5-2015

Large-Scale Graphene Film Deposition for Monolithic Device Fabrication

Khaled Al-Shurman
University of Arkansas, Fayetteville

Large-Scale Graphene Film Deposition for Monolithic Device Fabrication

Large-Scale Graphene Film Deposition for Monolithic Device Fabrication

A dissertation submitted in partial fulfillment
of the requirements for the degree of
Doctor of Philosophy in Microelectronics-Photonics

By

Khaled Al-shurman
Yarmouk University
Bachelor of Science in Physics, 1997
National University of Malaysia
Master of Science in Applied Physics, 2008

May 2015
University of Arkansas

This dissertation is approved for recommendation to the Graduate Council.

Dr. Hameed Naseem
Dissertation Director

Dr. Samir M. El-Ghazaly
Committee Member

Dr. Surendra Singh
Committee Member

Dr. Salvador Barraza-Lopez
Committee Member

Dr. Rick Wise
Committee Member

The following signatories attest that all software used in this dissertation was legally licensed for use by Khaled Al-shurman for research purposes and publication.

_____ _____

Mr. Khaled Al-shurman, Student Dr. Hameed Naseem, Dissertation Director

This dissertation was submitted to http://www.turnitin.com for plagiarism review by the TurnItIn company's software. The signatories have examined the report on this dissertation that was returned by TurnItIn and attest that, in their opinion, the items highlighted by the software are incidental to common usage and are not plagiarized material.

_____ _____

Dr. Rick Wise, Program Director Dr. Hameed Naseem, Dissertation Director

Abstract

Since 1958, the concept of integrated circuit (IC) has achieved great technological developments and helped in shrinking electronic devices. Nowadays, an IC consists of more than a million of compacted transistors.

The majority of current ICs use silicon as a semiconductor material. According to Moore's law, the number of transistors built-in on a microchip can be double every two years. However, silicon device manufacturing reaches its physical limits. To explain, there is a new trend to shrinking circuitry to seven nanometers where a lot of unknown quantum effects such as tunneling effect can not be controlled. Hence, there is an urgent need for a new platform material to replace Si.

Graphene is considered a promising material with enormous potential applications in many electronic and optoelectronics devices due to its superior properties.

There are several techniques to produce graphene films. Among these techniques, chemical vapor deposition (CVD) offers a very convenient method to fabricate films for large-scale graphene films. Though CVD method is suitable for large area growth of graphene, the need for transferring a graphene film to silicon-based substrates is required. Furthermore, the graphene films thus achieved are, in fact, not single crystalline. Also, graphene fabrication utilizing Cu and Ni at high growth temperature contaminates the substrate that holds Si CMOS circuitry and CVD chamber as well. So, lowering the deposition temperature is another technological milestone for the successful adoption of graphene in integrated circuits fabrication.

In this research, direct large-scale graphene film fabrication on silicon based platform (i.e. SiO_2 and Si_3N_4) at low temperature was achieved. With a focus on low-temperature graphene growth, hot-filament chemical vapor deposition (HF-CVD) was utilized to synthesize

graphene film using 200 nm thick nickel film. Raman spectroscopy was utilized to examine graphene formation on the bottom side of the Ni film and on the silicon-based substrate. Large-area bilayer graphene film was formed on silicon based platform.

COMSOL Multiphysics was used to investigate the CVD graphene growth on Ni films. Factors affecting CVD graphene synthesis include carbon solubility in Ni, growth time, growth temperature, as well as Ni film thickness. COMSOL model uses transport of diluted species, heat transfer in Ni thin film as well as deformed geometry module. In this particular research, the number of simulated graphene layers on Ni film was compared with experimental data. Also, the effect of many CVD parameters on graphene film fabrication is stated.

In conclusion, a novel method for direct large-scale graphene film fabrication on silicon based platform at low temperature was achieved using hot-filament chemical vapor deposition.

Acknowledgements

This Ph.D. Dissertation is the result of three years of work. I feel that this work would not have been possible without the help of a lot of people. First of all, I acknowledge Dr. Hameed Naeem for accepting me as Ph.D. student and allowing me to be working in this interesting study. I would like to thank all of my Ph.D. committee members; Dr. Samir M. El-Ghazaly, Dr. Surendra Singh, Dr. Salvador Barraza-Lopez, and Prof. Ken Vickers. I am very grateful to Dr. Rick Wise, Director of the microelectronics –photonics program at university of Arkansas. I wish to thank many people at the University of Arkansas' Department of Electrical Engineering; Dr. Juan C. Balda, Department Head, and Mr. Robert Saunders, P.E., Assistant Department Head. Also, I would like to thank many people at High Density Electronics Center (HiDEC) for their contribution and technical support; Dr. Michael Glover, Mr. Errol Porter, Mr. Mike Steger, and Mr. Tom Cannon. My grateful thanks are also extended to Arkansas Nano-Bio Materials Characterization Facility, specially, Dr. Mourad Benamara, facility director for his help in graphene film characterization. Many thanks to my friends; Dr. Husam Abu-Safe, Dr. Murtadha Alher, Omar H. Alzoubi, Aboozar Mosleh, Seyed Amir Ghetmiri, and Larry Cousar.

I would like to express my very great appreciation and thanks to my wife; Hanan Ali Abdallah Aljarrah. Hanan, this would not have been possible without your compassion and understanding. I am furthermore especially grateful to my kids; Zakaria, Mariam, Iman, and Zainab for their kindnesses. Finally, I am very grateful to my father, my mother, my brothers (Zakaria, Ibraheem, Ali, and Ahmed), and my sisters (Hanan, Taghreed, Abeer, Manal, and Noor).

Portions of this dissertation were published as:

Al-Shurman, K. M., and Hameed Naseem, "CVD Graphene Growth Mechanism on Nickel Thin Films," COMSOL Conference 2014, Boston, Massachusetts, USA, October 8 - 10, 2014. http://www.comsol.com/paper/download/194705/alshurman_paper.pdf.

Dedication

This dissertation is dedicated to my brother Zakaria.

Table of Contents

List of Figures

List of Tables

Chapter 1: Introduction and Motivation

Introduction

The nanoscience and nanotechnology field have been at the forefront of technology improvement over the last few decades due to its great potential applications [1]. The nanoscience and nanotechnology are interested in science and engineering at nanoscale [2].

Since 1958, the concept of integrated circuit (IC) has achieved great technological developments and helped in shrinking electronic devices. Nowadays, an IC consists of more than a million of compacted transistors.

The majority of current ICs use silicon as a semiconductor material. According to Moore's law, the number of transistors built-in on a microchip can be double every two years as shown in Figure 1.1. However, silicon device manufacturing reaches its physical limits. To explain, there is a new trend to shrinking circuitry to seven nanometers where a lot of unknown quantum effects such as tunneling effect can not be controlled. Hence, there is an urgent need for a new platform material to replace Si.

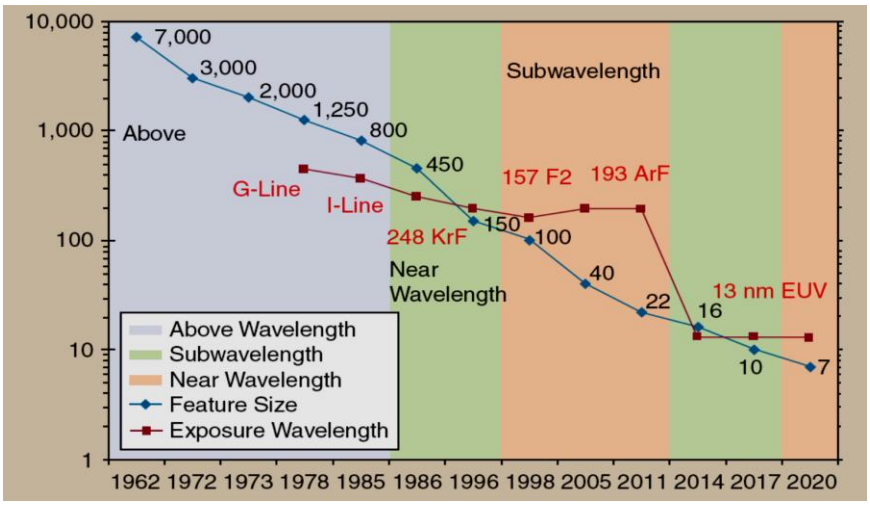

Figure 1.1[3]: Moore's law diagram

Graphene, which exhibits extraordinary electrical properties, can take over to allow the semiconductor industry to continue its journey toward smaller and faster electronic devices.

Graphene is one of the most recent carbon nanomaterials that have attracted widespread attention because of its superior properties and enormous potential for various applications [4]. Graphene is the basis of all graphitic forms. To clarify, graphene can be wrapped up into 0D buckyball, rolled into 1D nanotube, and stacked into 3D graphite as illustrated in Figure 1.2 [5].

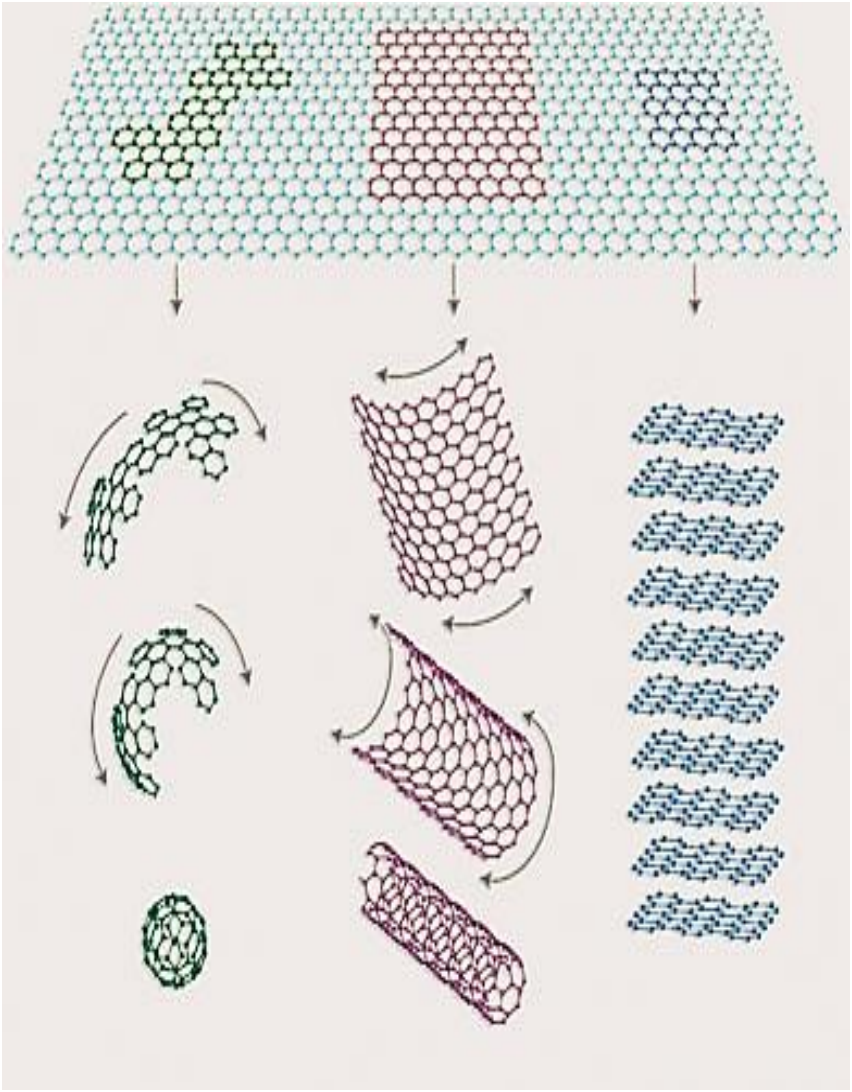

Figure 1.2 [1, 5]: Graphene; mother of all graphitic forms.

Graphene properties

1.1.1 Graphene lattice and band structure

Graphene is a single atomic layer, first isolated in 2004, of sp^2-bonded carbon atoms organized in a two dimensional hexagonal lattice structure as shown in Figure 1.2 [6]. The unit cell of graphene has two carbon atoms with carbon-carbon spacing, a equals 1.421 Å [7].
As illustrated in Figure 1.3, the lattice unit vectors are expressed by Equation 1.1 as following [8]:

$$a_1 = a\left(\frac{3}{2}, \frac{\sqrt{3}}{2}\right), \quad a_2 = a\left(\frac{3}{2}, -\frac{\sqrt{3}}{2}\right) \qquad \text{Equation 1.1}$$

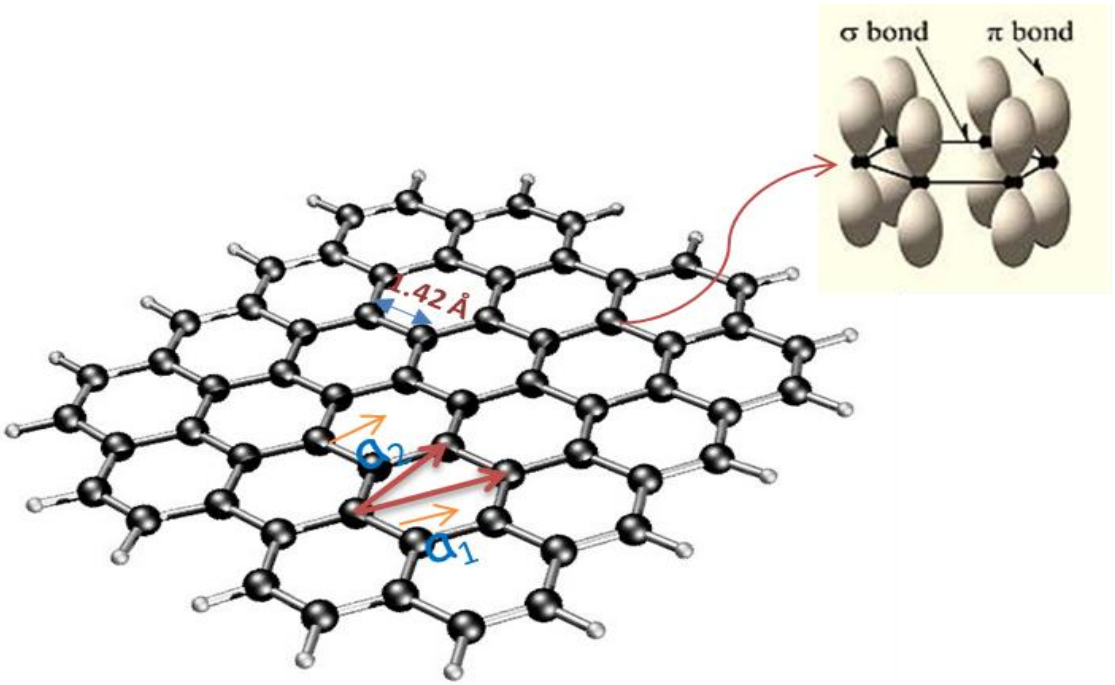

Figure 1.3: Hexagonal network of carbon – sp^2 bonding.

Each carbon atoms has six electrons; two electrons located in the innermost $1s^2$ state and four of them in the outer valence shell (i.e. 2s and 2p states) as displayed in Table 1.1.

Table 1.1: The electron configuration of carbon atom ground state.

Element		Shell				
Carbon	Z	K	L			
		1s	2s	$2p_x$	$2p_y$	$2p_z$
C	6	2	2	1	1	

In L shell, the sp^2 hybridization between the s and both p_x and p_y orbitals forms covalent C-C bonds between carbon atoms, the strongest bounds in nature [9]. This bond is called σ bond and it is the one which forms honeycomb lattice structure in graphene material. Hence, sp^2 hybrids have three electrons for σ bonding as illustrated in Figure 1.4.

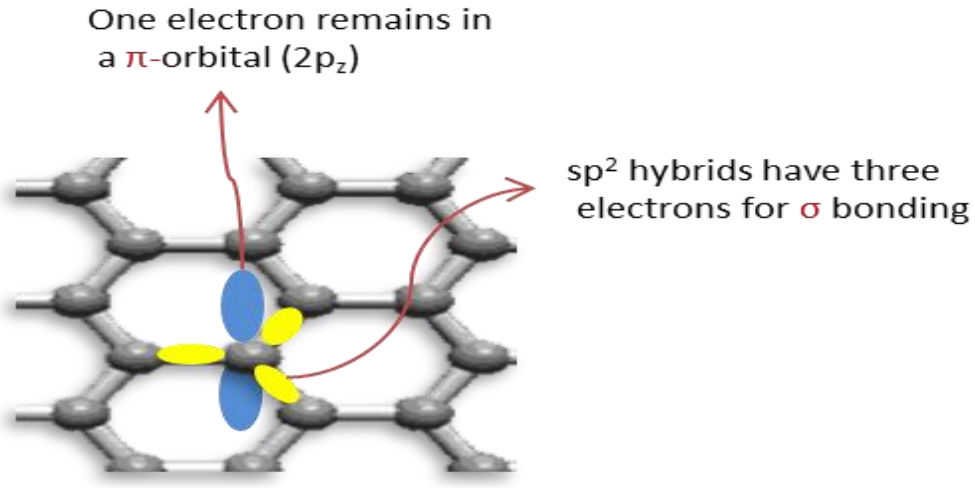

Figure 1.4: Bonds in Graphene

The p_z orbital is hybridized to form the valence band (π) and conduction band (π*) perpendicular to the plane of graphene atomic layer as shown in figure 1.3 [10]. The valence band (π) and conduction band (π*) meet at Dirac points; K and K' given by Equation 1.2 in the first Brillouin zone as shown in Figure 1.4 [11].

$$K=\left(\frac{2\pi}{3a}\ ,\ \frac{2\pi}{3\sqrt{3}\,a}\right),\quad K'=\left(\frac{2\pi}{3a}\ ,\ -\frac{2\pi}{3\sqrt{3}\,a}\right) \qquad \text{Equation 1.2}$$

Hence, graphene is considered a zero-gap semiconductor because graphene does not have band gap as illustrated in Figure 1.5 [12].

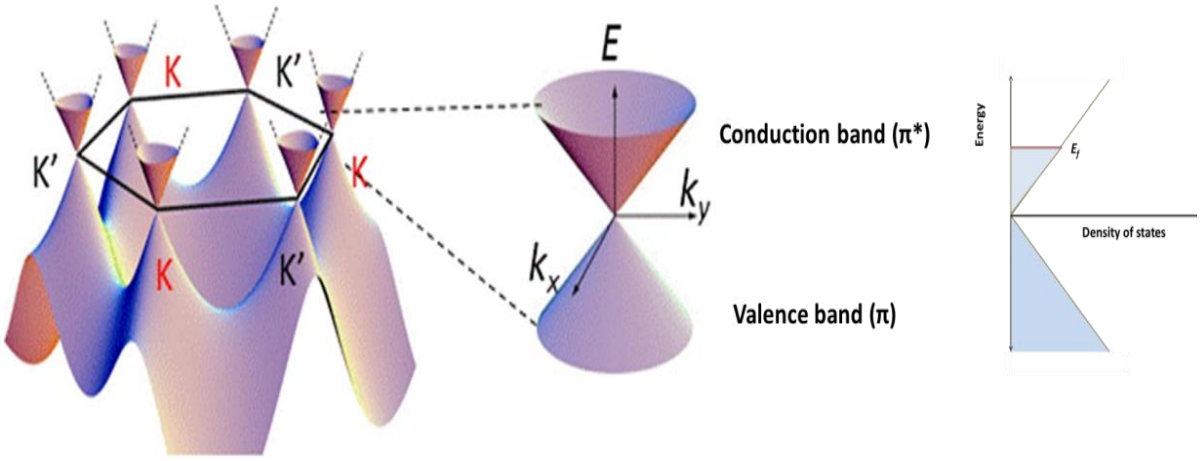

Figure 1.5 [12]: The energy dispersion relation and density of states of the graphene in the vicinity of K and K' points.

As displayed in the figure, In the vicinity of K and K' points, the low energy dispersion relations are linear and carriers behave as massless Dirac fermions with speed of light ~ 10^6 m/s. Hence, carriers are described by Dirac equation; Equation 1.4 [13].

$$E=\hbar v_F\sqrt{k_x^2+k_y^2} \qquad \text{Equation 1.3}$$

Where,

$\hbar = h/2\pi$: The reduced Plank's constant

k: The wave vector

v_F: The Fermi velocity ~ 10^6 m/s.

1.1.2 Electronic properties

The single-layer graphene is a semi-metal or zero-gap semiconductor, and has excellent electronic properties. Graphene's charge carriers (electrons) propagate through the hexagonal

lattice structure as massless Dirac fermions with Fermi velocity (v_F~ 10^6 m/s) with remarkably high electron mobility [14].

The measured electron mobility of graphene on SiO_2 substrates at room temperature is 40,000 $cm^2V^{-1}s^{-1}$ [14].Table 1.2 displays charge carriers mobility in graphene comparing with charge carriers mobility in the other well-known semiconductors materials like Si, Ge, and GaAs [15,16].

Table 1.2: Charge carriers mobility in graphene and in other well-known semiconductors materials

Property		Symbol	Unit	Si	Ge	GaAs	Graphene / SiO2
Mobility	Electron	μ_e	$cm^2V^{-1}s^{-1}$	1400	3900	8500	~40,000
	Hole	μ_h		471	1900	400	~40,000

In addition, graphene's charge carriers travel over hundreds of nanometers at a speed of 10^6 m/s, (300 times slower than that of light,) without scattering. So, the massless carriers and little scattering in graphene exhibit strong and strange relativistic quantum effects at room temperature [17].

1.1.3 Optical properties

Graphene also has extraordinary and unique properties. The free standing single layer of graphene transmits 97.7% of light that passes through it [18]. The transmission coefficient is given by Equation 1.4:

$T=1-\alpha\pi \approx 97.7\%$ Equation 1.4

Where,

T: The light transmission coefficient

$\alpha=e^2/4\pi\varepsilon_o\ \hbar c \approx 1/137$: The fine structure constant.

Hence, the free standing single layer of graphene absorbs approximately 2.3% of the incident white light that passes through it.

As shown in Figure 1.6, the light absorption is proportional to the number of graphene layers [19].

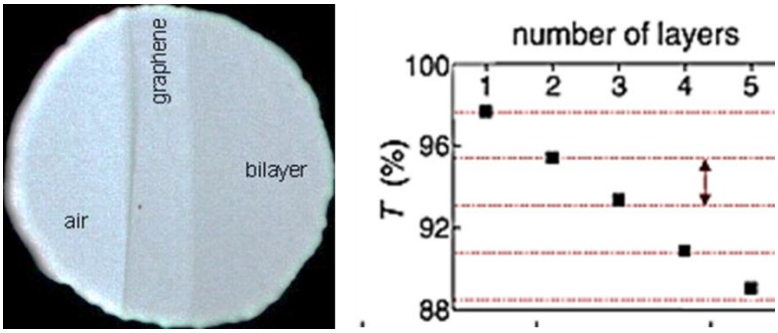

Figure 1.6 [19]: White light absorption by graphene layers.

In order to make graphene film visible for naked eye, graphene film is deposited on top of SiO_2/Si wafers. The visibility of graphene depends on both thickness of SiO_2 and light wavelength. The typical SiO_2 thickness on the Si wafer that is normally used to make graphene film visible is 300 nm as depicted in Figure 1.7 [20].

Figure 1.7 [20]: Graphene film on 300 nm SiO_2 imaged with white light.

1.1.4 Mechanical properties

Not only are graphene's electronic and optical properties extraordinary but also graphene has incredible mechanical properties. Suspended single layer graphene (SLG) has a large Young's modulus (1,100 GPa) and a breaking strength 42 N/m [21,22]. Graphene is stronger than steel and diamond [23]. Graphene is the strongest material ever known for two reasons. First, graphene is made of a single atomic layer of carbon atoms bonded together in a two

dimensional hexagonal lattice structure. Hence, the source of strength for graphene is due to very strong covalent bonds between atoms [24]. Second reason, 2D materials (e.g. graphene) have less defects comparing with bulk materials [25].

Graphene is bendable and stretchable [26]. To explain, graphene film can be bent, twisted and pulled to a certain range without breaking. Moreover, graphene is the thinnest and lightest material known ~ 0.77 mg per square meter [27].

1.1.5 Thermal properties

Furthermore, graphene also has extraordinary thermal properties. The intrinsic thermal conductivity of suspended single layer graphene (SLG) is dominated by phonons [28]. In fact, the intrinsic thermal conductivity of graphene is due to covalent sp^2 bonding between carbon atoms. It has been measured to be nearly 5000 W/mK [29]. Hence, suspended single layer graphene (SLG) conducts heat 10 times better than copper.

Table 1.3 shows a comparison between thermal conductivity values at room temperature of common materials used in semiconductors devices fabrication. It is clear from this table that the thermal conductivity value decreases with number of graphene layers.

Table 1.3: Thermal conductivity values at Room temperature of common materials used in semiconductors devices fabrication [30,31].

Materials	Room Temp Thermal Conductivity (W/mk)
Suspended Single Layer Graphene	1500–5000
Suspended Few Layer Graphene	1300–2800
Graphite	200 - 2000 (Orientation Dependent)
Carbon Nano-tubes (CNTs)	3000 - 3500
Diamond	1000 - 2200
Diamond-like Carbon (DLC)	0.1 - 10
Silicon (Si)	145
SiO2	1 - 13
Copper	400
Gold	~300

Motivation and objectives

Graphene is one of the most recent carbon nanomaterials that have attracted widespread attention because of its superior properties. The exceptional and unique properties of graphene create huge trends for many advanced electronic and optoelectronics devices, such as flexible thin-film transistors, biosensors, ultra capacitance devices, solar cells, and other innovations.

Graphene is a promising candidate to replace silicon material for monolithic device fabrication in next electronic device generations.

Chemical vapor deposition (CVD) offers a very appropriate technique to fabricate films for large-scale monolithic fabrication of graphene films. However, there are still several problems and challenges associated with CVD graphene synthesis. Direct deposition of graphene film on desired substrates such as silicon-based substrates without the need for transferring the deposited film from transition metal (Cu, Ni, etc.) is a scientist's concern nowadays. Therefore, one can avoid several problems related to graphene film transfer process such as chemical contamination, mechanical stresses, and potential graphene film damage. In addition, obtaining a large area single crystalline graphene layer, which is defect-free, is also researchers' hope. Hence, the single crystalline graphene layer could potentially provide carrier mobility in excess of 10^5 $cm^2/V.s$ as well as the other optimum properties. Also, lowering the deposition temperature is another objective that scientists hope to achieve in order to be able to utilize graphene in integrated circuits and meet the industrial requirements for graphene-based devices production.

In this study, we demonstrate large-scale graphene film deposition for monolithic device fabrication on different substrates; Si, SiO_2, Si_3N_4, diamond like carbon (DLC) and diamond. Large-scale graphene film was deposited at the interface between a Ni film and those substrates

at low temperature using hot-filament chemical vapor deposition (HF-CVD). Then, the Ni film was removed utilizing scotch tape and ferric chloride leaving graphene at the interface between a Ni film and Si-based substrate as shown in Figure 1.8. Hence, there is no more need for transfer process, which causes normally mechanical and/or chemical damage to the graphene film, of graphene from catalyst films. Also, graphene film was etched away using hydrogen atoms in order to selectively pattern the graphene film.

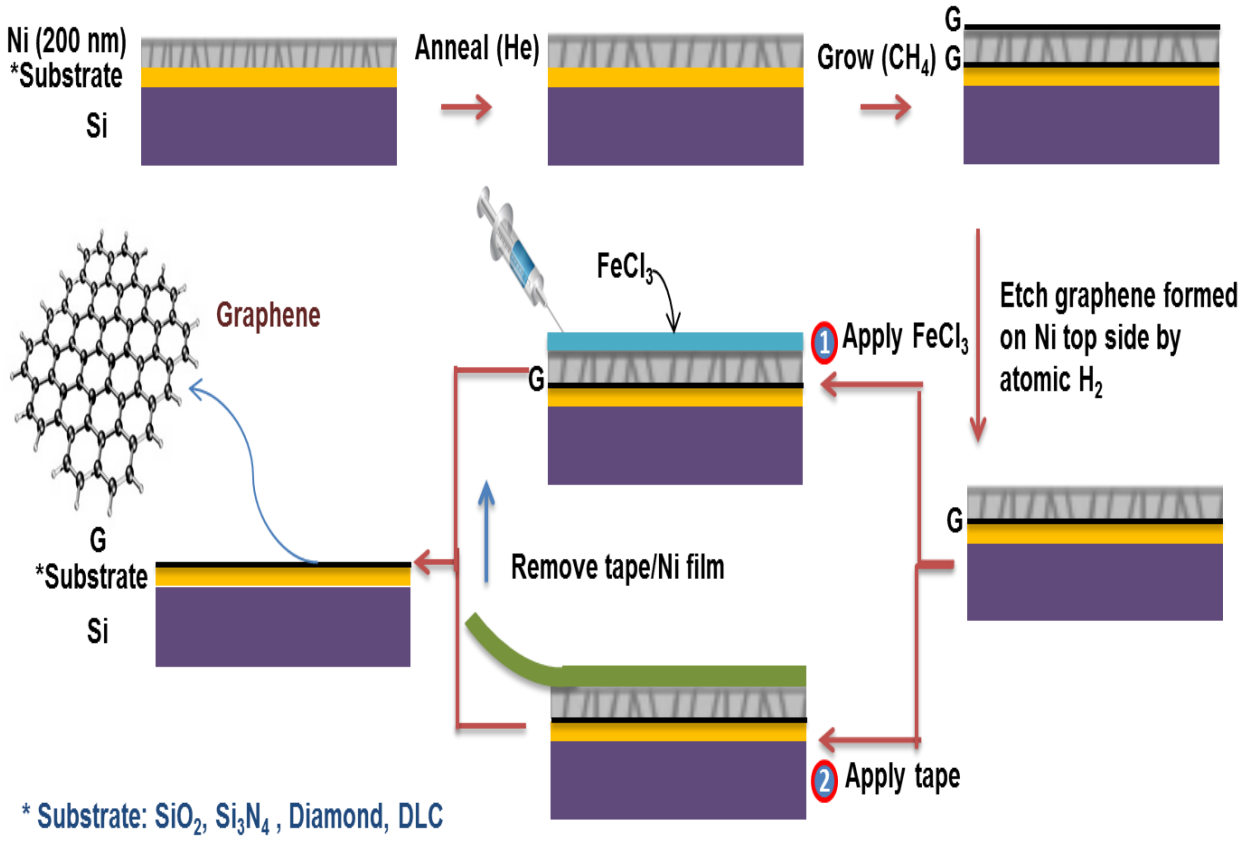

Figure 1.8: Proposed graphene growth process.

COMSOL Multiphysics software was used to simulate the process of graphene film growth using Ni thin film in order to be able to control the growth.

The research objectives of this project are:

a) At low temperature, direct deposition of graphene at the interface between a Ni film and Si-based substrate utilizing hot filament CVD.
b) Etching graphene film using atomic hydrogen
c) Peeling Ni film off easily using scotch tape.
d) Simulate graphene film growth mechanism using Ni film.

Dissertation outline

This dissertation consists of five chapters. The first chapter introduces graphene material. Then, graphene properties: graphene lattice and band structure, graphene electronic properties, graphene optical properties, graphene mechanical properties, and thermal properties are briefly explained. Chapter two is a literature review about graphene. In chapter three, the experiment al method that is used in thin film and graphene deposition are presented. In addition, COMSOL Multiphysics simulation for graphene growth mechanism using Ni film is explained. Also, in this chapter, a brief description of analytical characterizations such as Raman spectroscopy, scanning electron microscopy (SEM), energy dispersive x-ray spectroscopy, atomic force microscopy (AFM), and ellipsometry tools will be discussed. In chapter four, graphene film synthesis and simulation results are discussed. Finally, chapter five gives the conclusions of this study.

Chapter 2: Literature Review

2.1. Graphene synthesis

The novel properties of the graphene film, specifically monolayer of graphene, make graphene a promising material to utilize it for fabricating many novel electronic devices [32].

Obtaining a graphene film has been achieved using many techniques such as epitaxial growth using high temperature annealing of silicon carbide (SiC) and chemical vapor deposition (CVD).

Silicon carbide is a well-known material utilized in high-power electronics production. Si atoms sublimation method is used in order to obtain graphitic layers on the silicon or carbon faces of a silicon carbide wafer [33]. The number of graphitic layers can be controlled in order to obtain single graphene layer that has crystallites size ~ hundreds of micrometers [34].

Even though SiC method yields a very high quality of graphene film, this method has two disadvantages. The first disadvantage is the high cost of the SiC wafers. The second problem is the need for high temperature.

Currently, chemical vapor deposition is widely used to grow graphene films on different types of transition metals such as nickel and copper. Once the graphene film is formed on the surface of the transition metal, the graphene film is transferred to a desired film using multi-step process.

However, there are still many obstacles in obtaining a high quality continuous large-area of a monolayer and multilayer graphene (Figure 2.1) that is directly formed on an arbitrary substrate [35][36].

For instance, the capability of these techniques is limited in terms of scalability [21]. Also, the graphene film transfer operation causes a variety of structural defects and damages

(Figures 2.2) in the film and chemical contamination [37].

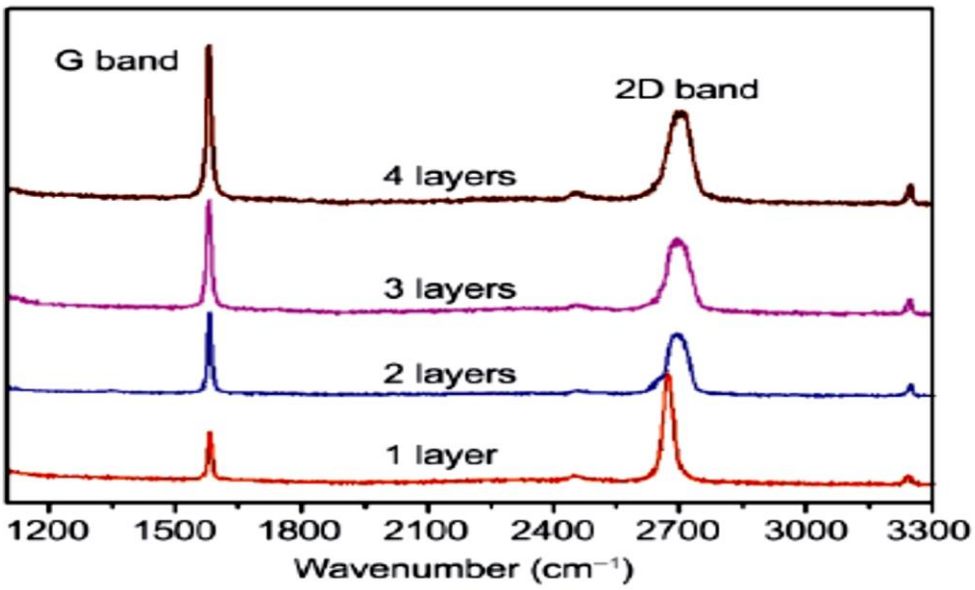

Figure 2.1[35]: Raman spectra of graphene film with 1, 2, 3, and 4 layers.

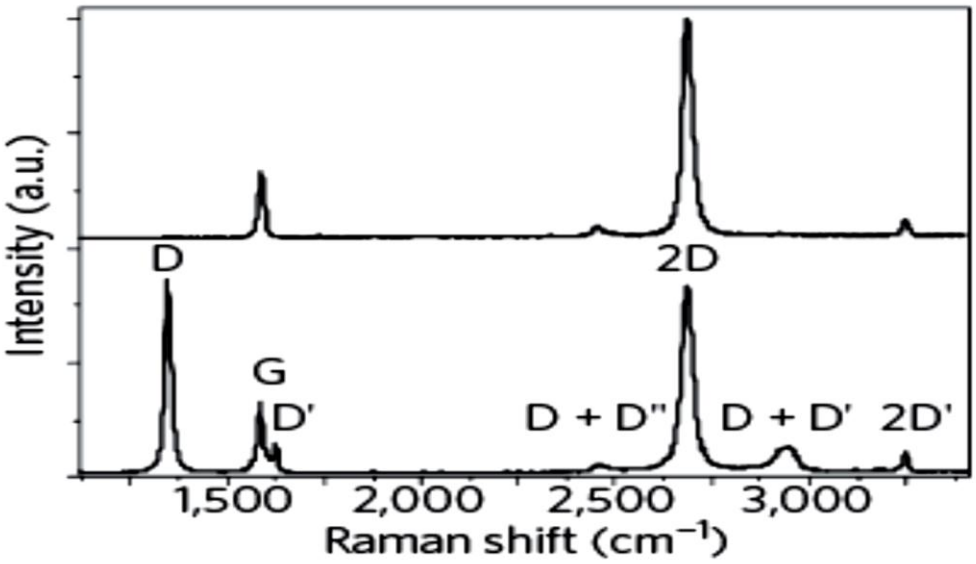

Figure 2.2 [37]: Raman spectra for damaged graphene film.

Raman spectroscopy is widely used to determine the number of graphene film. The number of graphene layers can be confirmed by I_{2D}/I_G as well as the symmetry and the lineshape

of the 2D-peak as clarified in Table 2.1 [38]. Also, the level of the defective and disordered structure of the graphene film can be extracted from the intensity ratio of the D to G peak (I_D/I_G). The quality of the graphene film is considered high if I_D/I_G intensity ratio less than 0.3.

Table 2.1: Graphene characterization using Raman spectroscopy.

I_{2D}/I_G	Graphene layers	2-D peak
2>	Single layer	Sharp
~1	Bi-layer	Broad
~0.3	Three layers	Broad
~0.2	Multi-layer	Broad

Graphene properties depend on fabrications methods. Table 2.2 displays the variation of each property based on production method.

Table 2.2[36]: Properties of graphene obtained by different methods.

Method	Crystallite size (μm)	Sample size (mm)	Charge carrier mobility (at ambient temperature) ($cm^2V^{-1}s^{-1}$)	Applications
Mechanical exfoliation	>1,000	>1	$>2x10^5$ and$>10^6$ (at low temperature)	Research
Chemical exfoliation	≤ 0.1	Infinite as a layer of overlapping flakes	100 (for a layer of overlapping flakes)	Coatings, paint/ink, composites, transparent conductive layers
Chemical exfoliation via graphene oxide	~100	Infinite as a layer of overlapping flakes	1 (for a layer of overlapping flakes)	Coatings, paint/ink, composites, transparent conductive layers
CVD	1,000	~1,000	10,000	Photonics, nano-electronics, transparent conductive layers
SiC	50	100	10,000	High-frequency transistors and other electronic devices

Currently, chemical vapor deposition (CVD) is considered a promising technique which provides a solution for the difficulties in obtaining a continuous monolayer and multilayer of large-area graphene. Also, the CVD technique meets the industrial requirements for graphene production [21].

In general, the graphene growth process using chemical vapor deposition (CVD) can be divided into four stages: a ramp-up stage, an annealing stage, a growth stage, and a cool down stage.

Chemical vapor deposition is a chemical process that is used to deposit fully dense thin solid films on different types of substrates such as metals and ceramics. To clarify, these thin solid films result from the decomposition of gaseous precursor(s) when they chemically react with a heated substrate as illustrated in Figure 2.3.

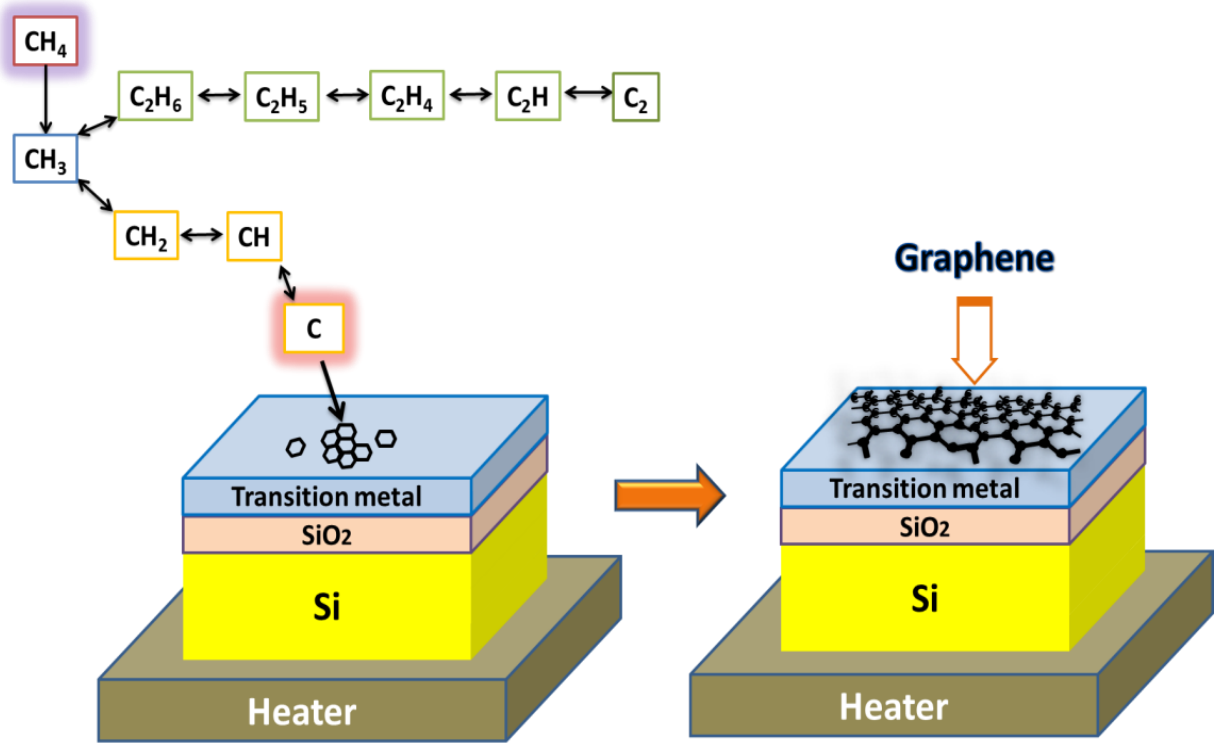

Figure 2.3: Graphene production using transition metals.

There are different forms of CVD processes including; Atmospheric Pressure Chemical Vapor Deposition (APCVD), thermal CVD, hot filament CVD, Plasma Enhanced Chemical Vapor Deposition (PECVD), Low Pressure Chemical Vapor Deposition (LPCVD), Metal-Organic Chemical Vapor Deposition (MOCVD), Laser Chemical Vapor Deposition (LCVD), Chemical Beam Epitaxy (CBE) [39].

Chemical vapor deposition systems come with different designs based on their form. However, there is a typical design (shown in Figure 2.4) that meets the minimum requirements for a chemical vapor deposition process [40].

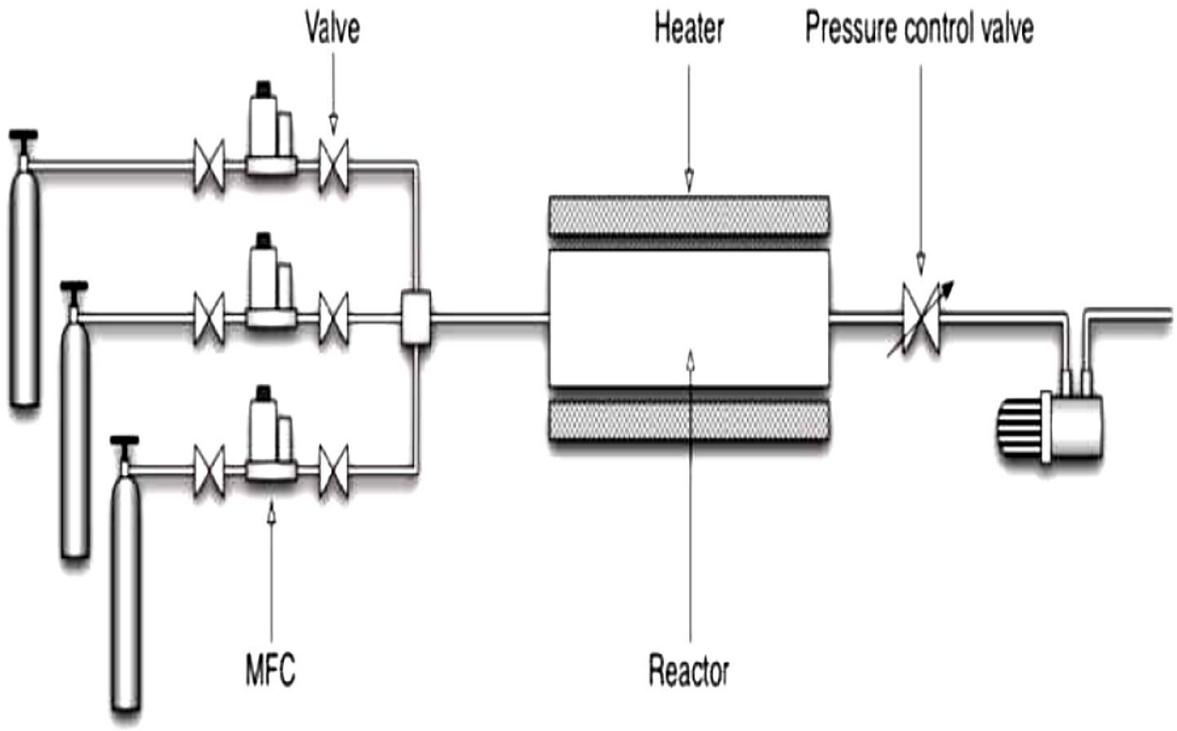

Figure 2.4 [40]: The minimum requirements chemical vapor deposition system.

2.2. Graphene CVD growth on transition metals

Chemical vapor deposition using hydrocarbon precursors can be carried out on the surface of various transition metals in group VIII such as Ni, Cu, and Co as shown in Table 2.3.

To explain, when a precursor such as methane or acetylene flows over a heated transition metal, it breaks into different forms of carbon. These forms of carbon will be either deposited or dissolved in the transition metal [41].

Presently, CVD graphene synthesis is widely conducted utilizing two transition metal substrates; Ni and Cu as a catalyst in order to obtain a large area of high quality graphene [42,43 ,44 ,45].

Table 2.3: Graphene obtained by different CVD parameters.

Precursor	Temperature	Pressure	Catalyst	Type of CVD	Ref.
Hydrocarbons		Std. P	Bi-metallic	RF-CVD	[46]
Hydrocarbons	900-1000 °C	Std. P	c-sapphire, Co/SiO_2 and H_2 (annealing)	Epitaxial CVD	[47]
Methane			Ni and Cu in ammonia		[48]
Ethylene			Bi-metallic	RF-CVD	[49]
Methane and H2	850-1000 °C		Ni thin film	CVD	[50]
Methane		Atm, Torr Vacuum	Cu	APCVD LPCVD UHVCVD	[51]
Methane and HOPG			Fe		[52]
Methane	1000 °C		Co and MgO Argon flow		[53]
Methane	700 °C		Fe	PECVD	[54]
Methane	1400-1900 °C		6H SiC	PECVD	[55]

Currently, chemical vapor deposition technique is considered a promising method for the synthesis of high quality graphene films utilizing various transition metals in group VIII such as Ni, Cu, and Co shown in Table 2.2. To explain, when a precursor such as methane or acetylene flow over a heated transition metal, it breaks into different forms of carbon. These forms of carbon will be either deposited or dissolved in the transition metal. These transition metals work as heterogeneous catalysts that enhance decomposition of the hydrocarbon materials such as methane (CH_4), acetylene (C_2H_2), and ethylene (C_2H_4). To clarify, heterogeneous catalysts lower

the activation energy required to break chemical bonds [40], hence, lowering the activation energy leads to increased reaction rate. However, catalysts not only help in dehydrogenation of hydrocarbons but also produce high quality crystalline graphite on their surface [56]. In the graphene CVD synthesis process, hydrocarbon decomposition on the surface of the catalyst releases carbon atoms as explained by Equation 2.1. However, some in-between chemical reactions including other hydrocarbons could be involved. For instance, methane conversion to graphene over the catalyst surface, S, can be described by the overall reaction as shown on Figure 2.5 [57]:

CH_4 + Surface (catalyst) → graphene + $2H_2(g)$ Equation 2.1

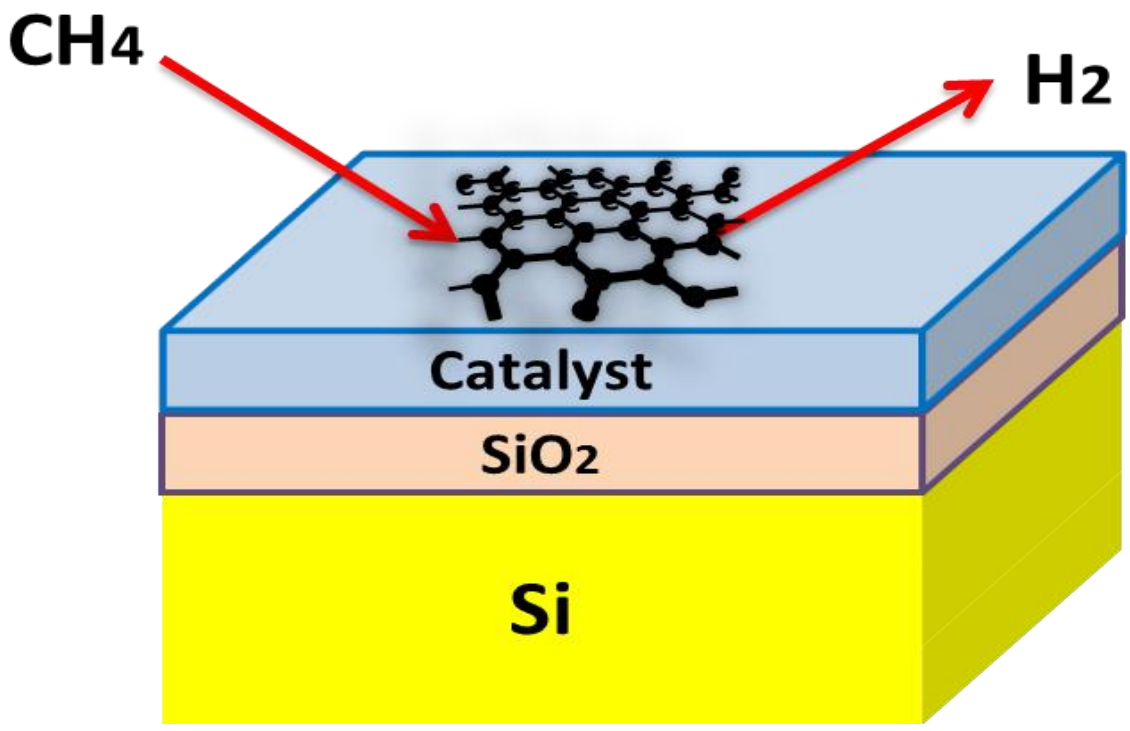

Figure 2.5: Basic conducting principle for graphene CVD deposition

Wafer-scale high-quality graphene film could only be achieved by controlling CVD parameters such as growth time, growth temperature, hydrocarbon pressure, cooling rate, and

hydrocarbon concentration [58]. In addition to these parameters, catalyst type plays a significant role in determining graphene growth mechanism, consequently defining the quality of the graphene film.

To date, there are two proposed mechanisms that explain the graphene synthesis process [40]. The two mechanisms could widely be described as [56]:

a) Graphene growth dissolution-precipitation: During the annealing period, the adsorbed carbon atoms diffuse into the bulk of the catalyst at high temperature. Then, the catalyst is cooled, whereby carbon atoms precipitate on the catalyst due to supersaturation.
b) Graphene growth direct deposition: Decomposed carbon atoms are deposited straight onto the catalyst surface.

Worldwide, graphene CVD growth has been achieved despite the fact the growth mechanisms are not fully understood and clear [59]. So, further theoretical and experimental research is needed to better understand the underlying mechanisms in order to control the quality of the graphene film.

2.3. Graphene transfer

Transfer of the grown graphene film to dielectric substrate is required for most applications. However, the graphene transfer process is very important and critical just as is graphene growth. There are many methods that have been used to transfer the graphene film into an insulating substrate. The first method is mechanical exfoliation using scotch tape and highly oriented pyrolytic graphite (HOPG) shown on Figure 2.6.

As illustrated in the figure, a highly oriented pyrolytic graphite crystal lattice consists of an ordered stacking of graphene sheets stacked in the sequence ABAB. Graphene sheets are slightly disoriented with respect to each other. Graphene sheet disorientation is characterized by

X-ray crystallography. The disorientation is determined based on the broadening of the (002) diffraction peak.

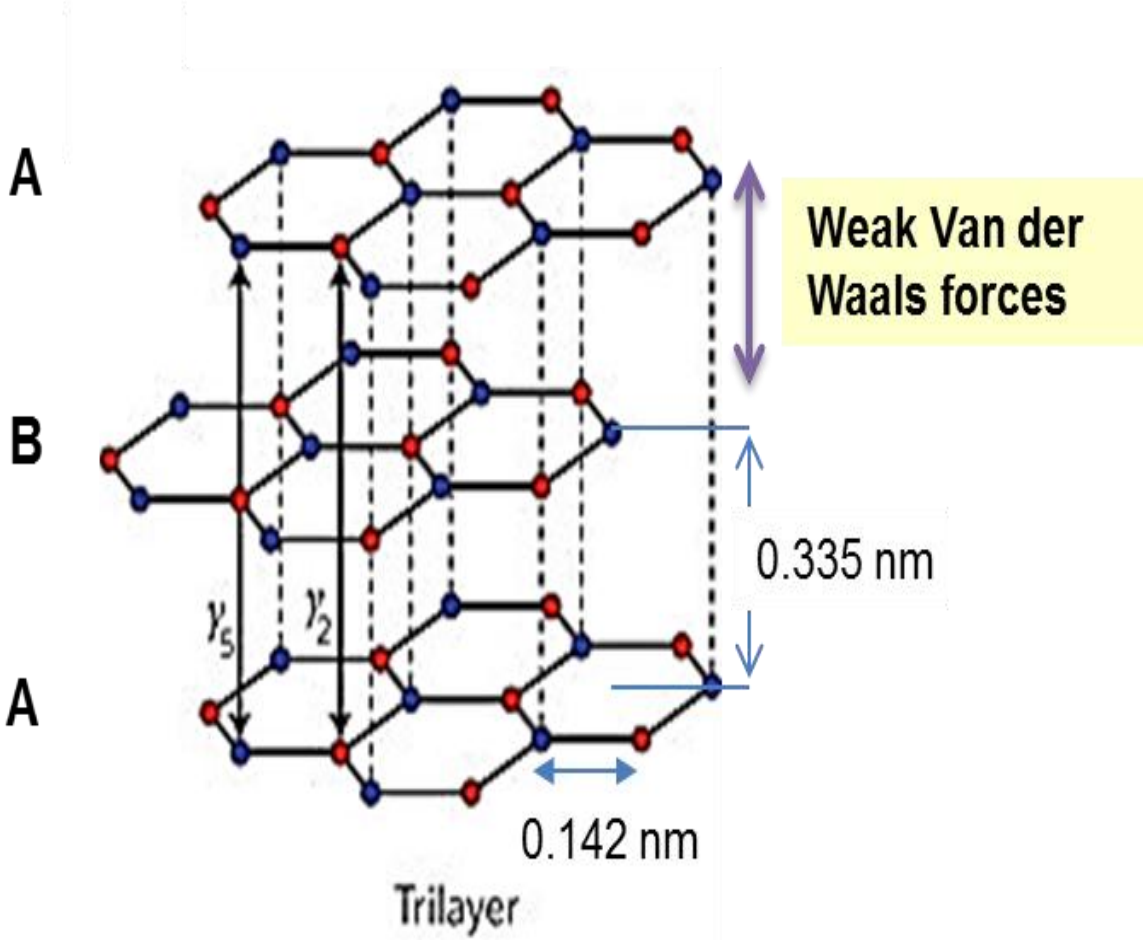

Figure 2.6: Highly oriented pyrolytic graphite (HOPG) structure.

Graphene film is peeled off from highly oriented pyrolytic graphite (HOPG) (depicted in Figure 2.7a surface utilizing scotch tape method as illustrated in Figure 2.7b. Graphene film obtained using the mechanical exfoliation method as of high quality properties and its crystal structure is reported to be excellent when comparing with graphene obtained by the other methods [60]. However, the sample size of the graphene obtained using this method is limited to a few micrometers.

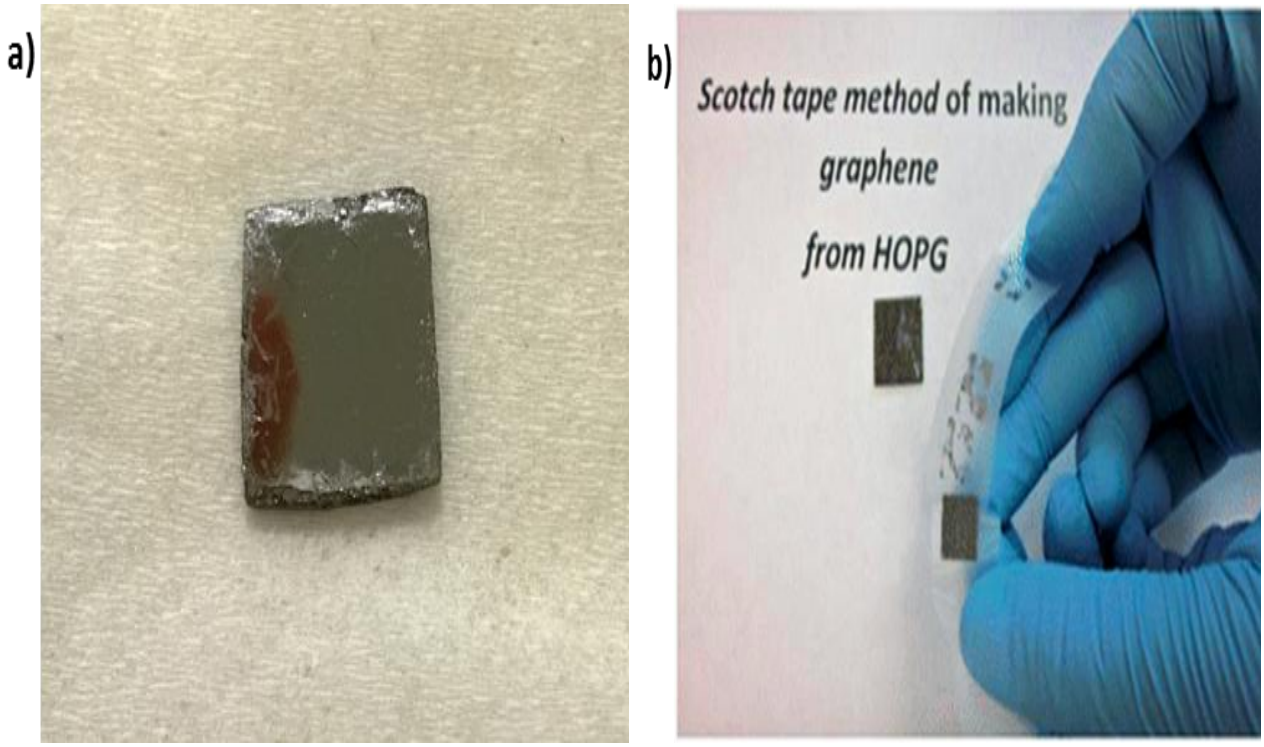

Figure 2.7 [61]: a) Highly oriented pyrolytic graphite (HOPG) sample; b) the mechanical exfoliation method using scotch tape.

The second method to transfer graphene films is conducted by utilizing poly(methyl methacrylate) (PMMA) or polydimethylsiloxane (PDMS) film. PMMA or PDMS is used to hold and transfer the graphene film as shown in Figure 2.8 [62, 63]. PMMA is deposited on the transition metal foil substrate that carries the graphene layer. Then, transition metal is etched away after PMMA is cured. Next, PMMA/graphene is transferred to desired substrate (e.g. SiO_2/Si). Finally, PMMA is removed by acetone. However, this transfer method leads to some defects to the transferred film as shown in Figure 2.8c. Recently, this method has been modified by adding additional steps in order to improve the quality of the transferred graphene film as illustrated in Figure 2.8b.

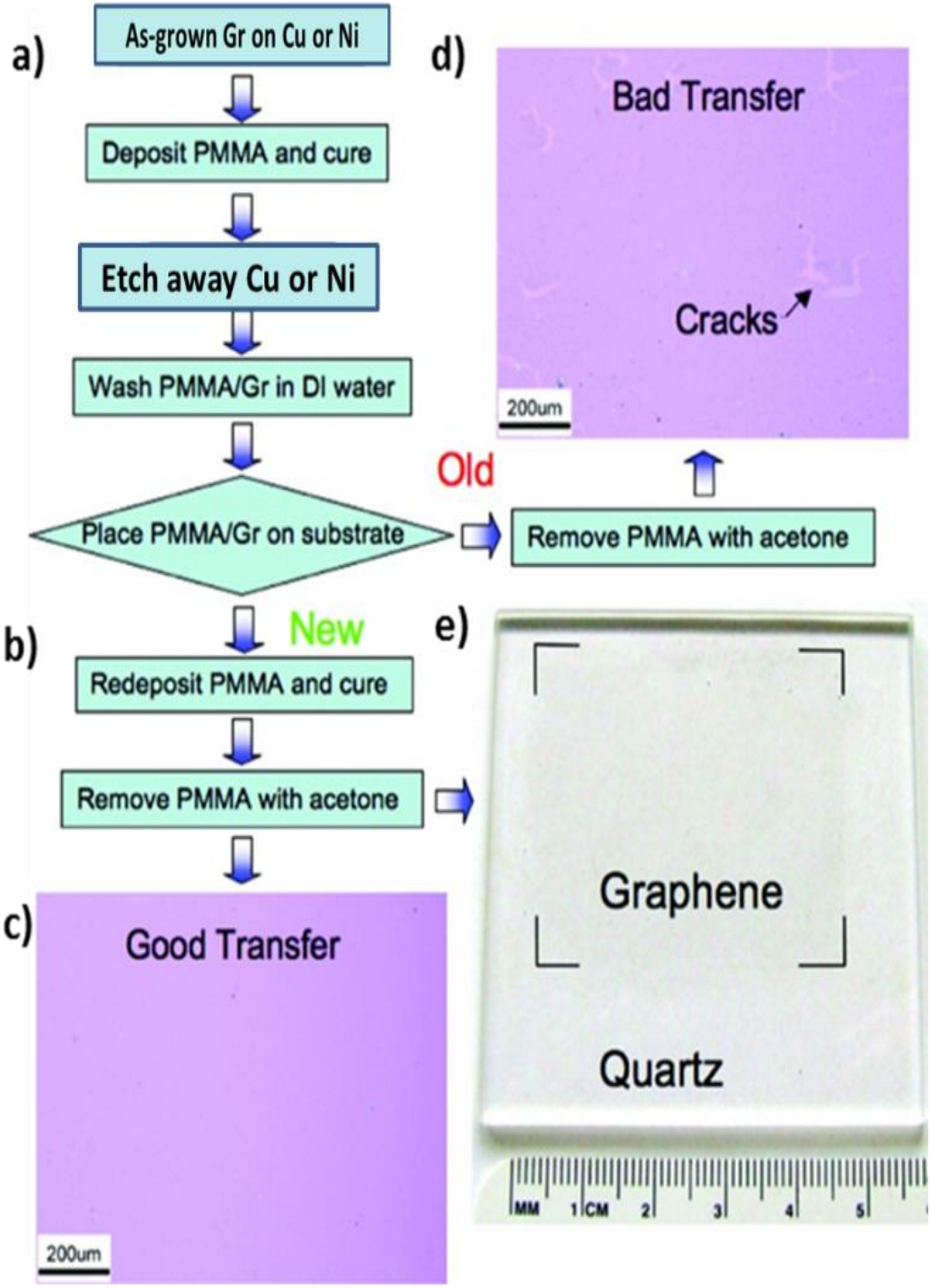

Figure 2.8 [62]: Graphene transfer methods. a) The old process for transfer of graphene films using PMMA. b) The current modified process for transfer of graphene films using PMMA. c) The optical micrographs of graphene transferred on SiO_2/Si wafers (285 nm thick SiO_2 layer) using the modified transfer method. d) The optical micrographs of graphene transferred on SiO_2/Si wafers (285 nm thick SiO_2 layer) using the old transfer method. e) A photo of a 4.5 × 4.5 cm^2 graphene on quartz substrate.

Another transfer method is called roll-to-roll method as illustrated in Figure 2.9. Bae and colleagues have successfully produced 30-inch graphene films grown by chemical vapor deposition onto flexible copper substrates [43].

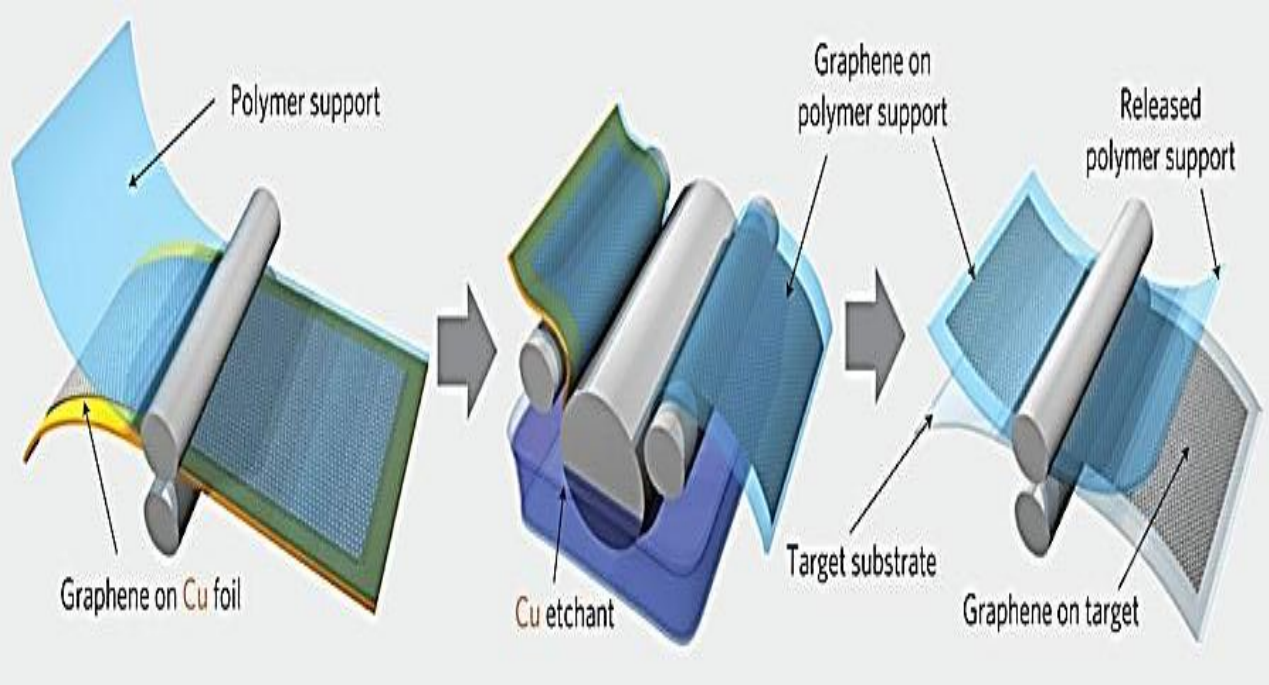

Figure 2.9 [43]: The roll-based production of graphene films grown on a copper foil.

The transfer of the graphene film to an insulating substrate is very essential for electronic applications in order to prevent electrical short when the electrical field flow through the graphene based device. However, transferring graphene film from metal substrates to an insulating or any desired substrate is very critical. To rephrase, the transfer of the graphene film will cause a lot of cracks and tears that create high electrical resistance and low optical transmittance in the film [62]. Also, the transfer process includes many wet chemical steps that can contaminate the graphene film [64]. Hence, in order to avoid a transfer process, depositing directly graphene film on dielectric substrates as shown in Figure 1.7. is proposed.

2.4. Graphene CVD growth on nickel (Ni)

There are two growth processes that work together to form graphene on Ni surface; carbon deposition from hydrocarbon precursors and carbon segregation from the bulk [40].

The graphene growth mechanisms primarily depend on the solubility and diffusivity of carbon in the transition metals as given in Equations 2.2 and 2.3, respectively [65,66]. The solubility of carbon atoms (S) in Ni is expressed by Equation 2.2:

$$S=S_o \exp(H/kT) \text{ (atoms cm}^{-3}\text{)} \quad \text{Equation 2.2}$$

where,

$S_o = 5.33 \times 10^{22}$ atoms cm^{-3}, an entropic pre-factor related to the density of sites where solute atoms sit.

H= −0.42 eV, the heat of precipitation.

K= Boltzmann's constant, 8.617 3324 ×10−5 eV K^{-1}

Equation 2.2 is an empirical equation that was proposed by Lander et al. [66] to describe the solubility process of the decomposed carbon atoms in Ni in the range 700 °C to 1300 °C. Also, carbon diffusivity can be expressed by utilizing diffusion coefficient of carbon atoms (D) in Ni using Equation 2.3;

$$D=D_o \exp(-E_D/kT) \text{ (cm}^2\text{ s}^{-1}\text{)} \quad \text{Equation 2.3}$$

where,

D_o= 2.48 cm^2 s^{-1} , an entropic pre-factor.

E_D = 1.74 eV, the diffusion activation energy.

K= Boltzmann's constant.

Also, the graphene growth mechanisms depend on the CVD growth conditions such as the growth temperature, the growth time, gas flow, the pressure, the cooling rate, and grain size.

So, the graphene growth mechanisms determine the topology and the thickness of the graphene film.

Depending on carbon solubility in the metal, the graphene grows on the metal substrate in two different ways [41]. In case of metals, which have relatively high carbon solubility (~1.3 atom% at 1000 °C) such as Ni, the dissolved carbon atoms at elevated temperature (700-1000 °C) precipitate from bulk to the metal surface upon cooling in order to form graphene. In contrast, carbon atoms grow on the surface of the metals that have relatively low carbon solubility such as Cu and Pt [67]. For instance, when a precursor such as methane (CH_4) or acetylene (C_2H_2) flows over a heated transition metal, it breaks into different forms of carbon. One of the potential ways for methane (CH_4) decomposition is $CH_3 \rightarrow CH_2 \rightarrow CH \rightarrow C$ which will be either deposited on or dissolved in the transition metal depends on carbon solubility in the metal [40]. Up to date, methane (CH_4) is extensively used as precursor for graphene growth for two reasons; CH_4 is stable at high temperature and has simple atomic structure.

In this research, Ni will be utilized as a catalyst for two reasons. First, Ni has a relatively higher melting point (1453 °C) as compared to Cu (1083 °C). In other words, using Ni will prevent formation a lot of metal contamination on the process chamber walls. Also, Ni has a high oxidation resistance while Cu reacts rapidly with O_2 producing copper oxide. So, using Cu means another required step in the graphene synthesis in order to get rid of CuO from graphene / Cu sample.

The CVD growth conditions which play significant role in obtaining large area, high quality graphene film have been investigated by many research groups.

Liu's group reported that the final thickness of the few layers of graphene is governed by three keys parameters; growth time, growth temperature, and sample cooling rate [68]. In their

experiment, chemical vapor deposition growth of graphene on 500 nm thick Ni film deposited on SiO_2/Si substrates have been carried out under 200 torr of H_2: 5% diluted CH_4 in Ar = 500:50 using a hot-wall CVD system.

Liu et al. reported that the three optimized graphene growth conditions are: 50 seconds for the growth time, 900 °C for the growth temperature, and 25 °C/s for the cooling rate. Also, they reported that single layer graphene regions of larger than 100 μm^2 have covered more than 50% of their 1 inch sample surface as shown in Figure 2.10.

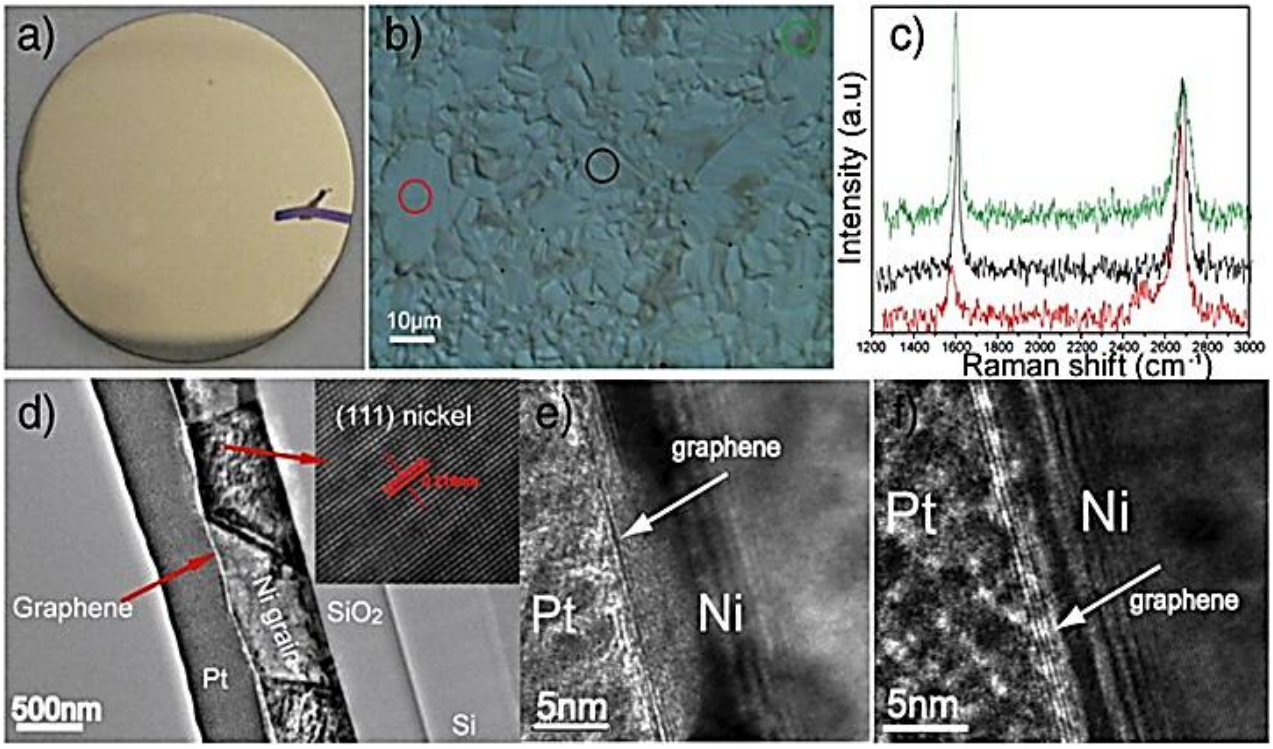

Figure 2.10 [68]: a) The optical digital image the wafer after graphene growths. b) Optical migrograph of the nickel surface after graphene growth. c) The Raman spectra corresponding to the three spots in b). d) XTEM of graphene on nickel with HRTEM shown in the inset. e) XTEM images of a single layer graphene region. f) XTEM image of a three layer graphene region are shown.

Then, the transfer process of the synthesized graphene film has been performed by soaking the samples in HCl solution. Cross-sectional transmission electron microscope (XTEM) and Raman

spectroscopy connected with optical microscopy were used to characterize the obtained graphene films.

Another group, Yu et al., synthesized a few layers of graphene on polished polycrystalline Ni foils with thickness of 0.5 mm [69]. First, the Ni foils were annealed in hydrogen for one hour and then exposed to a CH_4: H_2: Ar (0.15:1:2) environment at one atm for 20 min at 1000 °C. After that, the Ni foils were cooled at different rates 20 °C/s, 10 °C/s, and 0.1°C/s. Then, segregated graphene layers on Ni substrates were detached from Ni substrates using HNO_3 solution. Transmission electron microscopy (TEM) and Raman spectroscopy were used to characterize the quality of the films and the numbers of graphene layers formed on Ni.

Yu et al. found that the resulting thickness of the graphene layers depended on the cooling rate. Graphene can not be obtained by an extremely slow cooling rate whereas extremely fast cooling rate resulted in graphite film formation on the Ni foil surface. Graphene film can be produced using medium cooling rate as shown in Figure 2.11. Their results showed that a few layers of graphene (typically 3-4 layers) were produced with a cooling rate of 10 °C/s [69]. Also, they found that a high dosage of H_2 and smoother Ni substrates enhanced graphene film uniformity. In order to transfer the resulting graphene layers to an insulating substrate, they first coated the graphene/Ni foil with silicone rubber, and then covered it by a glass slide. After that, they etched the Ni using HNO_3.

Yoo et al. grew few-layer graphene films on Ni foils with thickness of 0.05 mm using an ethanol-CVD setup shown in Figure 2.12 [70].

First, pretreatment for Ni foils surface was performed in order to etch the native surface oxide which may reduce carbon solubility during fabrication process. Etching the native surface oxide was carried out by hydrofluoric acid for 5 seconds. Then, the Ni foil, which is placed in the

CVD chamber, was exposed to ethanol vapor when the temperature reached 900 °C for 5 min at a pressure of ~ 3 kPa. Then rapid cooling was carried out under argon gas flow of 300 sccm.

Scanning electron microscope (SEM), optical camera, and Raman spectroscopy have been used to study and characterize the synthesized graphene films.

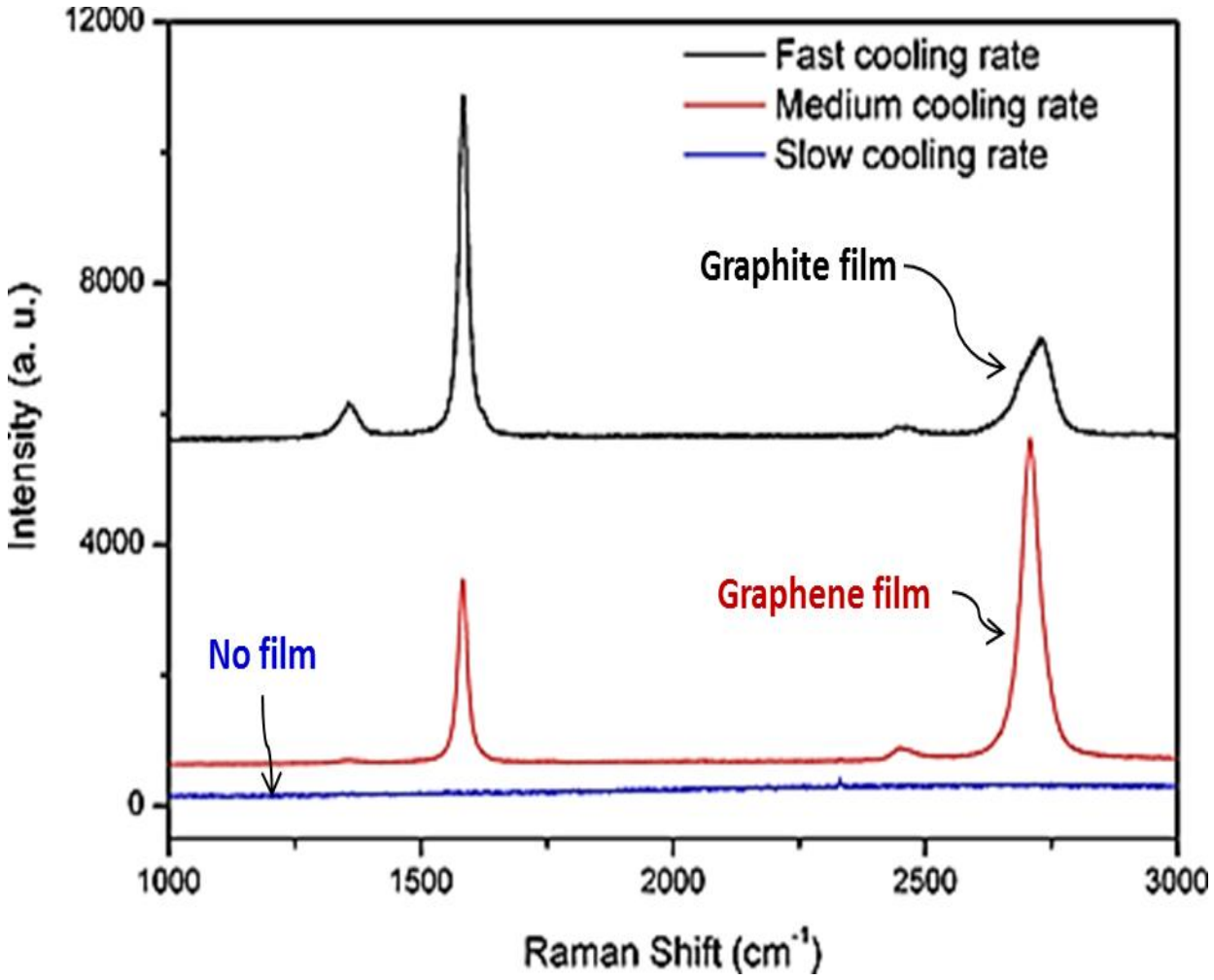

Figure 2.11 [69]: Raman spectroscopy of carbon film grown on the Ni foil surface at different cooling rate.

Yoo et al. showed that one can use ethanol, which is safe and cheap, to obtain multi-layers graphene (Figure 2.13) instead of using CH_4 gas, which is explosive and expensive [70].

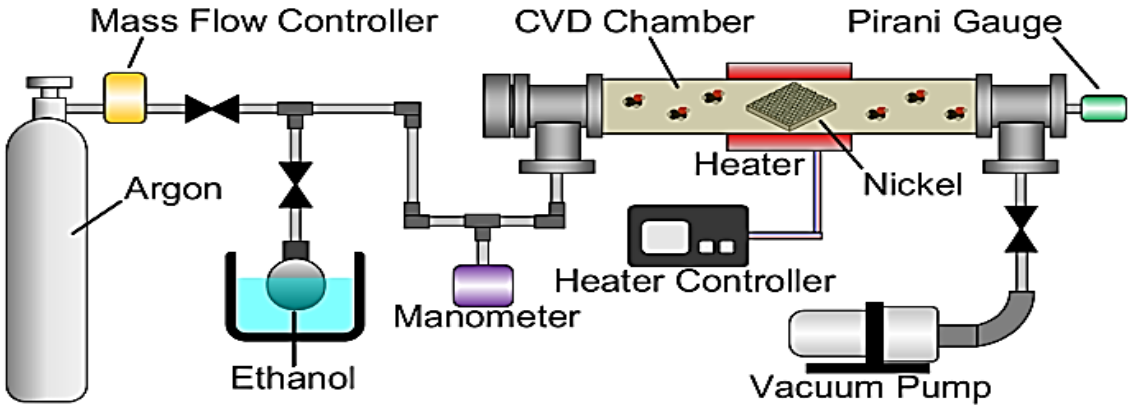

Figure 2.12 [69]: Schematic diagram of ethanol-chemical vapor deposition (CVD) system.

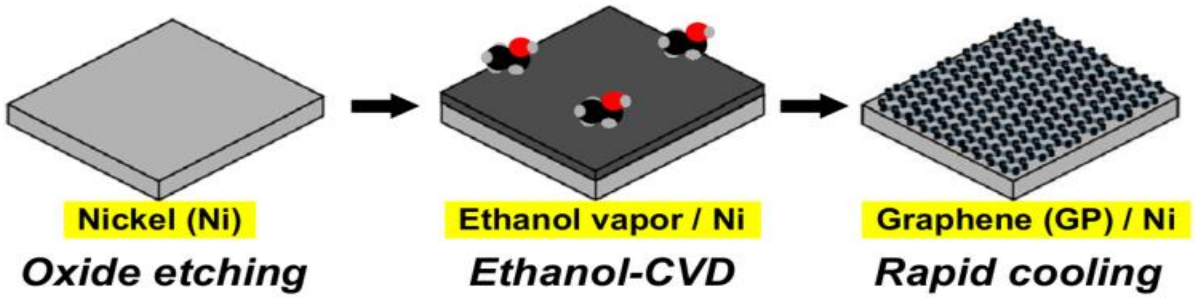

Figure 2.13 [70]: Graphene synthesis process via ethanol-CVD.

The growth of graphene on Ni was demonstrated in an atmospheric pressure chemical vapor deposition (APCVD) by Nayfeh et al. First, 30 nm adhesion layer of chromium (Cr) was deposited on SiO_2/Si. Then, 300 nm Ni was deposited on the chromium adhesion layer. Then, after putting the sample inside the APCVD furnace, a mixture of H_2 and Ar was flowed into the furnace while it was being ramped-up to 1000 °C. The annealing process was carried out for 20 min in order to remove Ni oxides and refine Ni microstructure. A small amount of CH_4 was introduced in the growth stage for 10 min. Finally, the system cools down, while still pumping the methane [71].

Nayfeh et al. [71] obtained monolayer graphene across the sample. However, they noticed that multilayers were formed on the Ni grain boundaries because the carbon precipitation is easy to be formed at these locations.

In order to synthesize a large area of high quality monolayer graphene directly on different types of transition metals, Yao et al. suggested an etching –aided chemical vapor deposition process as shown in Figure 2.14 [21]. Simply stated, after shutting down the carbon supply, an additional hydrogen etching process has been performed in order to remove the excessive dissolved carbon in the metal and prevent carbon precipitation on the metal surface during graphene growth time.

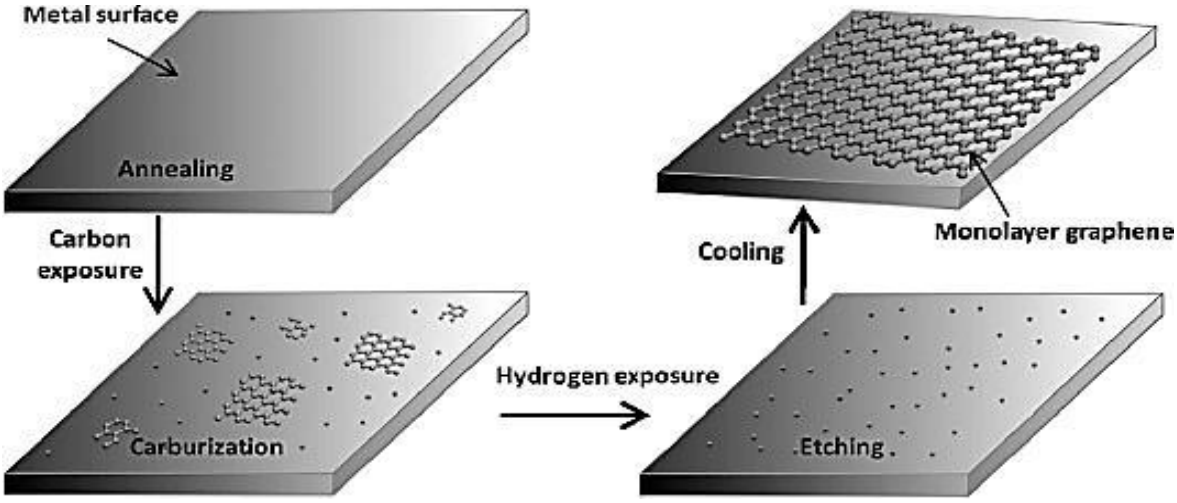

Figure 2.14 [21]: Schematic of etching-aided atmospheric pressure CVD growth of monolayer graphene on metal substrates.

In Yao et al.'s experiment, an annealing process at 1000 °C for 30 min was carried out for 100 μm metal foils such (Ni, Cu, Fe, and Co) under atmospheric pressure in the flowing of 500 sccm H_2 and 500 sccm Ar. Then, a carbon precursor (hexane vapor for Cu and methane for Ni, Co, and Fe) mixed with 500 sccm hydrogen was introduced into the furnace for 1 min in case of Cu, and 2 min in case of Ni, Co, and Fe. After finishing the carbon growth process, a

hydrogen etching was carried out at 1000°C for different periods of time (Cu: 1.5 min, Ni: 5min, Co: 5.5min, and Fe: 10min). Finally, the metal substrates were cooled down to room temperature under 500 sccm Ar with a cooling rate of 25°C/ min for Cu and 150°C/min for Ni, Co, and Fe to achieve one monolayer of graphene.

Yao et al. found that the additional hydrogen etching technique could be a solution for the bothersome carbon precipitation. Also, this technique could be extended to include other metals such as Au, Pt, Ru, and Pd. The additional hydrogen etching technique opens a new route for growth monolayer graphene on metal substrates that have high carbon solubility. For instance, varying hydrogen etching time enabled Yao et al to synthesize successfully monolayer graphene on Ni surface as shown in Figure 2.15.

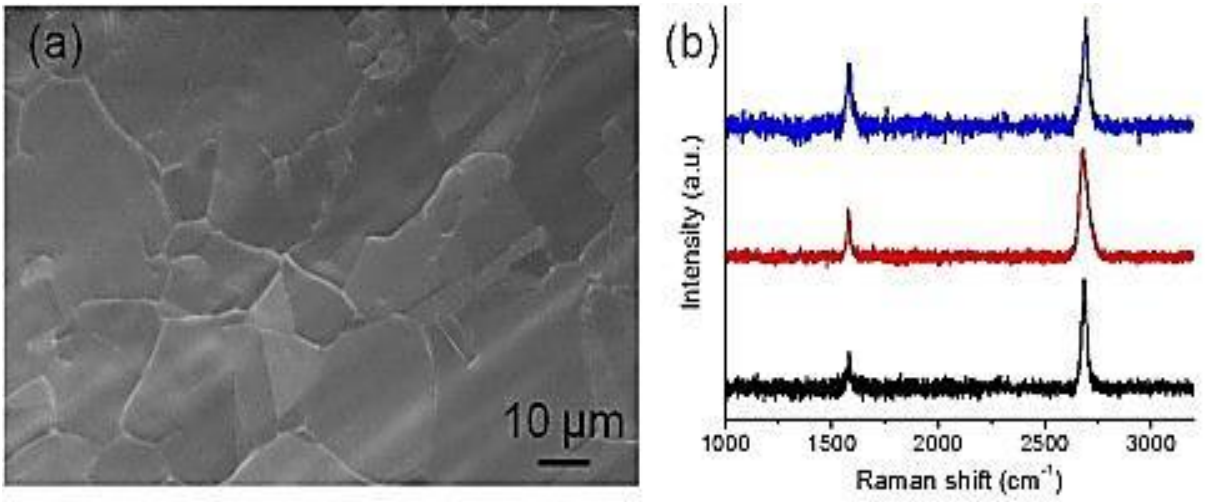

Figure 2.15 [21]: a) SEM image of single layer graphene grown on Ni surfaces b) Raman spectra of single layer graphene film grown on Ni at different locations.

Wafer scale, high- quality graphene films as large as 3 in on Ni and Cu under ambient-pressure has been synthesized by Lee et al as shown in Figure 2.16 [32]. Ni film of thickness 300 nm was deposited on SiO_2/Si. Then the substrate was loaded into a quartz tube furnace that was

ramped up to 1000°C under ambient pressure with flowing H_2 and Ar. A mixture of gases was introduced (CH_4:H_2: Ar=250:325:1,000) for 5 min before the system was rapidly cooled down to room temperature.

Lee et al. reported that high quality mono- or bi-layers of graphene are usually formed on Cu surface while multilayer is formed on Ni surface. Also, they claim that graphene film transfer does not change the quality of the graphene film [32].

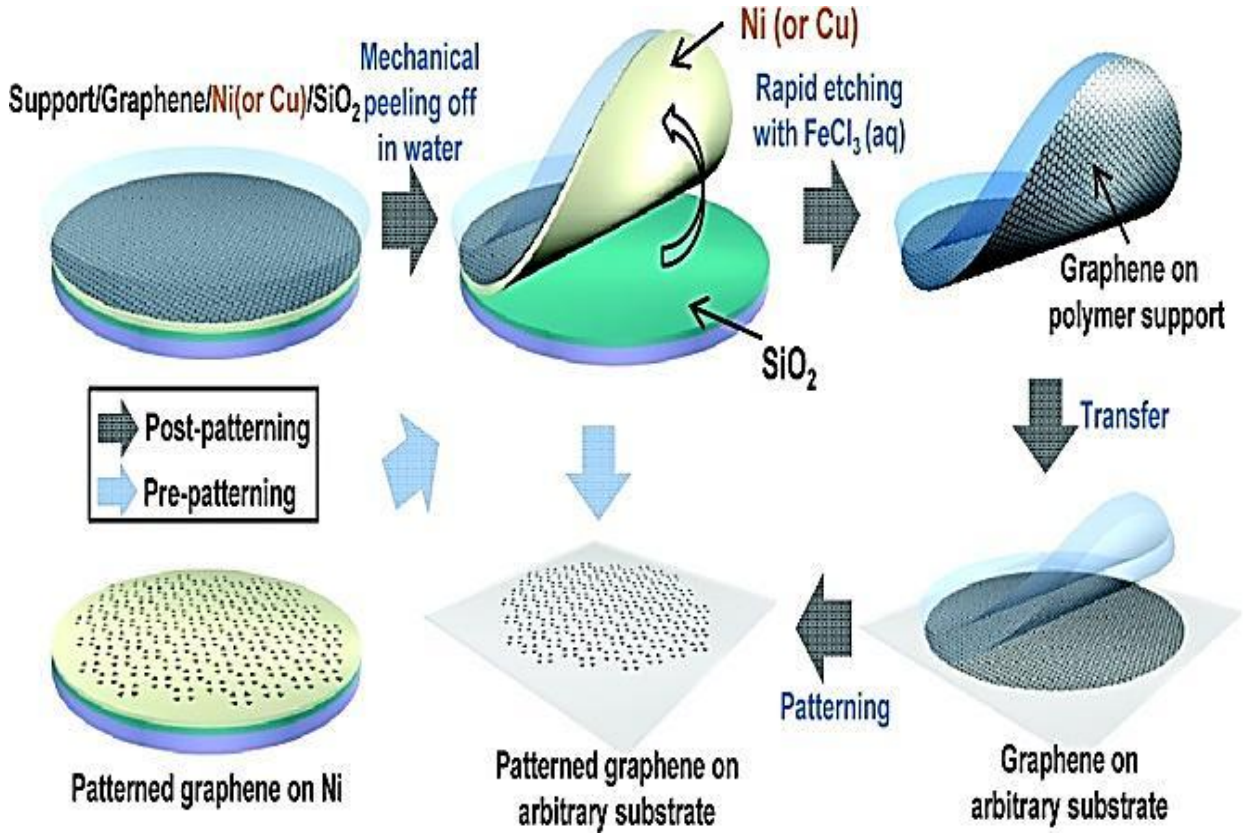

Figure 2.16 [32]: Schematic illustration for synthesis, etching, and transfer of large-area graphene films.

A research group from MIT used CVD in order to synthesize a large area of single- to few-layer of graphene films (~cm^2) on arbitrary substrates [42]. The grain size of single- or bilayer is 20 um. In their experiment, a 500 nm Ni film on a SiO_2/Si substrate was placed in a

CVD chamber. Then the system was ramped up for 10-20 minutes at 900-1000 °C under a 600 sccm Ar and 500 sccm H_2 flow. The CVD growth is performed for 5 to 10 minutes at 900 °C or 1000 °C under a 5-25 sccm CH_4 and 1500 sccm H_2 flow in atmospheric conditions.

The team reported that most of the obtained multilayer graphene was formed on the grain boundaries as shown in Figure 2.17b.

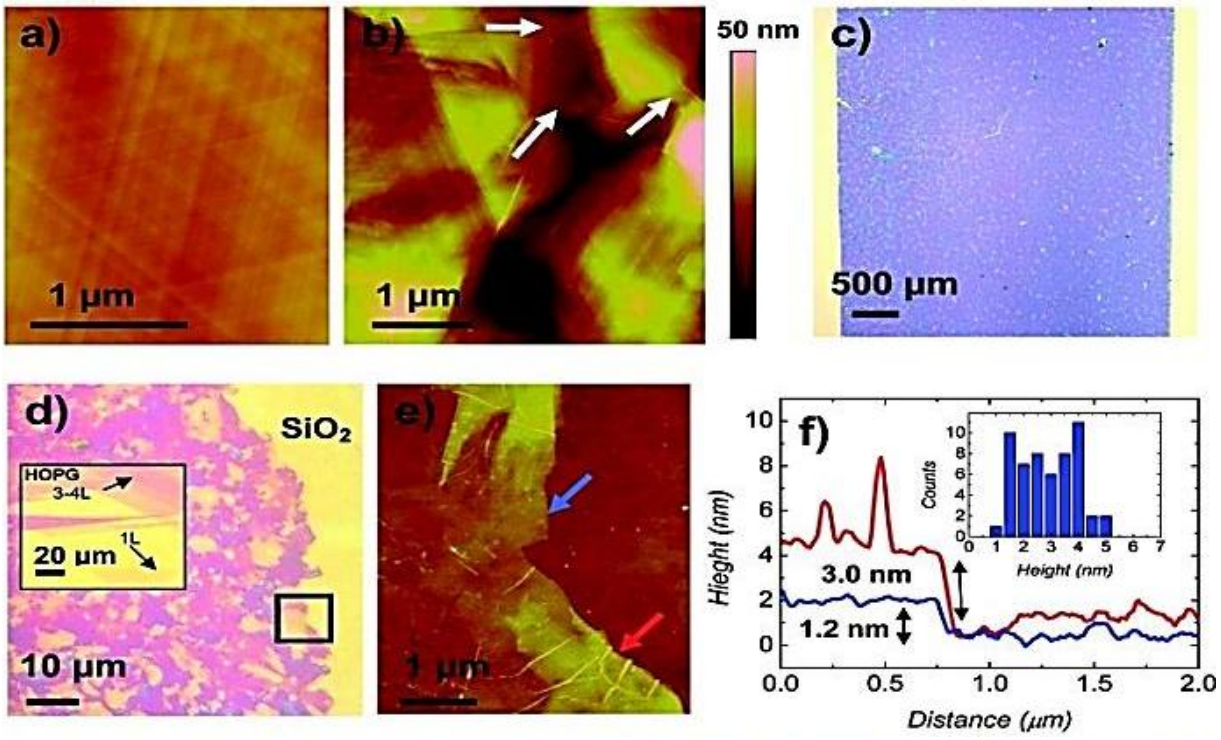

Figure 2.17 [42]: Graphene films grown by CVD on Ni. a) AFM image of the surface of a Ni grain after annealing. b) AFM image of a graphene film on polycrystalline Ni film after CVD synthesis. c) Optical image of the grown film (blue) on a SiO_2/Si substrate (yellow). d) Optical image of an edge of a graphene film deposited on a SiO_2/Si substrate. e) AFM image of the region surrounded by the black square in figure d. f) Graphene film thickness measurements on the two positions indicated in figure e.

Another group from the University of Southern California has reported results that match with the MIT group results in terms of a scalable method to synthesize single- and a few- layer graphene film on Ni film using CH_4-based CVD and grain boundary effects [72]. In their

experiment, a 100 nm Ni film was deposited on a 4 inch Si/SiO_2 wafer in order to use it as a substrate. The substrate was placed inside the tube as shown in Figure 2.18a. Then, the substrate was heated to 800 °C at a rate of 0.15 °C/min under 600 sccm of H_2. The substrate was then annealed at 800 °C in a 10:1 Ar: H_2 mixture. The deposition process was then performed for 8 min using a flow rate of 100 sccm of methane gas. Finally, the system was cooled at a rate of 0.15 °C/min.

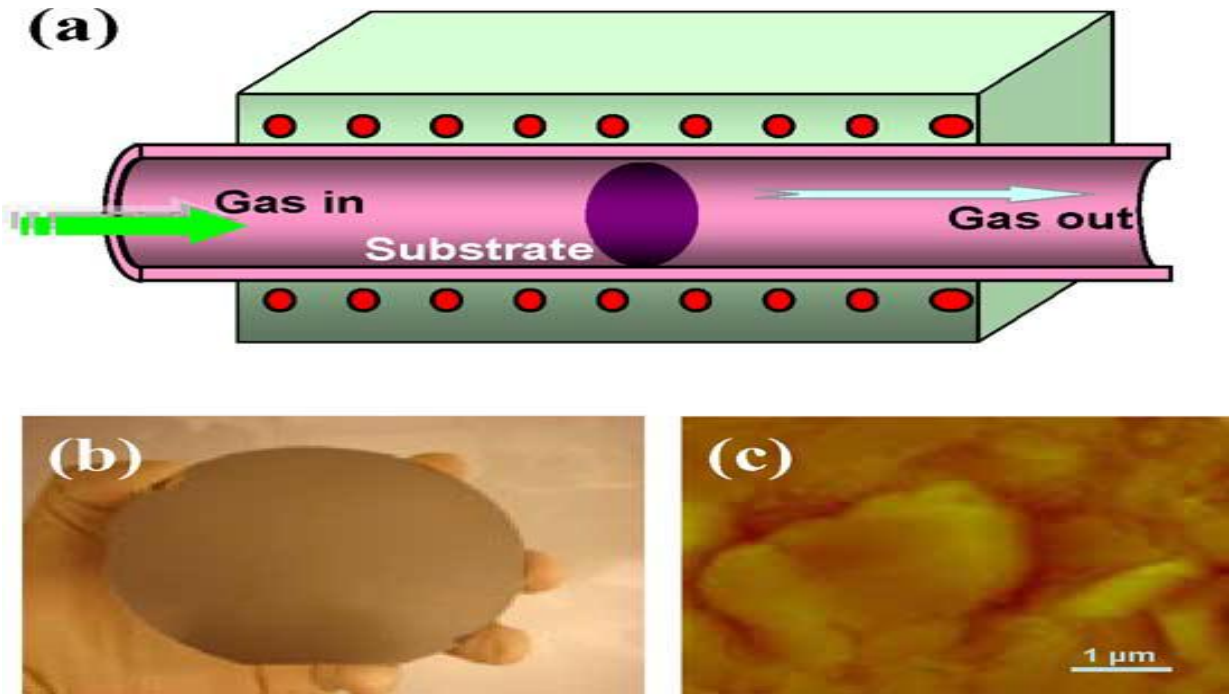

Figure 2.18 [72]: (a) Diagram of full-wafer scale deposition of graphene film on Ni film. (b) Nickel film evaporated on a 4 inch Si/SiO_2 wafer. (c) AFM image of Ni film after the CVD growth of graphene film.

Arco and his colleagues found that polycrystalline Ni domains were shaped due to heating and cooling effects Figure 2.18c [72].

CVD growth of graphene over polycrystalline Ni has been carried out at atmospheric pressure. As a result, continuous graphene film over the entire nickel area has been achieved because the graphene formed bridges across nickel grain boundaries [42, 72].

A study of comparison of graphene growth on single-crystalline and polycrystalline Ni by chemical vapor deposition showed monolayer/ bilayer graphene formation on single crystal Ni (111) due to the absence of grain boundaries. Whereas, multilayer graphene (>3 layers) formation on polycrystalline Ni was due to the existence of grain boundaries which acted as nucleation sites for multilayer growth as illustrated in Figure 2.19 [73].

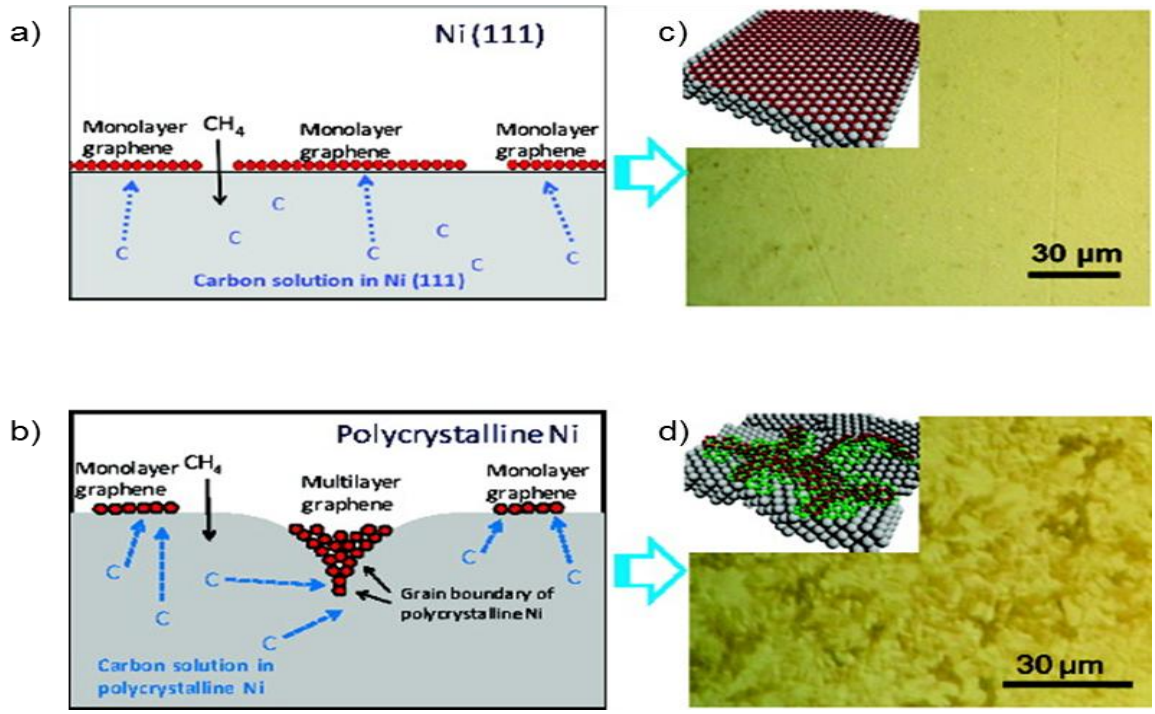

Figure 2.19 [73]: (a) graphene growth mechanism on Ni (111) film. b). graphene growth mechanism on polycrystalline Ni surface. (c) Optical image of a graphene/Ni (111) surface after the CVD process. (d) Optical image of a graphene/polycrystalline Ni surface after the CVD process.

This study by Zhang et al, a single crystal Ni (111) substrate and a polycrystalline Ni film of this 500 nm of Ni deposited on a SiO_2/Si wafer were loaded into a CVD chamber. Then, the CVD chamber was heated to 900 °C under 600 sccm H_2. Next, the substrates were annealed for 15 min under 900 °C at atmospheric pressure. Graphene films growth was conducted using

different methane concentrations; 0.5%, 0.65%, and higher than 12%. Then, the chamber was cooled to 500 °C at a rate of 16 °C /min.

Zhang et al. showed that the area percentages of monolayer/ bilayer graphene were 91.4% for the Ni (111) substrate and 72.8% for the polycrystalline Ni substrate, respectively, under comparable CVD conditions [73].

The correlation between the thickness variations of the graphene film with the grain size of the Ni film has been investigated by Thiele and his colleagues [74]. A 500 nm Ni was coated on SiO_2/Si substrate. Next, the substrate was placed into a quartz tube and ramped up in a CVD furnace to 900–1100 °C. Then, the annealing process was conducted under 200 sccm for H_2 and 800 sccm for Ar atmosphere. After that, the flow rate of H_2 was changed to 1300 sccm and Ar flow was shut down and at the same time 4 sccm CH_4 was introduced for 5 min. Samples were cooled to room temperature under H_2 and Ar.

Thiele and his colleagues reported that the minimization of the internal stress enhances grain growth with (111) orientation in the Ni film and increases the grain size. Also, SiO_2 substrate type, such as thermally grown SiO_2, low stress PECVD-grown SiO_2 and PECVD-grown SiO_2, affect the grain size [74].

A study on the effect of the growth temperature, the gas mixing ratio C_2H_2/H_2, and growth time on the CVD of acetylene/hydrogen, and quenching rate on the CVD of graphene was conducted by Chae et al. Their results showed that high temperature, high hydrogen concentration, and short growth time were important for making high quality few-layer graphene [75].

In a study reported by Chae et al., 0.5 mm Ni foil was first polished by chemical-mechanical polishing (CMP). The substrate was then placed inside a rapid thermal chemical

vapor deposition (RTCVD) chamber and heated up to 1000 °C in 5 min. Then, the annealing process was carried out under 45 sccm of H_2 for 30 min at 1000 °C. Then C_2H_2/H_2 =2/45 were introduced for 5 min at 1000 °C. Finally, the chamber was cooled to 500 °C at a rate of 160 °C/min.

A similar study to the Chae et al. study showed that cooling rate and short growth time played a significant role in reducing graphene thickness to grow single and bilayer graphene films [26].

Pan et al. demonstrated a direct of growth of large-area of graphene on SiO_2 substrate at temperatures ranging from 650 to 1000 °C using sputtered carbon and Ni film with rapid thermal processing as shown in Figure 2.20 [76]. The graphene film is achieved on SiO_2 insulator substrate with the removal of Ni using HCL.

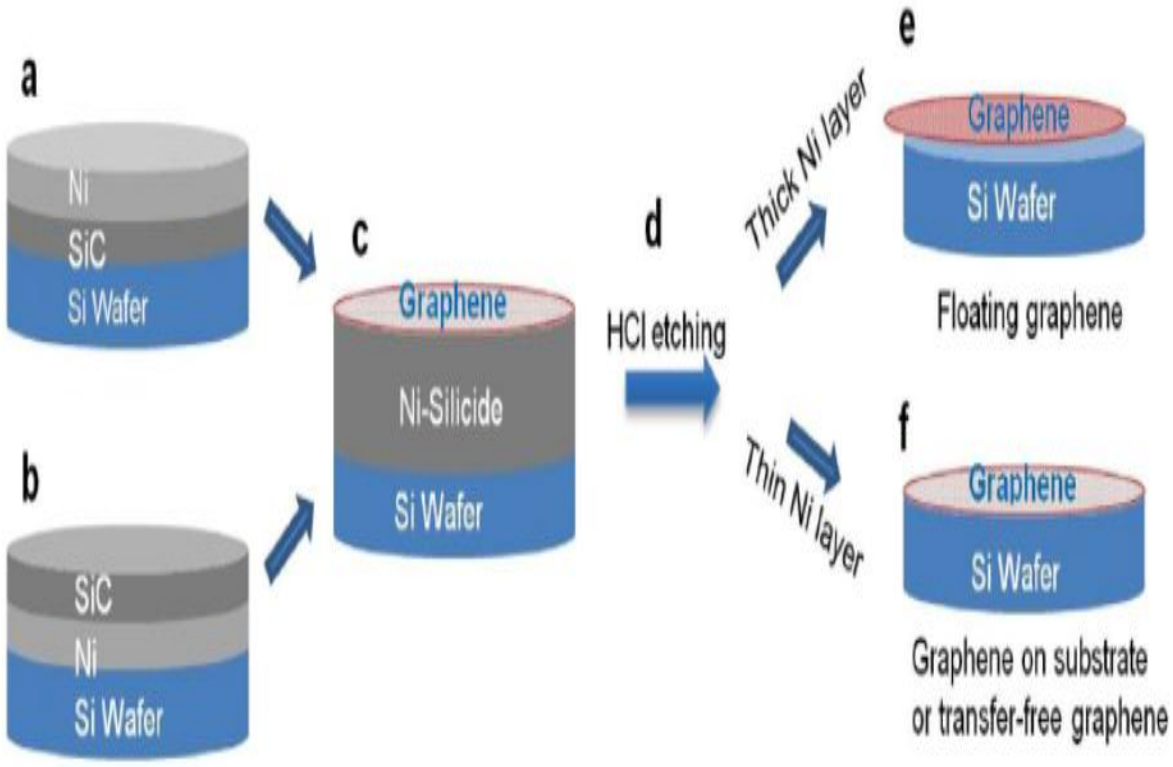

Figure 2.20 [76]: Schematic diagram of the graphene growth process using sputtered carbon and Ni film.

Tour et al. showed direct deposition of large-area and homogeneous bilayer graphene on various insulating substrates (SiO_2, h-BN, Si_3N_4, and Al_2O_3) at 1000 °C utilizing solid carbon sources as shown in Figure 2.21[77].

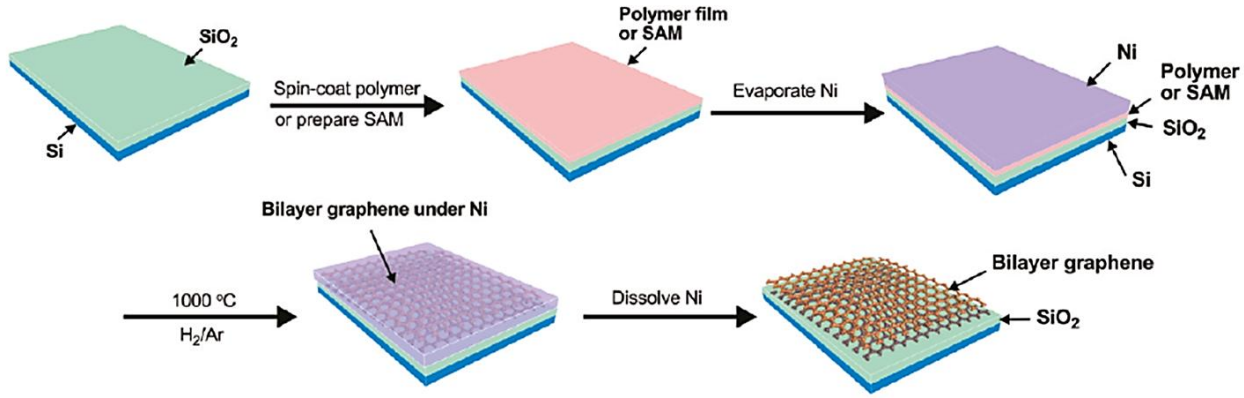

Figure 2.21: Schematic diagram of the graphene growth process using solid carbon sources.

A group at Massachusetts Institute of Technology and University of Michigan demonstrated a direct graphene growth on SiO_2 at ~900 °C using chemical vapor deposition method as presented in Figure 2.22 [78]. Graphene film deposition was followed by removal of the Ni film using an adhesive tape. The achieved patterned graphene film area was 1 cm ×1 cm.

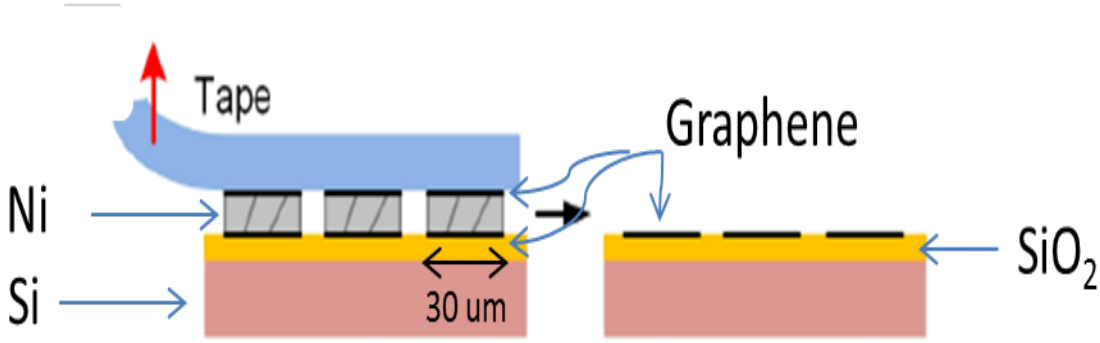

Figure 2.22: Schematic diagram of removal of Ni film leaving the patterned graphene on SiO_2.

Chapter 3: Experimental Methods

3.1. Introduction

This chapter describes the techniques, materials, procedures, and characterization tools utilized in this research. In this study, nickel thin films were deposited on different materials such as silicon, silicon dioxide, silicon nitride, diamond, and diamond-like carbon (DLC) in order to use them as substrates to grow graphene. Prior to Ni deposition, the substrate materials were cleaned with wet chemical cleaning processes. Diamond-like carbon was grown on the silicon samples using plasma- enhanced ultra-high vacuum chemical vapor deposition (PE UHV-CVD). Ni film was deposited on the samples using an e-beam evaporator at room temperature. After the Ni thin film deposition, the samples were annealed under hydrogen in the hot-filament chemical vapor deposition (HF-CVD) chamber. Then, graphene film was grown on Ni film through the surface catalytic pyrolysis of methane. The obtained graphene and diamond-like films were studied using different tools. Scanning Electron Microscopy (SEM) and Atomic force microscopy (AFM) were utilized in order to investigate the surface morphology of the graphene and diamond-like films. In addition, Energy Dispersive X-ray (EDX) spectroscopy was utilized to determine the constituent elements of the samples. Raman spectroscopy was used to characterize graphene and DLC material. In this chapter, a brief description of these analytical tools will be discussed.

3.2. Si Samples preparation

(100) oriented 5 inch silicon wafers were utilized to prepare the silicon substrate. The silicon wafers were cut into 1 inch x 1 inch silicon squares using a dicing saw shown in Figure 3.1 in the assembly lab at Engineering Research Center (ENRC), University of Arkansas.

Figure 3.1 : Micro Automation Model 1100 dicing saw.

3.3. Sample cleaning

Prior to any nano/microfabrication process, contaminants, such as foreign organic materials and metals, existing on the surface of the substrates must be removed due to their negative impact on the performance and high reliability of output nano/micro fabricated products. Thus, prior to graphene and DLC film growth, the samples were carried in a closed container to a class 100 clean room to do a wet chemical cleaning process. The substrates were ultrasonically cleaned with acetone. Then, the substrates were cleaned by methanol. Finally, the substrates were washed by deionized water and dried by N_2 in order to remove any hydrofluoric acid traces.

3.4. Silicon dioxide (SiO_2) sample preparation

A four-stack oxidation/diffusion furnace (Bruce BDF4) consists of four tubes was used; oxidation, boron diffusion, phosphorous diffusion, and hydrogen anneal tube as shown in Figure 3.2. The thermal oxidation processes for cleaned silicon samples were performed in the oxidation tube. After that, the final thickness of the thermal silicon dioxide (SiO_2) was approximately determined using a SiO_2 color chart. The color (i.e. dark violet to red violet) indicated that the final thickness of SiO_2 was approximately 100 nm.

Figure 3.2: Four-stack oxidation/diffusion furnace consisting of a field oxidation, boron diffusion, phosphorous diffusion and hydrogen anneal (Bruce BDF4).

3.5. Silicon nitride (Si_3N_4) sample preparation

Silicon nitride films were grown using Plasma Enhanced Chemical Vapor Deposition (PECVD) (Plasma Therm SLR730) shown in Figure 3.3 and in the University of Arkansas, High Density Electronics Center (HiDEC). The color of Si_3N_4 samples was light green. The color indicated that the thickness of the Si_3N_4 films was roughly 260 nm.

Figure 3.3: Plasma Enhanced Chemical Vapor Deposition (PECVD); Plasma Therm SLR730.

3.6. Ni for film deposition

A 200 nm thick Ni film was grown on the cleaned samples. The nickel film was deposited by an e-beam evaporator on different substrates; Si, Si/SiO_2, Si_3N_4, diamond like carbon, and diamond. As shown in Figure 3.4, the e-beam evaporator consisted mainly of an energy source, a deposition chamber, vacuum pump, permanent magnet, and a cooling system. Electron beam generated by thermionic emission using the electron gun was accelerated under high vacuum by a high voltage potential. The electron beam was directed and steered from the electron gun toward the material to be deposited using a magnetic field. The kinetic energy of the accelerated electrons was converted to thermal energy and used to melt the material such as gold

and copper that was to be deposited on a specific substrate. In order to achieve a uniform heating of the material, an additional electric field was used to sweep the electron beam over the material surface.

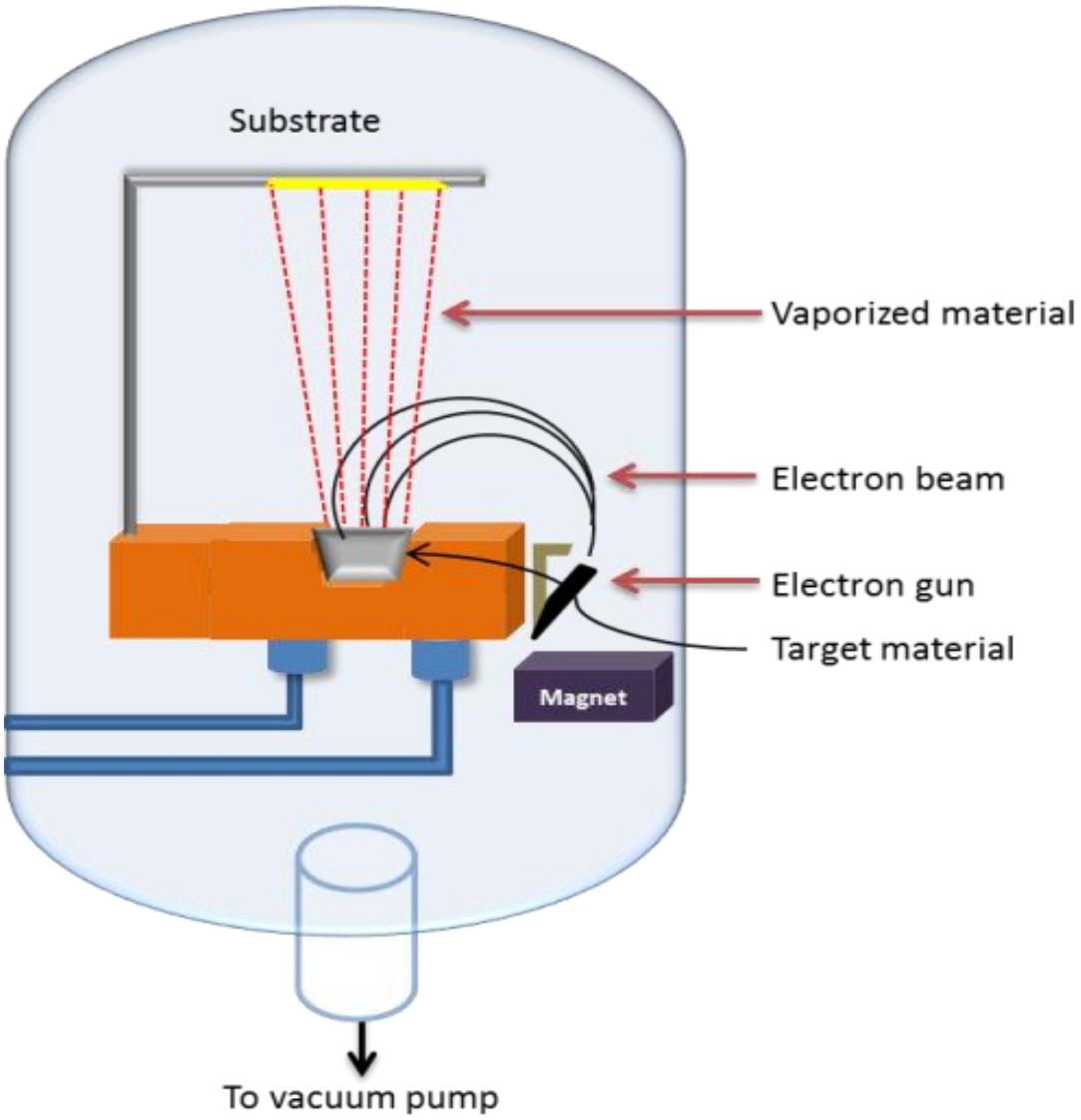

Figure 3.4: The schematic diagram of the electron beam.

3.7. Chemical vapor deposition (CVD) process

Chemical vapor deposition (CVD) is a chemical process used to deposit fully dense thin solid films on different types of substrates such as metals and ceramics. To clarify, these thin

solid films result from the decomposition of gaseous precursor(s) when they hit a heated substrate. Byproducts are produced and they are removed from the reaction chamber by a gas removal system.

In semiconductor fabrication processes, CVD is widely used in various films deposition such as polycrystalline, amorphous, and epitaxial silicon, SiO_2, silicon nitride, carbon nanotubes, diamond, diamond-like carbon, graphene.

Currently, among graphene synthesis methods, chemical vapor deposition (CVD) is considered a promising technique that provides the solution for the difficulties in obtaining a continuous monolayer and multilayer of large-area of graphene. Also, the CVD technique overcomes scalability limitations in graphene production [21].

Chemical vapor deposition (CVD) apparatus consists mainly of four systems as shown in Figure 3.5:

a) Delivery system: this system supplies precursors and carrier gases to a reaction chamber. The amount of required gas flow is delivered and regulated in standard cubic centimeter per minute unit (sccm) using valves and mass flow controllers.

b) Reaction system: chamber within which reactions and deposition on substrate surfaces take place at different temperatures and pressures.

c) Vacuum system: A system is used to remove undesirable byproducts from the reaction chamber.

d) Energy source: energy source such as resistive heating, radiant heating, radio frequency heating, and laser used to provide the required energy for the reaction occurring in the reaction chamber.

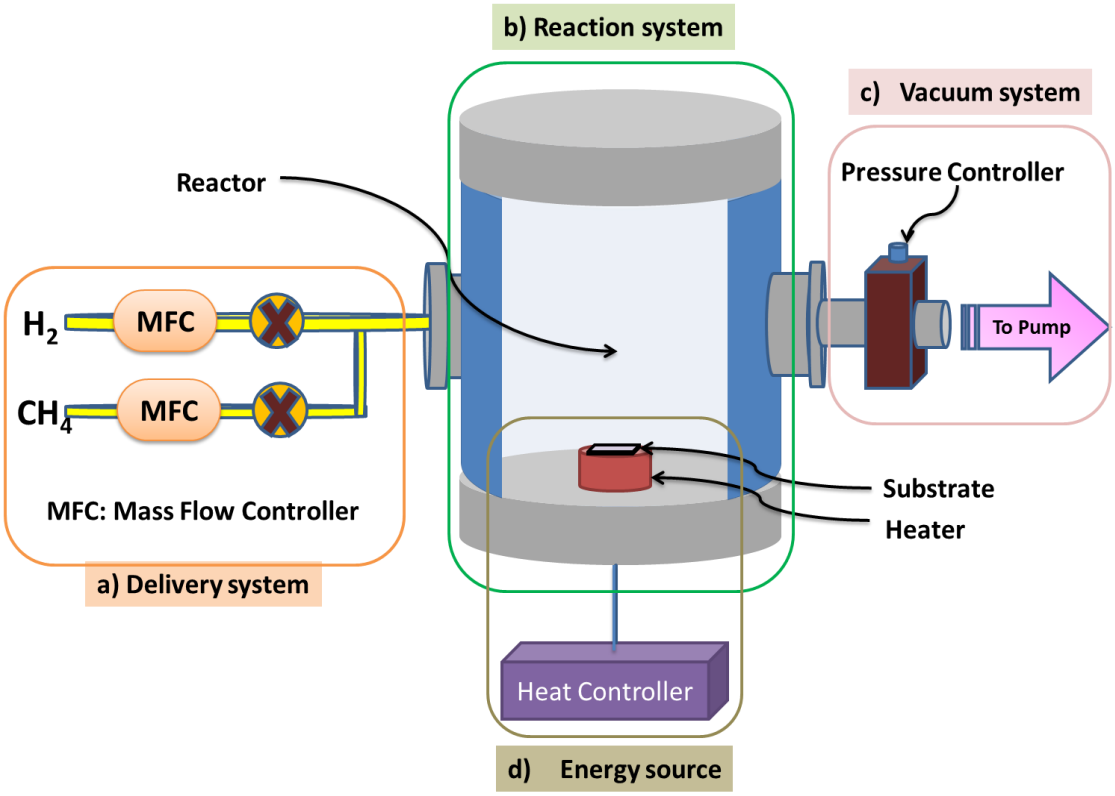

Figure 3.5: Schematic diagram of a typical graphene CVD system.

CVD processes can be classified into various types such as plasma-enhanced CVD (PECVD), atmospheric pressure CVD (APCVD), low-pressure CVD (LPCVD), microwave plasma-assisted CVD (MPCVD), hot filament CVD (HFCVD), and ultra-high vacuum CVD (UHVCVD).

In this research, two types of CVD systems, a unique ultra-high vacuum chemical vapor deposition (UHV-CVD) and the hot-filament chemical vapor deposition (HFCVD), were utilized in thin film fabrication processes.

3.8. Diamond-like carbon synthesis

Diamond like carbon (DLC) films were synthesized utilizing the PE CVD system depicted in Figure 3.6.

Figure 3.6: Photograph of the PE-CVD system at the ENRC, University of Arkansas.

Plasma, the fourth state of matter, is an ionized medium consisting of electrons, ions, and neutral atoms. Plasma consists approximately of equal numbers of positive ions and electrons. Hence, plasmas are influenced by electric and magnetic fields. Plasmas can be classified into two types:

a) Thermal plasma: In this type of plasma, particles (i.e. electrons, ions, and neutrals) are in thermodynamic equilibrium. Normally, flames, sparks, atmospheric arcs are utilized to produce thermal plasmas.

b) Non-thermal plasmas: There is no thermodynamic equilibrium between electrons and the other particles (i.e. ions and neutrals). In general, electrons temperature is higher than the heavier particles temperature. Figure 3.7 illustrates the principle of the plasma enhanced CVD system.

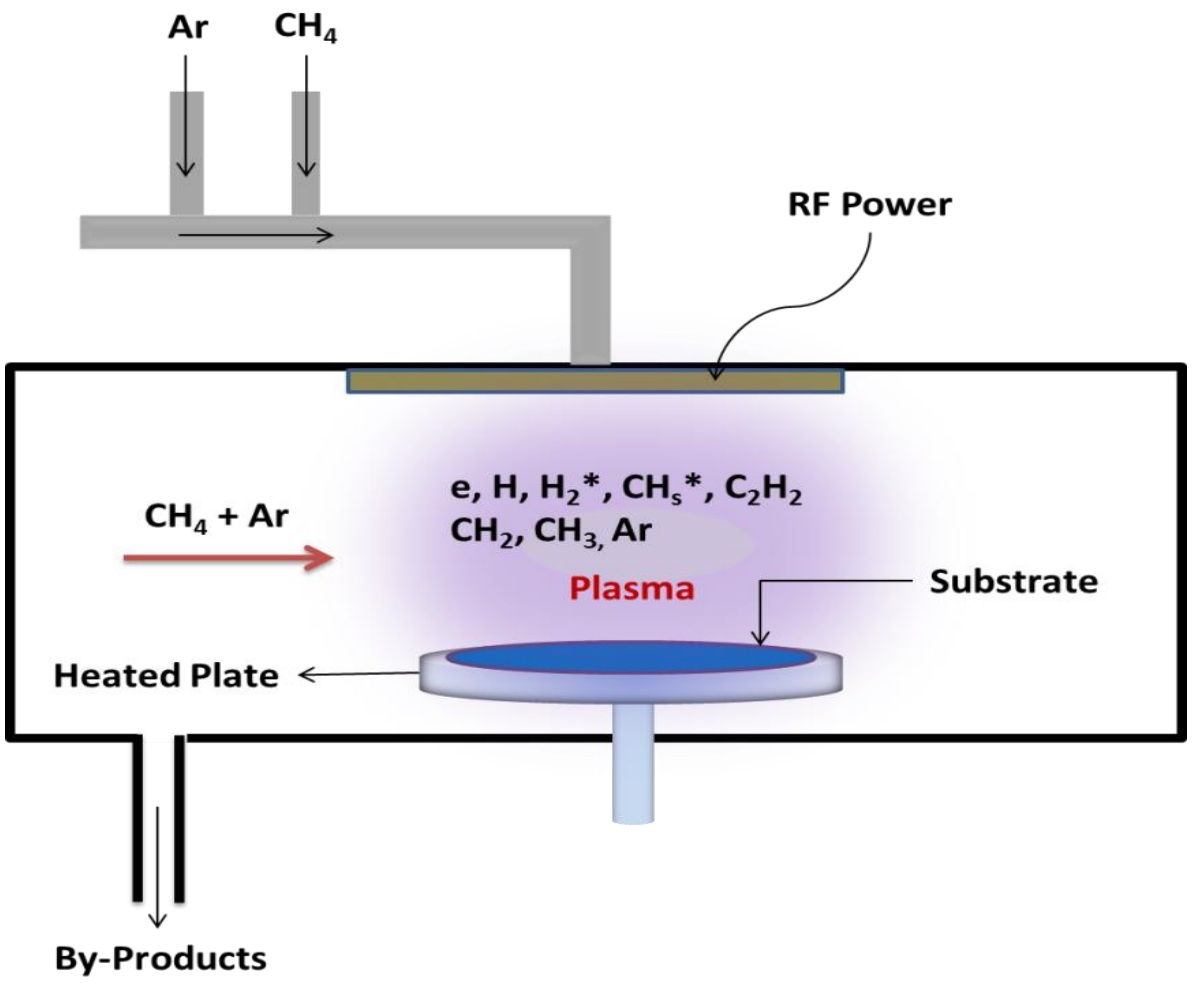

Figure 3.7: Schematic diagram of plasma enhanced CVD system.

Plasma sources can be categorized based on electric field excitation into two types:

1. DC discharges; and,
2. RF and microwave discharges.

Radio frequency (RF) discharge method was used in the DLC film deposition process. Normally, RF discharges operate in frequency range 1-100MHz, with a typical frequency = 13.56 MHz. In order to maximize the power transfer and minimize the reflected power, the power supply is connected with the reactor by an impedance matching network. The high

frequency electromagnetic energy is capacitively coupled or inductively coupled into the process chamber as shown in Figure 3.8 a and 3.8 b respectively.

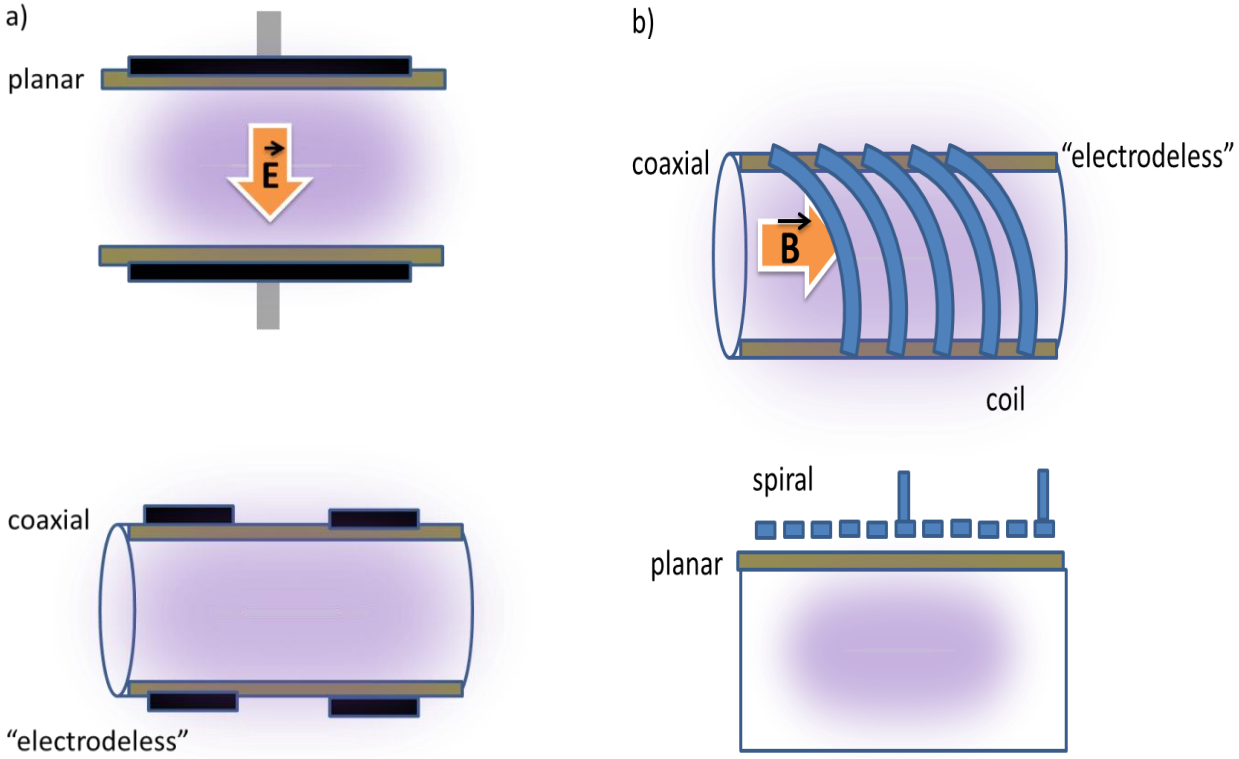

Figure 3.8: The high frequency electromagnetic energy is a) capacitively coupled or b) inductively coupled into the process chamber of the ultra-high vacuum chemical vapor deposition (UHV-CVD) system.

The PE-CVD system shown in Figure 3.6 is a home-built CVD. The home-built CVD was used in DLC films deposition. This system is considered unique for many reasons. The process chamber was cold wall, electro polished stainless steel chamber. The base pressure in the reaction chamber reached below 10^{-10} Torr using a turbo molecular pump and cryogenic pump. The cryogenic pump (<20°K) was utilized to remove water vapor and oxygen. The load lock chamber was pumped down 10^{-8} Torr prior to the growth process. The total internal volume of its reaction chamber was ~ 69.2 liters. Hence, this system had a capability to grow uniform thin

films on 4 inch wafers. Substrate heating temperature could reach up to 1000 °C. So, in situ, rapid thermal annealing could used in order to remove film defects without breaking vacuum. In this system, plasma provided the necessary energy for the chemical reaction of the precursors and allowed deposition at lower temperatures and at a very low pressure.

Methane (CH_4) as a precursor and Ar as carrier gas were used in DLC synthesis at low pressure and room temperature. The influence of CH_4/Ar flow rate ratio and the plasma power on the DLC growth was investigated.

The prepared and cleaned Si samples were mounted into the substrate holder . The samples were then placed into the load lock chamber. Then, the load lock chamber was pumped down to 10^{-3} Torr using a mechanical pump. When the pressure in the load lock chamber reached to 10^{-3} Torr , a turbo pump connected to the load lock chamber was used to depressurize the load chamber to 10^{-8} Torr. When the load chamber pressure reached 10^{-8} Torr, the gate valve, which isolates the load lock chamber from the process chamber, was opened. Then, the Si samples were transferred into the process chamber of the chemical vapor deposition (CVD) system using the linear sample transfer arm. Then, the gate valve was closed. Next, in order to reach the ultimate pressure of 10^{-10} Torr inside the process chamber, a helium cooled cryogenic pump was utilized in addition to the turbo and mechanical pump. The pressure in the system was constantly monitored using pressure gauges. Being in the process chamber, the sample was picked up by sample holder/ heating assembly. The DLC growth was conducted at room temperature utilizing CH_4 as a carbon atom source and Ar as carrier gas. Durng the DLC growth, RF plasma was generated under specific condition. MKS mass flow controllers and pneumatic valves, built in the system, were utilized to control precisely the mass flow rate of the precursor, methane. The outlet gases from the process chamber were exhausted and treated by Edwards Gas Reactor

Column (GRC). At the end of the growth stage, plasma, methane, and Ar sources were shut down and the process chamber was left to cool to room temperature. Then, the gate vlave was opened in order to transfer the samples to the load lock chamber. When the samples reached the load lock chamber, the gate valve was closed to isolate the process chamber. Next, the load chamber was vented with Ar. Finally, the samples were unloaded and kept in a closed container for charactrization.

3.9. Graphene synthesis

A single-chamber CVD system (hot filament activated CVD) shown in Figure 3.9 was used for performing graphene films deposition.

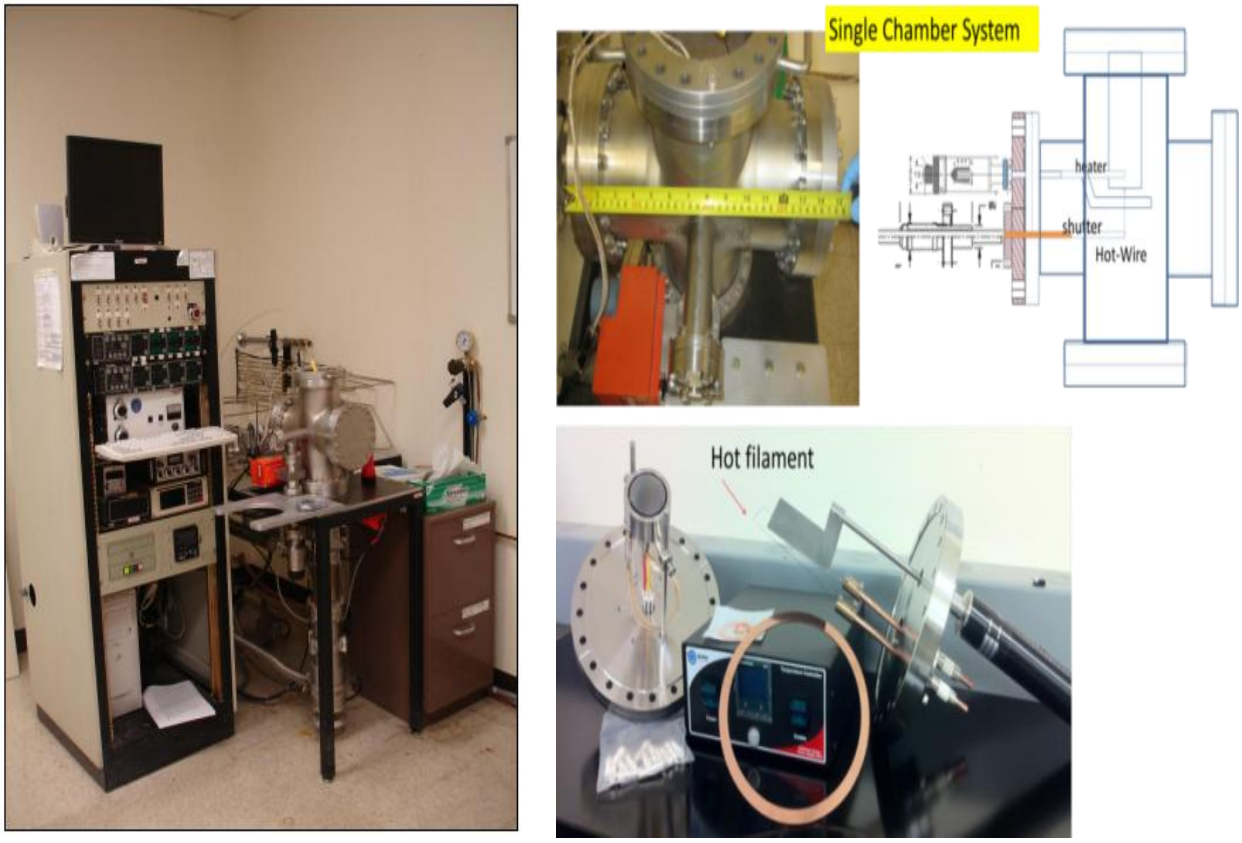

Figure 3.9: The single-chamber CVD system and its mean parts for graphene synthesis.

As illustrated in Figure 3.10, the basic set-up of the single-chamber CVD system consisted of:

a) A single stainless steel chamber.

b) A filament made out of tungsten, which is heated up to 2100 °C by a direct electrical current (dc) source around 16 A.

c) A substrate heater up to 800 °C.

d) A turbo molecular pump and a mechanical pump work together to pump the single-chamber CVD system down to 10^{-8} Torr prior to growth.

e) A delivery unit to deliver precursors and carrier gases to a process chamber. The amount of delivered gases such as hydrogen and methane is regulated by a number of valves and mass flow controllers.

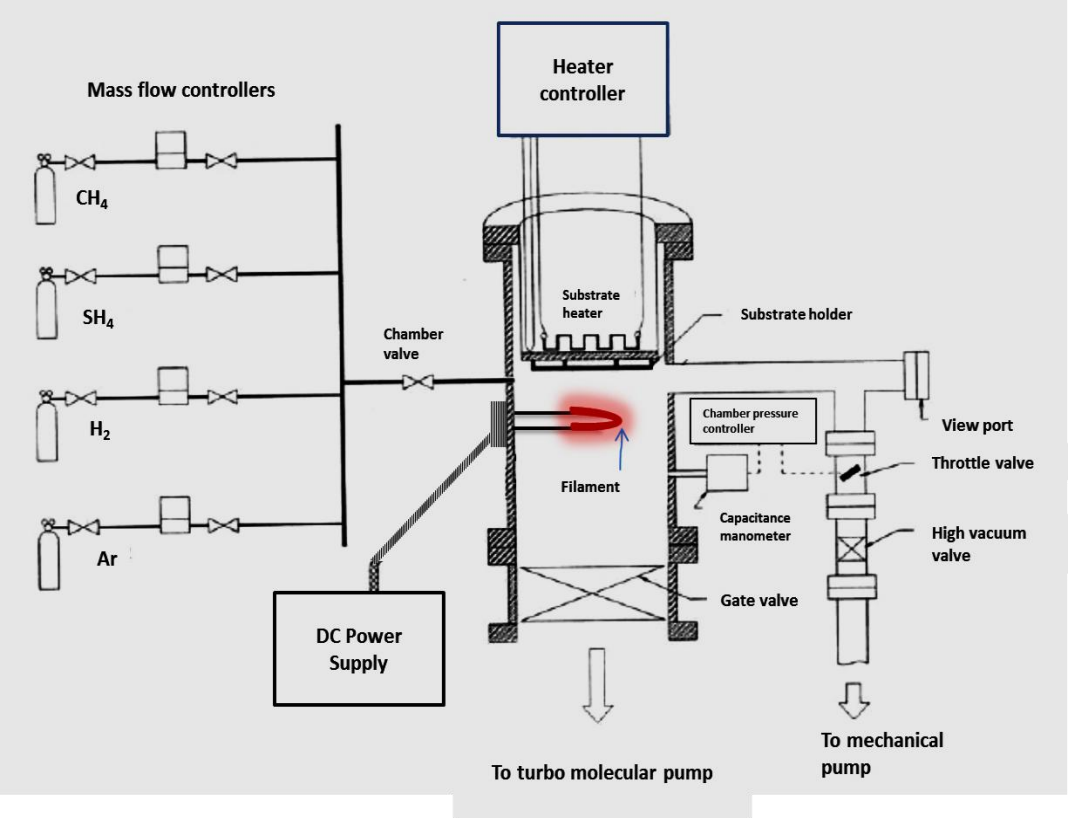

Figure 3.10: A schematic diagram of the hot filament CVD system.

Hot filament CVD (HF-CVD) method was originally developed by Matsumoto et al. in the early 1980s. The hot filament deposition process is the most and earliest method utilized for diamond growth under low pressures. This technique has been utilized extensively to deposit various silicon based and carbon based materials such as silicon thin films, silicon carbide films, carbon nanotubes, diamond like carbon films, and diamond.

The decomposition of precursor gases such as methane and silane is occurred on a heated filament (e.g. tungsten) leading to deposition of a solid film on a desirable substrate. Heat released from the filament is given by Equation 3.1;

$$P_{total}=2\pi.r_{filament}.l_{filament}.\varepsilon_{tungsten}.\sigma.T^4 \qquad \text{Equation 3.1}$$

Where,

P_{total}: The total power.

$r_{filament}$: The filament radius.

$l_{filament}$: The filament length.

$\varepsilon_{tungsten}$: The emissivity factor (generally frequency dependent).

σ: The Stefan–Boltzmann constant.

T: The temperature.

The hot-filament CVD technique has a number of significant benefits over conventional film deposition methods. Hot-filament chemical vapor deposition produces a large area deposition at low temperature. Also, the HF-CVD offers a high gas-decomposition and high deposition rate. In addition, hot-filament chemical vapor deposition relatively cheap and easy to operate compared with conventional CVD methods. There are several variables that have significant impact on the quality of the deposited film using HF-CVD methods such as substrate temperature, filament temperature, total growth pressure, and gases flow rates.

3.9.1. Graphene synthesis on different substrate materials

Hot-filament chemical vapor deposition (HF-CVD) shown in Figure 3.9 was used in order to grow graphene film on different substrate materials such as Si, SiO_2, Si_3N_4, DLC, and diamond. Carbon precursor, methane, (CH_4) and carrier gas, hydrogen (H_2) mixture, with different growth time and growth pressure were utilized in graphene film synthesis.

The graphene film growth process consisted of four steps as shown in Figure 3.11: ramp-up, annealing, growth, and cool down.

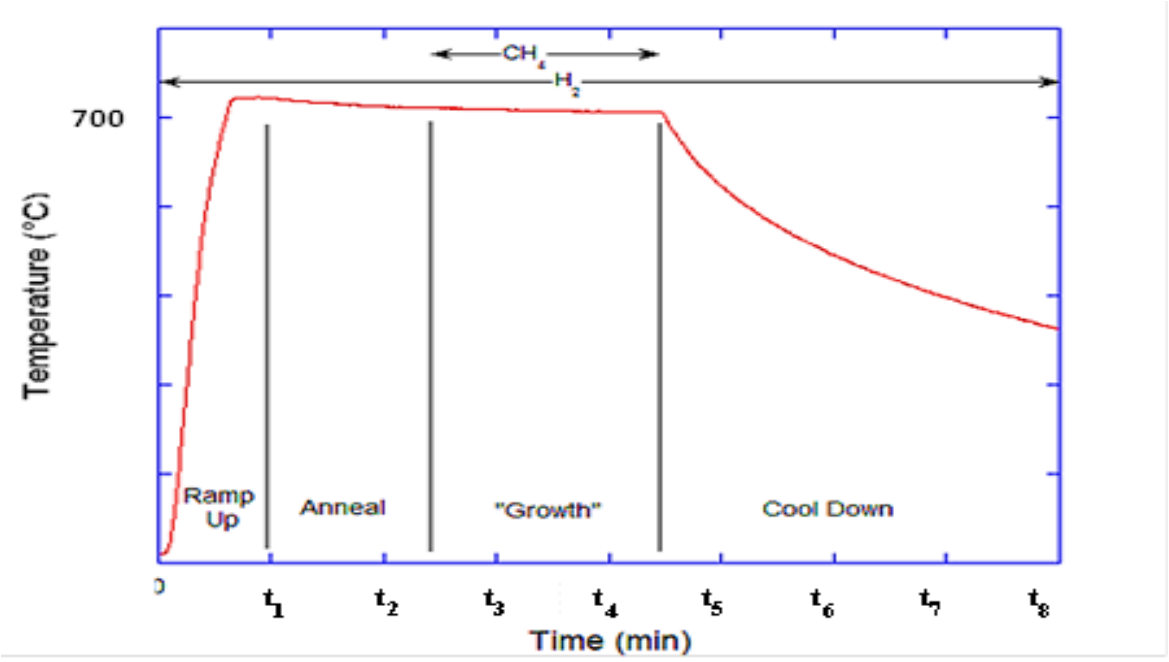

Figure3.11: The graphene film growth process at high temperature consisted of four steps.

The chamber of the hot-filament system was vented and the chamber was opened to load the cleaned samples. Next, the chamber was closed and pumped down to 10^{-3} Torr using a mechanical pump. When the pressure in the chamber reached to 10^{-3} Torr , a turbo pump connected to the chamber reduced the chamber pressure to 10^{-8} Torr. The pressure in the single chamber system was constantly monitored using pressure gauges. In the ramp-up step, the

process chamber was heated to the desired temperature (i.e. 700 °C) in Ar. Then, Ar source was closed while H_2 was introduced into the chamber. At the required temperature (i.e. 700 °C), the annealing stage (20 min- 30 min) was started.

The growth step was then started by introducing the precursor gas, CH_4 . The outlet product from the process chamber was exhausted and treated by a Gas Reactor Column (GRC). At the end of the growth step, methane and hydrogen flow sources were closed and an Ar source was simultaneously opened. Then, the process chamber was cooled to room temerature allowing carbon precipitates to form graphene on the top and bottom of the Ni surface. Finally, the sample was unloaded at room temperature and kept in labeled boxes for charactrization.

3.9.2. Effect of growth temperature on graphene synthesis using 200 nm nickel film-coated SiO_2/Si substrates

In order to investigate the effect of growth temperature on graphene synthesis, the hot filament chemical vapor system was used to synthesize large-area graphene film on 200 nm nickel film-coated SiO_2/Si substrates. The sample was loaded in the HF-CVD system. Then, the chamber was pumped down to $5.5x10^{-9}$ torr. Graphene films were synthesized at various substrate temperatures. Namely, the nickel substrates were heated to different temperature, 600, 650, 700, and 750 °C and maintained for 10 min in H_2 ambient at 0.5 torr. Next, H_2 was introduced into the deposition chamber with a flow rate of 5 sccm for 20 min. Then, a hydrocarbon gas, CH_4, with a flow rate of 10 sccm was introduced into the deposition chamber with a total pressure 1.5 torr. The process was held until the total growth pressure was stabilized. Then the power supply of hot filament was switched on for 10 min. After the deposition, the sample was cooled in Ar (150 sccm) to room temperature. The graphene films were deposited at a constant filament temperature of 2100 °C.

3.9.3. Effect of CH_4/H_2 ratio on graphene synthesis using 200 nm nickel film-coated SiO_2/Si substrates

200 nm nickel film-coated SiO_2/Si substrates were used to study the effect of CH_4/H_2 ratio on graphene synthesis. Graphene film was synthesized utilizing the HF-CVD system. The graphene films were fabricated using different CH_4/H_2 ratios; two, three, and five. The graphene film processes were performed under 1.5 torr at 700 °C for 10 min.

3.9.4. Effect of growth pressure on graphene synthesis using 200 nm nickel film-coated/Si_3N_4 substrates

In this study, the growth pressure effect on graphene synthesis on 200 nm nickel film-coated/Si_3N_4 substrates was investigated. Graphene films were grown at 700 °C using CH_4/ H_2 flow rate ratio of 15/5 sccm for 5 min with different pressure; 0.3, 0.5, and 1 torr.

3.9.5. Effect of growth temperature on graphene synthesis using 200 nm nickel film-coated/Si_3N_4 substrates

The effect of the temperature on graphene film grown on 200 nm nickel film-coated/Si_3N_4 substrates was examined. Graphene films were fabricated at different temperatures; 650, 700, and 720 °C. The other CVD parameters were kept constant. To explain, graphene films were grown at 1.8 torr using CH_4/ H_2 flow rate ratio 15/5 sccm for 5 min.

3.9.6. Graphene etching by atomic hydrogen

In order to etch graphene formed on the top surface on Ni films, many experiments were conducted using different recipes. Atomic hydrogen produced by hot filament CVD was used to etch graphene film grown on the top surface of Ni films. Five min was enough to completely etch graphene film at 500 °C with H_2 flow rate equals 5 sccm.

Graphene film synthesis at the top surface of thin Ni film by applying different effects such as temperature, pressure, and CH_4/ H_2 flow rate ratios was examined. The next step was checking graphene film deposition at the interface between Ni thin film and Si-based material.

3.10. Graphene direct deposition on Si-based substrate

The Ni thin film was removed by ferric chloride ($FeCl_3$) in order to examine graphene film formation at the interface between the Ni film and Si-based material. First, a photolithography process was used in order to pattern a frame to hold the graphene film that existed underneath the Ni film. Then, $FeCl_3$ was applied to etch away the Ni film as illustrated in Figure 3.12.

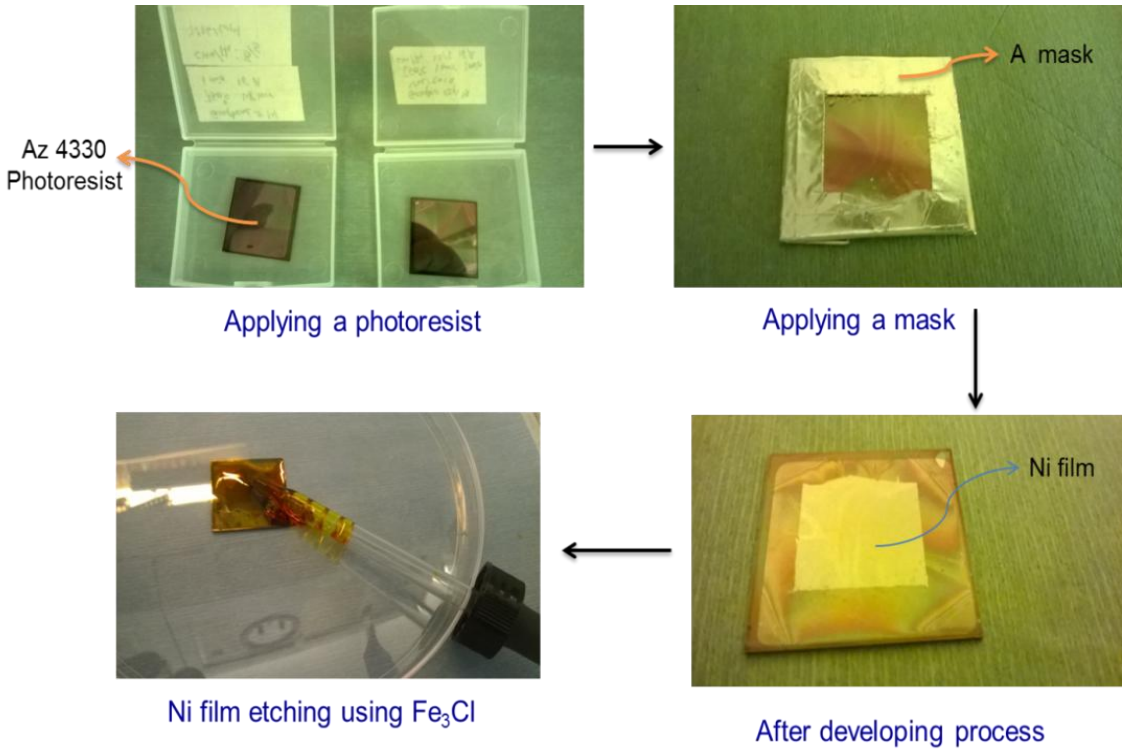

Figure 3.12: The process for removal of Ni thin film using Ferric chloride ($FeCl_3$).

Next, Raman spectroscopy was used to examine graphene formation under the removed Ni thin film.

3.11. Characterization Tools

3.12.1. Atomic force microscope (AFM)

In optical microscope or in scanning electron microscope, one can only see a 2D projection of a 3D system. So, there is no clear idea about the height of the feature, which is considered so important in nano-scale. However, atomic force scope (AFM) enables researchers to obtain a magnified 3D image with high resolution. Atomic force microscope (AFM) is considered one of the most important tools used to perform measurement of material properties such as topology, adhesion, stiffness, and friction of the studied material surface.

Atomic force microscope works on the principle of interaction forces between molecules or particles or surfaces. In reality, the interaction forces between the surface of the studied sample and a sharp tip surface can be described by the Lennard-Jones model as illustrated in Figure 3.13 [79].

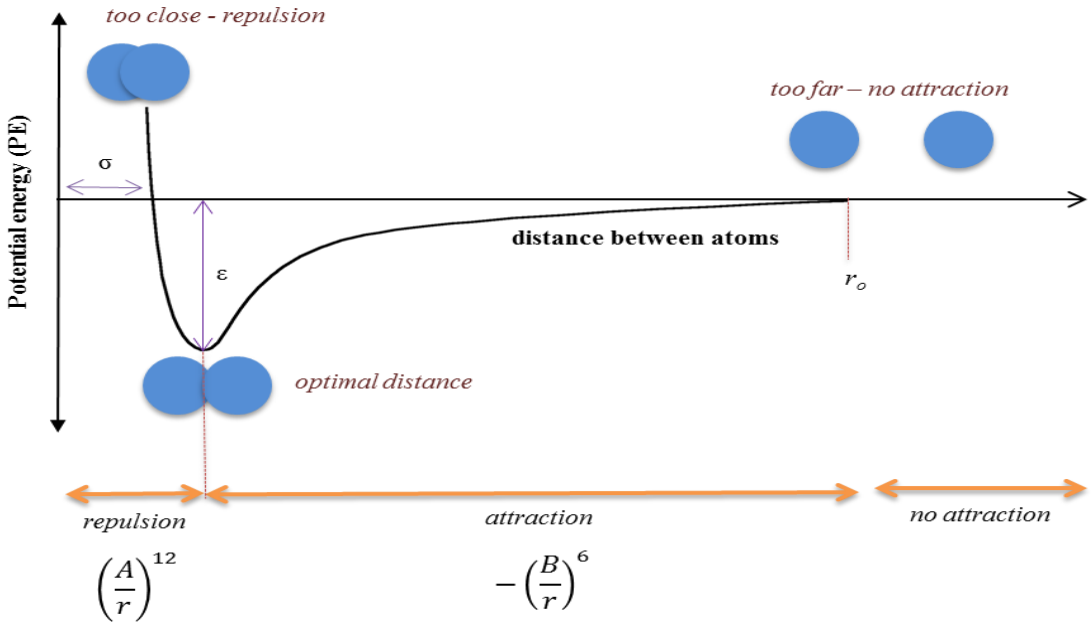

Figure 3.13: The Lennard-Jones model.

The Lennard-Jones potential is given by Equation 3.2:

$$V(r)=4\epsilon\left[\left(\frac{\sigma}{r}\right)^{12}-\left(\frac{\sigma}{r}\right)^{6}\right] \qquad \text{Equation 3.2}$$

Where,

$V(r)$: The potential energy between the two atoms or molecules.

ϵ: The well depth; a measure of how strongly the two atoms attract each other.

σ: The distance at which the potential energy between the two particles is zero.

r: Separation distance between the centers of one atom to the center of the other atom.

It is obvious from the equation that the potential energy equals zero for large separation distance, $r > r_o$. To explain both terms, attraction and repulsion force equals zero. For intermediate distance, $\left(\frac{\sigma}{r}\right)^{6} \gg \left(\frac{\sigma}{r}\right)^{12}$. This means that attraction force dominates at that distance. However, to further decrease in the distance between the two objectives (i.e. small *r*) leads to a repulsive force which dominates.

As shown in Figure 3.14, Atomic force microscope (AFM) consists mainly of:

- A tip which is considered the most important hardware part of the Atomic force microscope. Actually, the tip is utilized to physically touch the studied surface. In fact, the obtained resolution of the examined feature depends on tip size and geometry. Normally, in contact operation mode, tips are made of silicon nitride while for tapping mode, tips are mostly made of silicon.
- A cantilever used for mounting the tips. The length of the cantilever is roughly on the order of 100 to 200 um. A good cantilever has a low spring constant and the resonant frequency higher than instrument's data acquisition rate.

- A photo detector which is utilized to track the deflection of the cantilever. It is a position sensitive diode which generates a voltage when light with certain wavelength shines on it. The generated voltage is a function of the position at which the light falls.
- A laser source which reflects back from the shining area located on the backside of the cantilever
- A piezoelectric scanner for mounting the cantilever and demonstrating the change of stress as a change of generated voltage.
- A feedback control system is used to adjust and maintain the constant deflection.

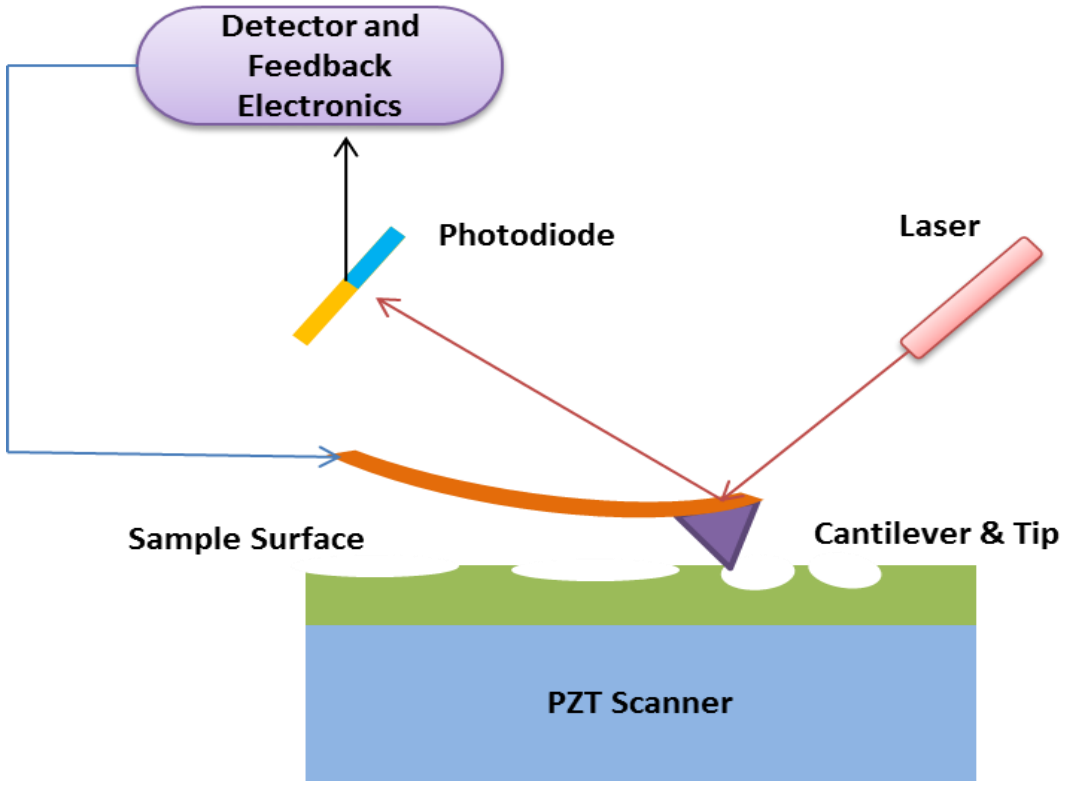

Figure 3.14: Schematic drawing of the Atomic Force Microscope (AFM).

Atomic force microscope utilizes the raster scanning method to image the surface of the sample. AFM works based on the beam bounce method for detecting the deflection of the

cantilever. The operating principle of AFM can be classified to contact and tapping mode as depicted in Figure 3.15. In contact mode, the tip, which is mounted on the cantilever surface, is in touch with the sample surface. Normally, this operation mode is utilized for investigating hard surfaces. For studying sticky and soft surfaces such as polymers, contact mode is preferred to image those surfaces.

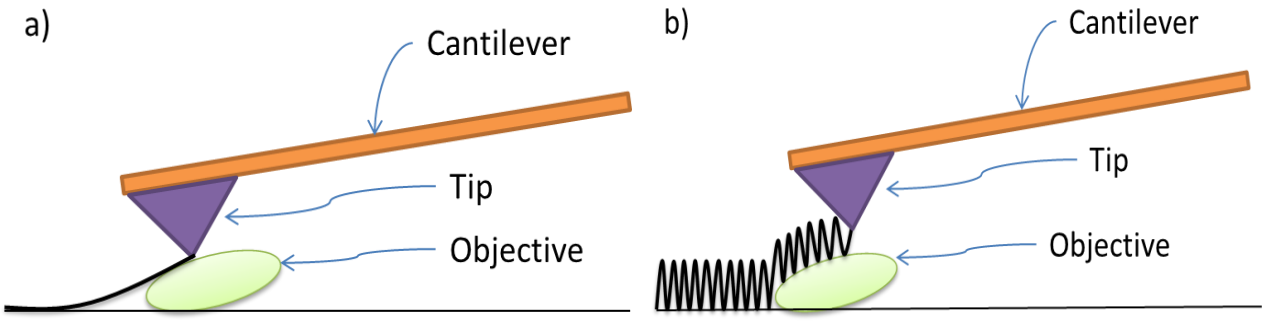

Figure 3.15: Atomic force scope (AFM) imaging modes: a) contact mode b) tapping or non-contact mode.

3.12.2. Raman spectroscopy

Raman spectroscopy is one of the most popular and powerful non-destructive technique utilized to identify and characterize the materials and their structural properties. Raman phenomenon effect was discovered in 1928 by C.V. Raman. Raman effect is based on the fact that when a monochromatic light with frequency $\boldsymbol{\nu}$o encounters a molecule, most of the light scatters with the same frequency of the incident light due to elastic scattering (i.e. Rayleigh scattering). However, a very small portion of incident photons are inelastically scattered with energy lower or higher than the incident energy. This shift of energy (i.e. h $\boldsymbol{\nu}$) is equal to the vibrational energy of molecules as illustrated in Figure 3.16. To explain, the shift energy; h$\boldsymbol{\nu}$ is related to the material properties.

At room temperature, most molecules are in the ground vibrational states. When the light interacts with these molecules, the molecules are excited and their energy jumps from the ground vibrational state to a virtual state for very short time. Then, the molecules relax by emitting light with lower energy (i.e. h $\boldsymbol{\nu}$o- h$\boldsymbol{\nu}$) called Stokes shift. However, a few of the molecules are naturally excited in a vibrational excited state. So, these molecules gain energy when they interact with the incident photons. Hence, they are excited to a virtual energy level. Then, they relax to the ground state by radiating photons with higher energy (i.e. h $\boldsymbol{\nu}$o+ h$\boldsymbol{\nu}$) called anti-Stokes shift.

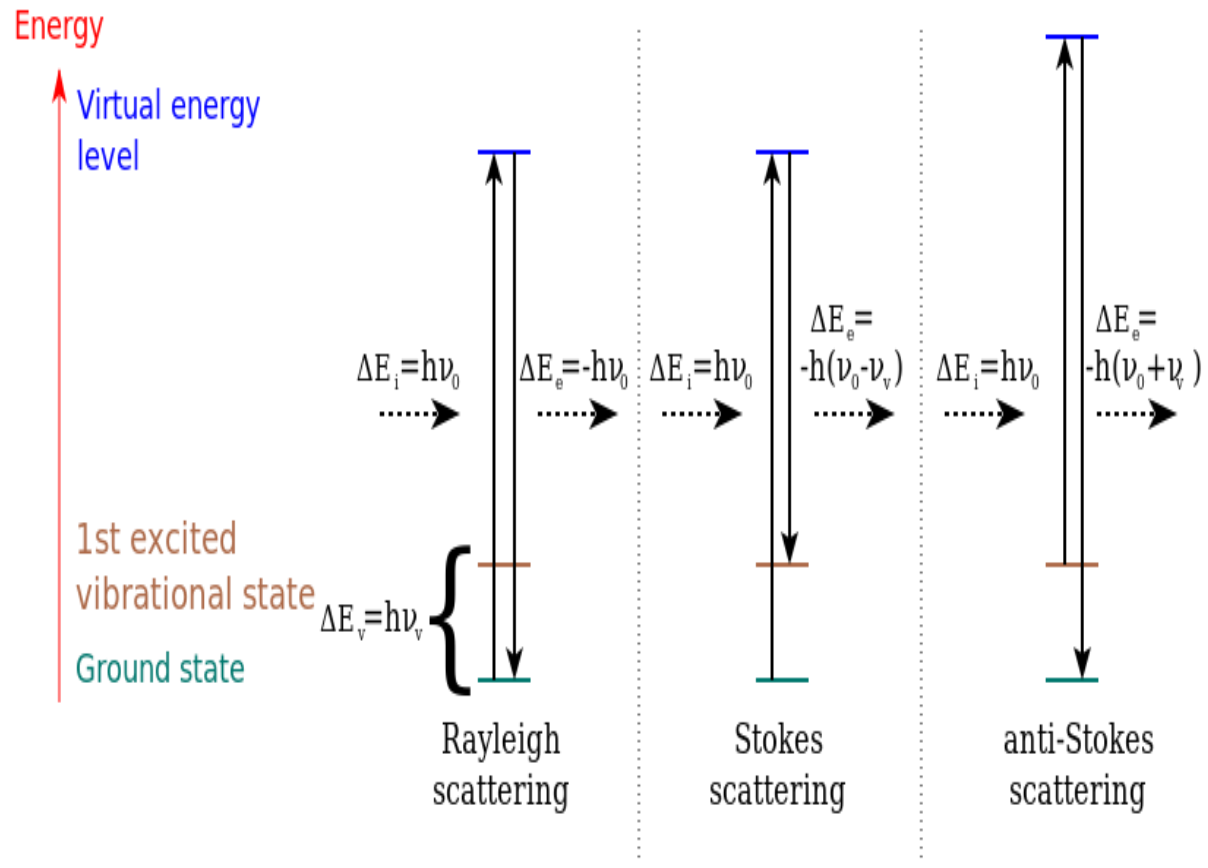

Figure 3.16: The different possibilities of light scattering.

As depicted in Figure 3.17, Raman spectrometer consists basically of many devices and tools such as:

- A pulsed or continuous monochromatic light source with a wavelength in the UV, visible or near IR wavelengths is used as excitation source. Usually, this light source is powerful laser.
- Laser line specific Rayleigh filters used to prevent Rayleigh scattering from entering the detector.
- High quality optical set such as lenses, mirrors, or optical fibers utilized to direct and collect the light.
- A dispersing device (grating or prism) coupled with a charge-coupled device CCD.

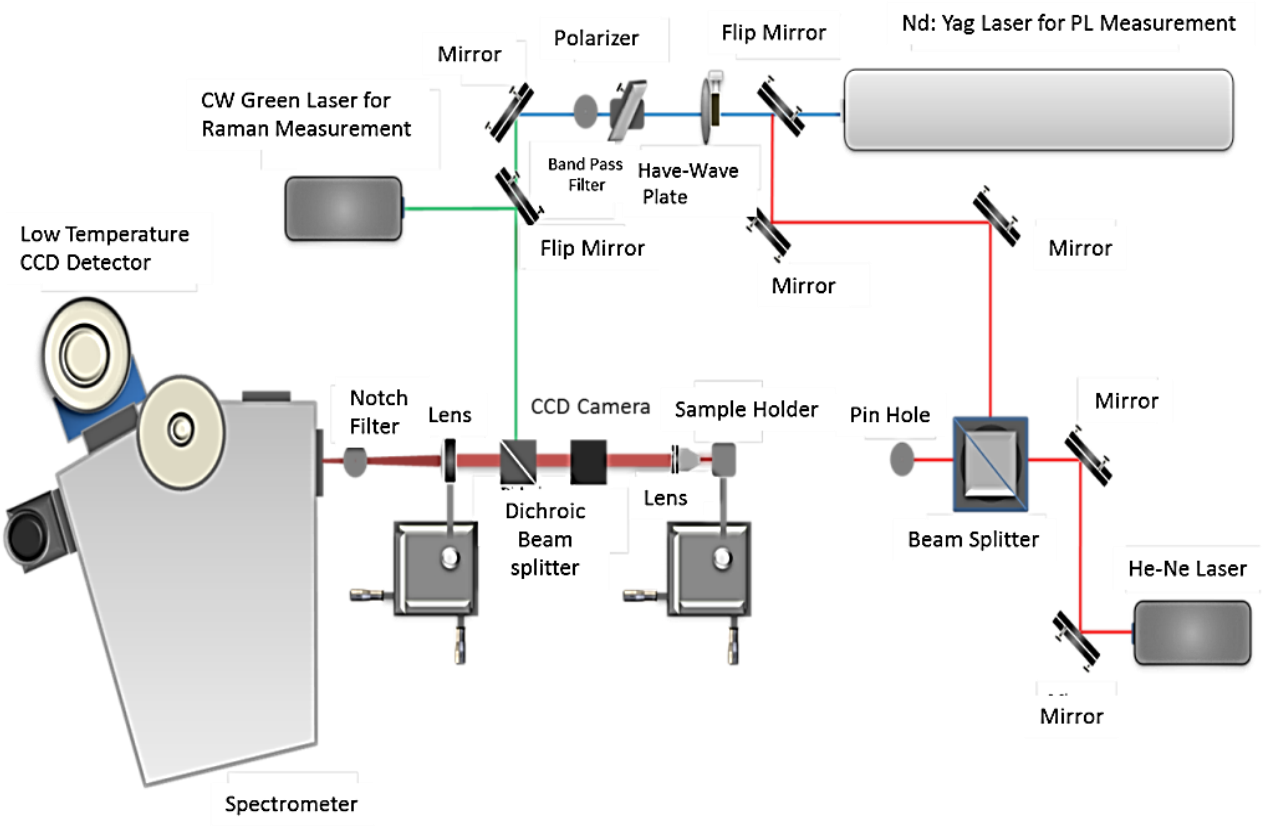

Figure 3.17: Schematic diagram of the Raman and PL spectroscopy system.

3.12.3. The scanning electron microscope (SEM)

A Scanning Electron Microscope (SEM) was used to study morphology of the graphene films fabricated in this research. Scanning electron microscope was used to image the surface of studied sample by scanning the surface utilizing a high energy beam of electronics. As illustrated in Figure 3.18, a scanning electron microscope (SEM) consists in general of:

- An electron gun: A v-shape tungsten wire, thermionic cathode is used to generate an electron beam by heating the tungsten wire utilizing electric current.
- Anode: A hollow metallic disk utilized to accelerate the generated electrons called primary electrons downwards.
- Electromagnetic lens: Used to focus the electron beam on the specimen surface.
- Raster scan generator: Utilized to direct and raster the electron beam over the specimen surface.
- Secondary electrons detector (SE): Utilized to detect and record the knocked out electrons, called secondary electrons, from the specimen surface.
- Positively biased grid: Placed in front of the secondary electron detector in order to increase the number of detected secondary electrons.
- Computer with a monitor: Used to compute the input signals and display them as magnified image.

The electron beam produced by the electron gun is directed by electromagnetic lens and electromagnet deflection toward the sample surface. Once the focused electron beam of high-energy electros hits the sample surface, different types of signals are produced such as secondary electrons (SE), back-scattered electrons (BSE), light (cathode luminescence) (CL), and characteristic X-rays.

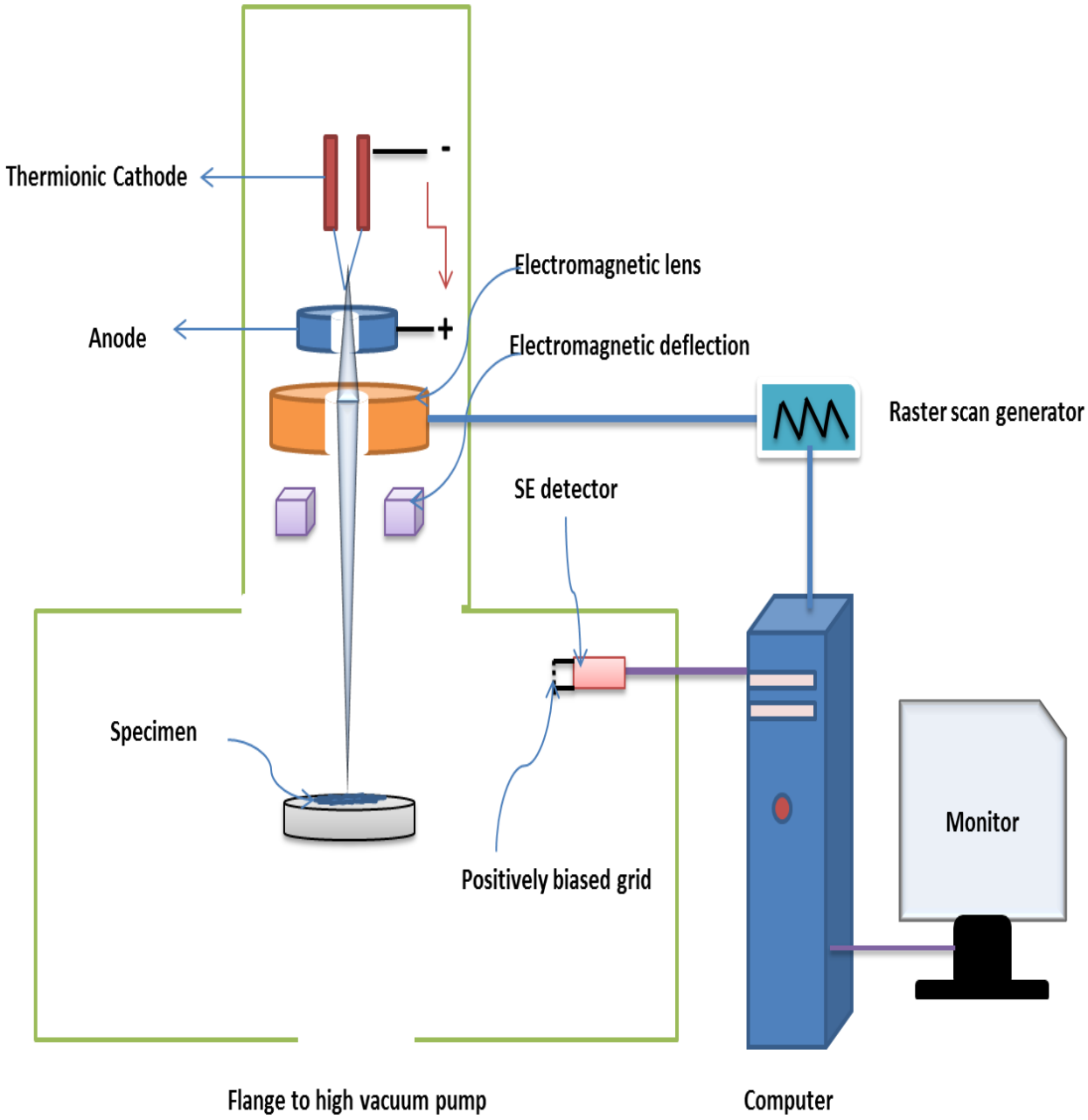

Figure 3.18: Lay-out of the scanning electron microscope.

For each type of signal, there is a specific detector used in order to collect the signal then convert it to a 2D image. These signals give significant information about the sample such as topography, chemical composition, crystalline structure, and electronic structure.

Secondary electrons (SE) are considered the most valuable signal used to obtain an image of the specimen surface. Back-scattered electrons (BSE) technique is used to study an elements distribution and chemical homogeneity of the specimen. Light cathode luminescence (CL) is utilized to study and characterize structure defects and impurities in the sample.

3.12.4. Energy dispersive X-ray spectroscopy (EDX, EDS, or XEDS)

Energy Dispersive X-ray analysis (EDX) is a non-destructive and in situ analytical technique utilized to detect and identify the composition of elements in the studied sample. EDX systems can be connected with several characterization techniques such as Scanning Electron Microscopy (SEM), Scanning Transmission Electron Microscopy (STEM), and Transmission Electron Microscopy (TEM). The impact of the primary electrons on the specimen produces x-rays that carry information about the elements present on the sample. The obtained data from Energy Dispersive X-ray analysis is displayed as peaks corresponding to the elements existing in the sample being examined.

Once the electron beam knocks electrons out of the examined material, holes are generated because the secondary electrons leave their positions in the electron shells they used to occupy. The atoms of the examined sample will be excited if the created holes are in the inner shells. So, electrons from outer shells will drop into the generated holes located in these inner shells resulting in energy in the form of X-rays as illustrated in Figure 3.19. Then, the produced X-ray can be measured by an energy-dispersive spectrometer.

Since the X-rays released from the atoms sample are characteristic of the difference in energy between the two shells to the element of the parent atom, this helps researchers in identifying and determining the elemental composition of the specimen.

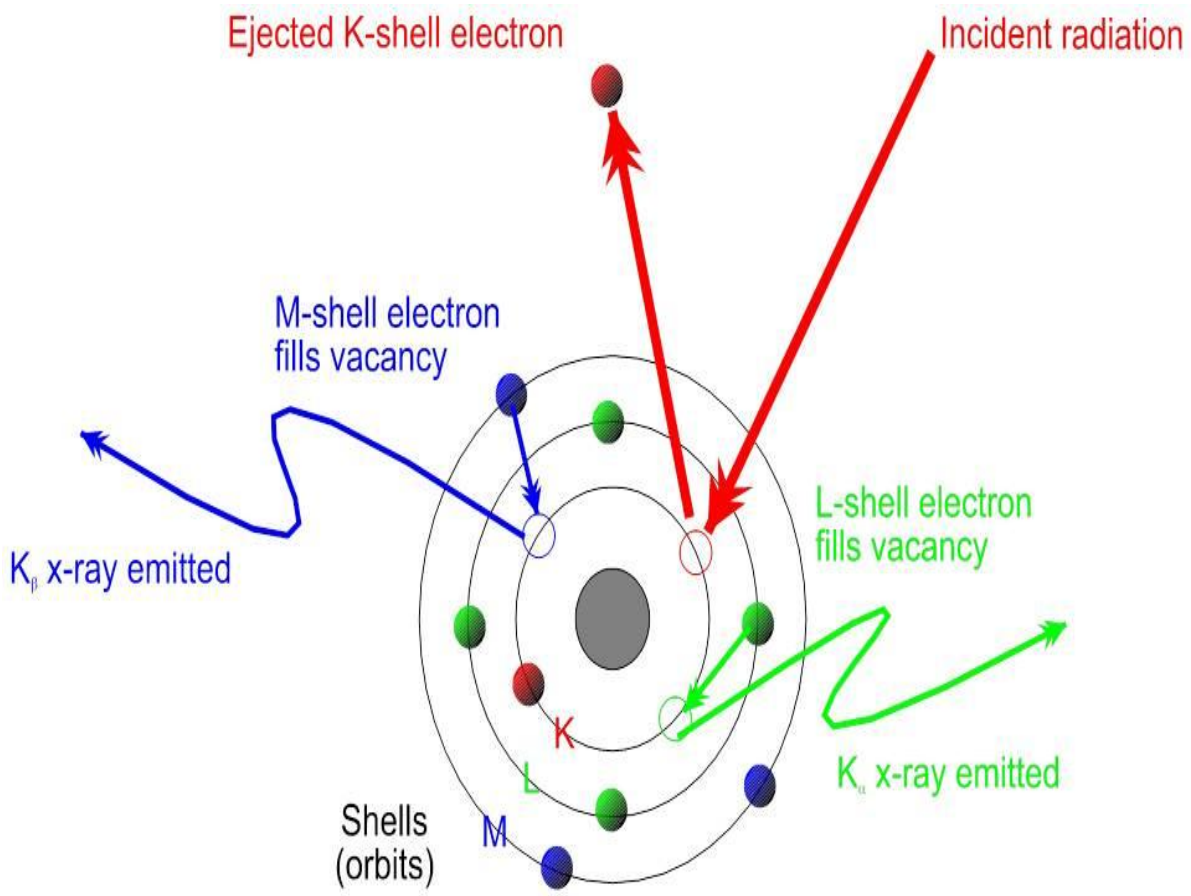

Figure 3.19: Operational principle of Energy dispersive X-ray spectroscopy (EDX).

3.12.5. Ellipsometry

Ellipsometry is a non-destructive and non-contact measurement technique utilized to measure film thickness and optical constant. Also, ellipsometry could be used to characterize material properties related with a variation in optical response such composition, crystallinity, surface roughness, and doping concentration. An ellipsometry apparatus consists primarily of a light source, polarizer, polarization analyzer, and photodetector. The principle of operation of the ellipsometry depends on measuring the polarization change and the phase difference when light reflects or transmits from a material structure as shown in Figure 3.20.

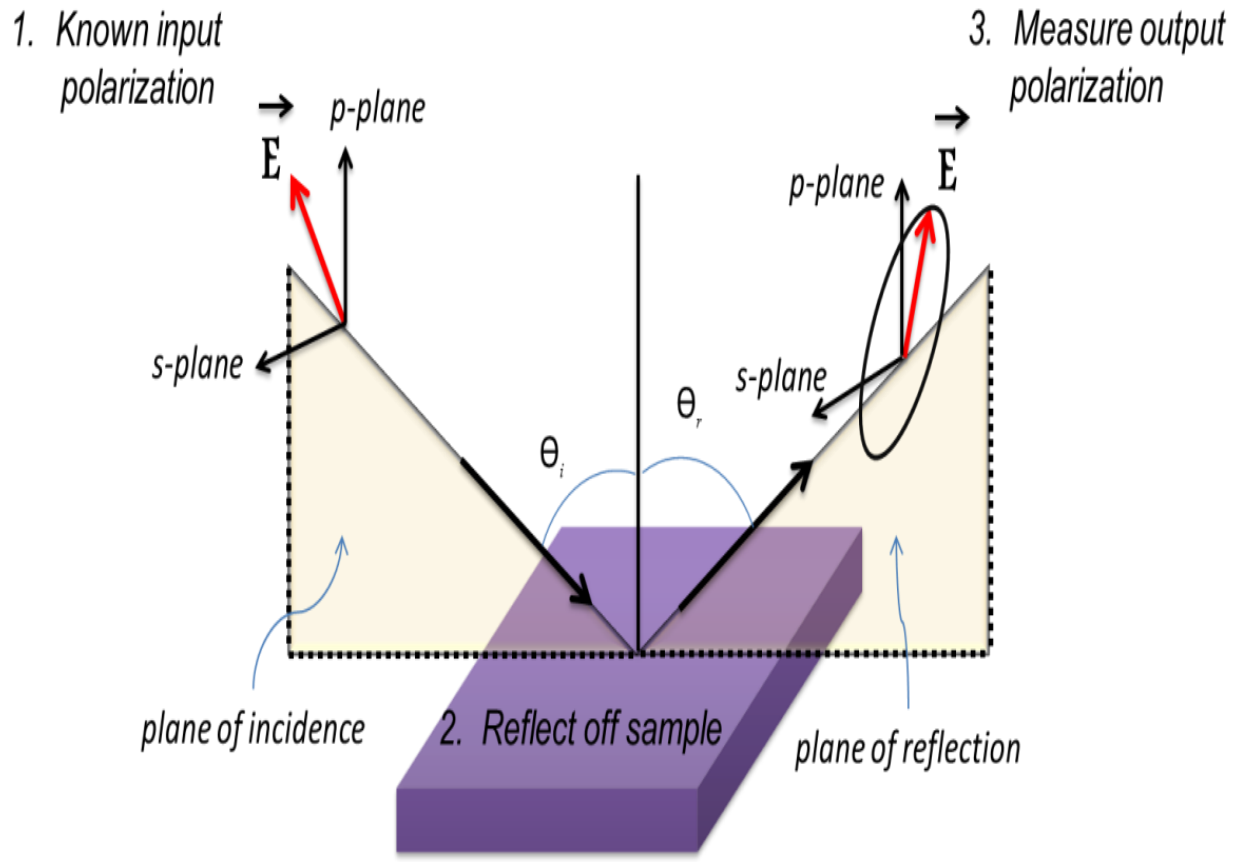

Figure 3.20: Typical ellipsometry configuration, a linearly polarized light reflects from the sample surface and the polarization change is measured to determine the sample thickness.

When a linearly polarized light reflects from the sample surface, it becomes elliptically polarized .The polarization change is measured and the film thickness film and optical properties are determined based on the given information such as input polarization, output polarization, refractive of index, incident angle, and reflected angle.

3.13. COMSOL Simulation

COMSOL Multiphysics software uses the Finite Element Method and computational meshing in solving various coupling physics and engineering problems [80].

COMSOL Multiphysics was applied to explain the growth mechanism of graphene on Ni thin film. To clarify, COMSOL simulation was performed in order to describe and explain the graphene growth mechanism using Ni film. Figure 3.21 illustrates the main simulation steps conducted using COMSOL Multiphysics.

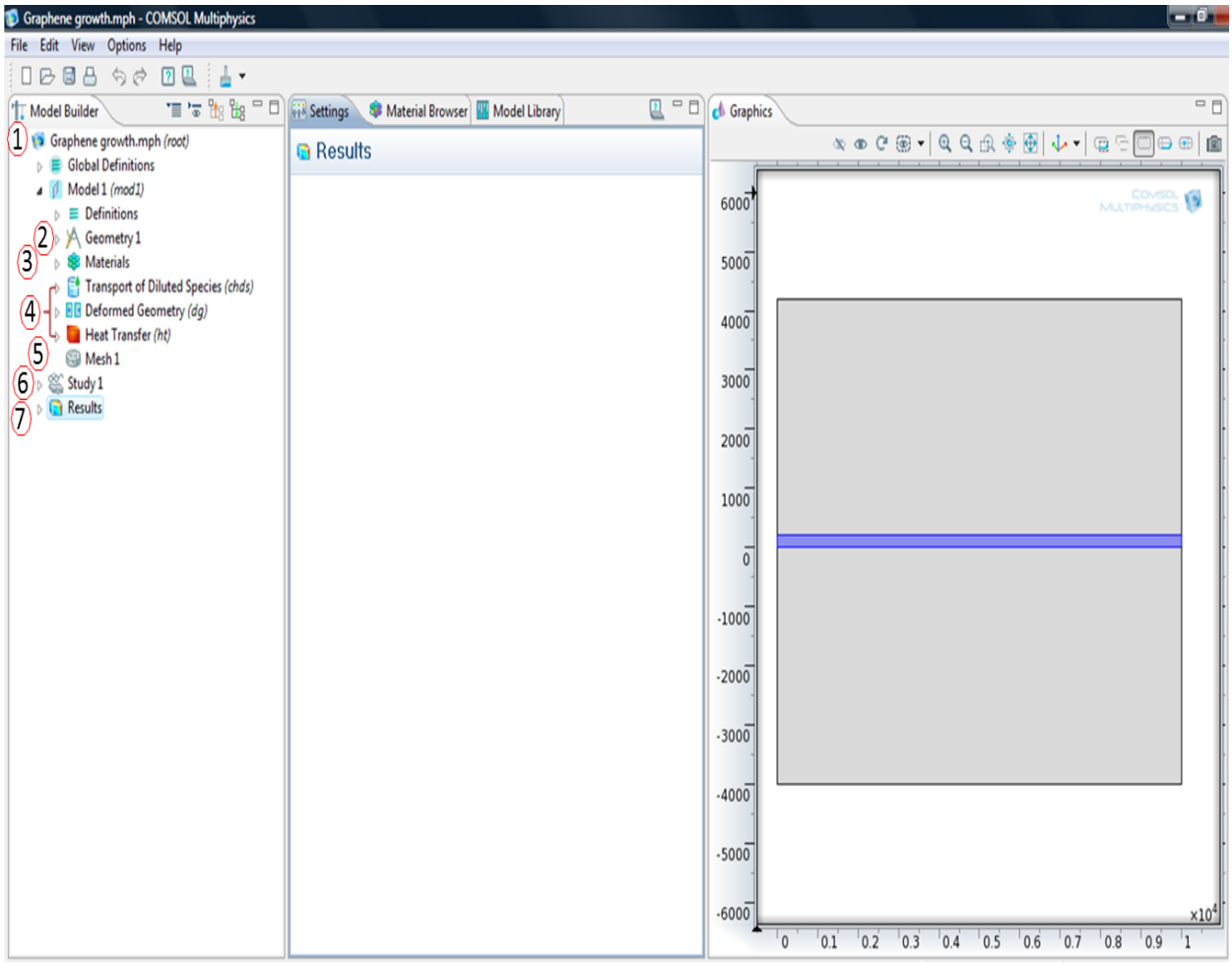

Figure 3.21: The main steps of the model construction process utilizing COMSOL Multiphysics.

In this work, both carbon dissolution and precipitation steps were simulated as illustrated in Figure 3.22. In addition, graphene film growth on Ni thin film at different condition such as growth time, growth temperature, carbon solubility, and Ni film thickness were investigated.

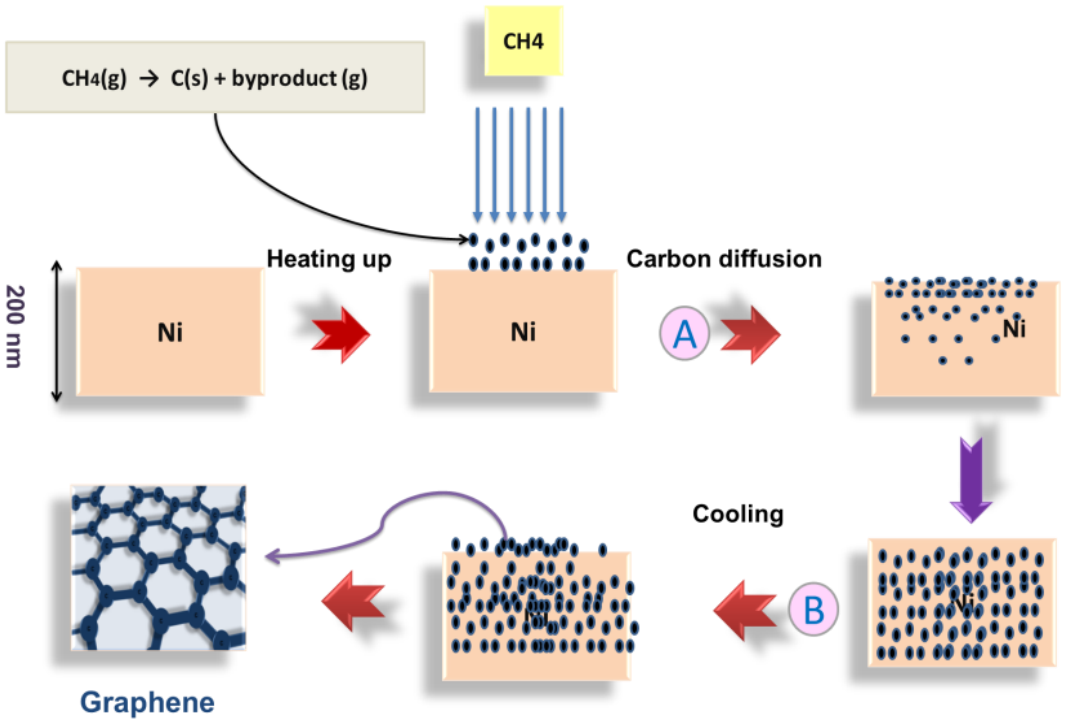

Figure 3.22.: Graphene CVD growth process using nickel film: a) carbon diffusion into the Ni film b) carbon precipitation on the Ni film surface.

COMSOL Multiphysics software was utilized to model graphene growth on Ni at high temperatures. As illustrated in Figure 3.22, graphene synthesis was performed in two essential steps:

A. Carbon diffusion in Ni film:

   In this research, carbon diffusion inside a Ni film was examined. When CH_4 hit the top surface of the 200 nm Ni thick heated to 1000 °C, CH_4 decomposed catalytically and released carbon atoms. Then, the adsorbed carbon atoms diffused into the Ni film at the same temperature, 1000 °C.

B. Carbon precipitation:

   During the cooling period, carbon atoms precipitation on Ni surface occurred due to supersaturation of the diluted carbon in Ni.

In this model, in order to simplify the graphene CVD synthesis method, the following assumptions were made:

- There was no diffusion of carbon atoms via grain boundaries.
- The bottom side of the nickel film was blocked. So, there was no diffusion thru this side.
- During the annealing stage, carbon atoms were homogeneously and uniformly distributed in the Ni film.
- During cooling period, precipitated carbon atoms segregated and distributed homogeneously on the surface of the Ni film.
- In the dissolution process, there was no direct deposition for carbon atoms on the surface of the Ni film.
- There was no carbide formation in the Ni film.

In this model transport of diluted species, heat transfer in Ni thin film and deformed geometry module were utilized as shown in Figure 3.23.

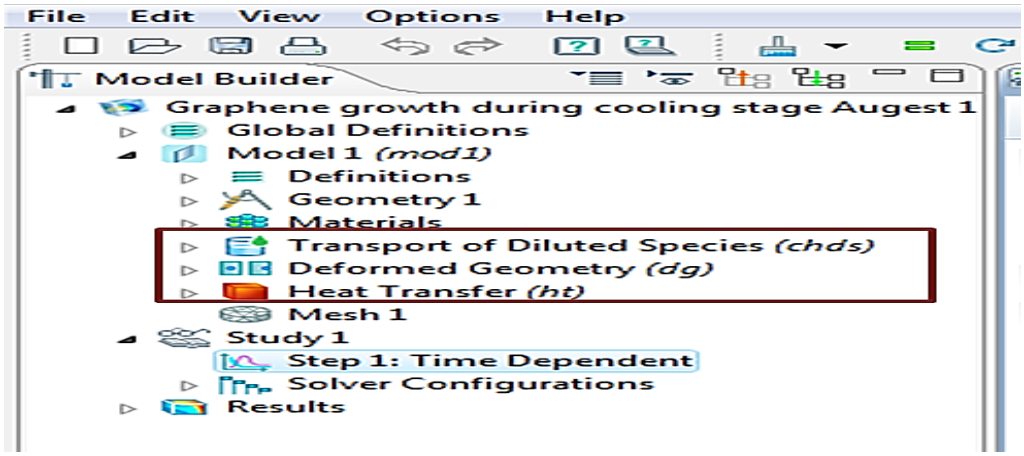

Figure 3.23: The COMSOL modules used in this study; transport of diluted species, heat transfer in Ni thin film and deformed geometry.

The geometry of the graphene synthesis model created in COMSOL is illustrated in Figure 3.24.

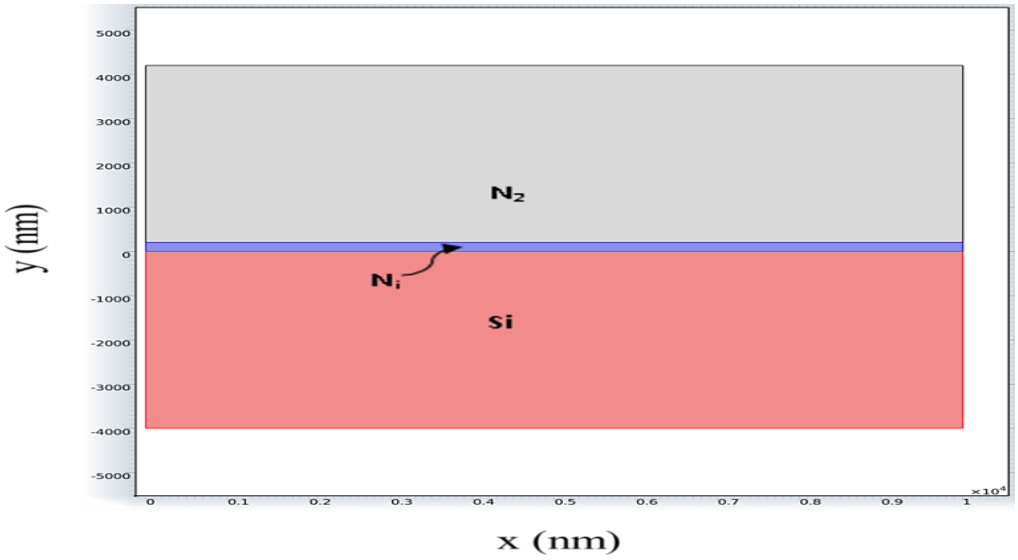

Figure 3.24: Model schematic diagram of graphene growth using Ni thin film.

Figure 3.25 shows the COMSOL mesh for the graphene synthesis model. The graphene synthesis model was extremely meshed.

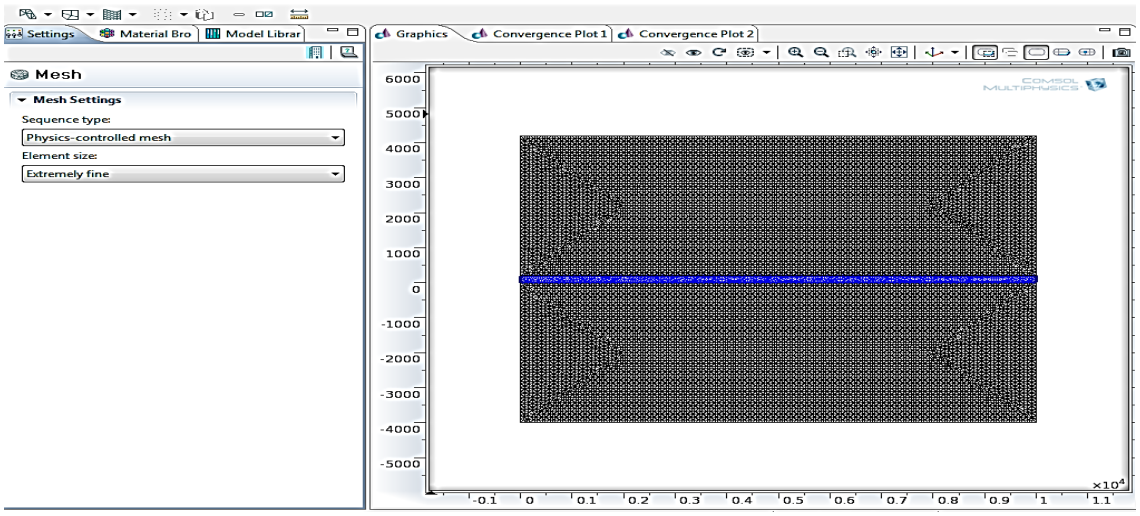

Figure 3.25: The graphene synthesis model; COMSOL mesh.

During the carbon dissolution and precipitation stage, carbon atoms were mainly transferred by diffusion process from the Ni film surface into its bulk. Hence, conservation of mass was used to described the carbon atoms transformation. The governing equation for carbon atoms transport is mathematically defined by Equation 3.3.

$$\frac{\partial c}{\partial t}=\nabla.(D\nabla c) \qquad \text{Equation 3.3}$$

Where c is the carbon atoms concentration and *D* is the carbon diffusion coefficient defined by Equation 2.3.

The heat transfers within the Ni film by conduction. So, heat transfer in Ni film is mathematically expressed by Equation 3.4.

$$\rho C_P \frac{\partial T}{\partial t}=\nabla.(\kappa\nabla T) \qquad \text{Equation 3.4}$$

Where

T: The temperature.

C_P : The specific heat capacity.

ρ : The mass density of the material.

κ: The thermal conductivity

In the dissolution period, the mass and heat transfer initial and boundary conditions for graphene synthesis model are illustrated in Figure 3.26. To clarify, as an initial condition, the concentration of carbon atoms in Ni film at t=0 was set as follows:

$$c\ (t=0)=0 \qquad \text{Equation 3.5}$$

Also, the temperature of the Ni film at t=0 was set as follows:

$$T\ (t=0) = T\ (t) = 1000\ °C \qquad \text{Equation 3.6}$$

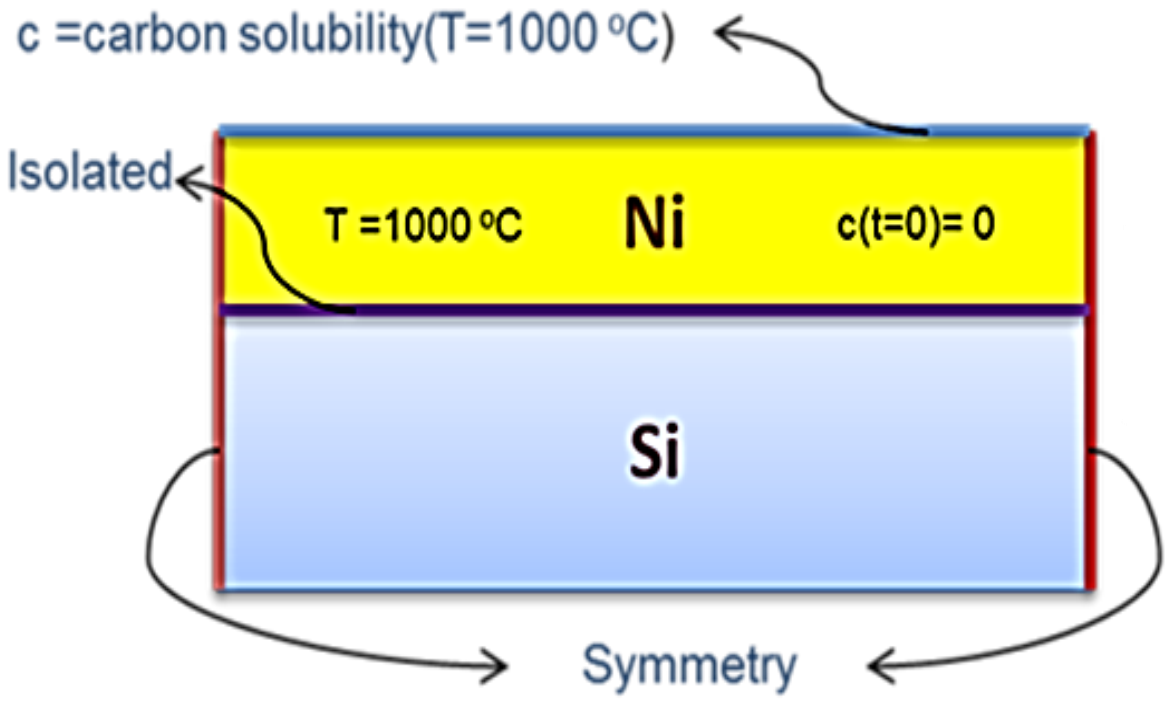

Figure 3.26: The mass and heat transfer initial and boundary conditions for graphene synthesis model during the dissolution stage.

The mass and heat boundary conditions during the dissolution time for this model are:

- The carbon concentration at the top surface of the Ni film is equal the solubility of carbon at a temperature equals the initial temperature of the Ni film:

  $c=S(T_{intial\_Ni})$ Equation 3.7

- There is no carbon flux or heat at the bottom surface of the Ni film :

  $-n.N_i=0$ Equation 3.8

- There is a symmetry of carbon flux and heat at the Ni film sides:

  $-n.N_i=0$ Equation 3.9

Figure 3.27 displays the mass and heat transfer initial and boundary conditions for graphene synthesis model during the precipitation phase.

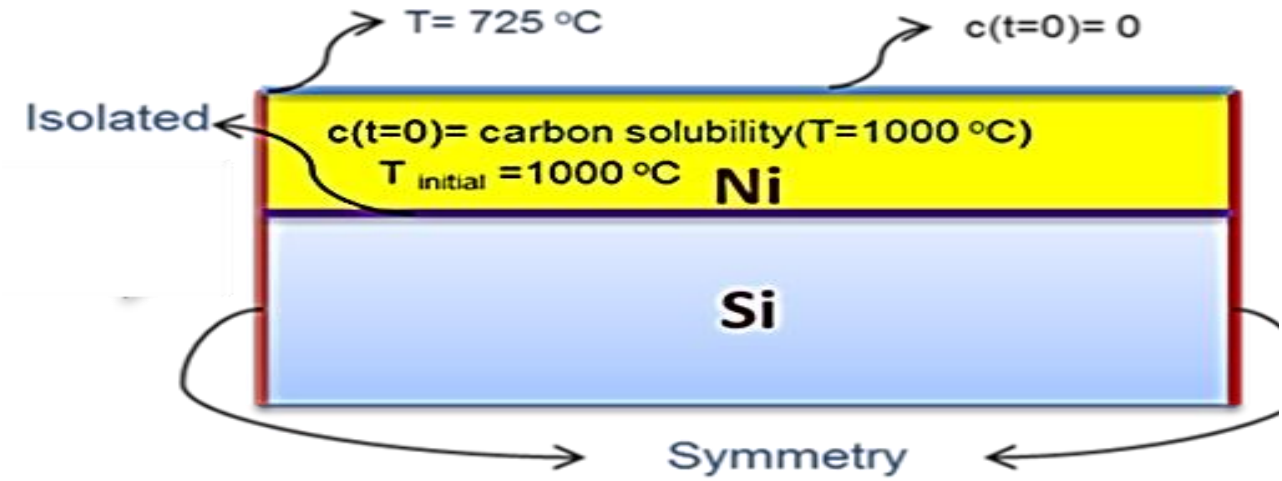

Figure 3.27: The mass and heat transfer initial and boundary conditions for graphene synthesis model during the precipitation period.

The initial conditions in this model for the precipitation phase were set as:

- The concentration of carbon atoms inside the Ni film at t=0 equals the carbon solid solubility limit in Ni at 1000 °C.

  c (t=0)=Carbon solid solubility limit (T=1000 °C) Equation 3.10

- The concentration of carbon atoms on the top surface of the Ni film at t=0 equals zero.

  c (t=0)=0 Equation 3.11

- The temperature of the Ni film at t=0 equals T=1000 °C

  T (t=0) = 1000 °C Equation 3.12

- The thickness of graphene film, d, on the top surface of the Ni film at t=o was zero.

  d(t=0)=0 Equation 3.13

Also, the boundary conditions for mass and heat transfer in the graphene film synthesis model were defined as:

- The temperature of the top surface equals the desirable temperature of the surface

$T=T_{desirable}$ (e.g. 750 °C) Equation 3.14

- The bottom surface of the Ni film was isolated:

$-n.(-k\nabla T) = 0$ Equation 3.15

- There was a symmetry of the heat flux and mass at the Ni film sides:

$-n.N_i=0$ Equation 3.16

- There was no carbon flux at the bottom surface of the Ni film :

$-n.N_i=0$ Equation 3.17

Chapter 4: Results and Discussion

4.1 Diamond-like carbon (DLC) synthesis on Si substrate

Diamond-like carbon (DLC) films were synthesized utilizing Plasma Enhanced Chemical Vapor Deposition system (PE -CVD). The effect CH_4/Ar flow rate ratio and plasma power on DLC fabrication were investigated using different recipes as illustrated in Table 4.1.

Table 4.1: Experimental parameters for the DLC deposition.

Recipe	CH_4/Ar flow rate ratio (sccm)	Growth time (min)	Power (watt)	Growth Temperature (°C)	Growth pressure (torr)
1	55/45	60	77	R.T.	0.3
2	90/10	60	77	R.T.	0.3
3	33/67	60	77	R.T.	0.3
4	10/90	60	77	R.T.	0.3
5	90/10	60	30	R.T.	0.3
6	50/50	60	30	R.T.	0.3

DLC films were successfully deposited on 2’’x 2’’ silicon (100) polished substrate and glass at room temperature as shown in Figure 4.1 and Figure 4.2, respectively.

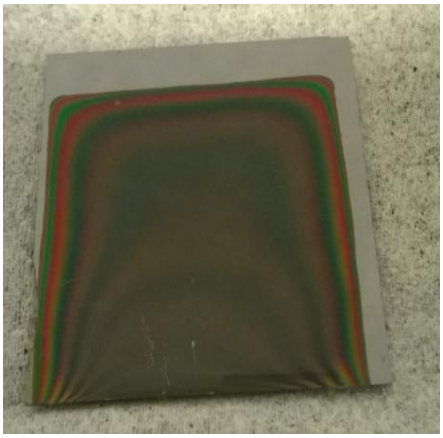

Recipe1: DLC on Si

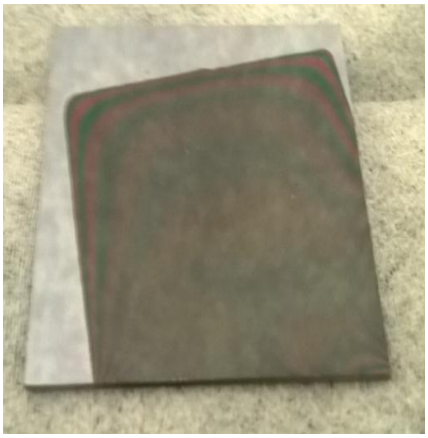

Recipe3: DLC on Si

Figure 4.1: Diamond-like carbon (DLC) films deposited on Si at room temperature utilizing PECVD.

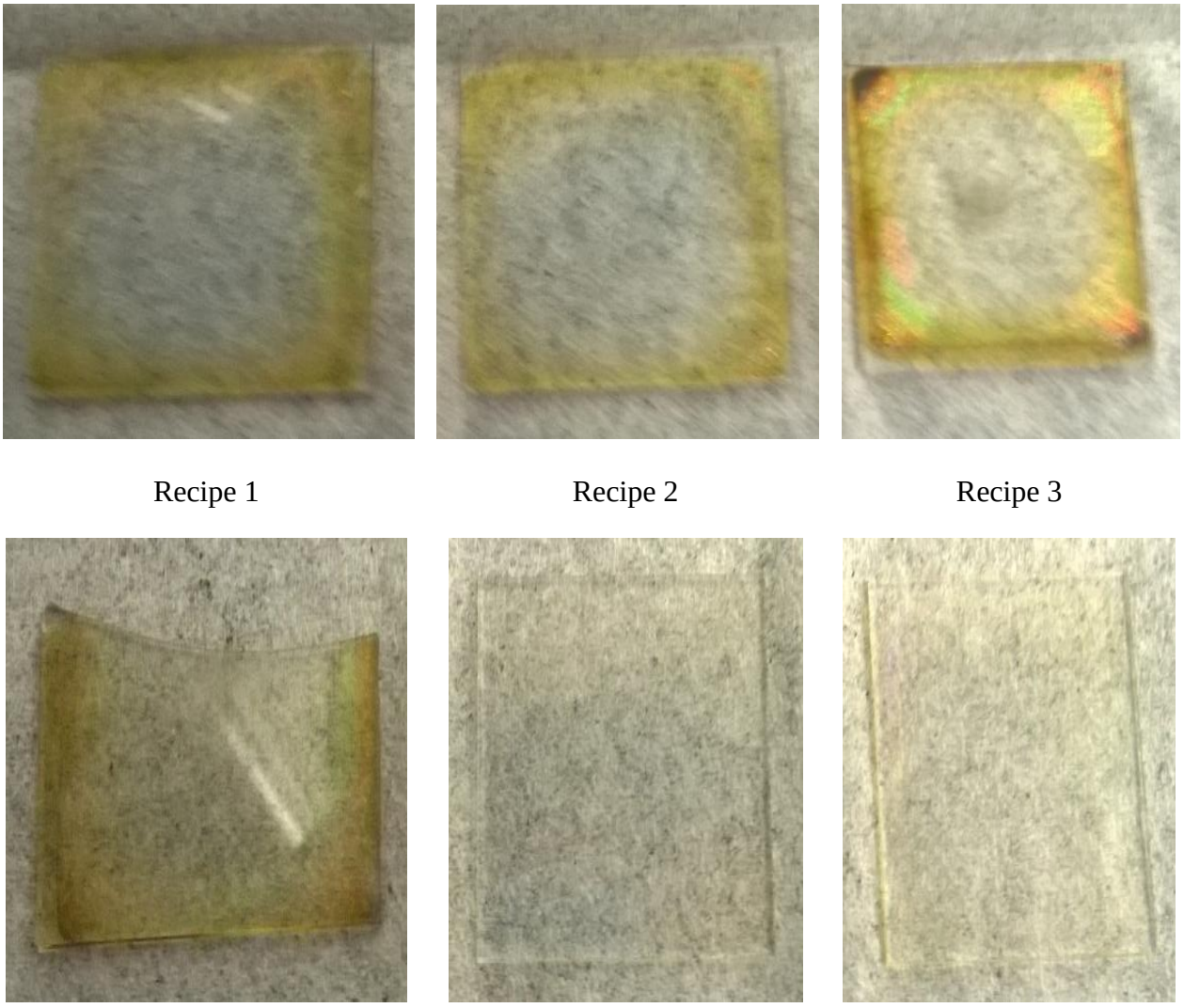

Recipe 1 Recipe 2 Recipe 3

Recipe 4 Recipe 5 Recipe 6

Figure 4.2: Diamonds like carbon (DLC) films deposited on glass by different recipes at room temperature utilizing PECVD.

The obtained DLC films were characterized by the micro-Raman spectroscopy utilizing an excitation wavelength of 532 nm. The Raman spectrum of DLC films consists typically of two broad peaks; G peak and D peak. The G peak, associated with the highly crystalline sp^2 graphite, appears at ~ 1580 cm^{-1}. The second peak; D peak, tetrahedral diamond form, is located at ~ 1350 cm^{-1}.

The Raman spectrums of the obtained DLC films synthesized by different CH_4/H_2 ratios at power equals 77 watt are presented in Figure 4.3. The broadness of Raman peak shown in Figure 4.3 implies that the DLC carbon films had an amorphous structure.

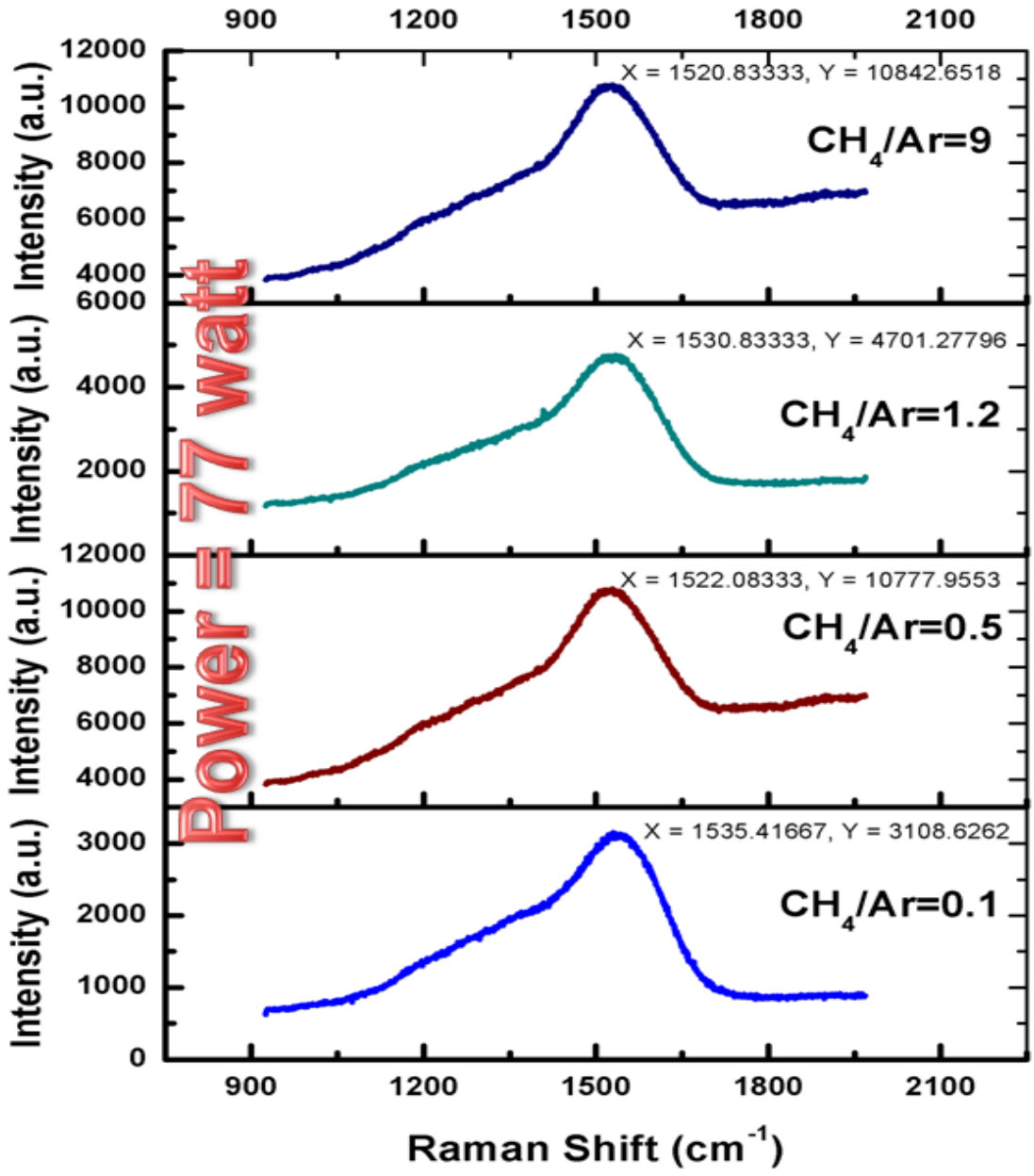

Figure 4.3: Raman spectra for DLC film deposited on Si substrate by different CH_4/Ar ratios at 77 watt.

As illustrated in Figure 4.4, the relation between G-peak position and CH_4/Ar ratio indicates that the G-peak position shifted lower with increasing CH_4/Ar ratio. This denotes a lower ratio of CH_4/Ar resulted in more sp^3 carbon bond. Also, the red shift of the G-peak demonstrated that the DLC film was in tensile stress.

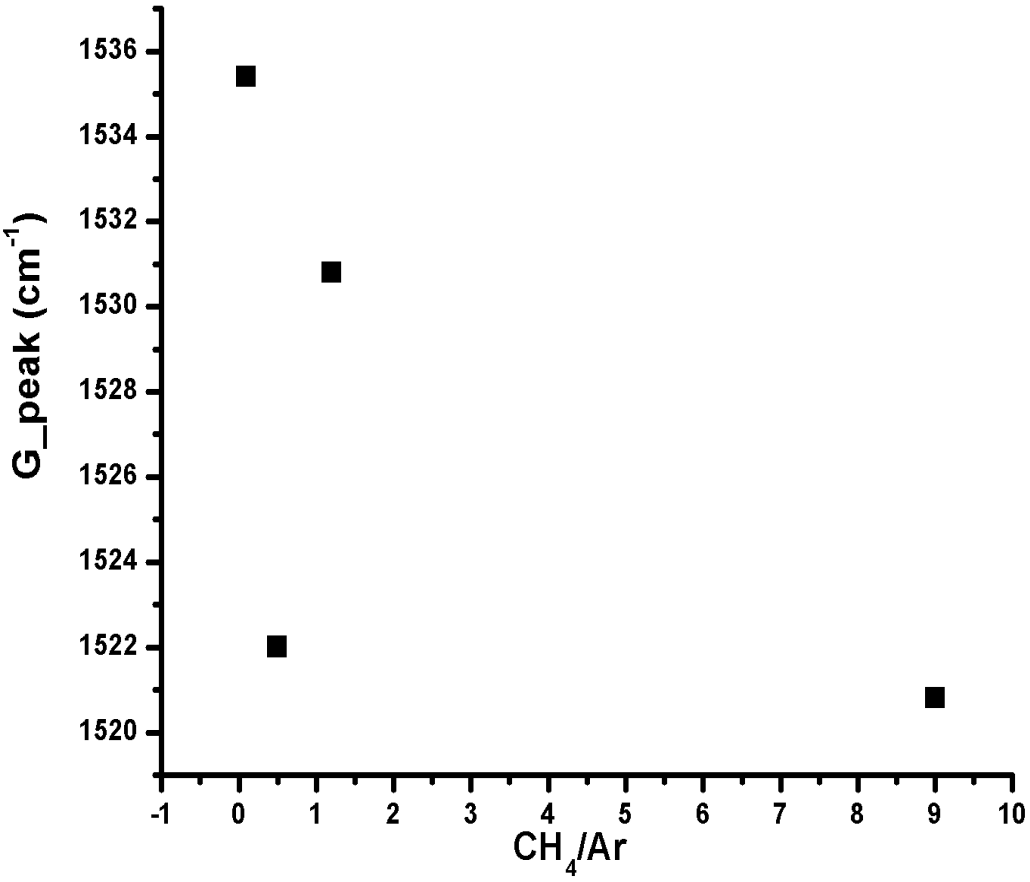

Figure 4. 4: The relation between G-peak position and CH_4/Ar ratio.

Also, the effect the power of plasma on DLC film synthesis was studied. DLC film fabrication was conducted using two values of the plasma power supply: 77 and 30 watt.

The Raman spectrums of the DLC films synthesized using 30 watt are shown in Figure 4.5. It is obvious from the figure that no DLC film was formed on the Si substrate at 30 watt.

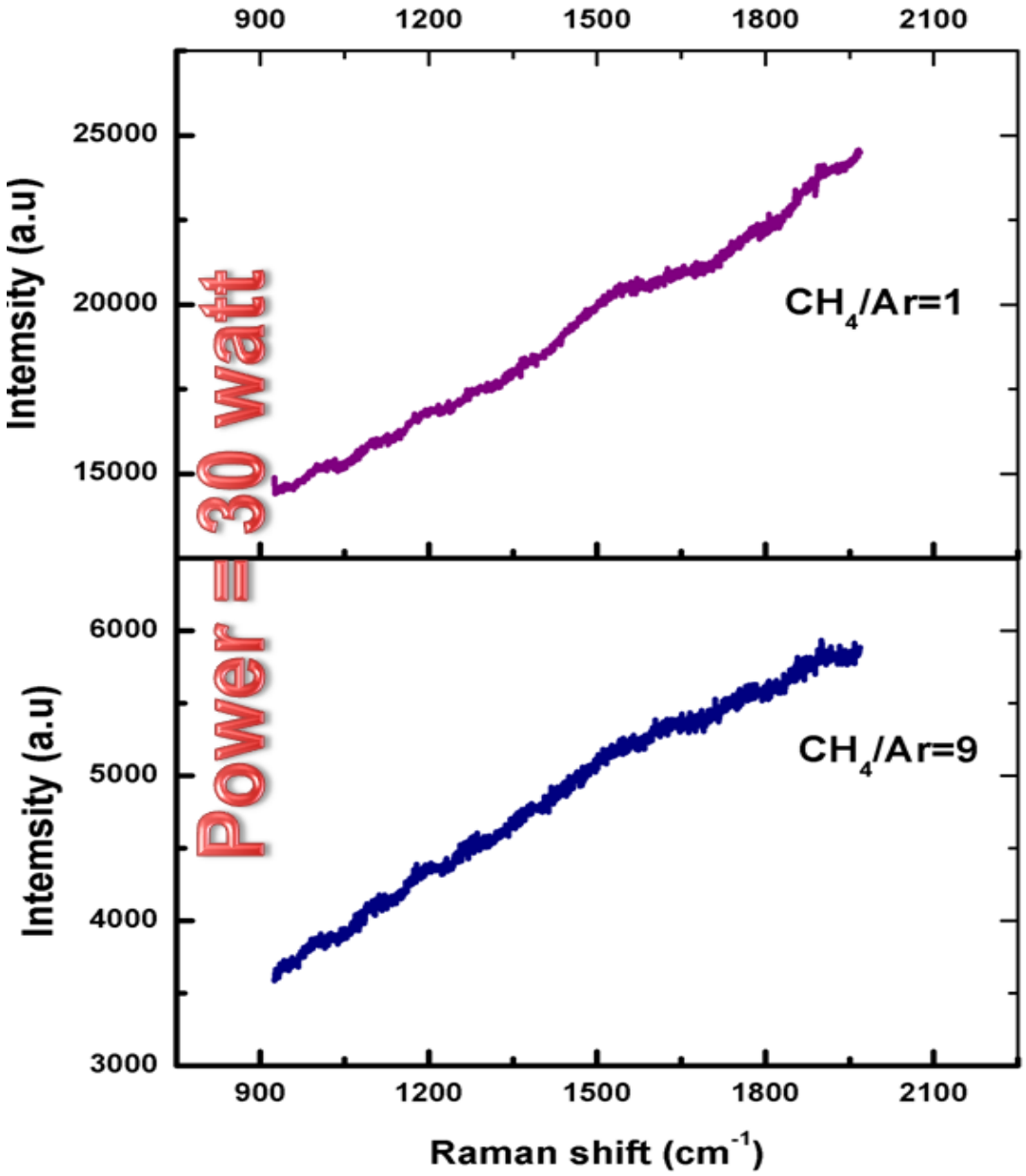

Figure 4.5: Raman spectra for DLC film deposited on Si substrate by different CH_4/Ar ratios at 30 watt.

SEM was used to investigate the surface morphology of the DLC films. The SEM micrograph in Figure 4.6 does not show visible defects on the surface of the DLC film.

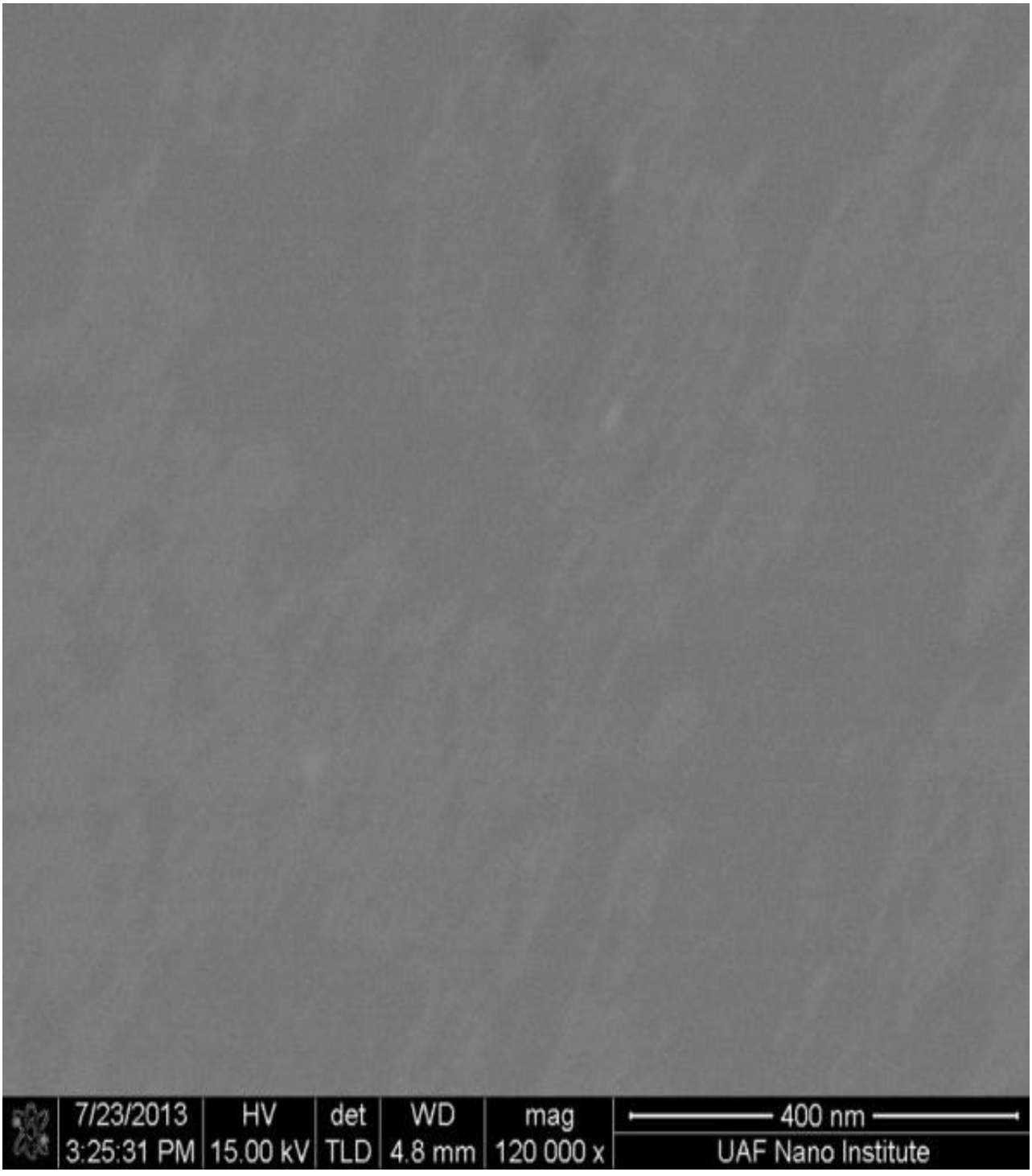

Figure 4.6: SEM image of DLC film deposited on Si substrate.

In addition, EDX was used for elemental analysis. From EDX analysis, carbon and silicon were found in the synthesized DLC film as depicted in Figure 4.7.

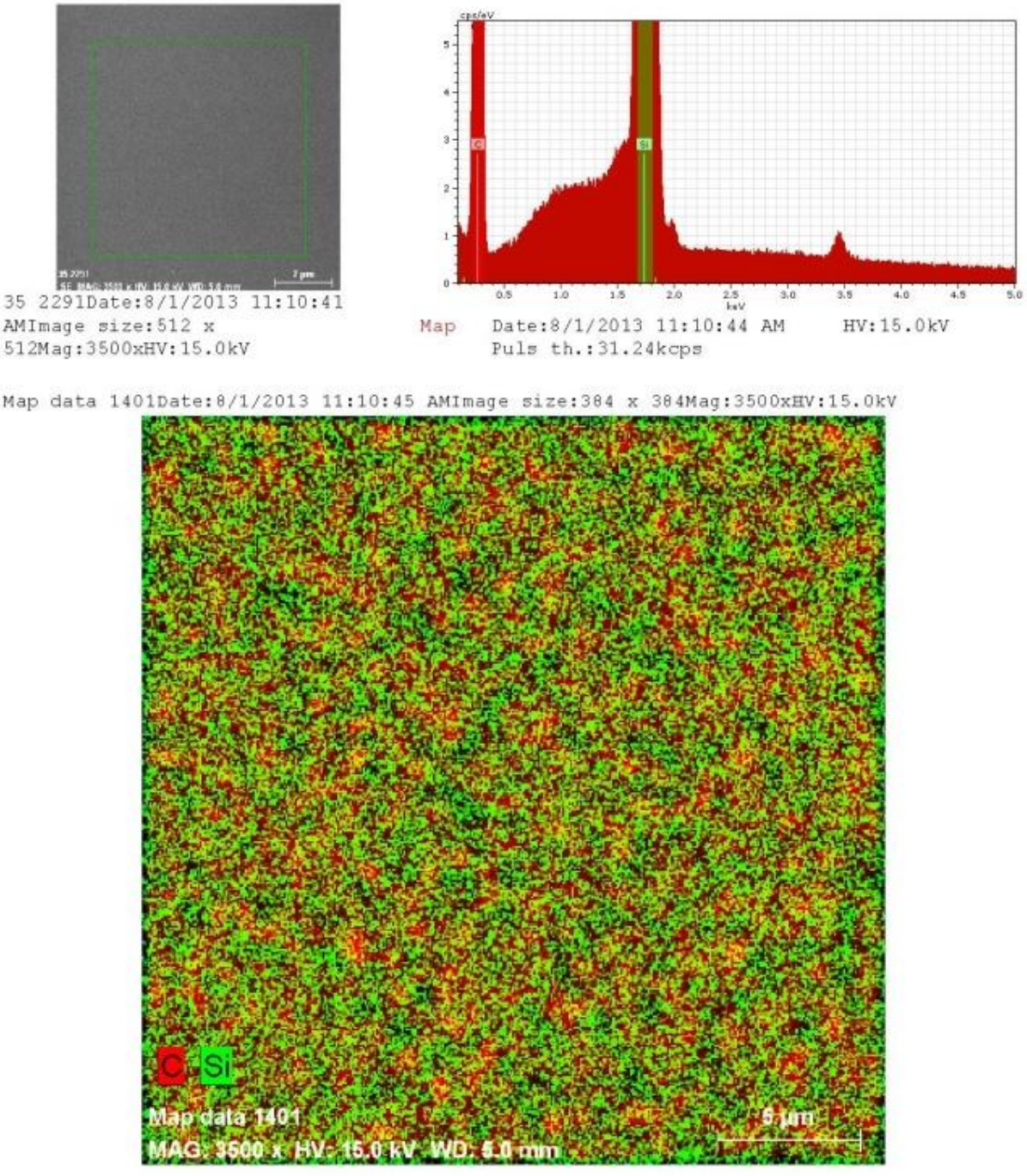

Figure 4.7: EDX image of DLC film deposited on Si substrate.

The surface roughness of the DLC films played a significant role in determining the adhesion force between the nickel film and the DLC film surface. To simplify, decreasing the roughness of the DLC films facilitated the removal of the nickel film from the surface of the DLC films. Therefore, Atomic Force Microscopy (AFM) was utilized to examine the DLC films surface.

AFM showed that the average roughness (Ra) of DLC sample (1μ×1μ) was 0.265 nm and the root mean square roughness (Rq) was 0.337 nm as shown in Figure 4.8 and Figure 4.9 .The average reported roughness is ~ 17 nm [41]. This means that the DLC films obtained in this research were ultra-smooth.

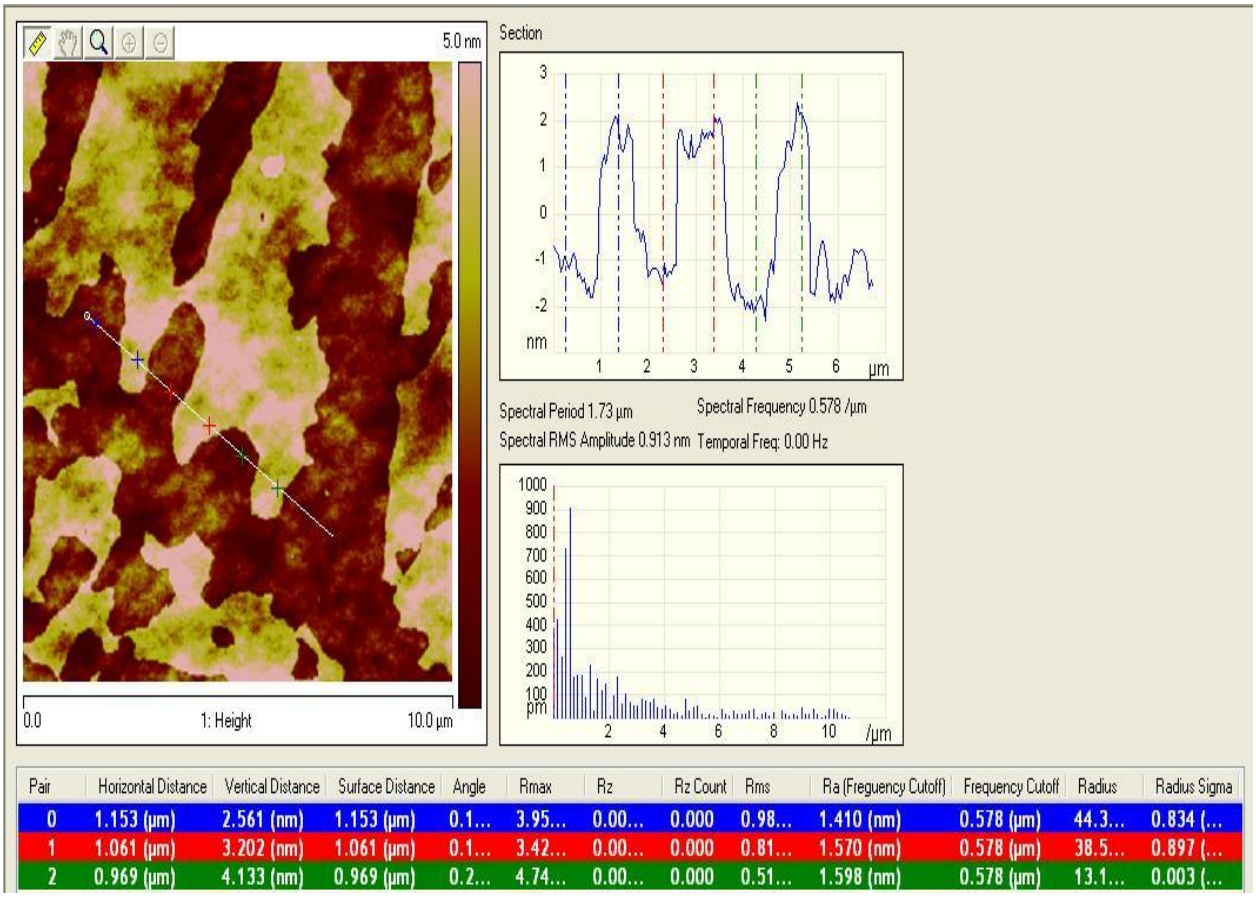

Pair	Horizontal Distance	Vertical Distance	Surface Distance	Angle	Rmax	Rz	Rz Count	Rms	Ra (Freguency Cutoff)	Frequency Cutoff	Radius	Radius Sigma
0	1.153 (μm)	2.561 (nm)	1.153 (μm)	0.1...	3.95...	0.00...	0.000	0.98...	1.410 (nm)	0.578 (μm)	44.3...	0.834 (...
1	1.061 (μm)	3.202 (nm)	1.061 (μm)	0.1...	3.42...	0.00...	0.000	0.81...	1.570 (nm)	0.578 (μm)	38.5...	0.897 (...
2	0.969 (μm)	4.133 (nm)	0.969 (μm)	0.2...	4.74...	0.00...	0.000	0.51...	1.598 (nm)	0.578 (μm)	13.1...	0.003 (...

Figure 4.8: AFM trace of DLC film deposited on Si substrate.

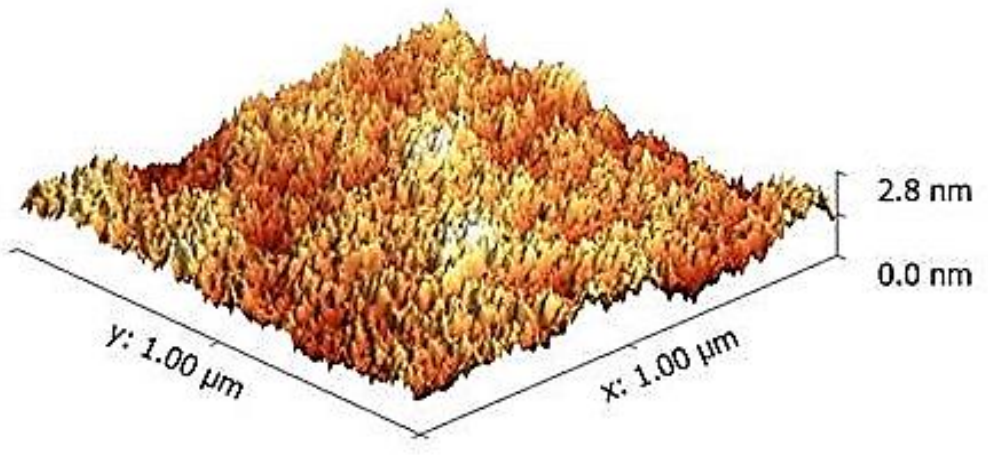

Figure 4.9: AFM image of DLC film deposited on Si substrate.

4.2 Graphene synthesis on different substrate materials

Graphene films were synthesized utilizing hot-filament chemical vapor deposition. Methane (CH_4) and Hydrogen (H_2) mixture with different growth time and growth pressure were used in graphene film synthesis.

In this study, the capability of the hot-filament CVD in fabricating a uniform growth of graphene film growth on different substrate at low temperature was investigated. The same Raman spectroscopy (i.e. 532 nm) was utilized to investigate the synthesized graphene films that formed on different substrate materials. Table 4.2 illustrates the CVD parameters used in graphene films synthesis on different substrates.

Table 4.2: Graphene CVD growth parameters.

Substrate material	CH_4/H_2 flow rate ratio (sccm)	Growth temperature (°C)	Growth pressure (torr)	Growth time (min)	Ni film thickness (nm)
Si	15/5	700	1.5	15	200
SiO_2	15/5	700	1.5	10	200
Si_3N_4	15/5	700	1	5	200
Diamond	15/5	700	1.5	10	200
DLC	15/5	700	1.5	10	200

The Raman spectra of the graphene films fabricated on different substrates – Si, Si_3N_4, diamond, and DLC – are illustrated in Figure 4.10 - Figure 4.13.

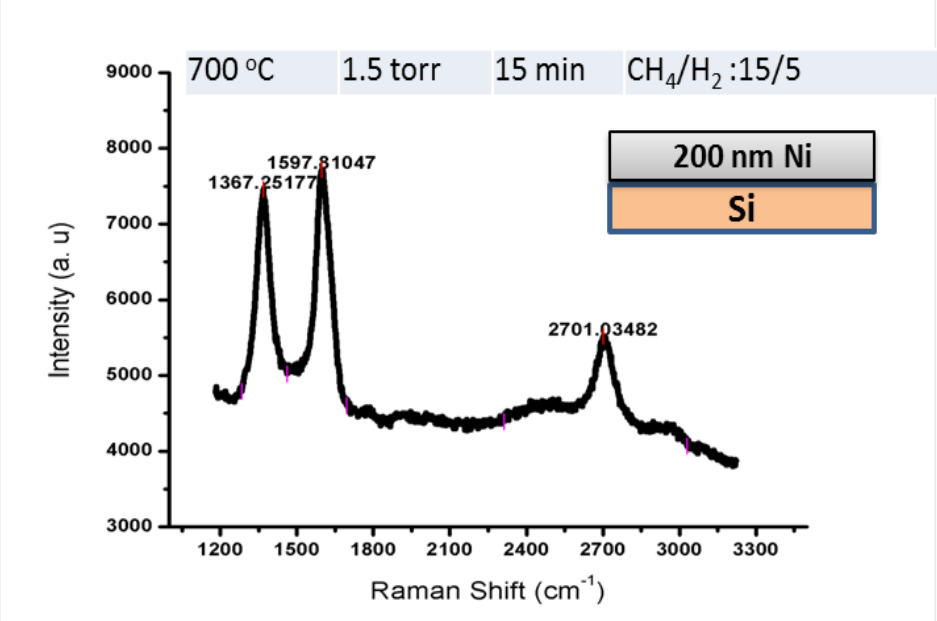

Figure 4.10: Raman spectra for graphene films synthesized on Ni (200 nm) /Si.

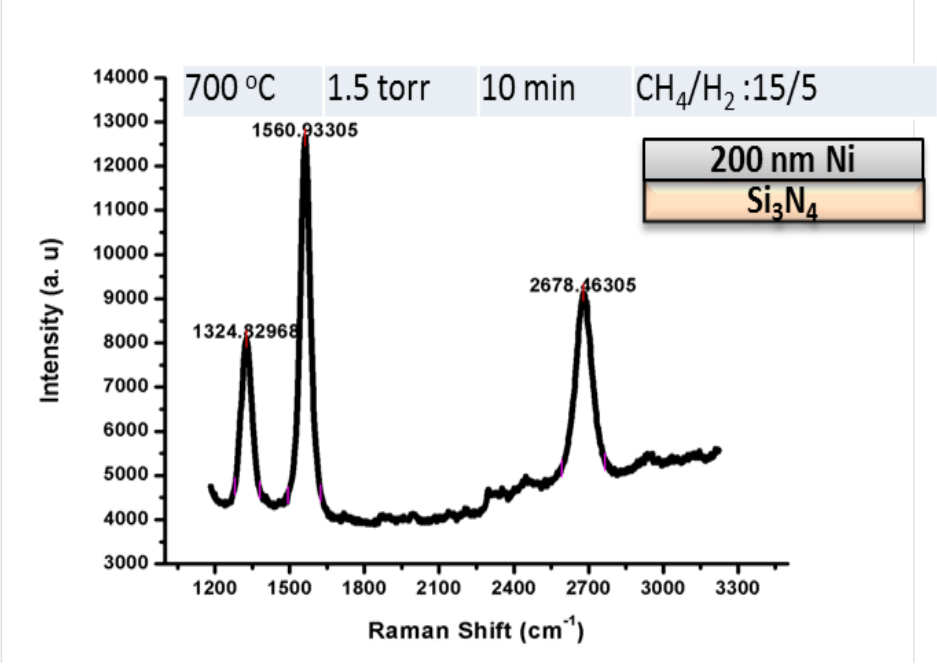

Figure 4.11: Raman spectra for graphene films synthesized on Ni (200 nm) /Si_3N_4.

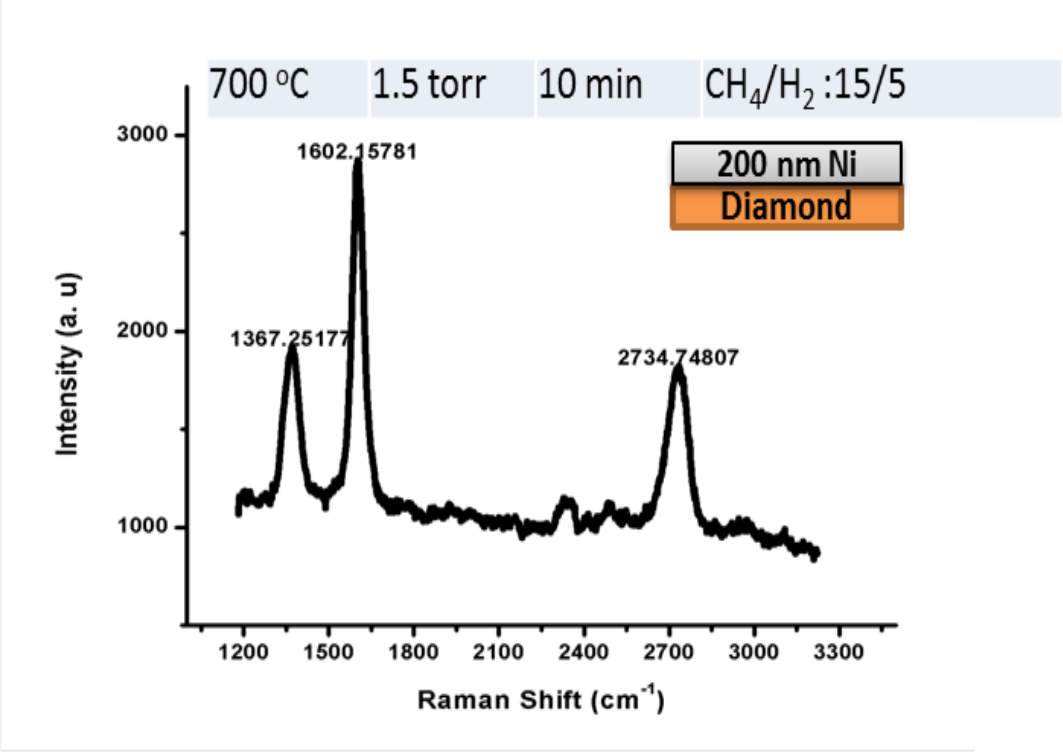

Figure 4.12: Raman spectra for graphene films synthesized on Ni (200 nm) /diamond.

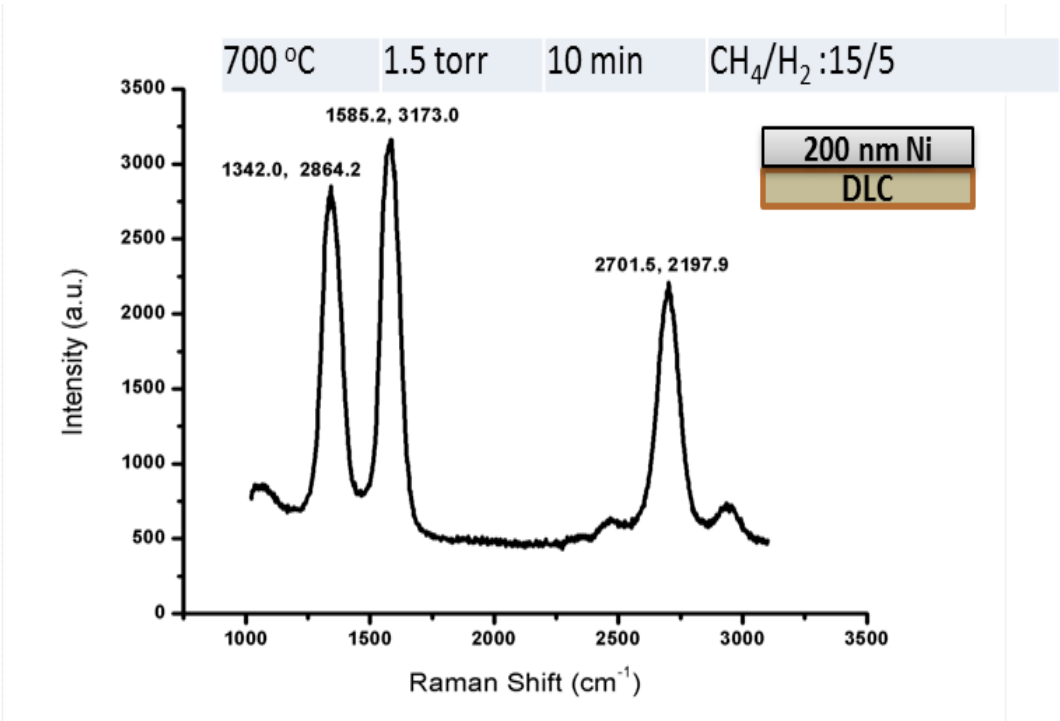

Figure 4.13: Raman spectra for graphene films synthesized on Ni (200 nm) /DLC.

The Raman parameters for each graphene film are shown in Table 4.3. Raman results show a few layers of graphene formed on 200 nm nickel film-coated different substrate (i.e. Si, SiO_2, Si_3N_4, DLC, and diamond).

Table 4.3: The Raman parameters for each graphene film deposited on Si, SiO_2, Si_3N_4, DLC, and diamond.

Substrate	D-peak center (cm^{-1})	G-peak center (cm^{-1})	2D-peak Center (cm^{-1})	I_D/I_G	I_{2D}/I_G	FWHM(2D-peak) (cm^{-1})
Si	1367.3	1597.8	2701.0	0.97	0.72	305
Si_3N_4	1325.3	1562.0	2682.3	0.64	0.72	94.5
DLC	1342.0	1585.2	2701.5	0.90	0.69	111.97
Diamond	1367.3	1602.2	2734.8	0.45	0.51	94.5

It is obvious that graphene film formed on Si substrate had a max value of I_D/I_G, 0.97. This means that this graphene film had more defects than the other graphene films formed on SiO_2, Si_3N_4, DLC, and diamond. Also, the value of I_{2D}/I_G for all the graphene falls within the range 0.333-1. So, these values demonstrate that approximately three layers of graphene were formed on those substrates as explained in section 2.1.

4.3 Effect of the substrate temperature on graphene synthesis using 200 nm nickel film coated SiO_2/Si substrates.

The effect of substrate temperature on graphene film synthesis was investigated. Graphene film was synthesized at different substrate temperatures; 600, 650, 700, and 750 °C. The other CVD parameters were kept fixed; time (10 min), gas flow rates (CH_4/H_2:10:5 sccm), pressure (1.5 torr), and hot-filament temperature (2100 °C). Table 4.4 depicts the CVD parameters utilized in studying the effect of growth temperature on graphene synthesis.

Table 4.4: The CVD parameters utilized in studying the effect of growth temperature on graphene synthesis using 200 nm nickel film-coated SiO_2/Si substrates.

Substrate material	CH_4/ H_2 flow rate ratio (sccm)	Growth temperature (°C)	Growth pressure (torr)	Growth time (min)	Ni film thickness (nm)
SiO_2	10/5	600	1.5	10	200
	10/5	650	1.5	10	200
	10/5	700	1.5	10	200
	10/5	750	1.5	10	200
	10/5	700	1.5	10	200

A scanning electron microscope (SEM) was used in order to do more investigation for the graphene film surface. SEM confirms graphene film formation on the top surface of the Ni film as shown in Figure 4.14.

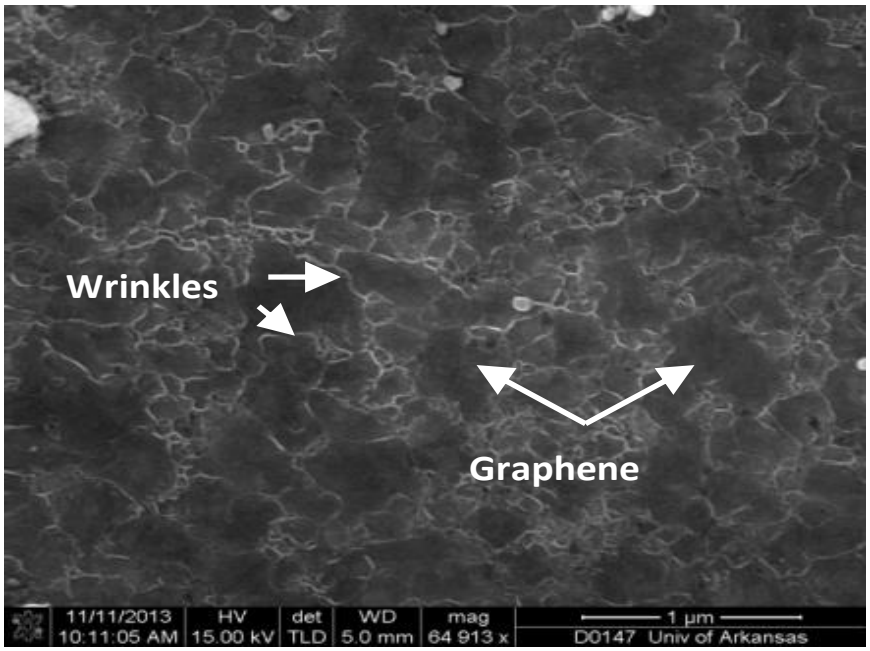

Figure 4.14: SEM image of graphene film formed on Ni film thickness of 200 nm.

It is clear that graphene wrinkles were distributed and formed on the Ni surface. To clarify from SEM image, the dark structures represent the graphene areas whereas the bright features represent the wrinkles of the graphene film.

Carbon atoms diffusion in the grain boundaries is faster than the one takes place at the grains themselves. Consequently, more graphene layers are formed at grain boundaries.

In order to confirm graphene film growth, Raman spectroscopy for the fabricated graphene films on Ni films at different substrate temperature were used as illustrated in Figure 4.15.

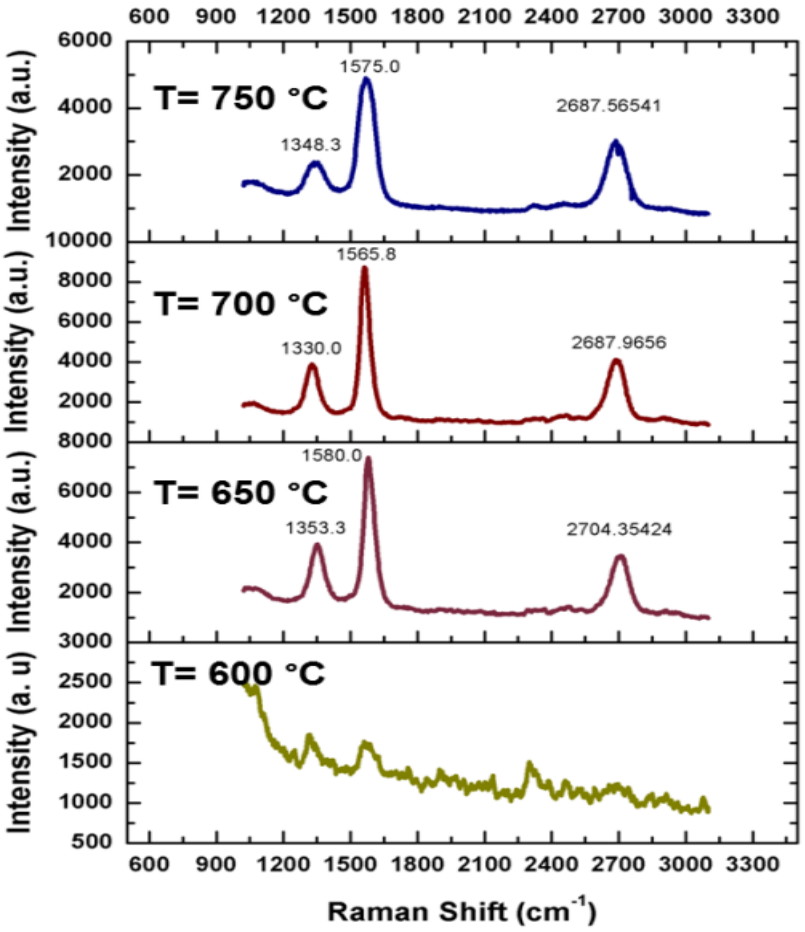

Figure 4.15: Raman spectra of graphene films grown on $Ni/SiO_2/Si$ substrate at different temperature.

It is clear from the figure that a few layers of graphene were formed on the Ni surface at 650, 700, and 750 °C. However, no Raman spectrum of graphene film was observed at a growth temperature of 600 °C as depicted in Figure 4.15.

In order to determine the number of graphene film, there are many ways. One of these methods is Raman spectroscopy. The number of graphene layers can be confirmed by I_{2D}/I_G as well as the symmetry and the lineshape of the 2D-peak [38]. The 2D-peak is considered the distinctive peak of graphene. It is obvious from Raman spectra of the synthesized film on $Ni/SiO_2/Si$ substrate that a few layers of graphene film were formed on the top surface of the Ni film.

The 2D-peak shifts to the left when the substrate temperature rises as shown in Figure 4.16. To clarify, the 2D-peak position appears at 2704.3, 2687.9, and 2687.5 cm^{-1} for the graphene films grown at 650, 700, and 750 °C, respectively, as depicted in Figure 4.16. The red shift of 2D-peak demonstrated a decrease in the number of the graphene layers formed on the top surface of the Ni film when the substrate temperature was increased.

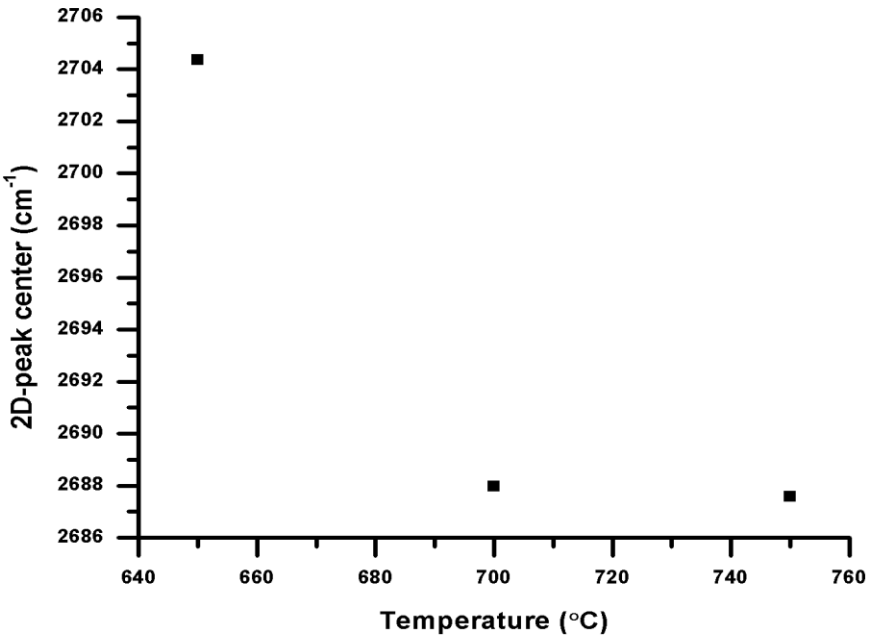

Figure 4.16: 2D- peak center as a function of the substrate temperature.

In order to study the effect of temperature on the number of graphene layers formed on the Ni film surface, I_{2D}/I_G vs. substrate temperature was plotted (Figure 4.17). I_{2D}/I_G increased when the substrate temperature increased as shown in the figure. So, the number of graphene layers decreases with substrate temperature. The values of I_{2D}/I_G show that approximately three to four layers of graphene were formed on the Ni surface.

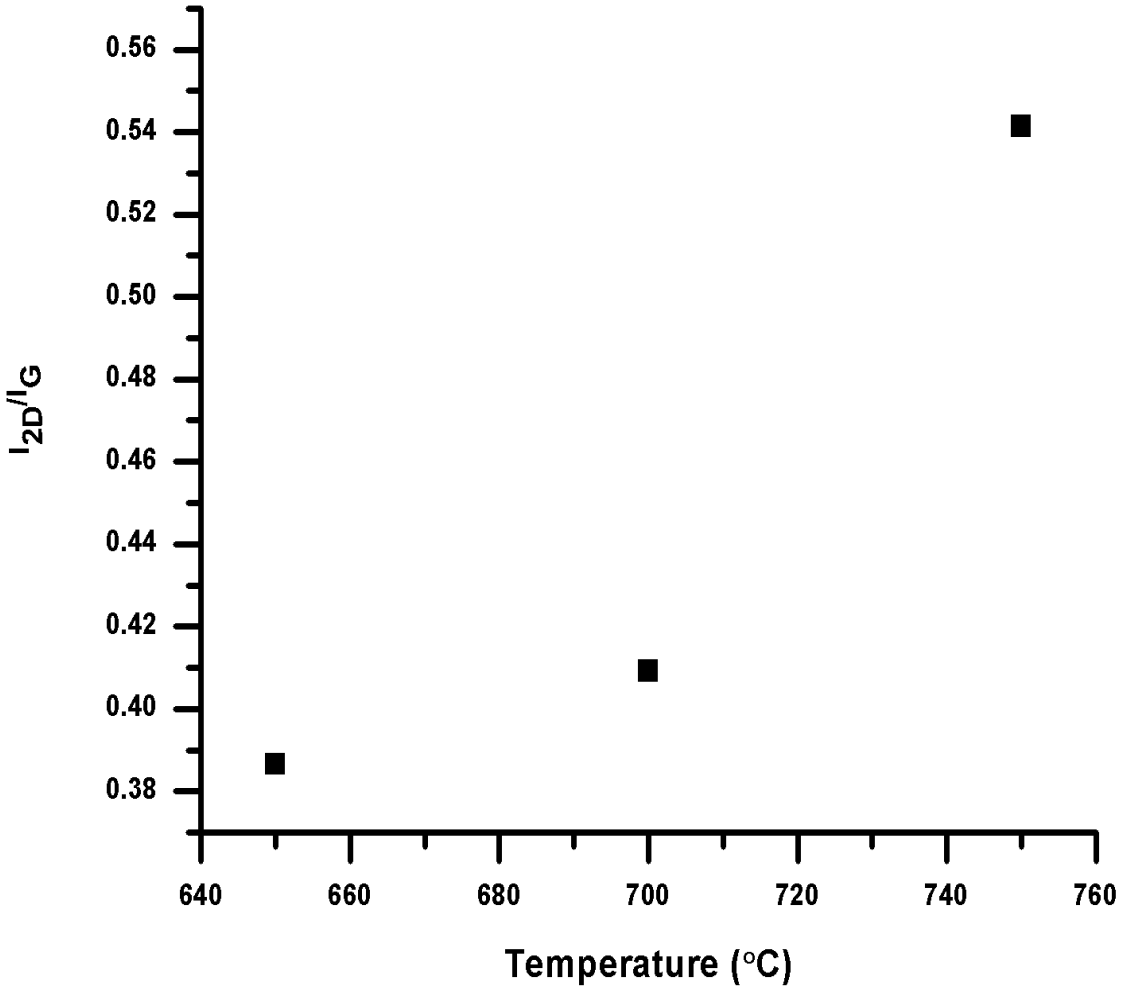

Figure 4.17: The I_{2D}/I_G intensity ratio of the graphene films as a function of the substrate temperature.

The level of the defective and disordered structure of the graphene film can be extracted from the intensity ratio of the D to G peak; I_D/I_G. So, in order to investigate the effect of the substrate temperature on graphene film quality, the relationship between I_D/I_G and temperature is represented in Figure 4.18.

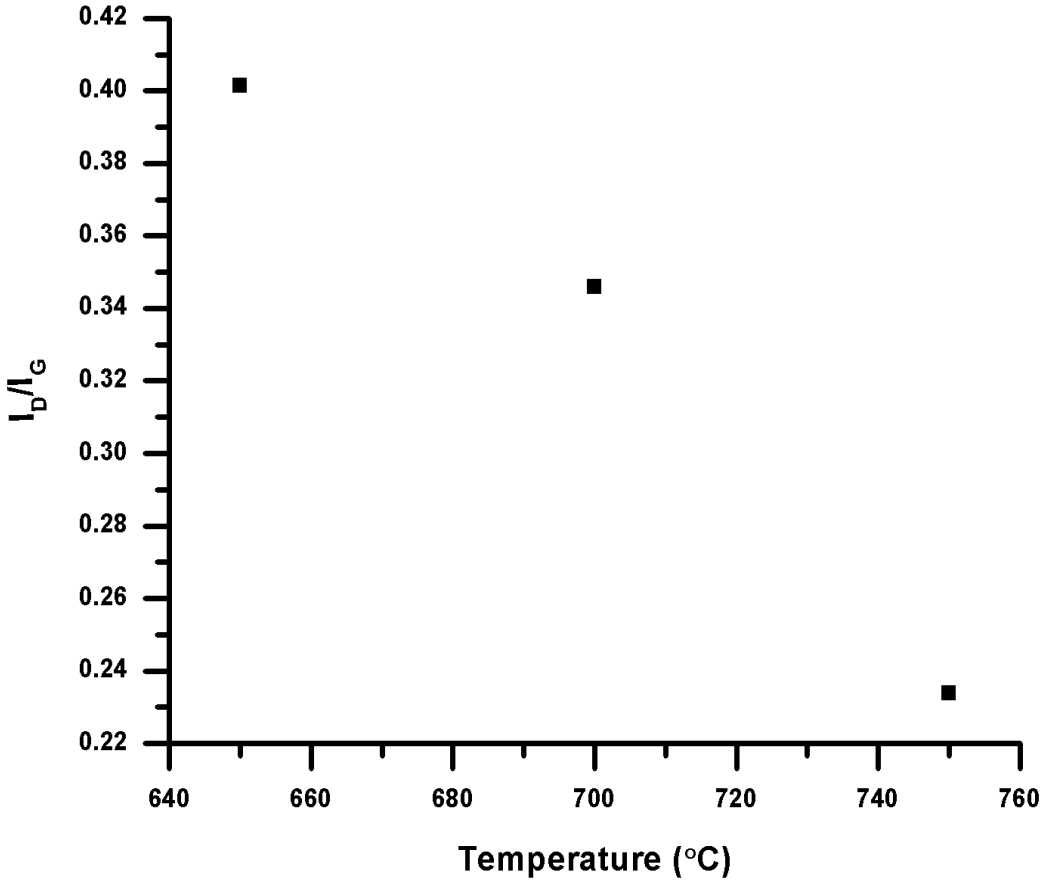

Figure 4.18: The I_D/I_G intensity ratio of the graphene films as a function of the substrate temperature.

It is obvious from Figure 4.18 that the I_D/I_G ratio decreases from 0.40 to 0.23 as the substrate temperature rises from 650 °C to 750 °C. The drop of the I_D/I_G values indicates an improvement in the quality of the graphene film as explained in section 2.1.

Tuinstra and Koenig's equation [81] (Equation 4.1) was utilized to calculate the average size of sp^2 domains (L_α) of the obtained graphene films.

$$L_\alpha = \left(2.4 \times 10^{-10}\right) \lambda_{laser}^4 \left(\frac{I_D}{I_G}\right)^{-1} \quad \text{Equation 4.1}$$

Where, λ_{laser} is the laser wavelength in nm.

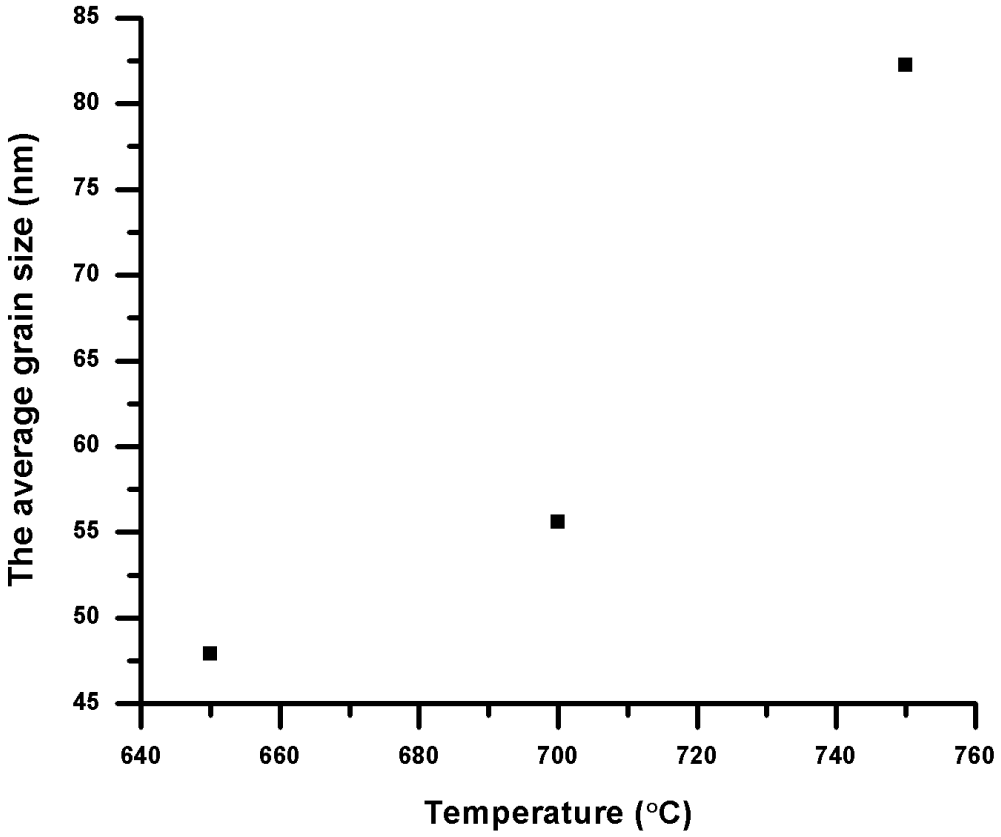

Figure 4.19: The average grain size (L_α) of graphene film as a function of the substrate temperature.

It is clear from Figure 4.19 that the calculated value of the average size of sp^2 domains (L_α) increased from 48 nm to 82 nm when the substrate temperature was raised from 650 °C to 750 °C.

4.4 Effect of CH_4/H_2 ratio on graphene synthesis using 200 nm nickel film-coated SiO_2/Si substrates.

The effect of CH_4/H_2 ratio on graphene films grown on 200 nm nickel film-coated SiO_2/Si substrates was investigated using Raman spectroscopy as shown in Figure 4.20.

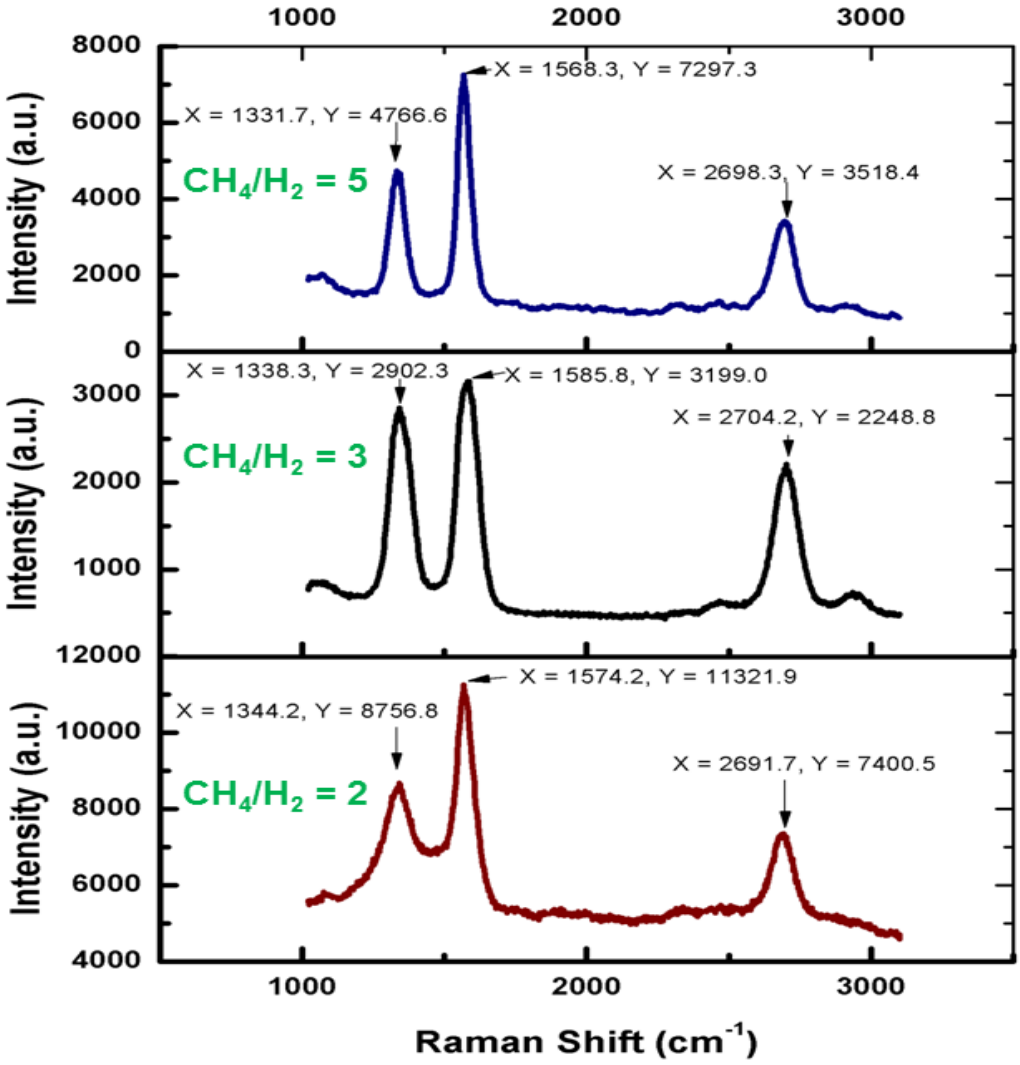

Figure 4.20: Raman spectra of graphene films grown on $Ni/SiO_2/Si$ substrate at different CH_4/H_2 ratios.

The graphene films were fabricated using different CH_4/H_2 ratios as illustrated in Table 4.5.

Table 4.5: the CVD parameters utilized in studying the effect of CH_4/H_2 ratios on graphene synthesis using 200 nm nickel film-coated SiO_2/Si substrates.

Substrate material	CH_4/ H_2 flow rate ratio (sccm)	Growth temperature (°C)	Growth pressure (torr)	Growth time (min)	Ni film thickness (nm)
SiO_2	10/5	700	1.5	10	200
	15/5	700	1.5	10	200
	10/2	700	1.5	10	200

I_{2D}/I_G ratios were calculated to determine how many layers of graphene were grown on the top surface of the Ni film.

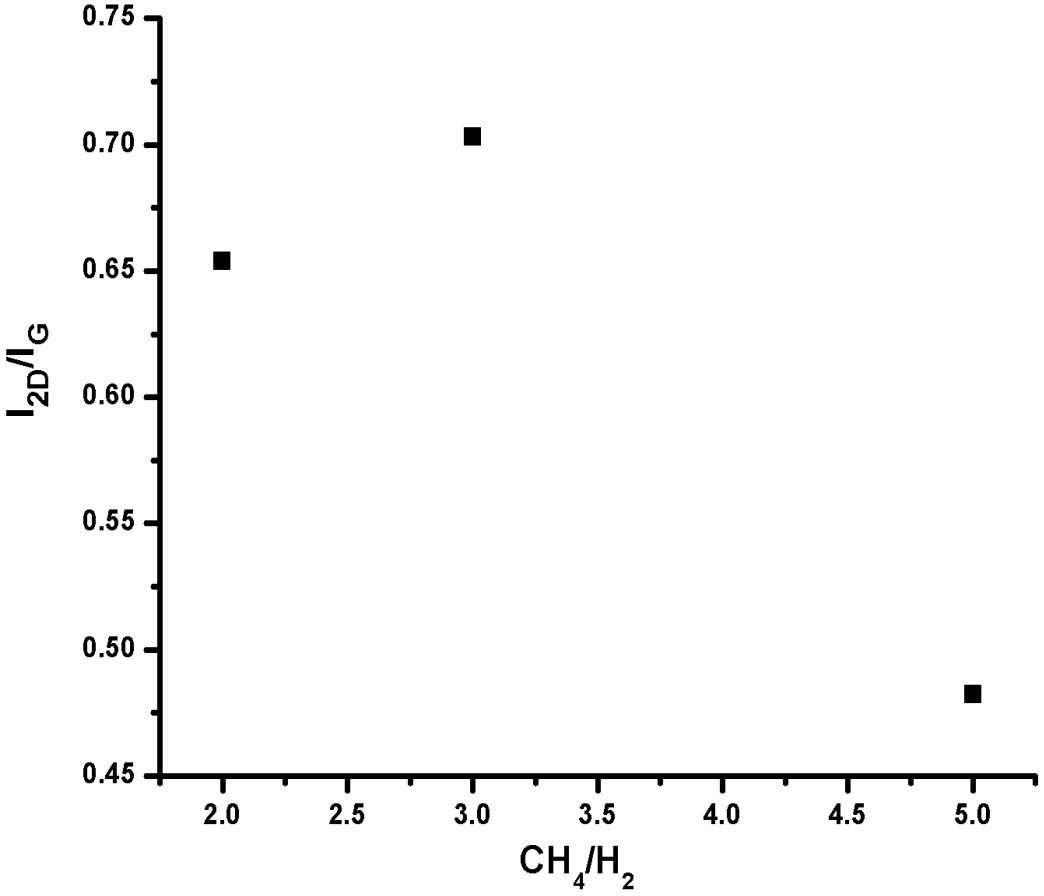

Figure 4.21: The I_{2D}/I_G intensity ratio of the graphene films as a function of CH_4/H_2 ratio.

As illustrated in Figure 4.21, there was a decreasing trend in I_{2D}/I_G intensity ratio values when CH_4/H_2 ratio decreased. So, the obtained number of graphene layers formed on $Ni/SiO_2/Si$ decreased markedly. This decrease of the number of graphene film was due to the increase of hydrogen atoms that etched away carbon material.

The quality of graphene film was investigated. The relationship between I_D/I_G and CH_4/H_2 ratio is shown in Figure 4.22.

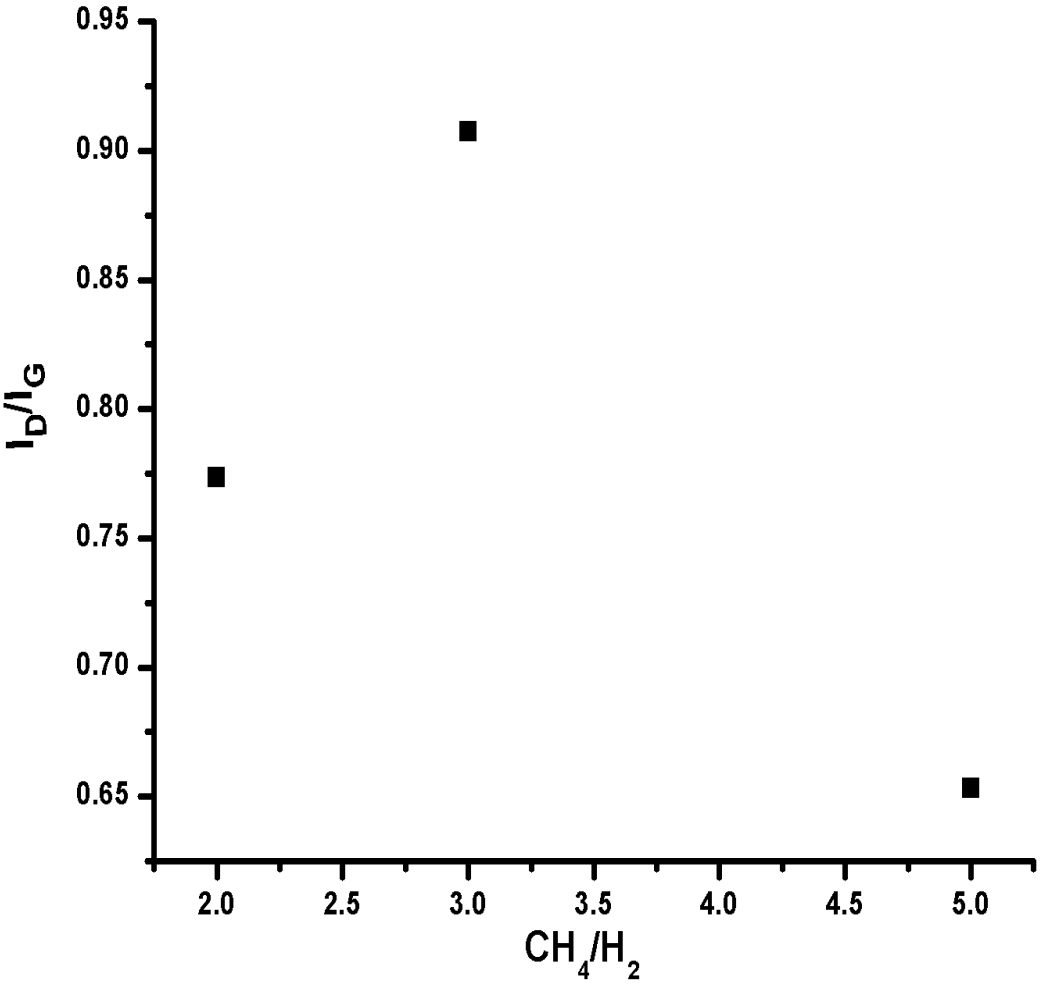

Figure 4.22: The I_D/I_G intensity ratio of the graphene films as a function of CH_4/H_2 ratio.

It is clear that there was a decreasing trend in the I_D/I_G intensity ratio when CH_4/H_2 ratio increased. The decrease of the I_D/I_G intensity ratio means a decreasing in graphene film defects. Hence, there was an improvement on graphene film quality when CH_4/H_2 ratio increased. The increase of hydrogen atoms helped etch away accumulated carbon materials formed at grain boundaries.

Equation 4.1 was used to calculate the average size of sp^2 domains (L_α) of graphene films grown on $Ni/SiO_2/Si$ substrate. This is plotted as a function of CH_4/H_2 ratio in Figure 4.23. The average grain size (nm) of graphene film had a rising trend when CH_4/H_2 ratio was increased. When CH_4/H_2 ratio was increased, more hydrogen was produced. So, hydrogen reduces the defects formed at Ni grain boundaries. As a result, decreasing the defects helps graphene grains reconnect.

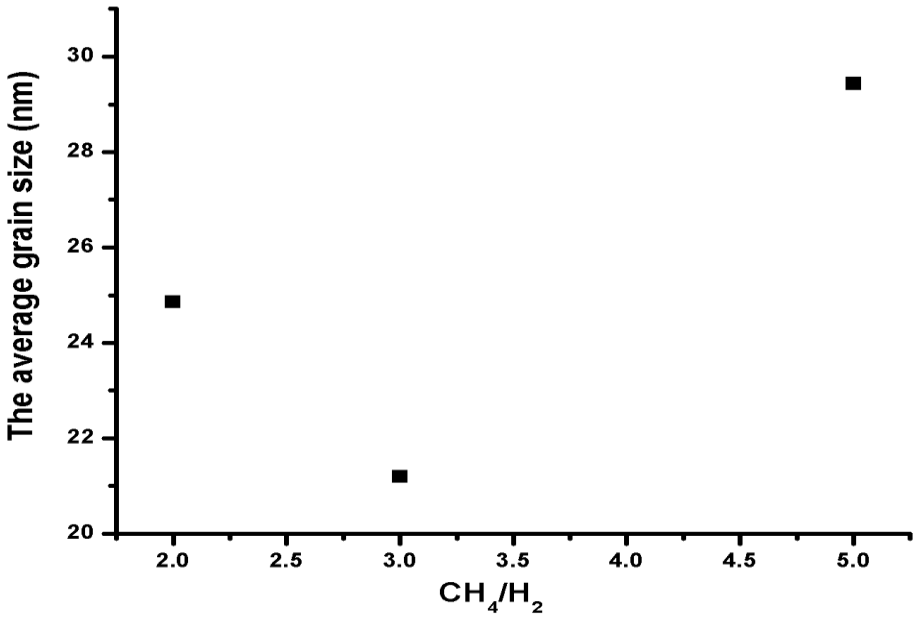

Figure 4.23: The average size of sp^2 domains (L_α) as a function of the CH_4/H_2 ratio.

The relationship between 2D-peak center and CH_4/H_2 ratios for graphene films grown on $Ni/SiO_2/Si$ substrate is illustrated in Figure 4.24. When the CH_4/H_2 ratio increased, the 2D peak center shifted up. This implies that the number of graphene films grown on the Ni film increased as described in section 2.1.

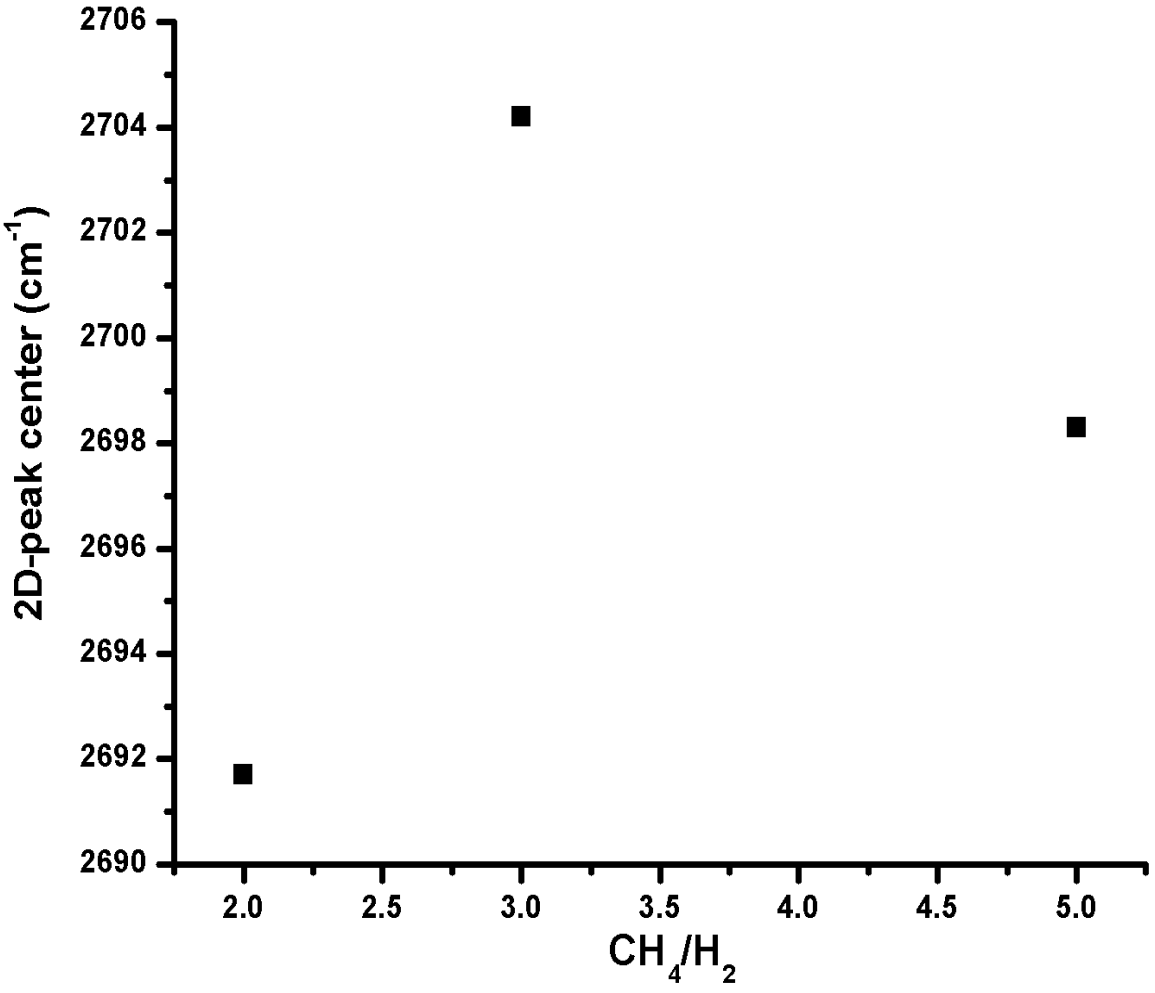

Figure 4.24: 2D-peak center as a function of the CH_4/H_2 ratio.

4.5 Effect of growth pressure on graphene synthesis using 200 nm nickel film-coated/Si_3N_4 substrates.

The effect of pressure on the synthesis of graphene formed on 200 nm nickel film-coated/Si_3N_4 substrate was investigated. Raman spectroscopy results of graphene film on Ni grown at 700 °C with different pressures (0.3, 0.5, and 1torr) are depicted in Figure 4.25.

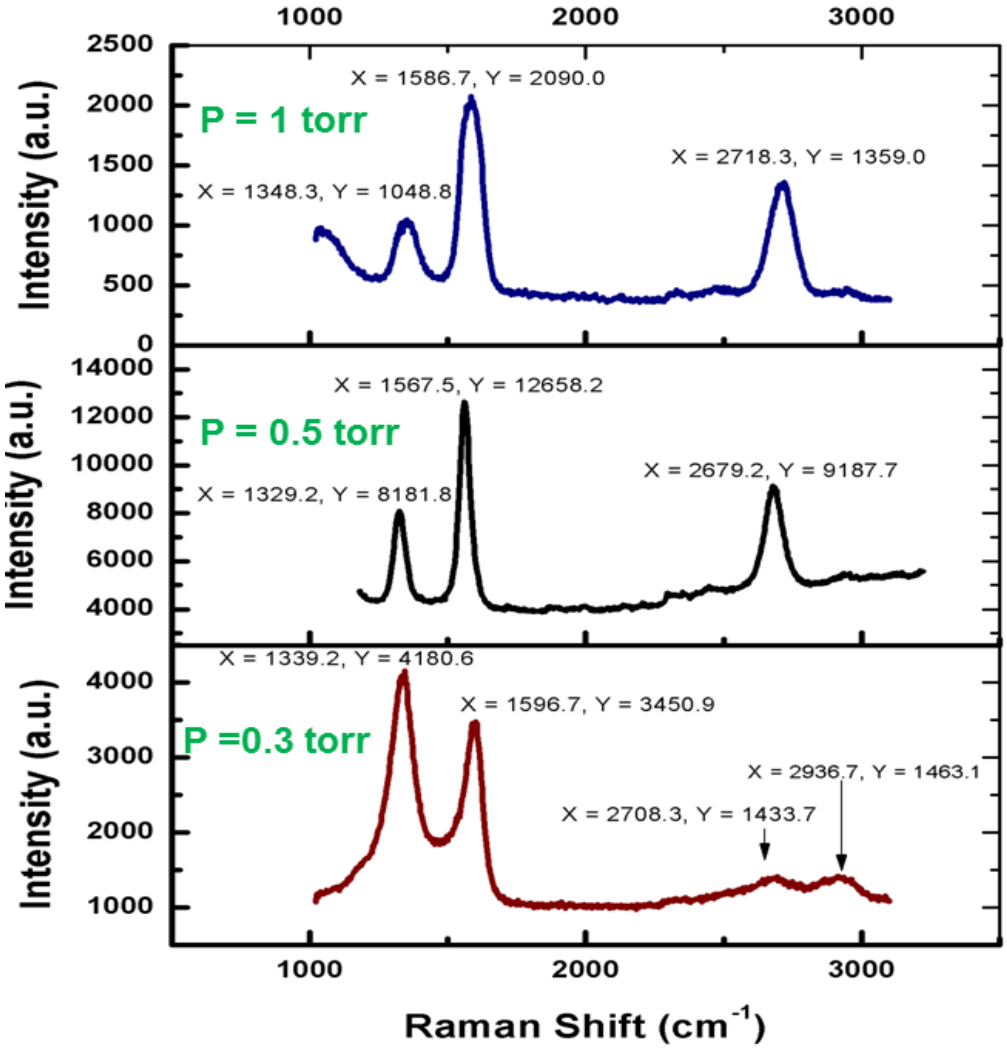

Figure 4.25: Raman spectra of graphene films grown on Ni/ Si_3N_4/Si substrate at different values of total pressure.

The CVD parameters used to study the effect of the total pressure on graphene film are illustrated in table 4.6

Table 4.6: The CVD parameters utilized in studying the effect of growth pressure on graphene synthesis using 200 nm nickel film-coated/Si_3N_4 substrates.

Substrate material	CH_4/ H_2 flow rate ratio (sccm)	Growth temperature (°C)	Growth pressure (torr)	Growth time (min)	Ni film thickness (nm)
Si_3N_4	15/5	700	0.3	5	200
	15/5	700	0.5	5	200
	15/5	700	1	5	200

In order to study the total pressure effect on graphene films grown at 700 °C on Ni/ Si_3N_4/Si substrate, Raman spectroscopy was utilized. I_{2D}/I_G is plotted vs. pressure in Figure 4.26.

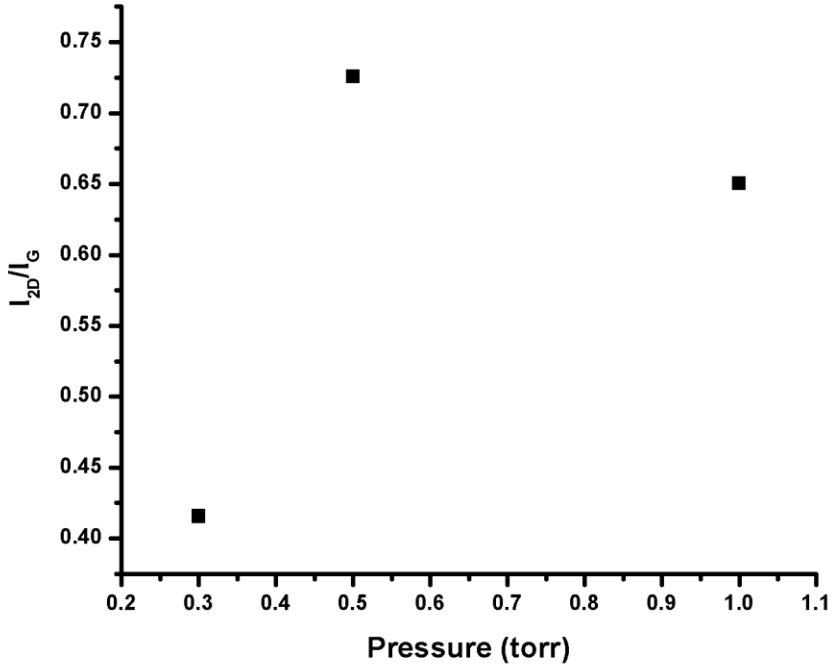

Figure 4.26: The I_{2D}/I_G intensity ratio of the graphene films as a function of the total growth pressure.

From Figure 4.26 there was a general upward trend in I_{2D}/I_G ratios when the pressure increased. Hence, the number of graphene films decreased. The relationship between the total pressure and the I_D/I_G intensity ratio in the graphene films is shown in Figure 4.27. Since the I_D/I_G intensity ratio was decreased with pressure, this means that the defects of the graphene film deposited on Ni/ Si_3N_4/Si substrate also decreased when the total pressure was increased.

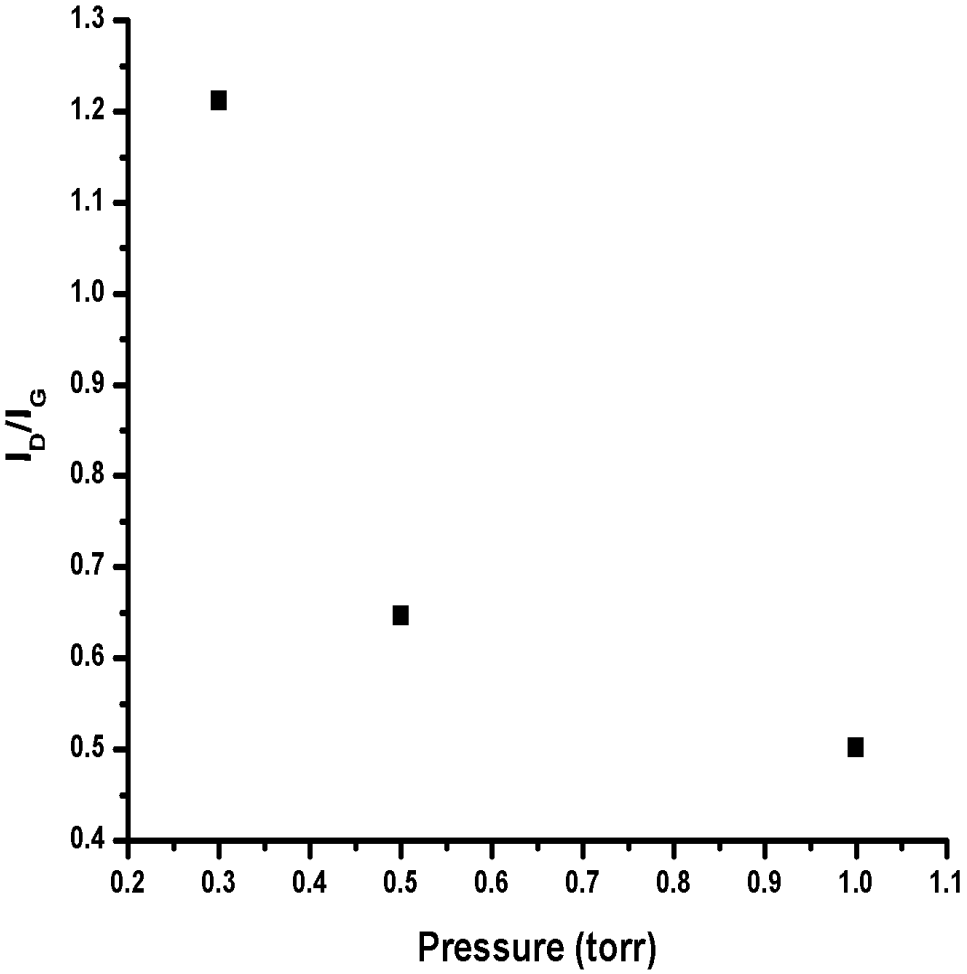

Figure 4.27: The I_D/I_G intensity ratio of the graphene films as a function of the total growth pressure.

The average size of sp^2 domains was calculated utilizing Equation 4.1 in order to investigate the relationship between sp^2 domain size and the I_D/I_G intensity ratio as well as the total pressure. As shown in Figure 4.28, the average grain size of graphene film decreased as the I_D/I_G intensity ratio increased. The average domain size of sp^2 dropped from 38 nm to 16 nm when the I_D/I_G intensity ratio increased from 0.5 to 1.2.

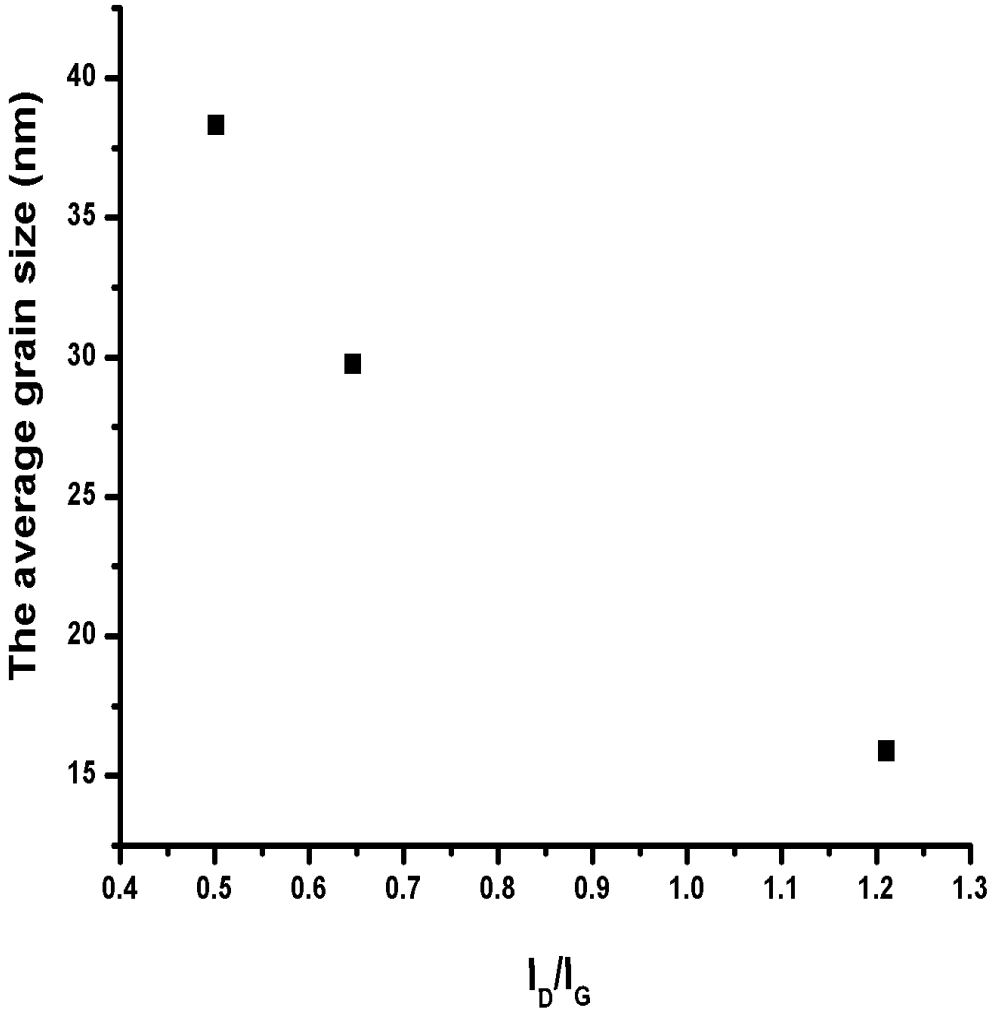

Figure 4.28: The relationship between the average grain size of graphene film (L_α) and The I_D/I_G intensity ratio of the graphene films.

Figure 4.29 illustrates the relationship between the average grain size of sp^2 domains and the total pressure. It is clear from the figure that the average grain size of graphene film increased when the growth pressure increased.

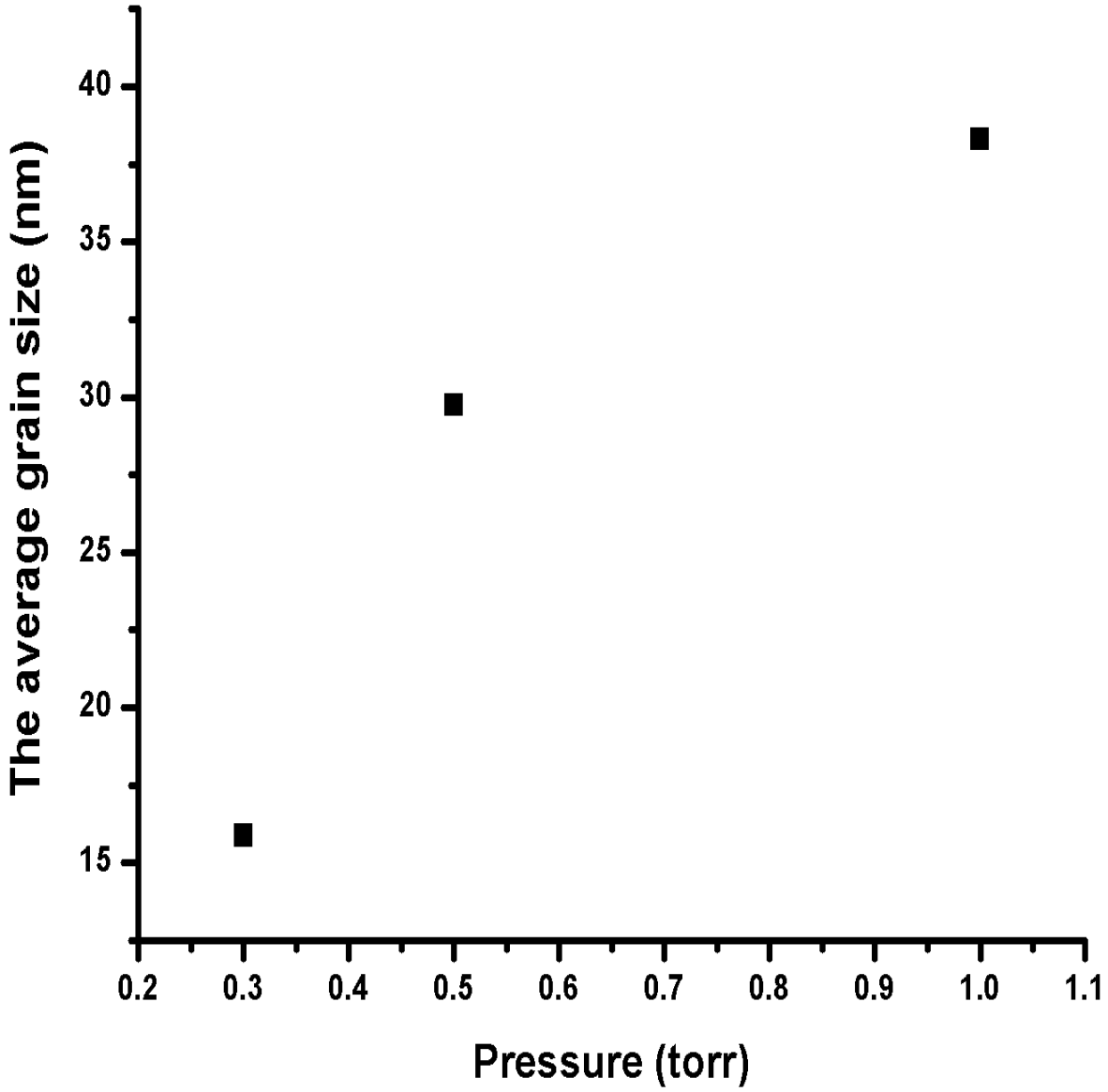

Figure 4.29: The average size of sp^2 domains (L_α) as a function of the total growth pressure.

4.6 Effect of growth temperature on graphene synthesis using 200 nm nickel film coated/Si_3N_4 substrates.

In this study, the effect of growth temperature on graphene film grown on Ni/ Si_3N_4/Si substrates at different temperatures was investigated using Raman spectroscopy. Raman spectra for graphene films fabricated at different temperatures are shown in Figure 4.30.

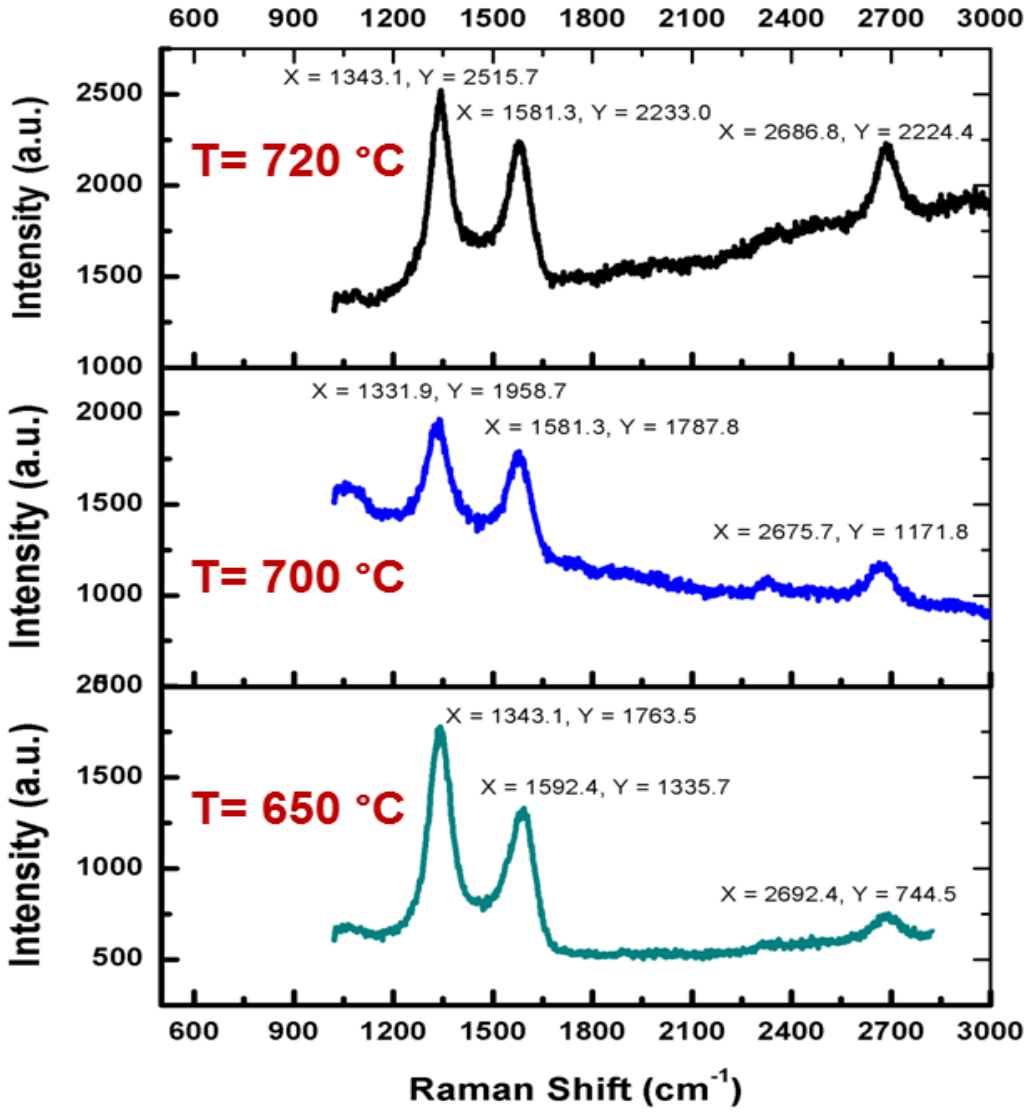

Figure 4.30: Raman spectra of graphene films grown on Ni/ Si_3N_4/Si substrate at different temperatures.

Graphene films were synthesized using different CVD parameters given in Table 4.7.

Table 4.7: The CVD parameters utilized in studying the effect of growth temperature on graphene synthesis using 200 nm nickel film-coated/Si_3N_4 substrates.

Substrate material	CH_4/ H_2 flow rate ratio (sccm)	Growth temperature (°C)	Total pressure (torr)	Growth time (min)	Ni film thickness (nm)
Si_3N_4	15/5	650	1.8	5	200
	15/5	700	1.8	5	200
	15/5	720	1.8	5	200

As shown in Figure 4.31, I_{2D}/I_G intensity ratio of the graphene films grown on Ni/ Si_3N_4/Si substrate increased with temperature. The number of graphene layers formed on the Ni/ Si_3N_4/Si substrate thus decreased when the growth temperature was increased.

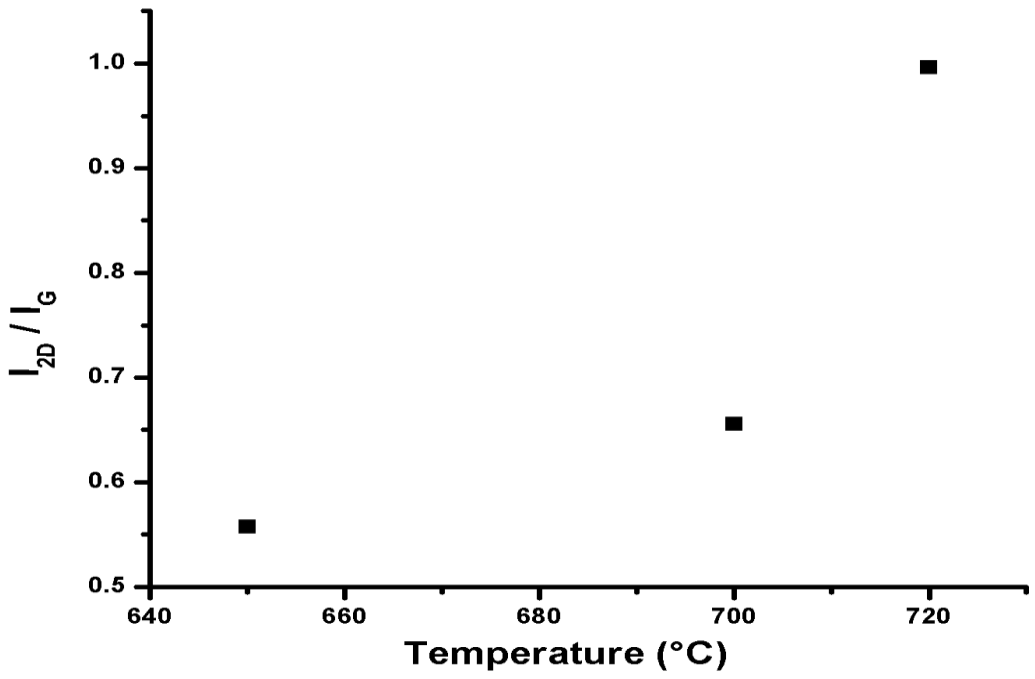

Figure 4.31: The I_{2D}/I_G intensity ratio of the graphene films grown on Ni/ Si_3N_4/Si substrate as a function of the growth temperature.

The I_D/I_G intensity ratio was used as an indicator to measure the quality of the graphene films. It is clear from the decrease in I_D/I_G that the quality of graphene film was improved as the growth temperature increased as depicted in Figure 4.32.

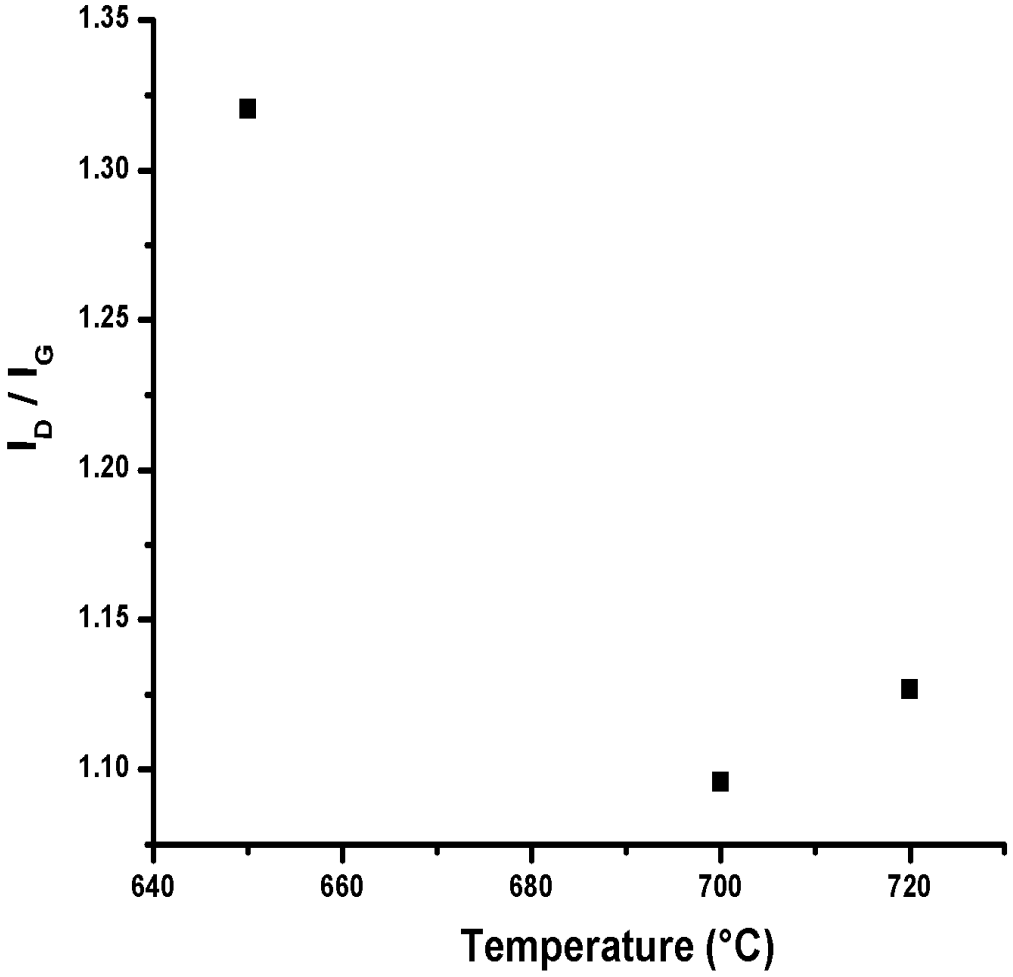

Figure 4.32: The I_D/I_G intensity ratio of the graphene films grown on Ni/ Si_3N_4/Si substrate as a function of the growth temperature.

The average calculated size of graphene film grains as a function of temperature is represented in Figure 4.33.

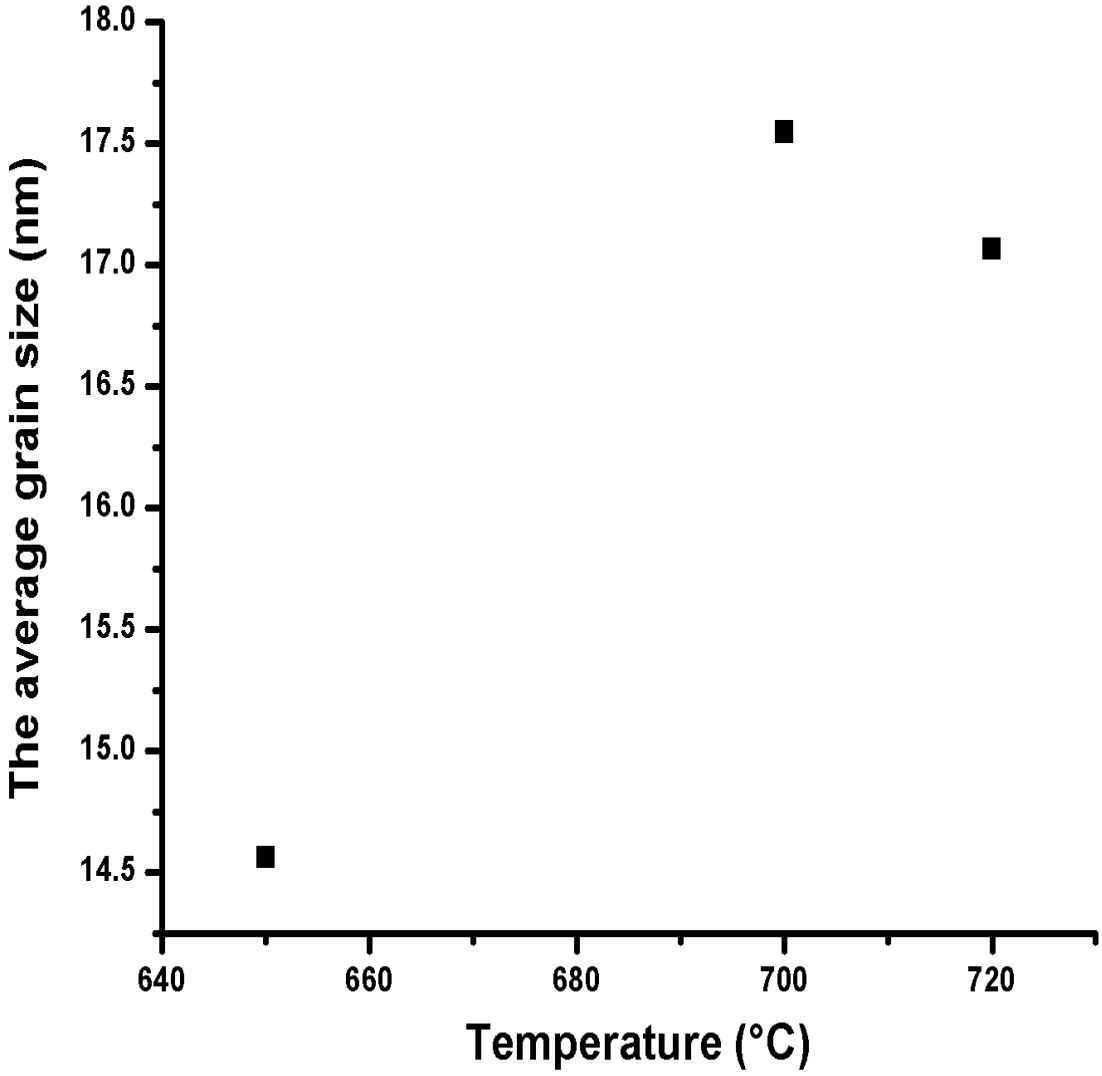

Figure 4.33: The average size of grain size (L_α) of the graphene films grown on Ni/ Si_3N_4/Si substrate as a function of the growth temperature.

Besides the graphene film quality improvement, Figure 4.33 shows that the average size of sp^2 domains (L_α) of the graphene films grown on Ni/ Si_3N_4/Si substrate increased as growth temperature increased.

Figure 4.34 illustrates the relationship between the centers of 2D-peak of the graphene films grown on Ni/ Si_3N_4/Si substrate and the growth temperature. It is observable from the figure that the 2D center of graphene films shifted to lower values as the growth temperature increased. This indicated that the number of graphene layers formed on Ni/ Si_3N_4/Si substrate decreased as the growth temperature increased.

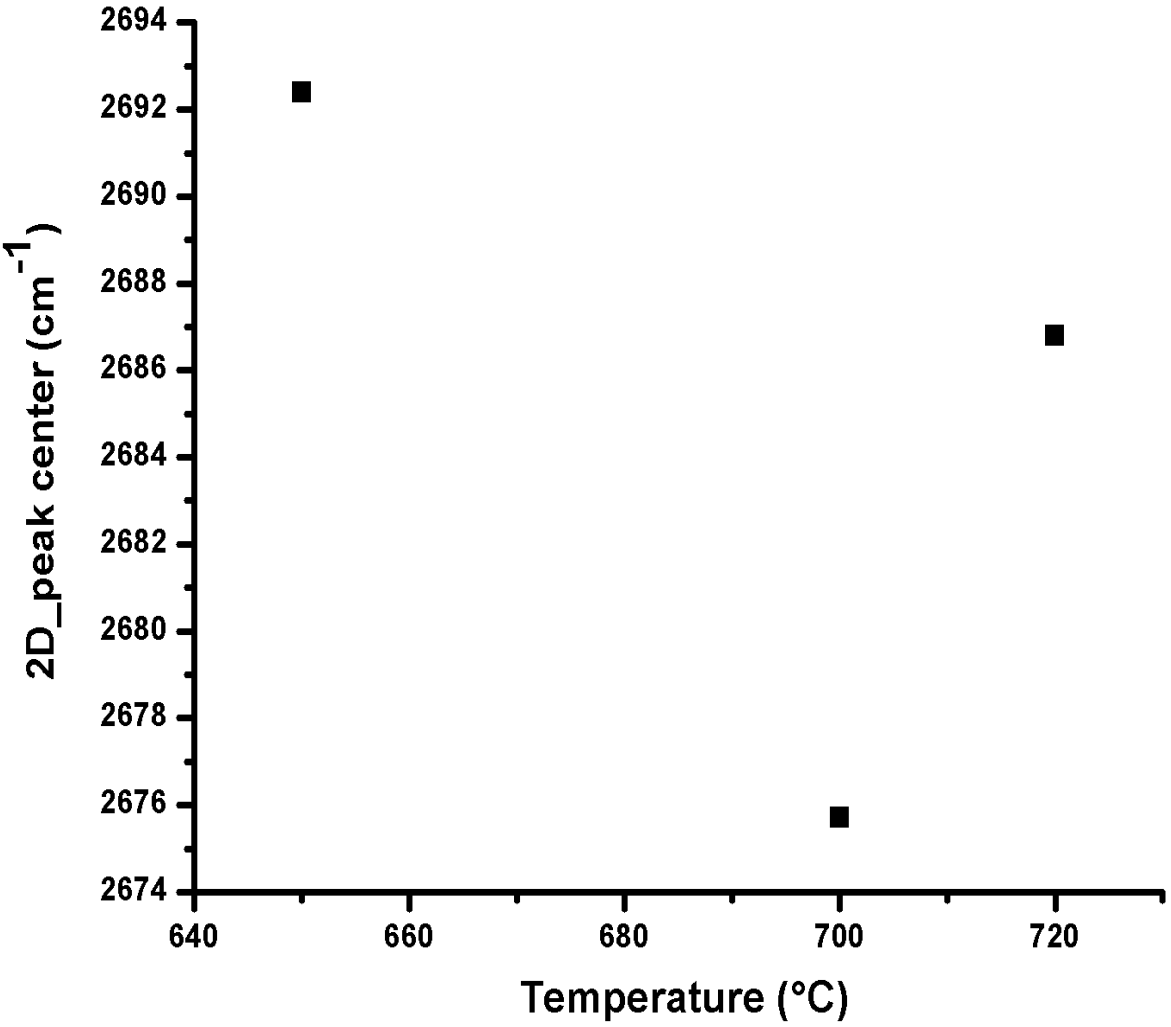

Figure 4.34: 2D-peak position the graphene films grown on Ni/ Si_3N_4/Si substrate as a function of the growth temperature.

4.7 Graphene etching by atomic hydrogen

In order to investigate the influence of atomic hydrogen on the etching of graphene formed on Ni surface. Different recipes were used in order to etch away the graphene film formed in the top surface of Ni film. Table 4.8 shows CVD parameters used to etch away the top graphene film in a minimum time of five minutes.

Table 4.8: Graphene etching CVD growth parameters using atomic hydrogen.

H_2 flow rate (sccm)	temperature (°C)	pressure (torr)	time (min)	Ni film thickness (nm)
5	500	0.5	5	200

Raman spectra for the surface of the Ni film before graphene deposition, after graphene deposition, and after graphene etching utilizing atomic hydrogen are shown in Figures 4.35, 4.36, 4.37, respectively.

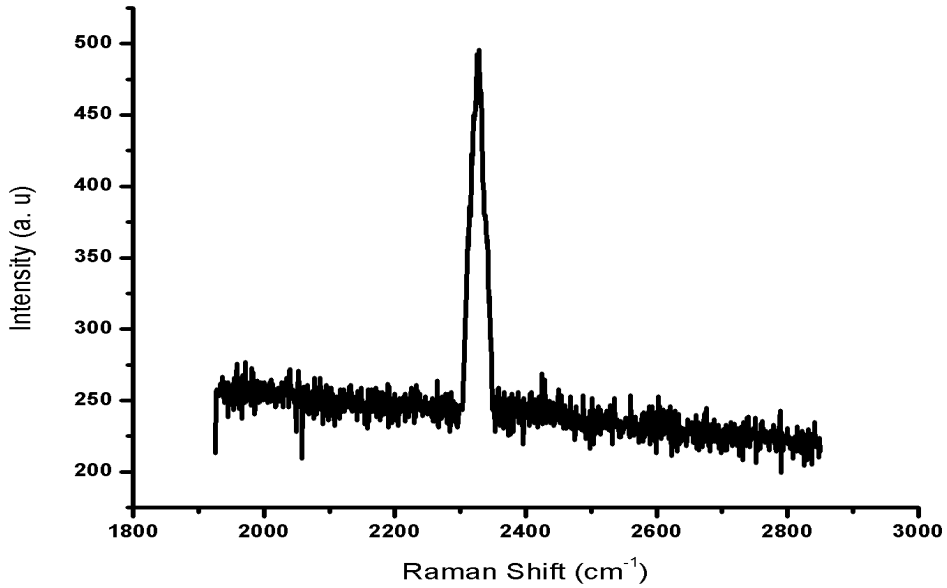

Figure 4.35: Raman spectra of Ni film before graphene deposition.

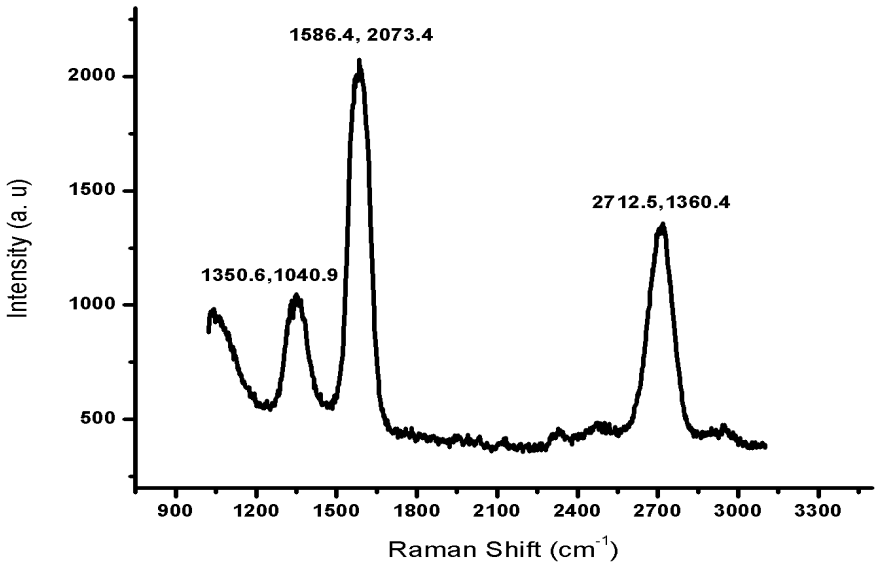

Figure 4.36: Raman spectra of graphene films grown on the top surface of Ni/ Si_3N_4/Si substrate after graphene deposition (and before atomic hydrogen etching).

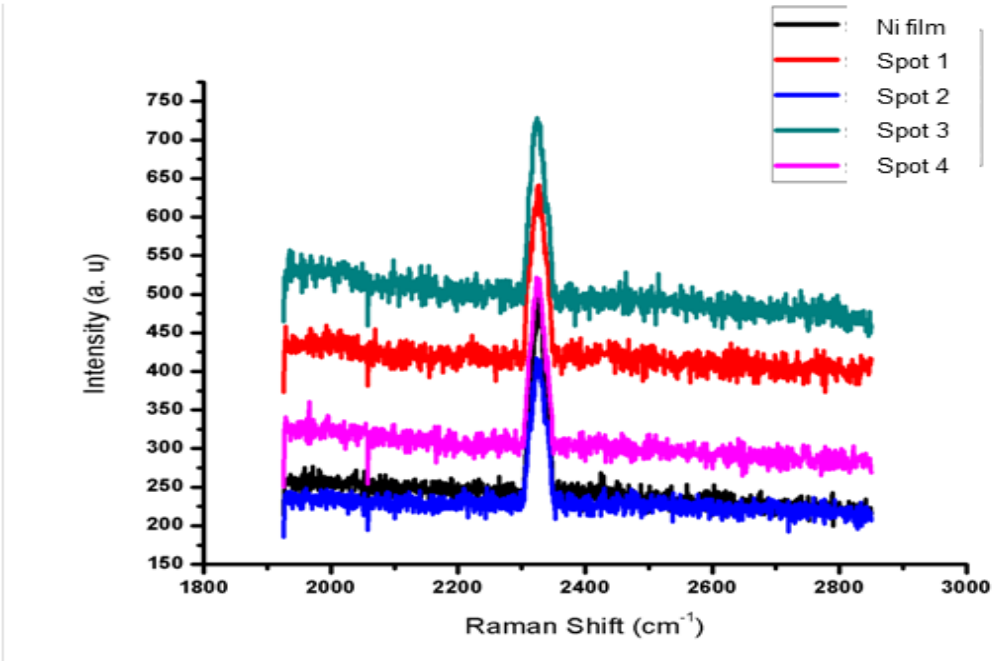

Figure 4.37: Raman spectra of graphene films grown on the top surface of Ni/ Si_3N_4/Si substrate after atomic hydrogen etching.

It is clear from the Raman spectra in Figure 4.37 that atomic hydrogen successfully etched the graphene film formed on the top surface of the Ni film.

The surface of the Ni film was imaged after graphene film etching by atomic hydrogen using scanning electron microscope (SEM) as illustrated in Figure 4.38. It is obvious from SEM image that atomic graphene film stacks up and agglomerate due to atomic hydrogen etching.

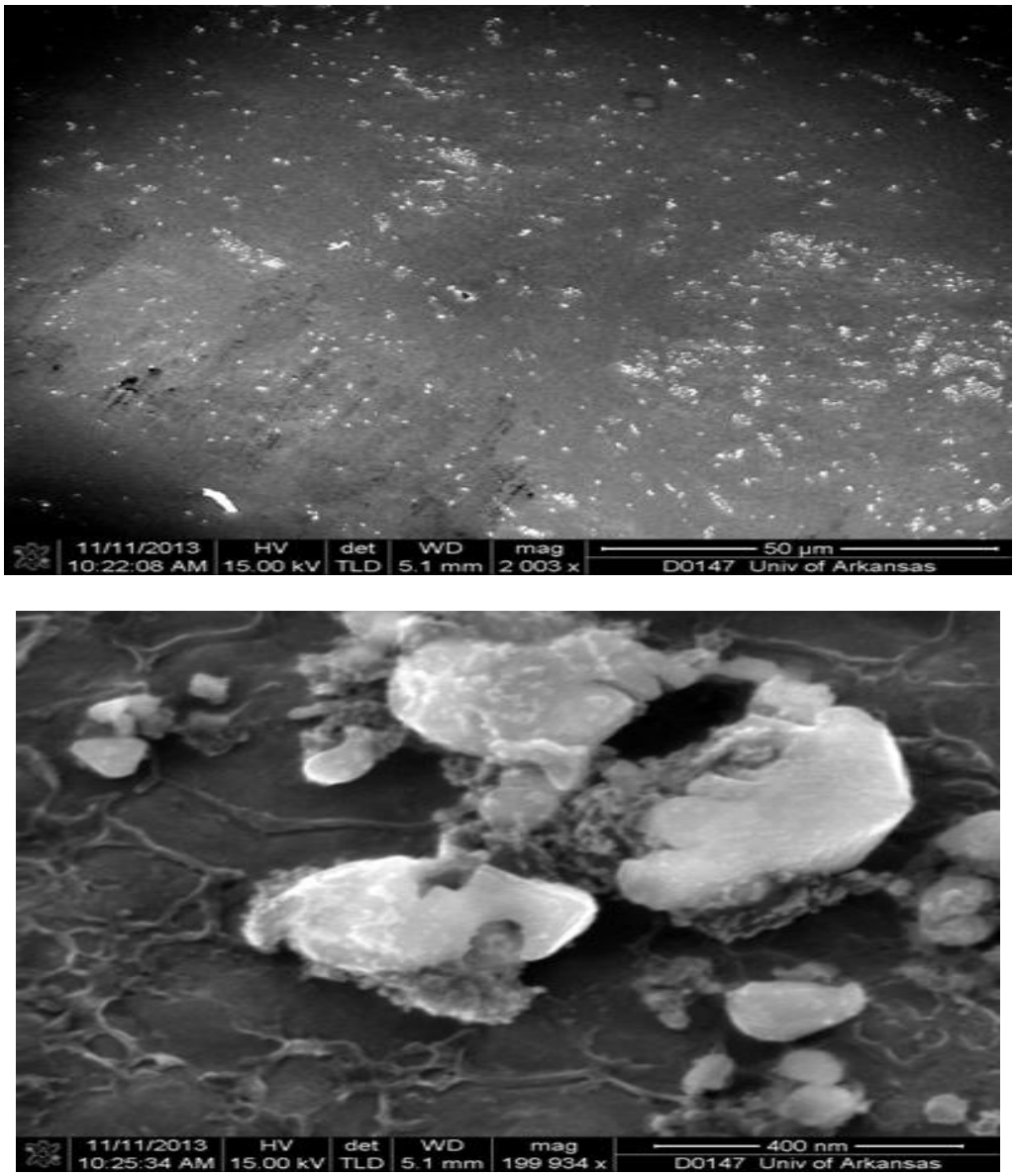

Figure 4.38: SEM image of graphene films grown on the top surface of Ni/ Si_3N_4/Si substrate after atomic hydrogen etching.

In addition, energy dispersive X-ray spectroscopy (EDX) was utilized for the elemental analysis of the top surface of Ni film. The EDX image in Figure 4.39 confirms that the graphene film and part of the Ni film were etched by atomic hydrogen.

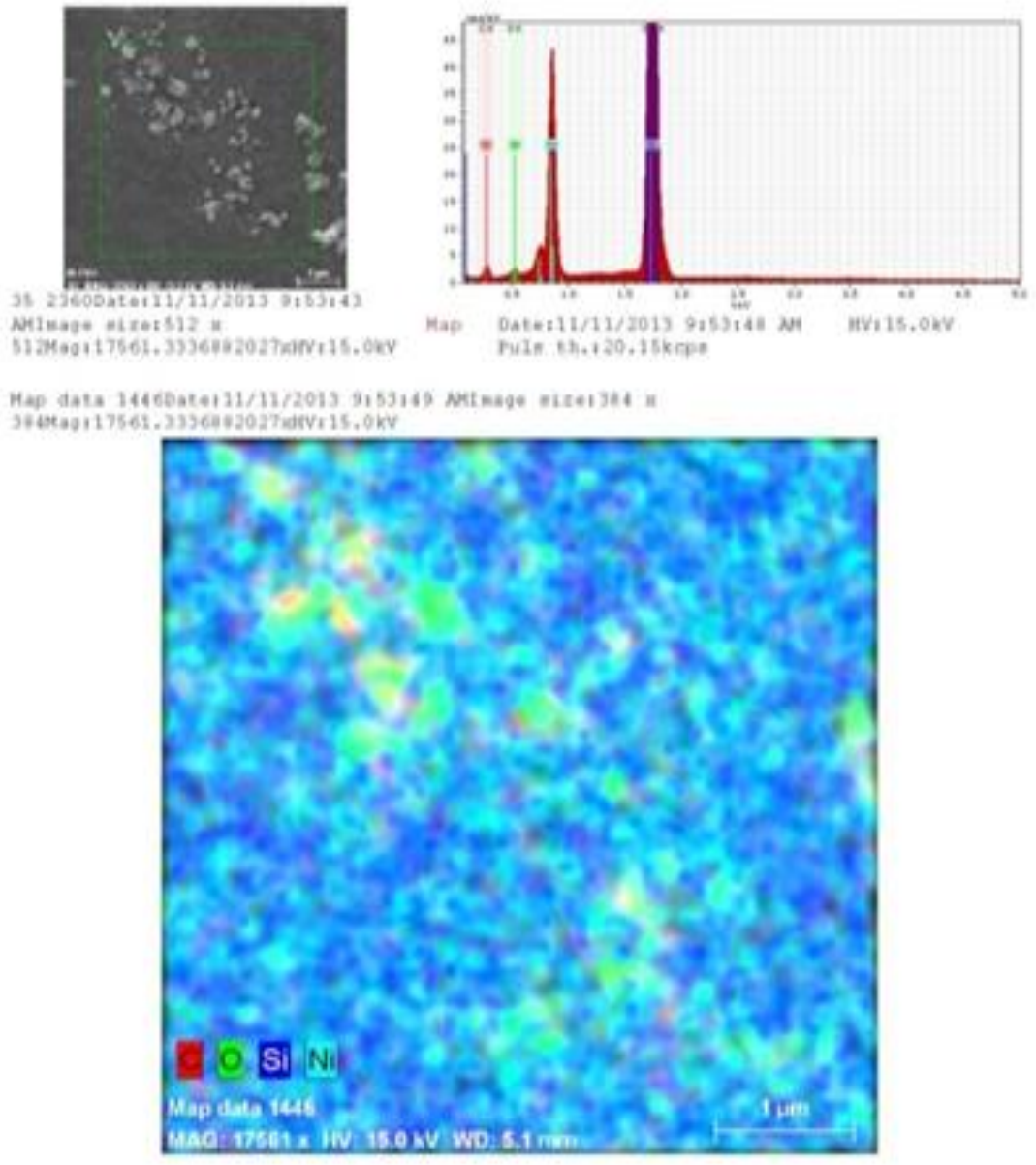

Figure 4.39: EDX image of graphene films grown on the top surface of Ni/ Si_3N_4/Si substrate after atomic hydrogen etching.

4.8 Graphene Formation at the interface between the Ni film and the Si-based substrates.

Large-scale graphene films (1 inch × 1 inch) were successfully grown at low temperature on the top surface of Ni thin films. The number of obtained graphene layers ranged from two to three as determined by the I_{2D}/I_G ratios of Raman peaks. Graphene films formed on the top surface of Ni films were etched away by hydrogen atoms to prepare Ni films for the next step – Ni removal. Removal of Ni film was achieved by scotch tape and $FeCl_3$ as described in section 1.3. Raman spectroscopy was then utilized to check for graphene formation at the interface between the Ni film and the Si-based substrates.

4.8.1 Graphene film formation on the backside of the Ni film deposited on Si_2N_3/Si and SiO_2/Si substrate:

During the graphene growth process, Ni films were annealed in Ar and H_2 ambient to facilitate the delamination of the Ni films. The adhesion of Ni films with different substrates; Si, SiO_2, Si_3N_4, DLC, and diamond were compared using scotch tape removal. The delamination of the Ni was easier for Ni films annealed in an Ar ambient compared with those annealed in a H_2 ambient. Among the substrates, the Ni film was found to have extremely poor adhesion (physical or chemical) with Si_3N_4/Si substrate and SiO_2/Si as shown in Figure 4.40 and Figure 4.43, respectively.

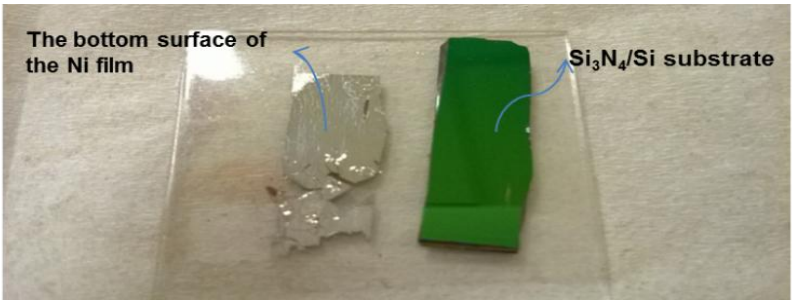

Figure 4.40: The photo of the backside of Peeled-off Ni film and Si_3N_4 substrate.

Graphene film formation on the backside of the Ni film deposited on SiO_2/Si substrate was examined. After removal of the Ni film, the graphene film on the backside of peeled off Ni film was investigated using Raman spectroscopy.

From the Raman spectra (Figure 4.41) of the graphene film formed on the backside of peeled off Ni film, it is clear that there was graphene formation, however, the peeling process caused a lot of damage to the graphene film as expected. Raman spectroscopy was also used to check graphene film formation on the Si_3N_4/Si substrate. There was no graphene film on Si_3N_4/Si substrate.

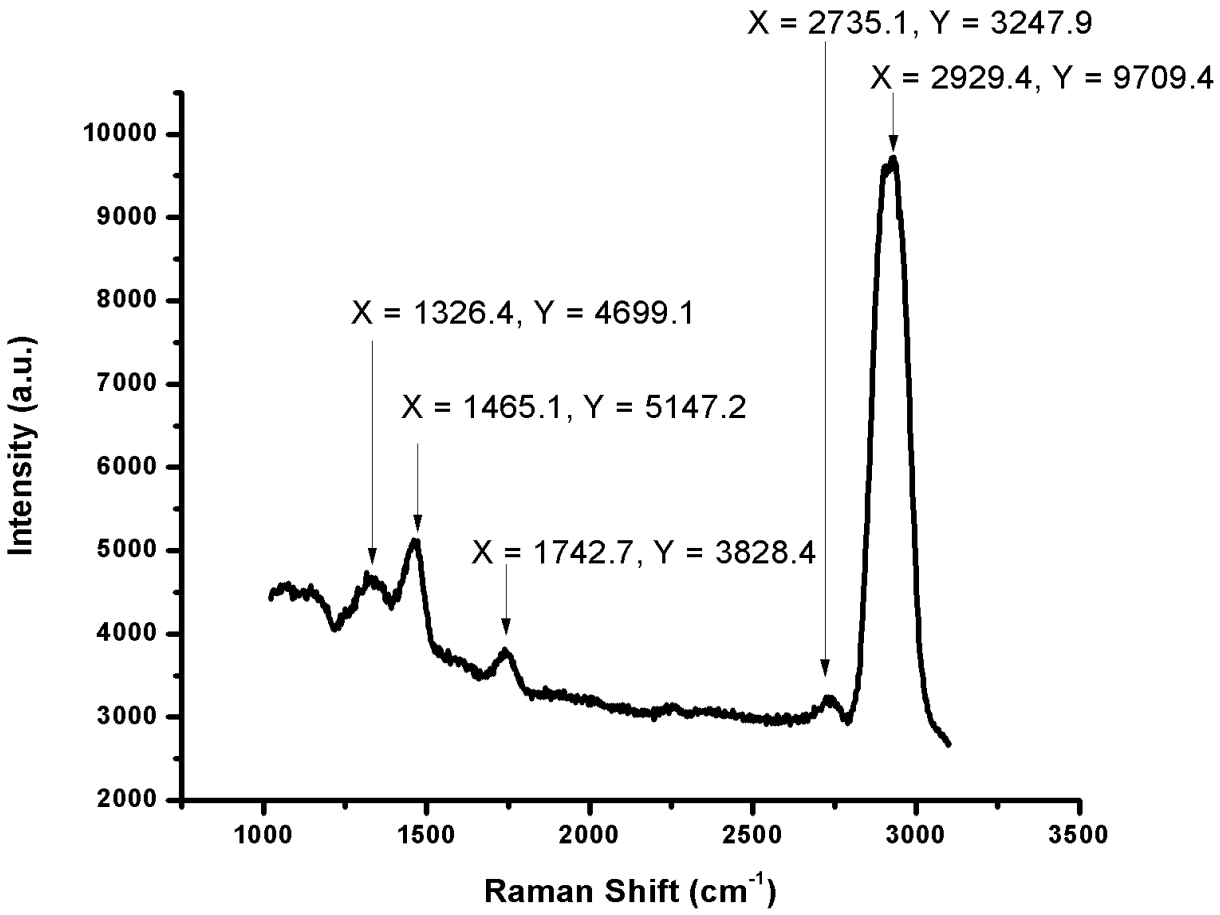

Figure 4.41: Raman spectra of graphene films grown on the bottom surface of the nickel film grown on Si_3N_4/Si substrate at 1 torr and 700 °C.

Figure 4.42 is the Raman spectra for the graphene film deposited on the topside of the Ni film for the same sample. The figure shows less defects compared with the level of the of graphene film defects illustrated in Figure 4.41.

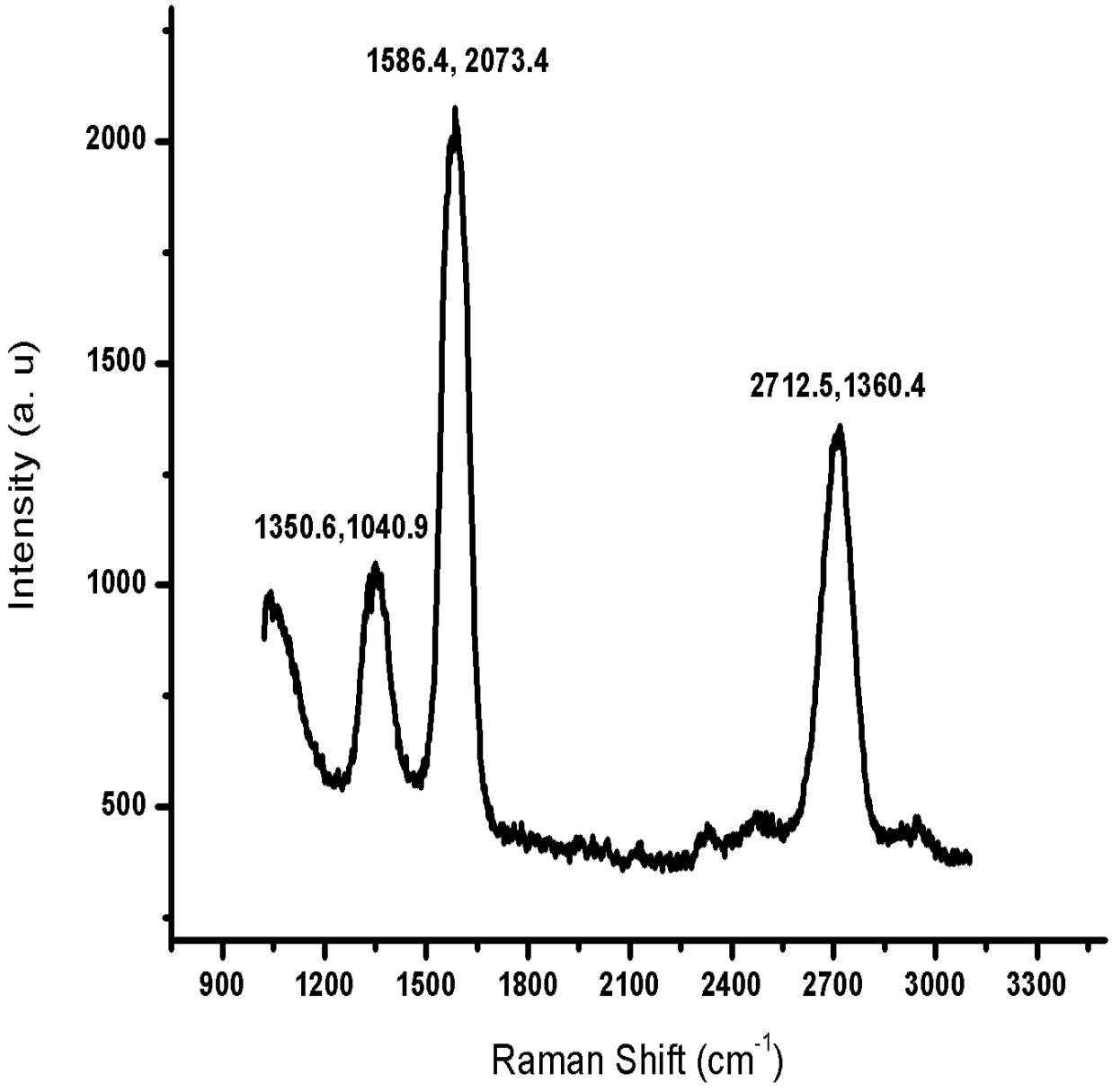

Figure 4.42: Raman spectra of graphene films grown on the top surface of the nickel film grown on Si_3N_4/Si substrate at 1 torr and 700 °C.

Also, graphene film formation on the backside of the Ni film deposited on SiO_2/Si substrate was investigated after Ni film removal using scotch tape. Figure 4.43 shows the top surface and back surface of Ni film deposited on SiO_2/Si substrate after removal of the Ni film using scotch tape. It may be seen in Figure 4.43 that the Ni film was not completely peeled off from the SiO_2/Si substrate. Raman spectroscopy was utilized to examine graphene film formation on the SiO_2 substrate and the bottom surface of the Ni film.

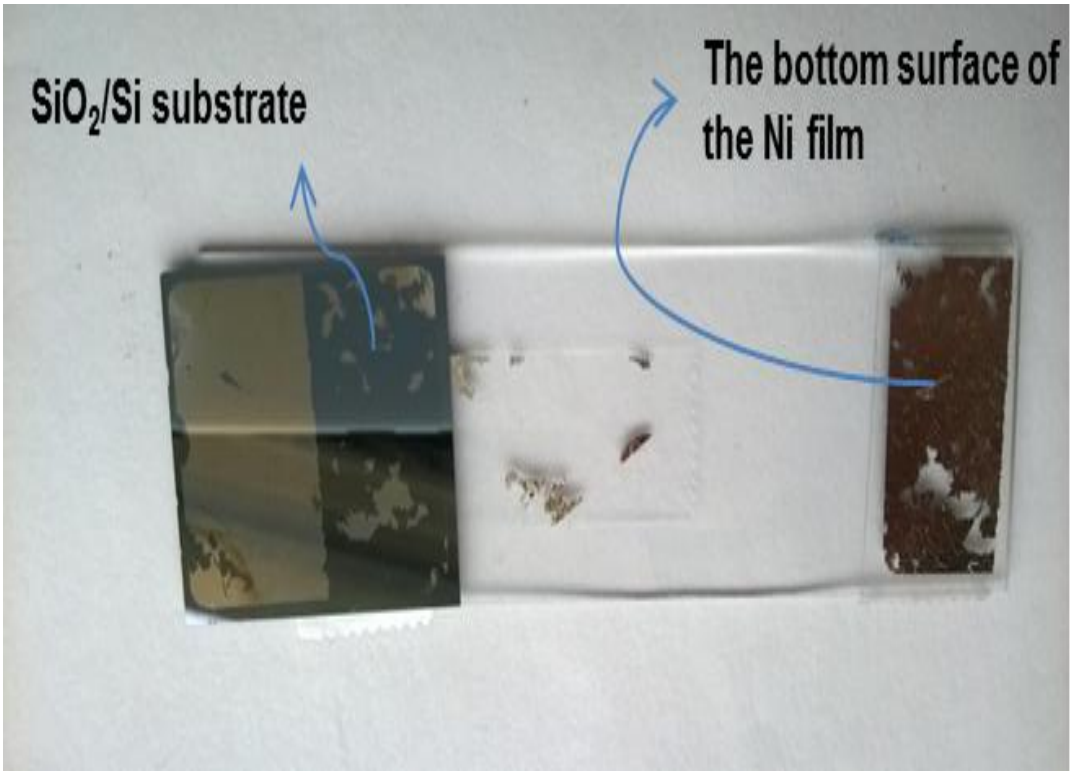

Figure 4.43: The photo of the backside of Peeled-off Ni film and SiO_2 substrate.

As illustrated in Figure 4.44, no graphene film was formed on the SiO_2 substrate. However, there was a growth of graphene film on the bottom surface of the Ni film. The peeling off process damaged the formed graphene film as indicated by the Raman spectra for the graphene film which had D+D', and which represents two-phonon defects, at 2930 cm^{-1}.

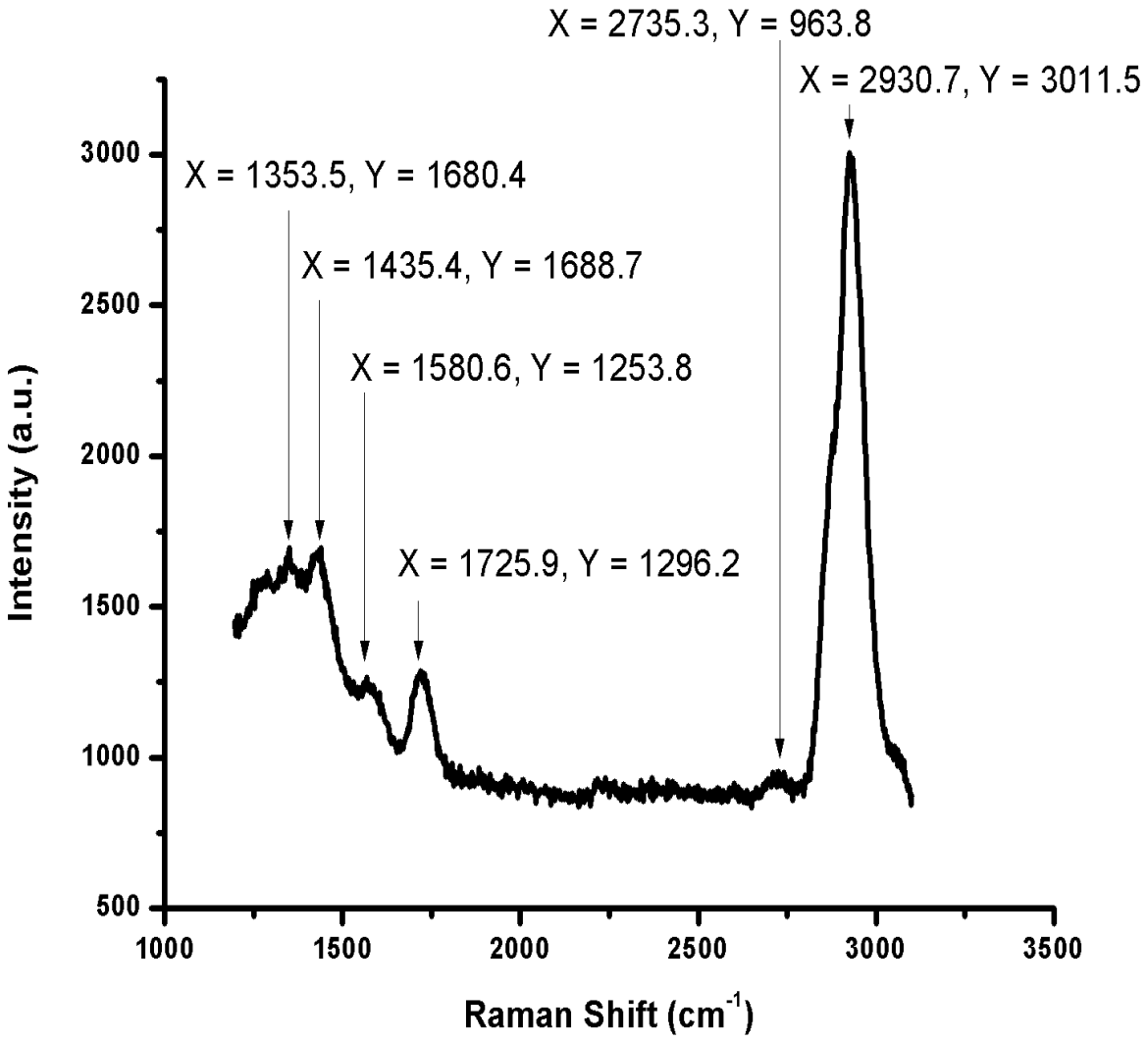

Figure 4.44: Raman spectra of graphene films grown on the bottom surface of the nickel film grown on SiO_2/Si substrate.

4.8.2 Graphene direct deposition on Si-based substrate

Ni thin film was removed utilizing ferric chloride ($FeCl_3$) in order to examine graphene film formation at the interface between the Ni film and Si-based material. Raman spectroscopy was used to ascertain whether graphene film existed under the removed Ni film.

Figure 4.45 shows Raman spectra for a sample where graphene film was grown on the top surface of the Ni film at 700 °C using CH_4/ H_2 flow rate ratio 10/5 sccm for 10 min with total pressure 1.5 torr.

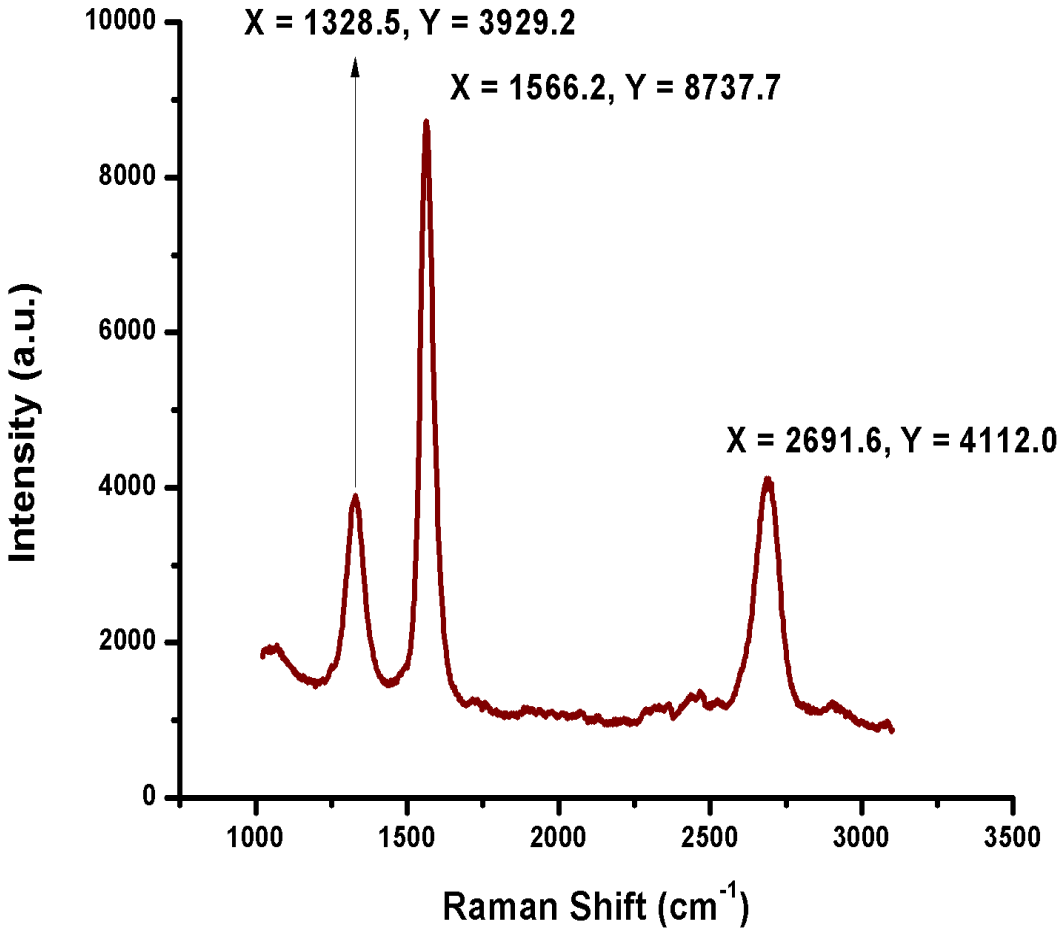

Figure 4.45: Raman spectra of graphene films grown on the top surface of the nickel film grown on SiO_2/Si substrate.

For the same sample shown in Figure 4.45, Raman spectroscopy was used to examine graphene formation after Ni etching using $FeCl_3$. Raman spectroscopy shows there was a direct formation of a graphene film on the SiO_2/Si substrate as shown in Figure 4.46.

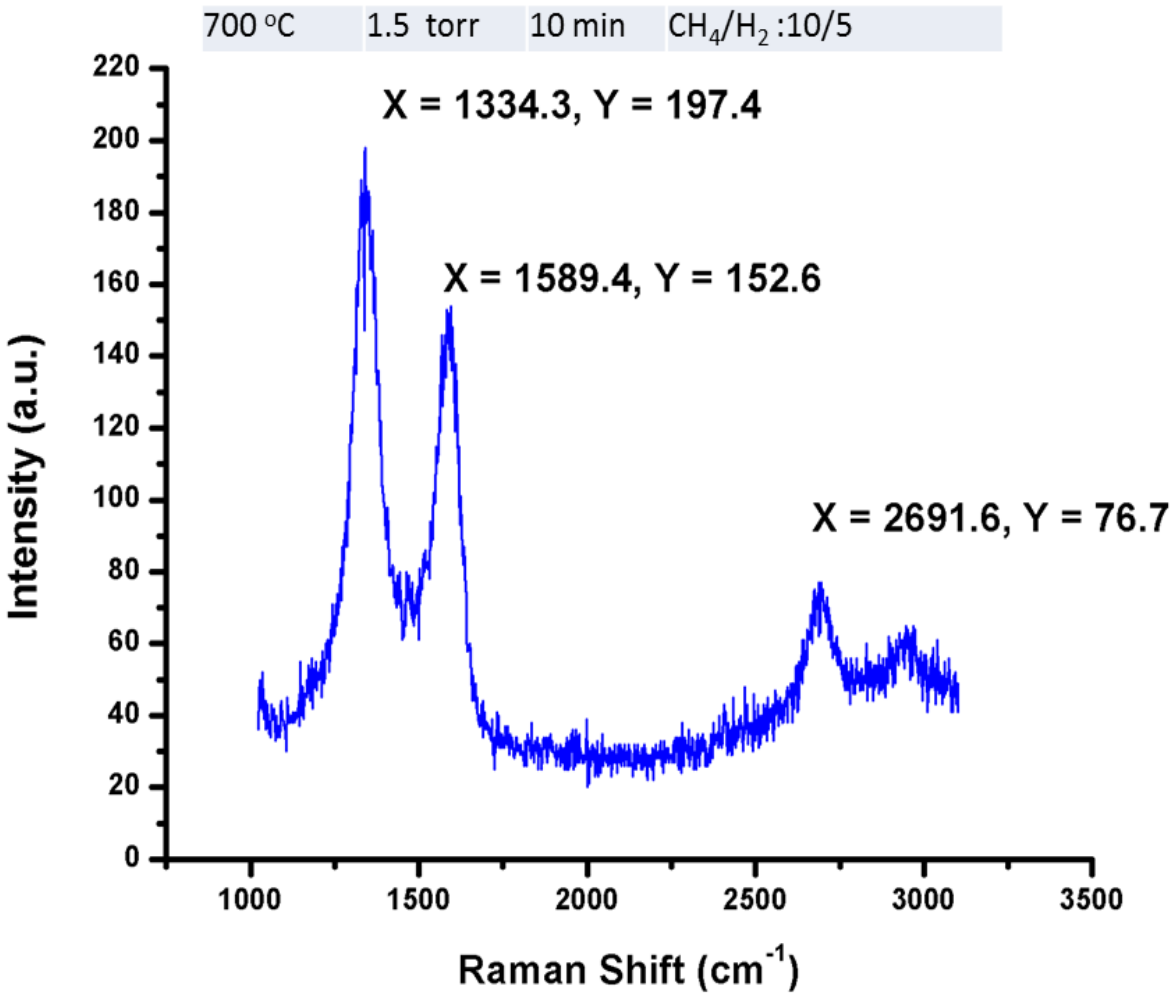

Figure 4.46: Raman spectra for graphene film formed directly on SiO_2 using CH_4/ H_2 flow rate ratio 10/5 sccm for 10 min.

From the Raman spectrum (Figure 4.46) of the graphene film, the I_{2D}/I_G intensity ratio indicates that there were three to four layers of graphene and a lot of defects on the obtained graphene film. The increase in the number of graphene layers and the high level of defects was due to the length of growth time (10 min). Also, there was not enough H_2 to inhibit the increase of the number of graphene layers and decrease the level the defects.

In contrast, when the time of graphene growth and the amount of hydrogen were increased, the number of graphene layers and the level of the defects were clearly decreased as shown in Figure 4.47.

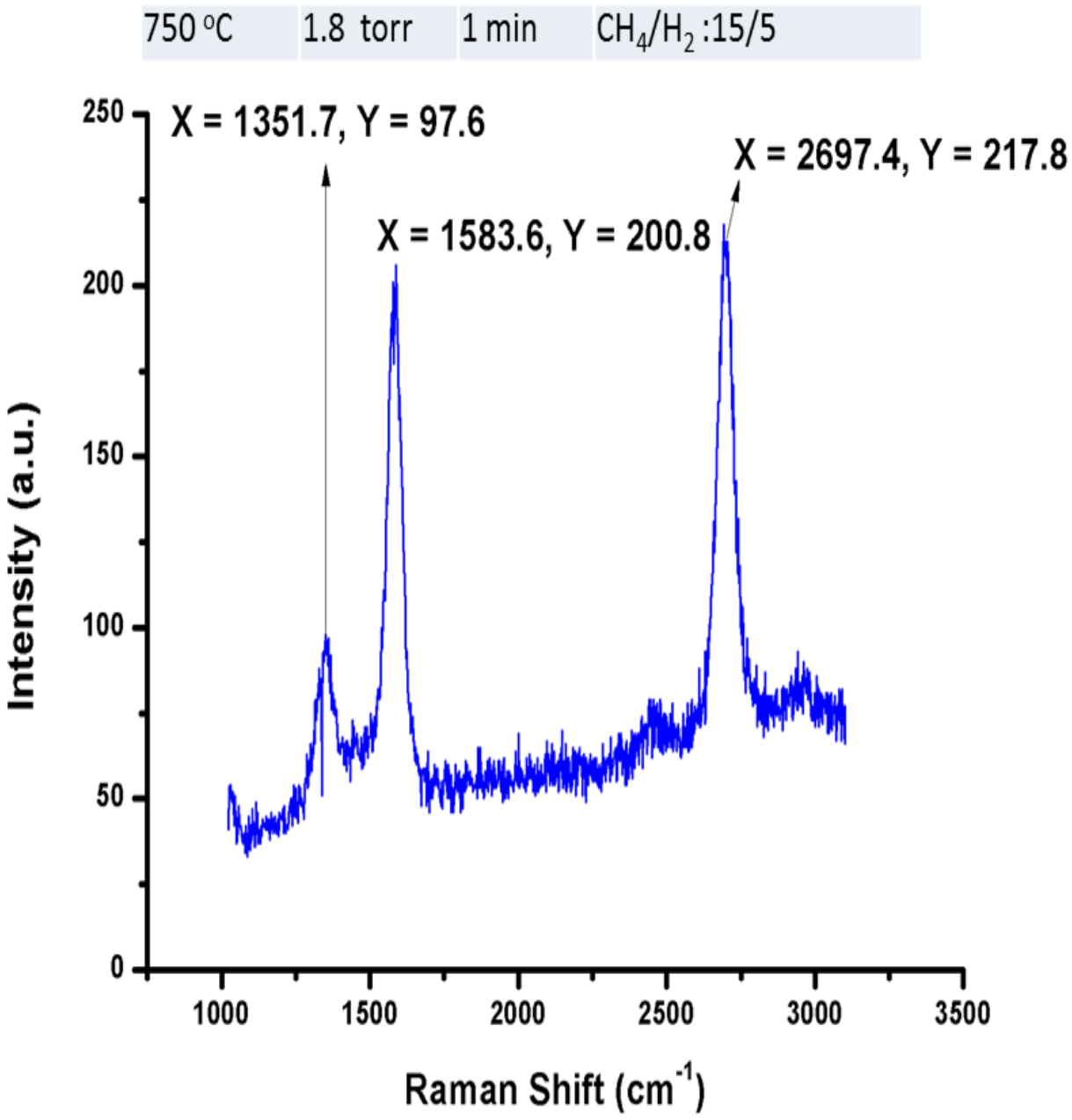

Figure 4.47: Raman spectra for graphene film formed directly on SiO_2 using CH_4/ H_2 flow rate ratio 15/5 sccm for 1 min.

Graphene film was deposited on the top surface of the Ni film at 750 °C using CH_4/ H_2 flow rate ratio 15/5 sccm for 1 min with total pressure of 1.8 torr; two layers of graphene were

formed on the SiO_2 substrate. Raman spectrum for the graphene film deposited on the top surface of the Ni film is shown in Figure 4.48 for this sample.

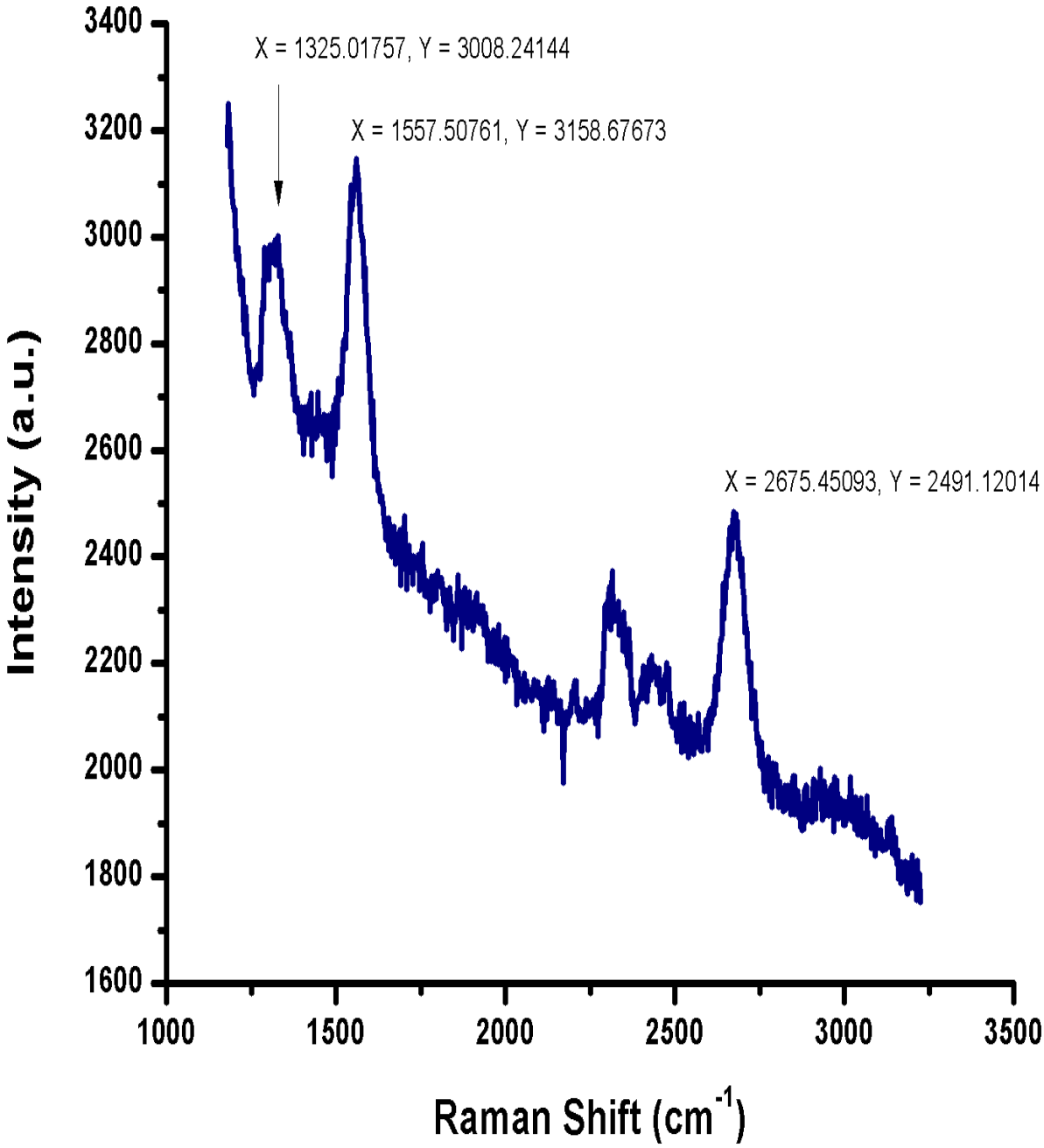

Figure 4.48: Raman spectra for graphene formed on the top surface of the Ni film using CH_4/ H_2 flow rate ratio 15/5 sccm for 1 min.

4.9 Simulated CVD graphene growth mechanism on nickel thin films

4.9.1 Carbon atoms inward diffusion in Ni film (Dissolution Stage)

The diffusion of Carbon atoms inside 200 nm thick Ni was simulated using COMSOL. The profile of carbon diffusion at 1000 °C into the Ni film at 0.05 sec is illustrated in Figure 4.49. The figure demonstrates carbon atoms diffusion inside the Ni film in -y-direction only.

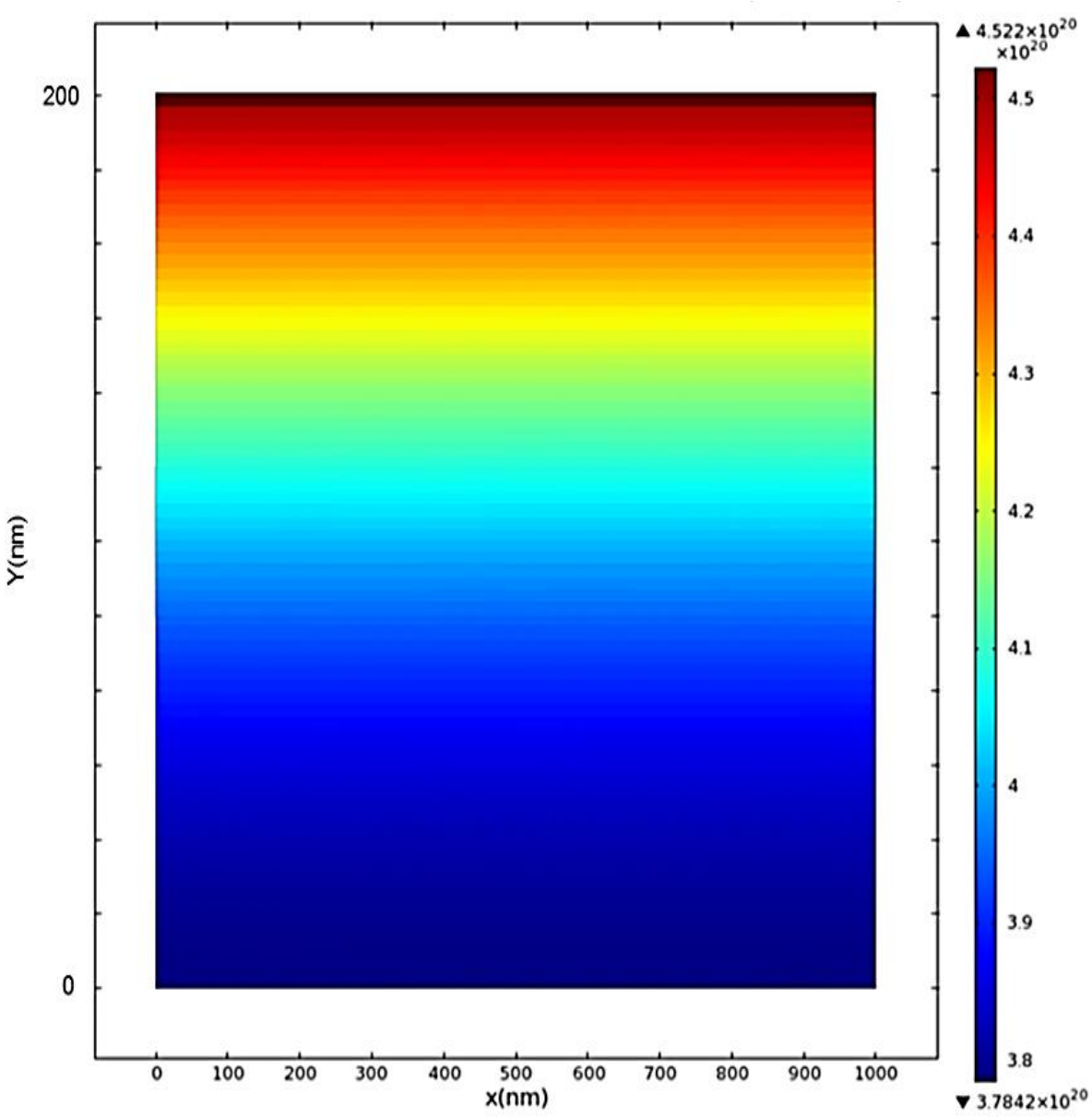

Figure 4.49: Calculated carbon atoms diffusion field at 1000°C inside 200 nm thick nickel film using COMSOL.

In order to investigate the influence of graphene growth temperature on carbon diffusion into the Ni film, the diffusion of carbon atoms was simulated with different temperature as shown in Figure 4.50. The figure clarifies how long it takes for the carbon diffusion process at 1000 °C to saturate 200 nm thick nickel film with carbon atoms. The Ni film reaches saturation in less than 0.05 second. The figure shows a faster diffusion of carbon atoms into the Ni film at higher growth temperatures.

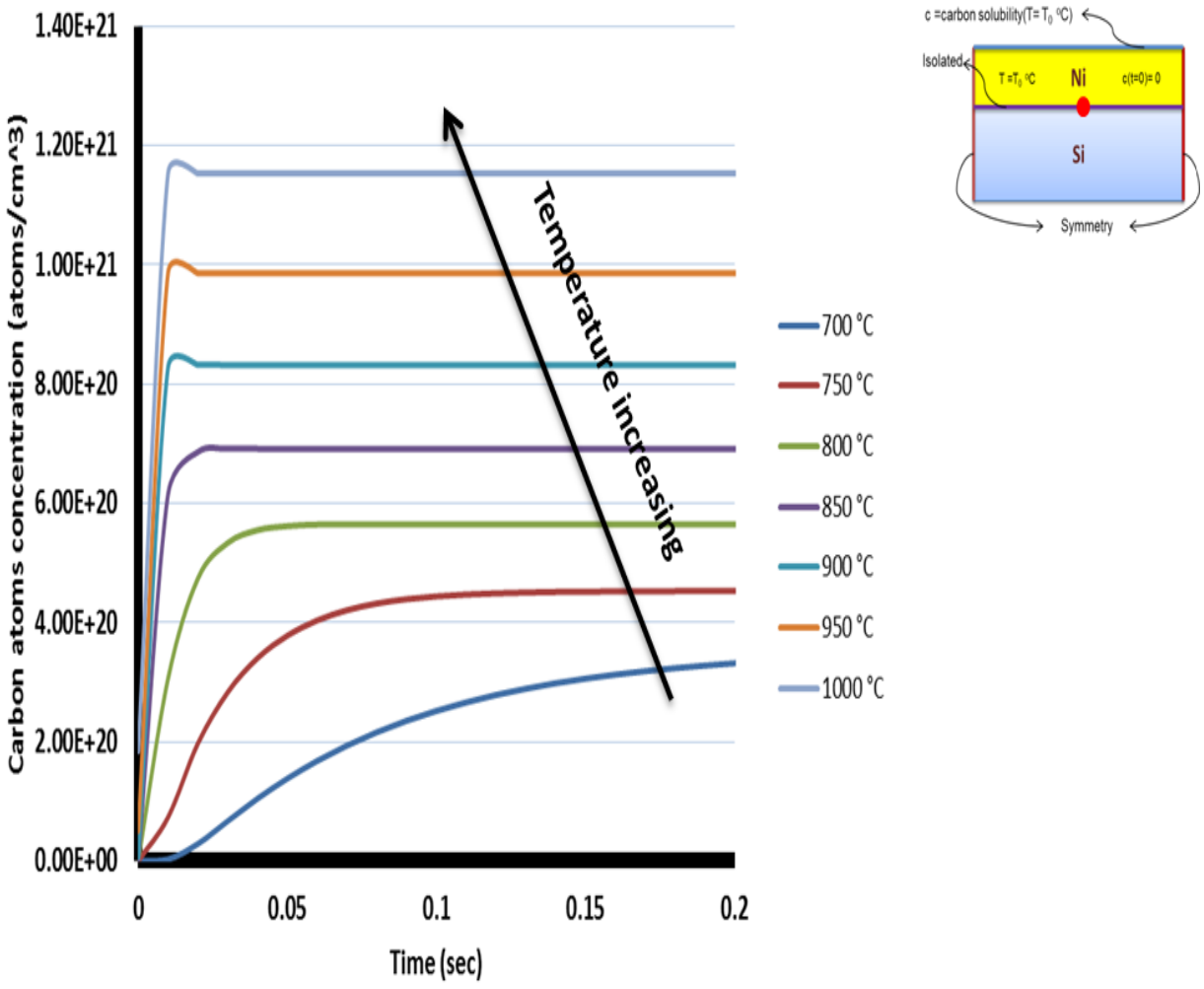

Figure 4.50: The influence of temperature on carbon atoms concentration at a point located on the bottom side of the Ni film during the carbon dissolution period.

Figure 4.51 shows that when the thickness of Ni film increases, the required time to reach the saturation level of carbon in the Ni film increases.

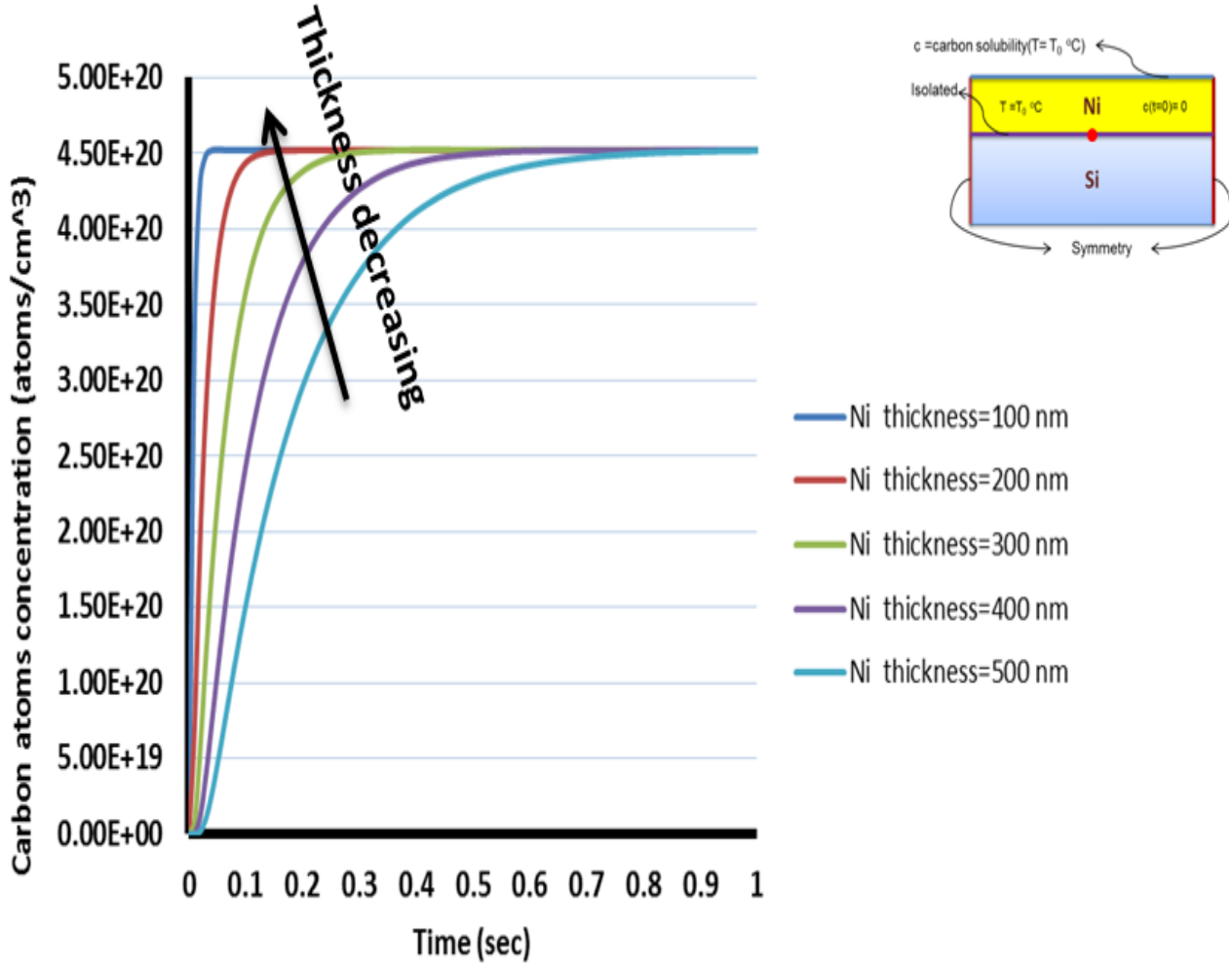

Figure 4.51: The influence of the Ni film thickness upon carbon atoms saturation in Ni film.

4.9.2 Carbon atoms outward diffusion in Ni film (Precipitation Stage)

In Chapter two, it was explained that carbon atom segregation occurs due to supersaturation upon cooling. The segregation of carbon atoms on the Ni film top surface during the cooling stage of graphene growth was simulated.

One can notice from Figure 4.52 that the carbon concentration inside the Ni film dropped from 1.0 x10^{21} (atoms/cm^{-3}) initially to 4.0 x10^{20} (atoms/cm^{-3}) in less than 0.2 sec when the Ni film temperature fell from 1000 °C to 725 °C.

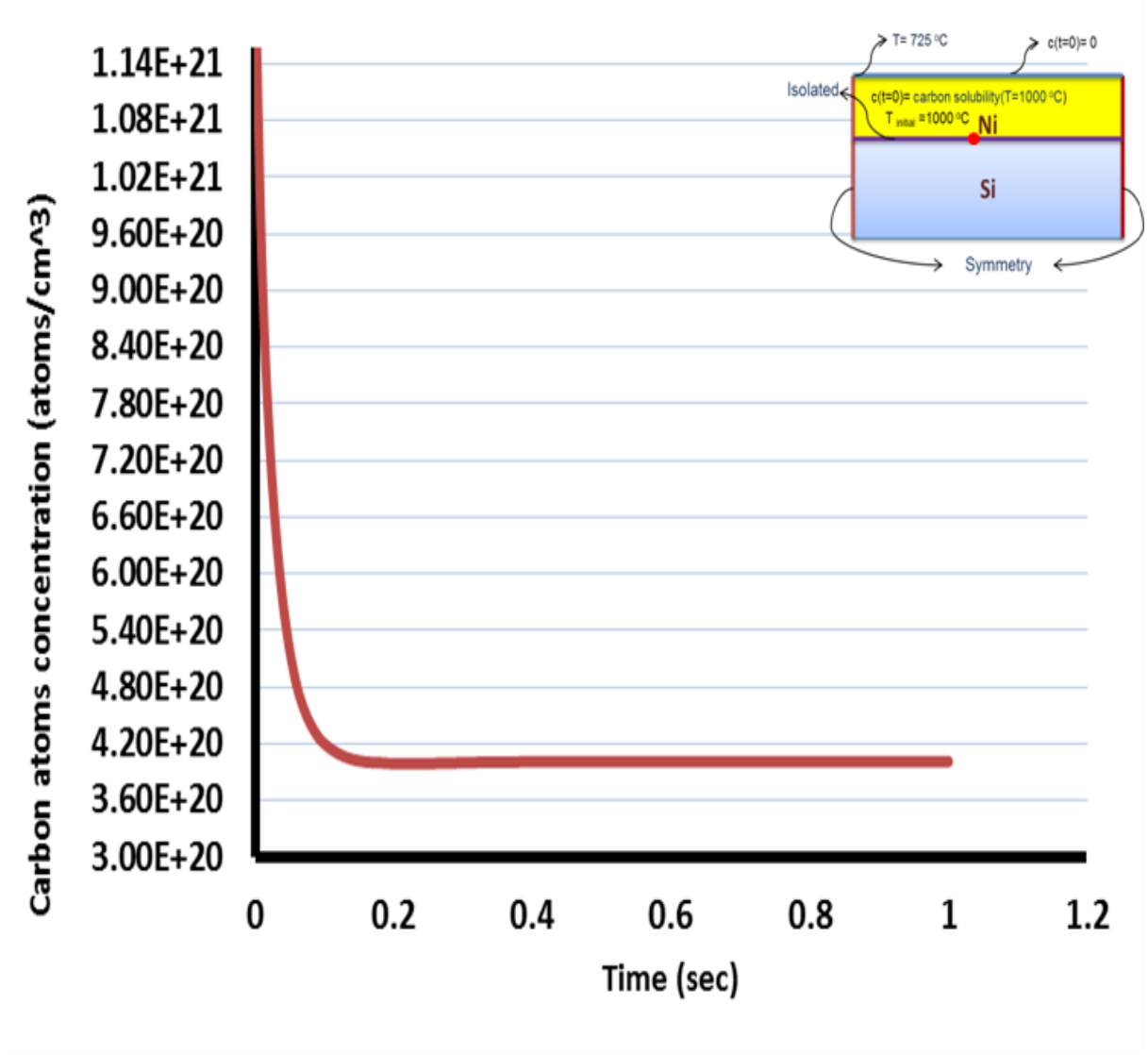

Figure 4.22: The decreasing in carbon atoms concentration due to the outward carbon atoms diffusion driven by supersaturation at a point located on the bottom side of the Ni during precipitation time.

Graphene layer formation on the top surface of the Ni film was simulated by a deforming mesh and diffusion transport model. It was initially assumed that the thickness of graphene film

on the top surface of the Ni film was zero. However, the thickness of graphene film increased by time due to the flux of carbon atoms in the y-direction through the interface between the Ni film domain and the nitrogen domain. So, in order to calculate the thickness of precipitated graphene film, the growth velocity in the +y-direction of the graphene film formed on the top surface of the Ni film was calculated using Equation 4.2.

$$v_y = \frac{\text{Carbon atoms flux}}{\text{The density of graphene}} = \frac{\vec{j}_m.\hat{n}_y}{\rho_{carbon}} \quad \text{Equation 4.2}$$

Where

v_y: The velocity the first participated graphene layer on the top surface of the Ni film

$\vec{j}_m.\hat{n}_y$: Carbon atoms flux in +y-direction

ρ_{carbon}: The density of graphene; 2.267 g/cm^3

Then, the thickness of the precipitated graphene film on the top surface of the Ni film was calculated utilizing Equation 4.3.

$$d = v_y * t \quad \text{Equation 4.3}$$

Where

d: The thickness of precipitated graphene film on the top surface of Ni film

t : Carbon atoms precipitation time

Hence, the number of obtained graphene layers (N) was calculated using Equation 4.4.

$$N = \frac{d}{\Delta d} \quad \text{Equation 4.4}$$

Where

N: The number of achieved graphene layers on the top surface of Ni film.

Δd: The thickness of single layer of graphene (0.335 nm) [35].

So, the number of precipitated layers of graphene film formed on the top surface of the Ni film could be calculated using Equations 4.2, 4.3, and 4.4.

Figure 4.53 illustrates the final thickness of the graphene film formed on the top surface of the Ni film in less than 0.2 sec was 7 Å when the 200 nm thick Ni film temperature was dropped from 1000 °C to 725 °C.

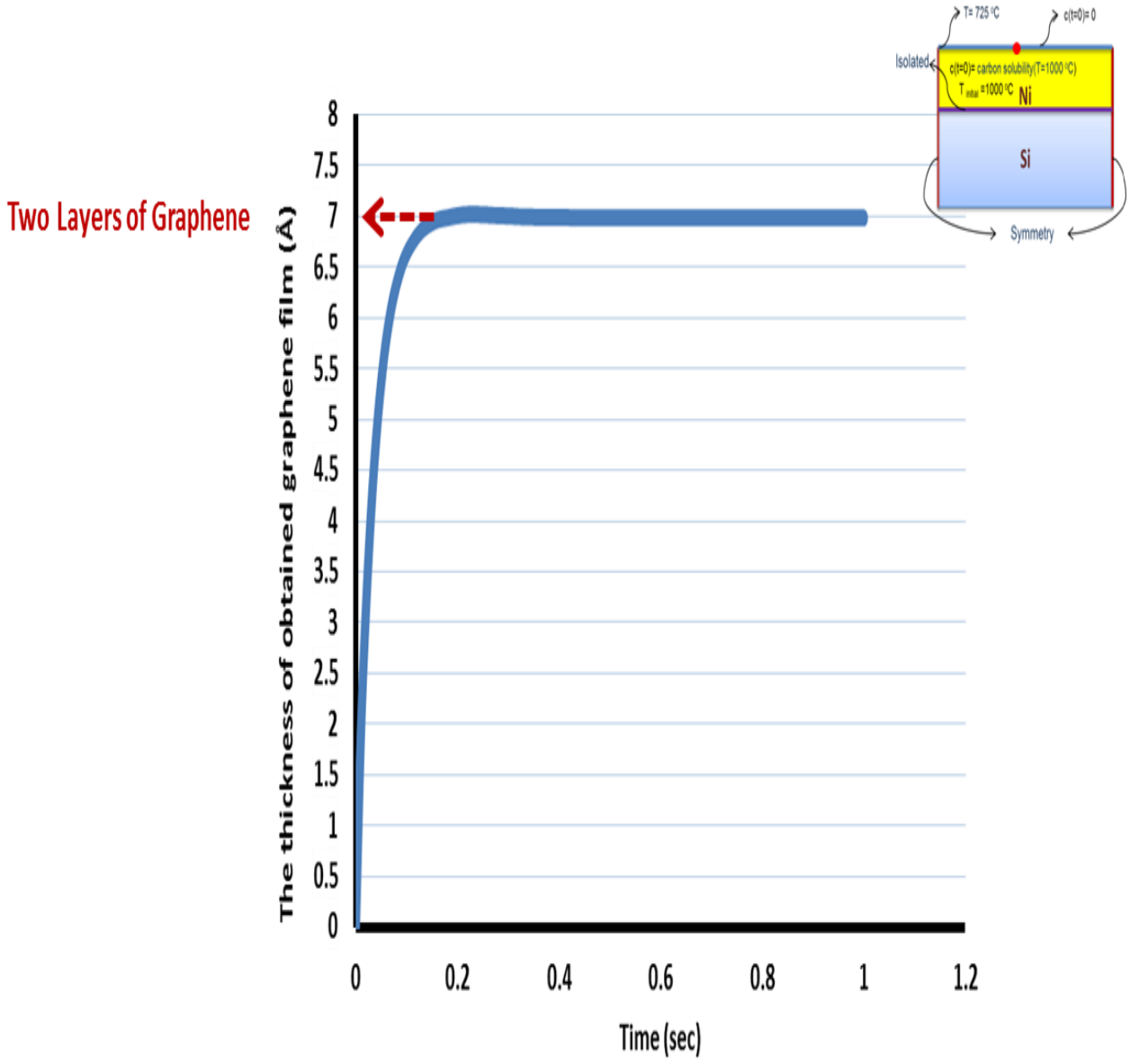

Figure 4.53: The thickness of the graphene film formed on the top surface of the Ni film when the Ni film temperature drops from 1000 °C to 725 °C.

When the 200 nm thick Ni film temperature was dropped from 900 °C to 725 °C, the number of calculated graphene film layers formed on the top surface of the Ni film within 0.4 sec was 1.7 layers as shown on Figure 4.54.

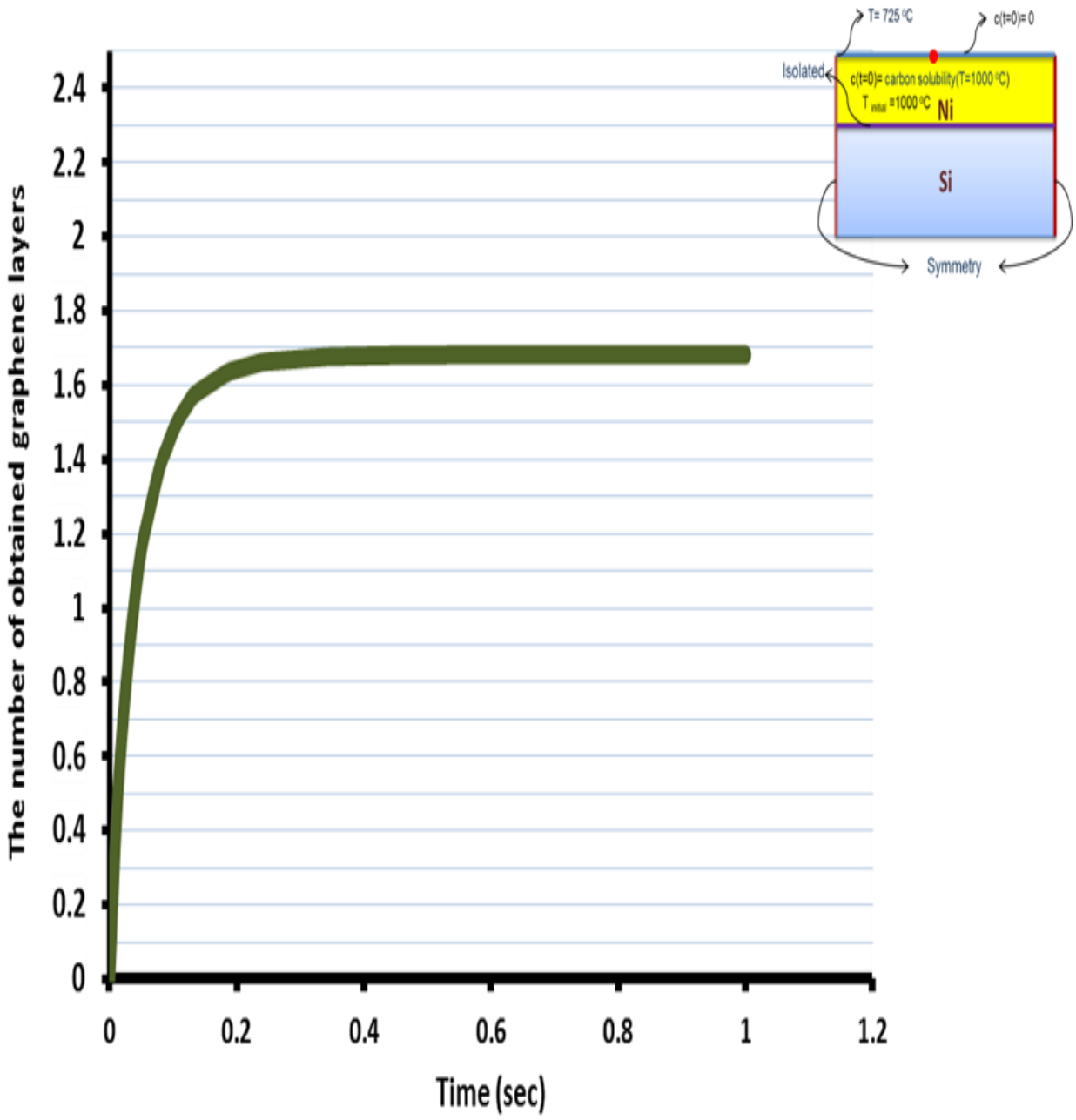

Figure 4.54: The number of the obtained graphene layers on Ni film surface after cooling from 900 °C to 725 °C.

More details on the effect of cooling an 200 nm Ni film on the formation of graphene layers on the nickel surface were studied. The number of graphene layers formed on the Ni film top surface when the Ni film cooled from 1000 °C to different temperatures is illustrated in Figure 4.55. For example, it is clear from this figure that when the nickel film was cooled from1000 °C to 725 °C, the number of graphene layers formed on the top surface of the Ni film was ~2 layers.

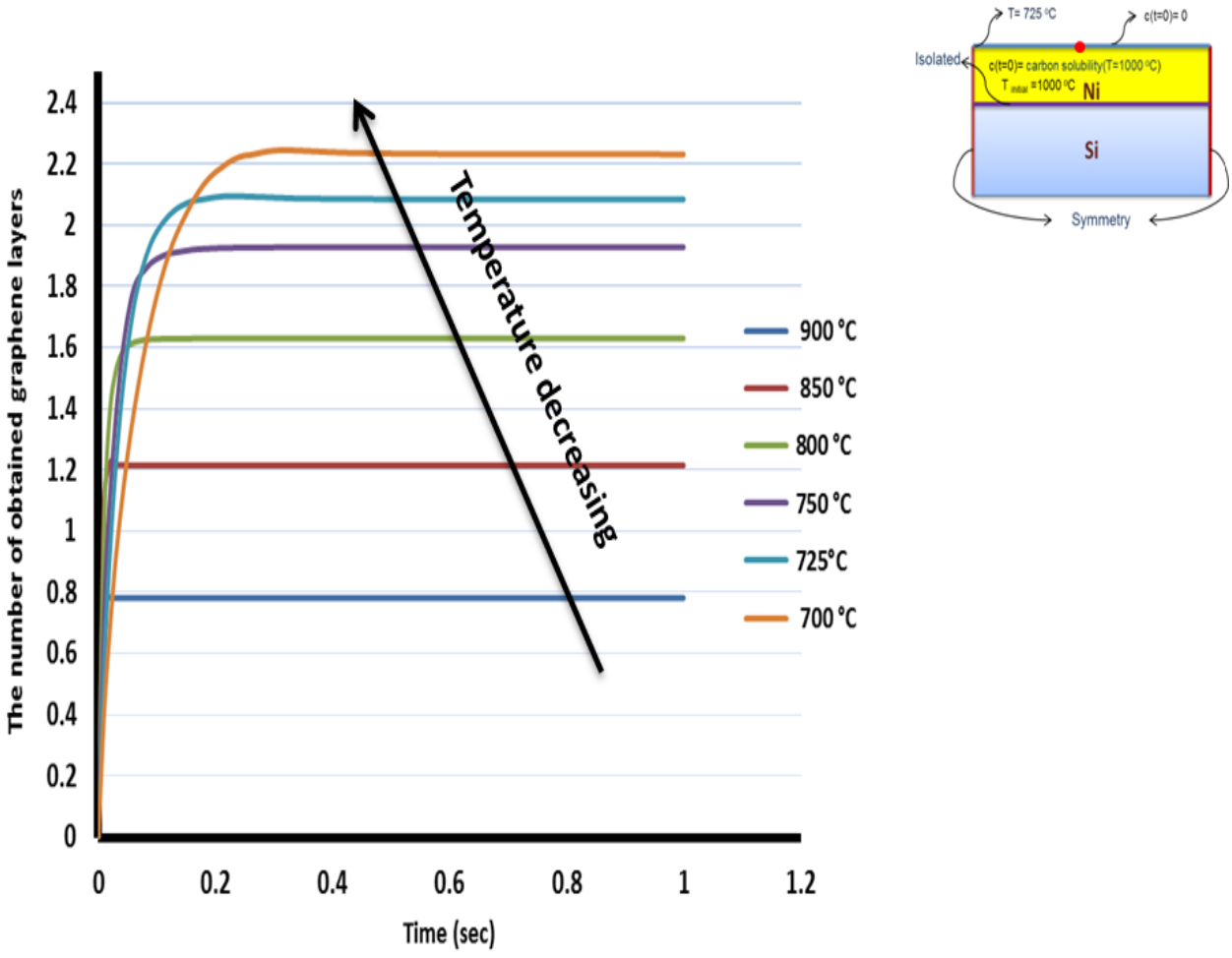

Figure 4.55: The number of the graphene layers grown on Ni film surface top surface after cooling from 1000 °C to different temperature.

4.9.3 Accuracy check

The simulated results were compared with experimental results conducted by Baraton et al. [82]. In their experiment, the graphene layers were formed using a precipitation mechanism. To clarify, graphene layers were experimentally produced on 200 nm thick Ni film without any participation of a direct carbon deposition mechanism in graphene formation. Their experimental results showed that the number of graphene layers formed on the Ni film when the temperature was dropped from 900 °C to 725 °C was two layers while the simulated results obtained in this work utilizing COMSOL MULTI -PHYSICS software was 1.7 layers.

Chapter 5: Summary and Conclusions

In this research, diamond-like carbon (DLC) films were deposited using plasma-enhanced ultra-high vacuum chemical vapor deposition system (PE-UHV-CVD). The effect of CH_4/Ar flow rate ratio and the plasma power on the DLC growth and quality was investigated.

A low-temperature synthesis of a few layers of graphene film on different 200 nm nickel film-coated substrates (Si, SiO_2, Si_3N_4, DLC, and diamond) using hot-filament chemical vapor deposition (HF-CVD) was conducted. The effect of growth temperature, growth pressure, CH_4/H_2 ratios, and graphene synthesis using the various 200 nm nickel film-coated substrates were investigated. Also, graphene etching utilizing atomic hydrogen was studied.

Ellipsometry was used to measure the thickness of SiO_2, Si_3N_4 films fabricated on Si substrate. Atomic force microscopy was used to investigate DLC films created using plasma-enhanced chemical vapor deposition system. AFM and SEM showed that ultra-smooth DLC films were formed on Si substrates.

In order to examine graphene films formed on 200 nm nickel film-coated Si, SiO_2, Si_3N_4, DLC, and diamond /Si substrates, scanning electron microscope energy dispersive X-ray spectroscope, and Raman spectroscope were used . SEM and EDX illustrated uniform growth of graphene films with wrinkles on the top and bottom surface of Ni films deposited on Si, SiO_2, Si_3N_4, DLC, and diamond /Si substrates. Raman spectroscopy was used to examine the quality and the number of graphene layers. I_{2D}/I_G values were used to determine the number of graphene layers formed on top and bottom surface of Ni film. Also, the intensity ratio I_D/I_G was used to determine graphene film quality. Moreover, the size of sp^2 domains (L_α) of the fabricated graphene films was approximately calculated using Tuinstra and Koenig's equation [77]. Raman

spectroscopy showed large-area uniform graphene films synthesized on both surfaces of Ni film top and bottom.

CVD graphene growth on nickel thin films by the dissolution-precipitation mechanism was modeled using COMSOL MULTIPHYSICS software. Heat transfer, mass transfer, and deformed geometry models were employed to simulate inward and outward carbon diffusion in the Ni film as well as the number of achieved graphene layers. Simulation showed that cooling 200 nm thick Ni film saturated with carbon atoms from 900 °C to 725 °C resulted in precipitating of 1.7 graphene layers on the Ni film surface. This simulated number of graphene layers was compared with experimental results. The COMSOL result matched well with experimental results, which gave two layers.

Large-scale suspended graphene film was formed on Si-based materials at low temperature. This could be a breakthrough for future device fabrication enabling graphene to replace Si or be used as a complimentary material to Si. Also, graphene film was completely etched away using atomic hydrogen. This could be very useful to pattern and selectively shape graphene films. Annealing and cooling graphene film in Ar atmosphere facilitated removal of Ni film from Si-based materials.

Graphene film can be obtained on Ni surfaces using the precipitation method. Moreover, one can use the Ni thin film as a sieve to control graphene film deposition at the bottom surface of the Ni film.

References

1. Salamanca-Buentello F, Persad DL, Martin DK, Daar AS, Singer PA. Nanotechnology and the developing world. PLoS Medicine 2005;2(5):e97.

2. Balzani V. Nanoscience and nanotechnology: A personal view of a chemist. Small 2005;1(3):278-83.

3. Zhang L. Silicon process and manufacturing technology evolution: An overview of advancements in chip making. Consumer Electronics Magazine, IEEE 2014;3(3):44-8.

4. Katsnelson MI. Graphene: Carbon in two dimensions. Materials Today 2007;10(1):20-7.

5. Trbovic J, Schönenberger C. Fabrication and electrical characterization of graphene. 2007.

6. Meyer JC, Geim AK, Katsnelson M, Novoselov K, Booth T, Roth S. The structure of suspended graphene sheets. Nature 2007;446(7131):60-3.

7. Lee J, Min K, Hong S, Kim G. Ab initio study of adsorption properties of hazardous organic molecules on graphene: Phenol, phenyl azide, and phenylnitrene. Chemical Physics Letters 2015;618:57-62.

8. McCann E, Koshino M. The electronic properties of bilayer graphene. Reports on Progress in Physics 2013;76(5):056503.

9. Carbon-Carbon bonds: Hybridization [Internet] Department of Physics - Freie Universität Berlin; c20112/3/15]. Available from: http://www.physik.fu-berlin.de/einrichtungen/ag/ag-reich/lehre/Archiv/ss2011/docs/Gina_Peschel-Handout.pdf. Accessed on 2/21/2015.

10. Avouris P, Chen Z, Perebeinos V. Carbon-based electronics. Nature Nanotechnology 2007;2(10):605-15.

11. Neto AC, Guinea F, Peres N, Novoselov KS, Geim AK. The electronic properties of graphene. Reviews of Modern Physics 2009;81(1):109.

12. Novoselov KS, Geim AK, Morozov SV, Jiang D, Zhang Y, Dubonos SV, Grigorieva IV, Firsov AA. Electric field effect in atomically thin carbon films. Science 2004 Oct 22;306(5696):666-9.

13. Peres N, Neto AC, Guinea F. Dirac fermion confinement in graphene. Physical Review B 2006;73(24):241403.

14. Zhu Y, Murali S, Cai W, Li X, Suk JW, Potts JR, Ruoff RS. Graphene and graphene oxide: Synthesis, properties, and applications. Adv Mater 2010;22(35):3906-24.

15. Y. Obeng, P. Srinivasan, H. Iwai, D. W. Hess, S. De Gendt, D. Misra, Z. Karim, H. Grebel, editor. Graphene and emerging materials for post-CMOS applications. ECS transactions; May 25-29, 2009; NJ: Electrochemical Society; 2009.

16. Dorgan VE, Bae M, Pop E. Mobility and saturation velocity in graphene on SiO2. Appl. Phys. Lett 2010;97(8):082112.

17. GRAPHENE: A NEW STAR IN MATERIAL SCIENCE [Internet]: Department of Physics, National Institute of Technology, West Bengal, India; c7/9/2014 [cited 2014 6/10/2014]. Available from: http://physics.unipune.ernet.in/~phyed/27.3/1374.pdf. Accessed on 3/10/2015.

18. Bonaccorso F, Sun Z, Hasan T, Ferrari A. Graphene photonics and optoelectronics. Nature Photonics 2010;4(9):611-22.

19. Nair RR, Blake P, Grigorenko AN, Novoselov KS, Booth TJ, Stauber T, Peres NM, Geim AK. Fine structure constant defines visual transparency of graphene. Science 2008 Jun 6;320(5881):1308.

20. Blake P, Hill E, Neto AC, Novoselov K, Jiang D, Yang R, Booth T, Geim A. Making graphene visible. Appl Phys Lett 2007;91(6):063124.

21. Yao Y, Wong C. Monolayer graphene growth using additional etching process in atmospheric pressure chemical vapor deposition. Carbon 2012;50(14):5203-9.

22. Cai D, Song M. Recent advance in functionalized graphene/polymer nanocomposites. Journal of Materials Chemistry 2010;20(37):7906-15.

23. Edwards RS, Coleman KS. Graphene synthesis: Relationship to applications. Nanoscale 2013;5(1):38-51.

24. Xuan Y, Wu Y, Shen T, Qi M, Capano MA, Cooper JA, Ye P. Atomic-layer-deposited nanostructures for graphene-based nanoelectronics. Appl Phys Lett 2008;92(1):013101,013101-3.

25. Wei Y, Wu J, Yin H, Shi X, Yang R, Dresselhaus M. The nature of strength enhancement and weakening by pentagon–heptagon defects in graphene. Nature Materials 2012;11(9):759-63.

26. Kim KS, Zhao Y, Jang H, Lee SY, Kim JM, Kim KS, Ahn J, Kim P, Choi J, Hong BH. Large-scale pattern growth of graphene films for stretchable transparent electrodes. Nature 2009;457(7230):706-10.

27. Roussak O, Gesser H. Carbon-based polymers, activated carbons. In: Applied chemistry. Springer; 2013. .

28. Balandin AA. Thermal properties of graphene and nanostructured carbon materials. Nature Materials 2011;10(8):569-81.

29. Balandin AA, Ghosh S, Bao W, Calizo I, Teweldebrhan D, Miao F, Lau CN. Superior thermal conductivity of single-layer graphene. Nano Letters 2008;8(3):902-7.

30. Renteria JD, Nika DL, Balandin AA. Graphene thermal properties: Applications in thermal management and energy storage. Applied Sciences 2014;4(4):525-47.

31. Yan Z. Thermal properties of graphene and applications for thermal management of high-power density electronics. United States -- California: University of California, Riverside; 2013. https://escholarship.org/uc/item/8m67d089. Accessed on 1/7/2015.

32. Lee Y, Bae S, Jang H, Jang S, Zhu SE, Sim SH, Song YI, Hong BH, Ahn JH. Wafer-scale synthesis and transfer of graphene films. Nano Letters 2010;10(2):490-3.

33. Forbeaux I, Themlin J, Debever J. Heteroepitaxial graphite on 6 H-SiC (0001): Interface formation through conduction-band electronic structure. Physical Review B 1998;58(24):16396.

34. Ohta T, Bostwick A, Seyller T, Horn K, Rotenberg E. Controlling the electronic structure of bilayer graphene. Science 2006 Aug 18;313(5789):951-4.

35. Ni Z, Wang Y, Yu T, Shen Z. Raman spectroscopy and imaging of graphene. Nano Research 2008;1(4):273-91.

36. Novoselov K, Fal V, Colombo L, Gellert P, Schwab M, Kim K. A roadmap for graphene. Nature 2012;490(7419):192-200.

37. Ferrari AC, Basko DM. Raman spectroscopy as a versatile tool for studying the properties of graphene. Nature Nanotechnology 2013;8(4):235-46.

38. Malard L, Pimenta M, Dresselhaus G, Dresselhaus M. Raman spectroscopy in graphene. Physics Reports 2009;473(5):51-87.

39. Jasinski J, Meyerson B, Scott B. Mechanistic studies of chemical vapor deposition. Annu Rev Phys Chem 1987;38(1):109-40.

40. Miao C, Zheng C, Liang O, Xie Y. Chemical vapor deposition of graphene. In: Sergey Mikhailov, editor. Physics and applications of graphene - experiments. Rijeka, Croatia: InTech; 2011: 37-34. http://www.intechopen.com/books/physics-and-applications-of-graphene-experiments/chemical-vapor-deposition-of-graphene. Accessed on 1/17/2015.

41. Kumar S, McEvoy N, Kim H, Lee K, Peltekis N, Rezvani E, Nolan H, Weidlich A, Daly R, Duesberg GS. CVD growth and processing of graphene for electronic applications. Physica Status Solidi (b) 2011;248(11):2604-8.

42. Reina A, Jia X, Ho J, Nezich D, Son H, Bulovic V, Dresselhaus MS, Kong J. Large area, few-layer graphene films on arbitrary substrates by chemical vapor deposition. Nano Letters 2008;9(1):30-5.

43. Bae S, Kim H, Lee Y, Xu X, Park J, Zheng Y, Balakrishnan J, Lei T, Kim HR, Song YI. Roll-to-roll production of 30-inch graphene films for transparent electrodes. Nature Nanotechnology 2010;5(8):574-8.

44. Yu Q, Jauregui LA, Wu W, Colby R, Tian J, Su Z, Cao H, Liu Z, Pandey D, Wei D. Control and characterization of individual grains and grain boundaries in graphene grown by chemical vapour deposition. Nature Materials 2011;10(6):443-9.

45. Hu B, Ago H, Ito Y, Kawahara K, Tsuji M, Magome E, Sumitani K, Mizuta N, Ikeda K, Mizuno S. Epitaxial growth of large-area single-layer graphene over cu (111)/sapphire by atmospheric pressure CVD. Carbon 2012;50(1):57-65.

46. Dervishi E, Li Z, Shyaka J, Watanabe F, Biswas A, Umwungeri JL, Courte A, Biris AR, Kebdani O, Biris AS. The role of hydrocarbon concentration on the synthesis of large area few to multi-layer graphene structures. Chemical Physics Letters 2011;501(4):390-5.

47. Ago H, Ito Y, Mizuta N, Yoshida K, Hu B, Orofeo CM, Tsuji M, Ikeda K, Mizuno S. Epitaxial chemical vapor deposition growth of single-layer graphene over cobalt film crystallized on sapphire. Acs Nano 2010;4(12):7407-14.

48. Park HJ, Skakalova V, Meyer J, Lee DS, Iwasaki T, Bumby C, Kaiser U, Roth S. Growth and properties of chemically modified graphene. Physica Status Solidi (b) 2010;247(11-12):2915-9.

49. Dervishi E, Li Z, Shyaka J, Watanabe F, Biswas A, Umwungeri J, Courte A, Biris A, Biris A. Large area graphene sheets synthesized on a bi-metallic catalyst system. Nanotechnology 2010:234-7.

50. Lee B, Yu H, Jeong G. Controlled synthesis of monolayer graphene toward transparent flexible conductive film application. Nanoscale Research Letters 2010;5(11):1768-73.

51. Bhaviripudi S, Jia X, Dresselhaus MS, Kong J. Role of kinetic factors in chemical vapor deposition synthesis of uniform large area graphene using copper catalyst. Nano Letters 2010;10(10):4128-33.

52. Kholmanov I, Cavaliere E, Cepek C, Gavioli L. Catalytic chemical vapor deposition of methane on graphite to produce graphene structures. Carbon 2010;48(5):1619-25.

53. Wang X, You H, Liu F, Li M, Wan L, Li S, Li Q, Xu Y, Tian R, Yu Z. Large-Scale synthesis of Few-Layered graphene using CVD. Chemical Vapor Deposition 2009;15(1-3):53-6.

54. Malesevic A, Vitchev R, Schouteden K, Volodin A, Zhang L, Van Tendeloo G, Vanhulsel A, Van Haesendonck C. Synthesis of few-layer graphene via microwave plasma-enhanced chemical vapour deposition. Nanotechnology 2008;19(30):305604.

55. Cambaz ZG, Yushin G, Osswald S, Mochalin V, Gogotsi Y. Noncatalytic synthesis of carbon nanotubes, graphene and graphite on SiC. Carbon 2008;46(6):841-9.

56. Reina A, Kong J. Graphene growth by CVD methods. In: Raghu Murali, editor. Graphene nanoelectronics. Springer; 2012: p 167-203.

57. Kim H, Saiz E, Chhowalla M, Mattevi C. Modeling of the self-limited growth in catalytic chemical vapor deposition of graphene. New Journal of Physics 2013;15(5):053012.

58. Regmi M, Chisholm MF, Eres G. The effect of growth parameters on the intrinsic properties of large-area single layer graphene grown by chemical vapor deposition on cu. Carbon 2012;50(1):134-41.

59. Zhang X, Yuan Q, Shu H, Ding F. Mechanisms of graphene chemical vapor deposition (CVD) growth. Graphene Chemistry: Theoretical Perspectives 2013:255-90.

60. Morozov S, Novoselov K, Katsnelson M, Schedin F, Elias D, Jaszczak J, Geim A. Giant intrinsic carrier mobilities in graphene and its bilayer. Phys Rev Lett 2008;100(1):016602.

61. Singh V, Joung D, Zhai L, Das S, Khondaker SI, Seal S. Graphene based materials: Past, present and future. Progress in Materials Science 2011;56:1178-271.

62. Li X, Zhu Y, Cai W, Borysiak M, Han B, Chen D, Piner RD, Colombo L, Ruoff RS. Transfer of large-area graphene films for high-performance transparent conductive electrodes. Nano Letters 2009;9(12):4359-63.

63. MingáLi C. Nanoelectronic biosensors based on CVD grown graphene. Nanoscale 2010;2(8):1485-8.

64. Regan W, Alem N, Alemán B, Geng B, Girit C, Maserati L, Wang F, Crommie M, Zettl A. A direct transfer of layer-area graphene. Appl Phys Lett 2010;96(11):113102,113102-3.

65. Wu Y, Chou H, Ji H, Wu Q, Chen S, Jiang W, Hao Y, Kang J, Ren Y, Piner RD. Growth mechanism and controlled synthesis of AB-stacked bilayer graphene on Cu–Ni alloy foils. Acs Nano 2012;6(9):7731-8.

66. Lander J, Kern H, Beach A. Solubility and diffusion coefficient of carbon in nickel: Reaction rates of Nickel-Carbon alloys with barium oxide. J Appl Phys 1952;23(12):1305-9.

67. Wei D, Wu B, Guo Y, Yu G, Liu Y. Controllable chemical vapor deposition growth of few layer graphene for electronic devices. Acc Chem Res 2013 JAN 15; 46(1):106-15.

68. Liu W, Chung CH, Miao CQ, Wang YJ, Li BY, Ruan LY, Patel K, Park YJ, Woo J, Xie YH. Chemical vapor deposition of large area few layer graphene on si catalyzed with nickel films. Thin Solid Films 2010;518(6):S128-32.

69. Yu Q, Lian J, Siriponglert S, Li H, Chen YP, Pei SS. Graphene segregated on ni surfaces and transferred to insulators. Appl Phys Lett 2008;93:113103.

70. Kwanghyun Yoo, Y. Takei, Bo Hou, S. Chiashi, S. Maruyama, K. Matsumoto, I. Shimoyama. Direct physical exfoliation and transfer of graphene grown via ethanol chemical vapor deposition. Micro electro mechanical systems (MEMS), 2011 IEEE 24th international conference on; 2011.

71. Dubey M, Nambaru R, Ulrich M, Ervin M, Nichols B, Zakar E, Nayfeh OM, Chin M, Birdwell G, O'Regan T. Graphene-based nanoelectronics. Adelphi MD: U.S. Army Research Laboratory; 2012. Report nr ARL-TR-5451.

72. De Arco LG, Zhang Y, Kumar A, Zhou C. Synthesis, transfer, and devices of single-and few-layer graphene by chemical vapor deposition. Nanotechnology, IEEE Transactions on 2009;8(2):135-8.

73. Zhang Y, Gomez L, Ishikawa FN, Madaria A, Ryu K, Wang C, Badmaev A, Zhou C. Comparison of graphene growth on single-crystalline and polycrystalline ni by chemical vapor deposition. The Journal of Physical Chemistry Letters 2010;1:3101-7.

74. Thiele S, Reina A, Healey P, Kedzierski J, Wyatt P, Hsu PL, Keast C, Schaefer J, Kong J. Engineering polycrystalline ni films to improve thickness uniformity of the chemical-vapor-deposition-grown graphene films. Nanotechnology 2010;21:015601.

75. Chae SJ, Güneş F, Kim KK, Kim ES, Han GH, Kim SM, Shin HJ, Yoon SM, Choi JY, Park MH. Synthesis of Large-Area graphene layers on Poly-Nickel substrate by chemical vapor deposition: Wrinkle formation. Adv Mater 2009;21(22):2328-33.

76. Pan G, Li B, Heath M, Horsell D, Wears ML, Al Taan L, Awan S. Transfer-free growth of graphene on SiO 2 insulator substrate from sputtered carbon and nickel films. Carbon 2013;65:349-58.

77. Yan Z, Peng Z, Sun Z, Yao J, Zhu Y, Liu Z, Ajayan PM, Tour JM. Growth of bilayer graphene on insulating substrates. ACS Nano 2011;5(10):8187-92.

78. McNerny DQ, Viswanath B, Copic D, Laye FR, Prohoda C, Brieland-Shoultz AC, Polsen ES, Dee NT, Veerasamy VS, Hart AJ. Direct fabrication of graphene on SiO2 enabled by thin film stress engineering. Scientific Reports 2014;4.

79. Johnson JK, Zollweg JA, Gubbins KE. The lennard-jones equation of state revisited. Mol Phys 1993;78(3):591-618.

80. Salandrino A, Engheta N. Far-field subdiffraction optical microscopy using metamaterial crystals: Theory and simulations. Physical Review B 2006;74(7):075103.

81. Faggio G, Capasso A, Messina G, Santangelo S, Dikonimos T, Gagliardi S, Giorgi R, Morandi V, Ortolani L, Lisi N. High-temperature growth of graphene films on copper foils by ethanol chemical vapor deposition. The Journal of Physical Chemistry C 2013;117(41):21569-76.

82. Baraton L, He Z, Lee CS, Maurice J, Cojocaru C, Lee YH, Pribat D. Study of graphene growth mechanism on nickel thin films. In: Graphita 2011. Springer; 2012.

Appendix A: Description of Research for Popular Publication

No more sand in your electronic devices

Electronic devices are basically made of sand. To explain, sand is treated in order to extract silicon. The majority of current ICs use silicon as a semiconductor material. Since 1958, engineers kept shrinking circuitry size in order to get high performance and high speed devices. However, silicon device manufacturing reaches its physical limits. No more shrinking of the size of the electronic devices can be achieved due to the heat generated in the devices. Hence, there is an urgent need for a technical solution for this sophisticated problem. The best solution for this problem is a new platform material to replace Si.

Graphene is a candidate material for future heat-free electronic devices. Graphene is a single atomic layer of carbon atoms organized in a two dimensional hexagonal lattice structure. Graphene is considered a promising material with enormous potential applications in many electronic and optoelectronics devices due to its superior properties. Electrons behave as a massless particle with high speed in graphene. Also, graphene is a flexible and transparent material. These amazing properties encourage researchers around the world to replace Si with graphene. However, a direct deposition of a high quality of graphene film on a desired substrate is still not achieved in terms of industry requirements. Current methods used to obtain graphene film on Si-based material require a multi-step transfer process. This transfer process does not match with electronic device manufacturing and degrades graphene properties as well.

In this research a very simple method for a direct deposition of graphene on Si-based material was achieved. A thin Ni film was deposited on Si-based material. Methane was decomposed catalytically and released carbon atoms when it hit the top surface of Ni film. Then, the adsorbed carbon atoms diffused into the Ni film at the same temperature, 1000 °C, until they

reached the Si-based material. The thin Ni film was used as sieve to control graphene formation on the Si-based material. This method can be used in electronic device industry enabling graphene to replace Si or be used as a complimentary material to Si.

Appendix B: Executive Summary of Newly Created Intellectual Property

The objectives of this research were:

a) Growing graphene film directly and selectively on a desired substrate at low temperature utilizing chemical vapor deposition (CVD) method.
b) *In situ* graphene film etching using atomic hydrogen.
c) Removing Ni film successfully using physical and chemical processes.
d) Simulating graphene film growth mechanism in Ni film.

The following list of new intellectual property items were created in the course of this research project and should be considered from both a patent and commercialization perspective.

1. The method for growing a large-scale suspended graphene film on Si-based materials at low temperature.
2. The process of etching away graphene film using atomic hydrogen.
3. The method for using the Ni thin film as a sieve to control graphene film deposition at the bottom surface of the Ni film.
4. The method for simulating CVD graphene growth on nickel thin films by the dissolution-precipitation mechanism using COMSOL MULTIPHYSICS software.

Appendix C: Potential Patent and Commercialization Aspects of listed Intellectual Property Items

C.1 Patentability of Intellectual Property (Could Each Item be Patented)

The three items listed were considered first from the perspective of whether or not the item could be patented.

1. The method for growing a large-scale suspended graphene film on Si-based materials can be patented because graphene films were grown at low temperature.
2. The process of etch away graphene film using atomic hydrogen can be patented. This process can be used to pattern the graphene film used in integrated circuit fabrication.
3. The method for using the Ni thin film as a sieve to control graphene film deposition at the bottom surface of the Ni film can be patented. This process can be used to grow different types of 2D materials.

C.2 Commercialization Prospects (Should Each Item Be Patented)

The three items listed were then considered from the perspective of whether or not the item should be patented.

1. The method for growing a large-scale suspended graphene film on Si-based materials should be patented. The graphene growing process is a low cost process and meets IC fabrication requirements.
2. The process of etching away graphene film using atomic hydrogen should be patented. This may be considered as a new method to pattern a graphene film.
3. The method for using the Ni thin film as a sieve to control graphene film deposition at the bottom surface of the Ni film should be patented. This process can be used to grow a large area of different types of 2D materials.

Appendix D: Broader Impact of Research

D.1 Applicability of Research Methods to Other Problems

In this research a novel method for direct large-scale graphene film formation on silicon based platform at low temperature was achieved using hot-filament chemical vapor deposition. Ni thin film was used as a sieve to control graphene film formation on Si-based substrates. The same method could be utilized to grow 2D materials on Si-based substrates. The COMSOL model could be used to study the growth mechanism of 2D materials.

D.2 Impact of Research Results on U.S. and Global Society

Large-scale suspended graphene film was formed on Si-based materials at low temperature. This could be a breakthrough for future device fabrication enabling graphene to replace Si or be used as a complementary material to Si. Therefore, graphene, which exhibits extraordinary electrical properties, can allow the semiconductor industry to continue its journey toward smaller and faster electronic devices.

D.3 Impact of Research Results on the Environment

Since 1958, the concept of integrated circuit (IC) has achieved great technological developments and helped in shrinking electronic devices. Nowadays, an IC consists of more than a million of compacted transistors. However, shrinking circuitry generates an intense heat which is radiated in all directions. So, always there is a need to cool the electronic devices. This requires more burning of fossil fuels to produce electricity for powering the cooling units in the devices.

Replacing Si used in the majority of current ICs with graphene will help in reducing the heat generated in electronic devices.

Appendix E: Microsoft Project for MS MicroEP Degree Plan

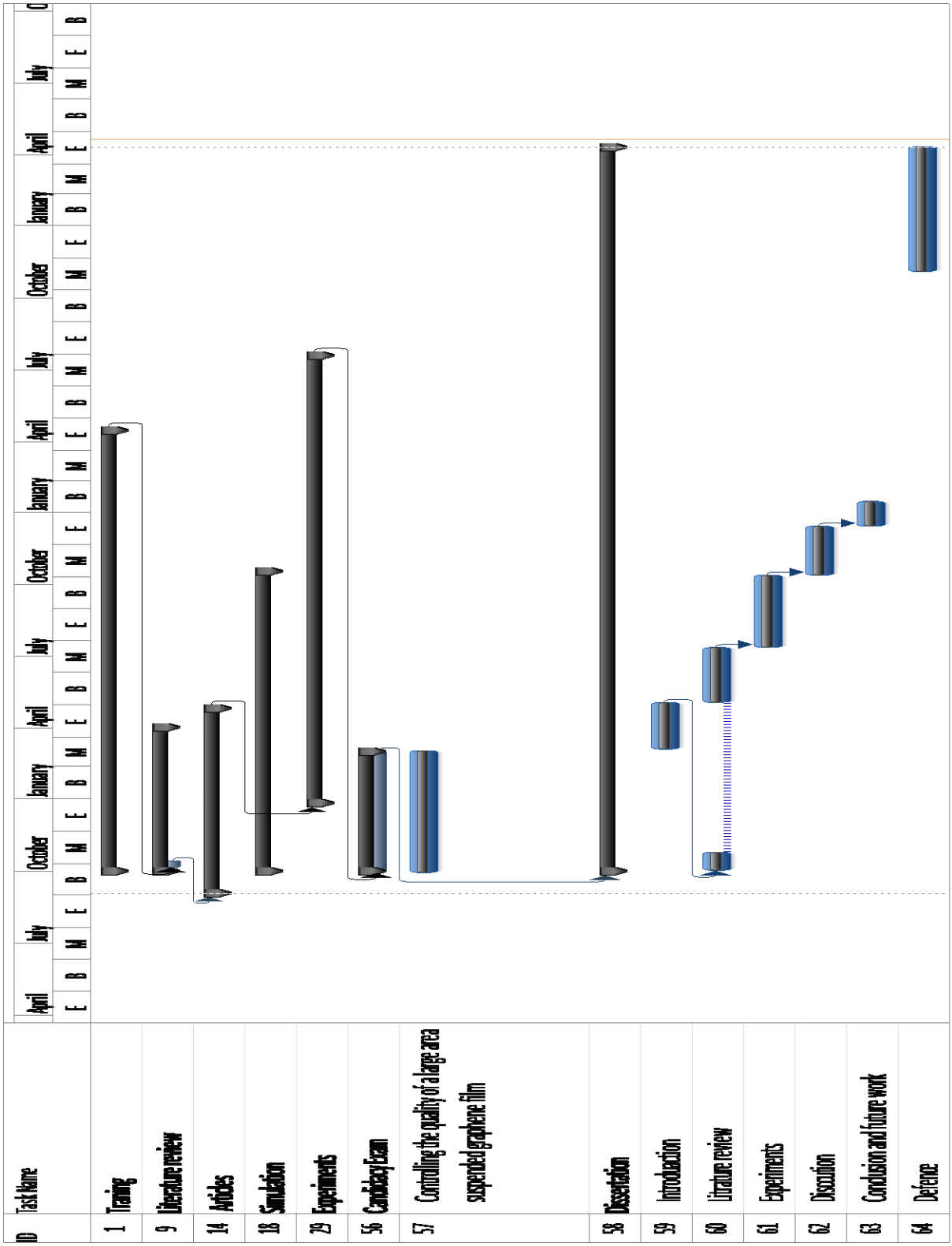

Appendix F: Identification of All Software Used in Research and Dissertation Generation

Computer #1:

Model Number: Dell Dimension 8300

Serial Number: R3615 W04

Location: ENRC 3615

Owner: Dr. Hameed Naseem

Software #1:

Name: Microsoft Office 2010

Purchased by: UA Electric Engineering Dept.

Software #2:

Name: COMOSOL MULTIPHYSICS

Purchased by: Microelectronics-Photonics Program

Software #3:

Name: Origin 9.1

Purchased by: Dr. Shui-Qing Yu

Computer #2:

Model Number: CORSAIR

Serial Number: 13118802

Location: ENRC 2933

Owner: Dr. Shui-Qing Yu

Appendix G: All Publications Published, Submitted and Planned

1. Al-Shurman, K. M., Husam Abu-Safe, Murtadha Alher, Omar Alzoubi, and Hameed Naseem, "Large-Area synthesis of Uniform Graphene on Nickel Films at Low Temperature Using Hot-Wire Chemical Vapor Deposition," MRS/New Diamond and Nano Carbons Conference (NDNC 2014), Chicago, IL, USA, May 25-29, 2014. www.mrs.org/ndnc-2014-tuesday-program/.

2. Al-Shurman, K. M., and Hameed Naseem, "CVD Graphene Growth Mechanism on Nickel Thin Films," COMSOL Conference 2014, Boston, Massachusetts, USA, October 8 - 10, 2014. http://www.comsol.com/paper/download/194705/alshurman_paper.pdf.

3. Al-Shurman, K. M., and Hameed Naseem, "CVD Graphene Growth Mechanism on Nickel Thin Films," COMSOL Conference 2014, Boston, Massachusetts, USA, October 8 - 10, 2014. http://www.comsol.com/paper/download/194711/alshurman_abstract.pdf

4. Alzoubi, O. H., Husam Abu-Safe, Khalid Alshurman, Hameed A. Naseem. "Broadband Absorptance High Efficiency Silicon Nanowire Fractal Arrays for Photovoltaic Applications," MRS/ Spring Meeting & Exhibit (2014 MRS), San Francisco, CA, USA, April 21-25, 2014. https://mrsspring14.zerista.com/event/member/112934

5. Al-Shurman, K. M., Husam Abu-Safe, Murtadha Alher, Omar Alzoubi, and Hameed Naseem, "Large-Area Synthesis of Uniform Graphene Film on Graphene Synthesis on Different Substrate Materials at Low Temperature," Year 4 ASSET II Annual Meeting, Little Rock, AR.USA, September 4-5, 2014.